Dynamics of neat ionic liquid, binary mixtures and liquids under confinement: Theoretical and simulation study

Thesis Submitted for the Degree of

Doctor of Philosophy (Science)

of

Jadavpur University

By

Snehasis Daschakraborty

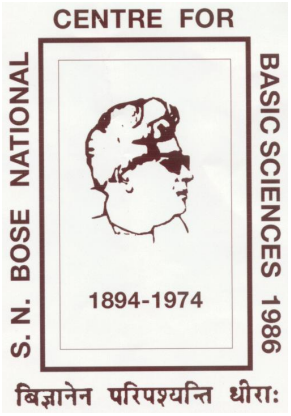

Department of Chemical, Biological and Macromolecular Sciences,

S. N. Bose National Centre for Basic Sciences,

Block-JD, Sector-III, Salt Lake City,

Kolkata-700098, India

Dedicated to

My Father Sri Ranjit Daschakraborty

And

Mother, Smt. Rekha Daschakraborty

CENTRE FOR BASIC SCIENCES 1986
S. N. BOSE NATIONAL
1894 - 1974
विज्ञानेन परिपश्यन्ति धीराः

सत्येन्द्र नाथ बसु राष्ट्रीय मौलिक विज्ञान केन्द्र
SATYENDRA NATH BOSE NATIONAL
CENTRE FOR BASIC SCIENCES
সত্যেন্দ্র নাথ বসু জাতীয় মৌল বিজ্ঞান কেন্দ্র

CERTIFICATE FROM THE SUPERVISOR(S)

This is to certify that the thesis entitled **"Dynamics of neat ionic liquid, binary mixtures, and liquids under confinement: Theoretical and simulation study"** submitted by **Sri Snehasis Daschakraborty** (Index no. 18/12/Chem./21), who got his name registered on 18/04/12 for the award of Ph. D. (Science) degree of Jadavpur University, is absolutely based upon his own work under the supervision of **Dr. Ranjit Biswas** and that neither his thesis nor any part of it has been submitted for either any degree/diploma or any other academic award anywhere before.

Ranjit Biswas 25.07.13

Dr. Ranjit Biswas

Associate Professor,

Department of Chemical, Biological and Macromolecular Sciences

S. N. Bose National Centre for Basic Sciences

Block – JD, Sector – III, Salt Lake, Kolkata – 700098, West Bengal, India

DR. RANJIT BISWAS
Associate Professor
S. N. Bose National Centre for Basic Sciences
Block-JD, Sector-III, Salt Lake
Kolkata-700 098, India

FUNDED BY DEPARTMENT OF SCIENCE & TECHNOLOGY, GOVERNMENT OF INDIA
निधिवद्ध विज्ञान और प्रौद्योगिकी विभाग भारत सरकार द्वारा

Acknowledgement

I spent about five years at the S. N. Bose National Centre for Basic Sciences (SNBNCBS), Kolkata, as a research scholar in the department of Chemical, Biological and Macromolecular Sciences (CBMS). I have learnt so many things here and therefore I would like to express my gratitude and heartiest thanks to all connected to my activity and well-being here.

I would like to express my deep gratitude to my research supervisor Dr. Ranjit Biswas for giving me an excellent supervision and enormous encouragement to shape up my scientific skills. His kind and affectionate attitude has always motivated me to perform my best. He has taught me how to deal with a research problem and treat professionally. He has always helped me how to build a clear understanding on a research problem. I have also felt and enjoyed his guidance towards the journey of becoming a true human being. I truly see him as my friend, philosopher and guide.

I would like to thank Prof. Arup Kumar Roychowdhury, the Director, S. N. Bose National Centre for Basic Sciences, for providing an excellent research atmosphere at the Centre. I am highly obliged to Prof. Abhijit Mookerjee for giving me positive energy in my research works. I would like thank sincerely Dr. Gautam Gangopadhyay, Dr. Jaydeb Chakrabarti, Dr. Samir Kumar Pal, Dr. Priya Mahadevan, and Dr Chhayabrita Biswas for their deep concern, care and affection throughout my stay at the Centre.

I am grateful to Prof. Biman Bagchi, Solid State and Structural Chemistry Unit, Indian Institute of Science, Bangalore, India and Prof. Mark Maroncelli, Dept. Of Chemistry, Penn State University, USA, for various important suggestions, insightful discussion and encouragement. I also convey my deep regards to Prof. Amalendu Chandra, Dept. of Chemistry, Indian Institute of Technology Kanpur, Kanpur, India and Prof. Sanjoy Bandyopadhyay, Dept. of Chemistry, Indian Institute of Technology Kharagpur, Kharagpur, India for their overwhelming support in many ways. I acknowledge with respect the help and assistance received from Dr. Pradip Kumar Ghorai, IISER, Kolkata and Prof. Partha Dastidar, IACS, Kolkata during my Ph. D. tenure.

I heartily thank my present labmates (PCCPians), Biswajit-da, Tamisra, Anuradha, Sandipa, Kallol and Suman for their constant encouragement and support in many ways. I am really grateful to them and will never forget such a beautiful homely bonding. I am also extremely indebted to the ex-members of my lab, Tuhin-da, Hemant-da, and Harun-da for their

contributions in my research and also in many non-academic things. I thank Prabhat Prakash, who did a short term summer project in our laboratory, for his company and charm.

Apart from the academic personals and friends, I would like to convey my regards to all the non academic official members of the Centre who have assisted me in many ways during my PhD tenure.

I convey my regards to Dr. Parijat Das, whom I supposed as a member of my lab, for her caring attitude and great hospitality at her home. I would like to express my deep feelings to sweet Rwitoban and Arshaman for their cuteness.

I express my gratitude to the security personals in the Centre for their caring and responsive attitude, which has always made me feel secured inside the campus.

I would also like to thank the *canteen-boys* in the centre, Bidyasagar, Sanatan, Hari, Sumanta, Subhankar, Mrinmay, Sudip, Bappa for their extreme care for providing a good quality food. My sincere thanks are for Bhai-da, Haren-da, Nares-da, Dulal-da, and Bharat-da for their support in many ways.

I am really grateful to my late Grandfather and maternal grandfather for their heavenly blessings that showered upon me, and other members of my family: my father, my mother, my old grandmother, my dida, my sister (Mou-di), and my brother-in-law (Jamaibabu). I want to express my deep affection to my bhagni (Ankesha), and bhagna (Ankan) for their sweet attitude, which has given me an extra energy to scale the difficult terrains of research, publications and beyond.

Finally, I acknowledge the Council of Scientific and Industrial research, New Delhi for granting me a research fellowship.

Abstract

In this Thesis, we have presented theoretical studies of Stokes shift dynamics of a fluorescent probe dissolved in pure ionic liquids, and binary mixtures of it with various common dipolar solvents. In addition, theoretical study on how charge-charge interaction decouples from orientational relaxation in ionic liquids, and computer simulations on structural and dynamical features of various model liquids are also presented. Ionic liquid, being an environmentally benign solvent, has been attracted interests by many researchers in molecular level investigation. Moreover, it has been shown that ionic liquids possess micro-heterogeneity with strong implications on various relaxation processes. This thesis therefore primarily focuses on understanding relaxation dynamics in terms of microscopic picture. We have developed molecular theories for this purpose and molecular mechanism has been ascribed via facilitating direct comparison between theoretical predictions and measurements. In some cases, where experimental data are not available yet, our predictions on dynamical features motivate new experiments and/or simulations. Recent fluorescence upconversion measurements of (ionic liquid + water) system have revealed semi-quantitative agreement between experimental data and our theory. We have also developed a molecular theory for understanding the dielectric relaxation of ionic liquid where we have focussed on the importance of dipole-dipole, ion-dipole and ion-ion interactions for their relative roles in dielectric relaxation and collective rotation. Computer simulations have been carried out to understand the structural and dynamical behaviours of model liquids in bulk and confinement.

The thesis contains twelve chapters including Introduction (Chapter 1), describing the motivations of the works presented in the thesis with literature survey, and Conclusion (Chapter 12), where main results in various works are summed-up and some future problems discussed. In Chapter 2 and 3 we have discussed our theoretical understanding on the Stokes shift dynamics of two non-conventional ionic liquids. Chapter 4 consists of the theoretical study of solute probe dependence on Stokes shift dynamics in ionic liquid. The probable origin of ultrafast time scale, originated from Three Pulse Photon Echo Peak Shift (3PEPS)

measurements for ionic liquid has been described in Chapter 5. Chapter 6 and 7 deals with the theoretical study of Stokes shift dynamics of a solute probe in binary mixture of ionic liquid and dipolar solvent. We have described in Chapter 8 the theoretical description for the study of dielectric relaxation in ionic liquid. Chapter 9, 10 and 11 describe the computer simulation investigation of dynamics of some model liquids in bulk and confined environment.

List of Publications

1. "*Stokes' Shift Dynamics in (Ionic Liquid + Polar Solvent) Binary Mixtures: Composition Dependence*" by **Snehasis Daschakraborty** and Ranjit Biswas, *Journal of Physical Chemistry B*, **2011**, *115*, 4011.

2. "Stokes' Shift Dynamics in Alkylimidazolium Aluminate Ionic Liquids: Domination of Solute-IL Dipole-Dipole Interaction"by **Snehasis Daschakraborty** and Ranjit Biswas, *Chemical Physics Letters*, **2011**, 510, 202.

3. "*Fluorescence Dynamics in Supercooled (Acetamide + Calcium Nitrate) Molten Mixtures*" by Harun Al Rasid Gazi, Biswajit Guchhait, **Snehasis Daschakraborty** and Ranjit Biswas, *Chemical Physics Letters*, **2011**, *501*, 358.

4. "*Does Polar Interaction Influence Medium Viscosity? A computer Simulation Investigation Using Model Liquids*" by **Snehasis Dascharaborty** and Ranjit Biswas, *Journal of Chemical Sciences*, **2012,** *124*, 763.

5. "*Stokes shift dynamics of [Na][TOTO] - a new class of ionic liquids: A comparative study with more common imidazolium analogs*" by **Snehasis Daschakraborty** and Ranjit Biswas, *Chemical Physics Letters*, **2012,** *545*, 54.

6. "*Ultrafast Solvation Response in Room Temperature Ionic Liquids: Possible Origin, and Importance of the Collective and the Nearest Neighbour Solvent Modes*" by **Snehasis Daschakraborty** and Ranjit Biswas, *Journal of Chemical Physics*, **2012,** *137*, 114501.

7. "*Medium Decoupling of Dynamics at Temperatures ~100 K Above Glass-Transition Temperature: A Case Study with (Acetamide+Lithium Bromide/Nitrate) Melts*" by Biswajit Guchhait, **Snehasis Daschakraborty** and Ranjit Biswas, *Journal of Chemical Physics*, **2012**, *136*, 174503.

8. "*Transport Properties of Binary Mixtures of Asymmetric Particles: A Simulation Study*" by **Snehasis Daschakraborty** and Ranjit Biswas, In "*Concepts and Methods in Modern*

Theoretical Chemistry (Vol-2)"; Ghosh, S. K., Chattaraj, P. K. Eds.; CRC Press; Taylor & Francis Group: London, UK, 2013; pp 21-35.

9. "*Stokes shift Dynamics of Ionic Liquids: Solute Probe Dependence, Effects of Dielectric Relaxation Window and Solvent Librations*" by **Snehasis Daschakraborty**, Tamisra Pal and Ranjit Biswas. *Journal of Chemical Physics*, **2013** (submitted).

10. "*Composition Dependent Stokes Shift Dynamics in (Ionic Liquid + Dipolar Solvent) Binary Mixtures: Comparison between Theory and Experiments*" by **Snehasis Daschakraborty** and Ranjit Biswas. *Journal of Physical Chemistry B*, **2013** (to be submitted soon).

11. "*Dielectric Relaxation of Ionic Liquid: Role of Ion-Dipole and Ion-Ion Interactions and Effects of Heterogeneity*" by **Snehasis Daschakraborty** and Ranjit Biswas. *Journal of Physical Chemistry B* **2013** (to be submitted soon).

12. "*Solvation Dynamics in Ionic Liquids: Competitive Roles of Translational and Rotational Motions*" by Ranjit Biswas, **Snehasis Daschakraborty** and Tamisra Pal *Journal of Physical Chemistry B* (Feature article) **2013** (to be submitted soon)

13. "*Medium Heterogeneity in Presence of a Structure Breaker: Temperature Dependent Fluorescence Studies of Deep Eutectic (Alkylamide+Electrolyte) Melts*" by Biswajit Guchhait, **Snehasis Daschakraborty** and Ranjit Biswas, *Journal of Physical Chemistry B* **2013** (to be submitted soon).

14. "*Inhomogeneity in Structure and Dynamics in Binary Mixture of Asymmetric Particles Inside a Cylindrical Nanopore: Investigation Using Molecular Dynamics Simulation*" by **Snehasis Daschakraborty** and Ranjit Biswas (In Preparation).

15. "*Calculation of Critical Solution Temperature of Anisotropic Binary Fluid Mixtures: A Molecular Dynamics Simulation Study*" by **Snehasis Daschakraborty** and Ranjit Biswas (In Preparation).

16. "*Stokes shift dynamics of aqueous solution of Guanidinium salts: A Theoretical Approach*" by **Snehasis Daschakraborty** and Ranjit Biswas (In Preparation).

Contents

Chapter 1

Introduction

Molecular level understanding of dynamics in liquids is extremely important in the area of chemical kinetics and reaction dynamics, where either neat liquid or liquid mixture is often used as a reaction medium. This is because both medium polarity and dynamics critically regulate the reaction rate either via modifying the reaction barrier or coupling dynamically to the reactive mode[1-11]. The reaction medium can affect the reaction rate by facilitating the stabilisation of the intermediate species through solvation.[12-17] Solvents can even control a reaction by forcing a specific pathway to follow.[18-23] Simple collision theory[24] of reaction states that when reactant particles collide against each other, only a certain fraction of such collisions can induce chemical change; these are called successful collisions. Thus by tuning the number of collision, the rate of the reaction may be controlled. A detailed knowledge of solvent dynamics can therefore assist in achieving better understanding of solvent effects on rate of a reaction. Apart from chemical reactions, several important biological phenomena, such as, protein folding, formation of lipid bilayer, ion permeation through channels etc. demand a detail understanding of solvent effects and the relevant control.[25-36]

Liquid mixtures are sometimes more useful as reaction media than neat liquids because medium effects can be tuned via simply altering the mixture composition. For example, medium polarity varies with the composition of the binary mixture. Transport properties, such as, viscosity and diffusion will also be a function of composition. As a result, binary mixtures provide a better control for a given chemical reaction. This is a key for using binary mixtures as designer reaction media for tailoring a reaction. Naturally, researchers have devoted enormous interest in exploring various static and dynamical properties of pure liquids and binary mixtures.[37-41]

Another class of solvents, which has the potential to be used as environment-friendly reaction medium, is ionic liquids. These are molten electrolytes at or near room temperature and composed of large organic cations and anions. Multiple long alkyl chains attached to

cations for typical ionic liquids provides the entropic gain to overcome the charge-charge coulombic interaction between oppositely charged ions and drive the ions to be displaced from their designated places in a crystal lattice. Interestingly, ILs are known for about a century, with one of the earliest truly RTILs being ethylammonium nitrate (T_m ~285 K)[42].

However, the research on ILs has grown rapidly over the last two decades because of several useful solvent properties such as, low vapour pressure[43], high thermal stability,[44] good solvating ability for a wide variety of organic, inorganic and organometallic compounds,[45,46] high electrical conductivity[47], low nucleophilicity, and capability of providing weekly coordinating or non-coordinating environments. Consequently, ILs find applications in chemical and pharmaceutical industries, nuclear fuel processing, electrochemical cell assemblies, etc.[48-50] The growing interest for using ILs as environmentally benign reaction media[51-56] necessitates a thorough molecular level understanding of the interaction and dynamics of these Coulomb systems. This is the key reason for a spurt of research activities in this area using theory, experiment, and computer simulation techniques.[57-126]

Addition of polar solvents strongly influences viscosities and electrical conductivities of parent ILs which may make these mixtures alternative media for certain chemical and electrochemical applications.[124] On other hand, the miscibility of ILs in water may be a serious threat to the environment because it may enter into the food chain to affect the entire ecosystem.[51] The possible advantages and disadvantages of these binary mixtures demand detailed study so that interactions between a conventional solvent and ionic liquid are properly understood. Moreover, the molecular level understanding of the dynamical features may indicate how screening can affect the over-all dynamics of such mixtures.

Similar to conventional polar liquids, time resolved fluorescence Stokes shift (TRFSS) technique has been employed rather extensively to access the dynamical information in these systems.[66,73-82,126] These and dielectric relaxation (DR)[57,64,65,104-112] studies of pure imidazolium ILs have revealed, in addition to viscosity-controlled slow timescales, the presence of extremely fast time scales like in common dipolar solvents. Another interesting

feature in these TRFSS studies includes observation of large dynamic Stokes shifts[77,78,82,85,126] suggesting strong average polarity for these media. However, DR measurements report static dielectric constant (ε_0) to be around 12 for imidazolium ILs at room temperature.[57,64,65,104-112] These apparently contradictory results seem to suggest strong roles for both solute-IL dipole-dipole and dipole-ion interactions in determining the experimental shifts in these systems. Indeed, a semimolecular approach has been developed to understand experimental Stokes shift dynamics in terms of these two different types of solute-IL interactions.[67-72] This theory, when applied for Stokes shift dynamics of dipolar probes in several imidazolium ILs, predicts solute-IL dipolar interaction contribution to the observed shift is ~60%. In addition, predicted dynamics tracks well the measured solvation response functions where slow long time tail originates from the relaxation of the ion dynamic structure factor. Interestingly, this semi-molecular theory suggests the experimentally observed sub-picosecond solvation response in imidazolium ILs has its origin in the collective rotation of the dipolar ions. Moreover, this theory has successfully explained the reason behind the break-down of the existing continuum-model based dielectric theories for solvation. The separation between dipole-dipole interaction contribution from dipole-ion component in this theory enables one to test the interrelationship between dynamic solvent response and frequency dependent dielectric function for ionic liquids.

The above approach, when suitably expanded for binary mixtures of ILs with common dipolar solvents, has been found to predict successfully experimental results.[71] The composition independence of the Stokes shift in experiment has been observed in the theoretical predictions as well. The theory predicts the total dynamical solvent response in such mixtures are a combination of three contributions arising from (i) solute-IL dipole-dipole interaction, (ii) solute-IL dipole-ion interaction and (iii) solute-cosolvent dipole-dipole interaction.

The present thesis is divided in several chapters where the next chapter (chapter 2) contains the application of a semimolecular theory (developed earlier)[67,68] to predict the Stokes shift dynamics for a dipolar solute, coumarin 153 (C153), in six different low viscous alkylimidazolium ILs containing a fixed anion, tetra (hexafluoroisopropoxy) aluminate[109,110].

Calculated shifts in these ILs at ~343 K range are seen to be higher than common imidazolium ILs, and an overwhelming contribution (~75-85%) arises from the solute-IL dipole (dipole-dipole) interaction. Inclusion of solvent-libration enhances the amplitude of the ultrafast component in the total dynamics. Although the predicted dynamics is faster than in other ILs, calculated shifts follow the same linear correlation with ion size-ratio. Furthermore, model calculations explore the solute-IL size-ratio dependence of the interaction contributions to the shift, and investigate the relative importance of solvent rotational and translational modes for IL dynamics.

The same theory has also been applied in chapter 3 to study the temperature dependent Stokes shift dynamics of C153 probe in sodium 2,5,8,11-tetraoxatridecan-13-oate ([Na][TOTO]) (a highly viscous IL)[111,112], and compared with imidazolium ionic liquids (ILs). Note in these ILs the dipole-dipole interaction contribution to the dynamics arises from the interaction between the anion and the solute which is different from imidazolium ones where it is the cation which participates in such interactions. The theory has used the experimental DR data measured earlier. Predicted dynamic Stokes shift for [Na][TOTO] has been seen to be slightly lower than that calculated for imidazolium ILs. The calculated biphasic dynamics is extremely slow because of large viscosity, average solvation time ($\langle \tau_{ss} \rangle$) being in ~1 s - 10 ns range at $254 \leq T/(K) \leq 344$. This is much slower than those in imidazolium ILs ($0.1 \leq \langle \tau_{ss} \rangle / ns \leq 6$ at $278 \leq T/(K) \leq 338$). Predicted temperature dependence of shift is very weak and suggests near-Arrhenius behavior for the dynamics.

Recently dynamic Stokes shift measurement of a fluorescent probe, C153, has been done with a combination of broad-band fluorescence upconversion (FLUPS) and time correlated single photon counting (TCSPC) in order to determine the complete solvation response of various ILs.[126] This measurement has revealed different Stokes shift and dynamics from earlier study[77] of a different probe, DCS, using a combination of Kerr-gated emission (KGE) and TCSPC techniques. The solvation relaxation time scales, the corresponding amplitudes, and the stretching exponent have been changed in the new measurements. Moreover, the new measurements suggests initial part of the solvation response to be Gaussian in nature, in contrast to earlier simple exponential representations. Here, the question is whether this difference is real and originates from the use of different experimental techniques. Also, one

would like to investigate how much of this difference is related to the usage of different probes in separate measurements. We investigate these questions in chapter 4. Inclusion of librational contributions[127] along with DR data[106] improves the agreement between theory and experiments for the systems considered. Here the probe dependence on Stokes shift dynamics has also been investigated. The sensitivity of the theory towards the dielectric relaxation data, measured at different frequency region, has been checked and studied in detail.

Recent three-pulse photon echo peak shift (3PEPS) measurements with several RTILs have revealed multi-exponential dynamics with ultrafast solvation timescale in the range, $20 < \tau_1/\text{fs} < 250$, for both imidazolium and phosphonium RTILs.[66] This is striking for two reasons: (i) the timescale is much faster than those reported by the TRFSS experiments[77] and (ii) sub-hundered femtosecond solvation response in phosphonium ionic liquids is reported for the first time. In chapter 5, a mode coupling theory based calculation[128-130] has been presented, where such ultrafast solvation in 3PEPS measurements has been visualized to originate from the nearest neighbour solute-solvent interaction. Consideration of Lennard-Jones interaction for the nearest neighbour solute-solvent non-dipolar interaction leads to biphasic dynamics with a predicted ultrafast time constant in the ~100-250 femtosecond range, followed by a slower one similar to that reported by the 3PEPS measurements[66]. In addition, the calculated fast time constants and amplitudes are found to be in general agreement with those from computer simulations. Different microscopic mechanisms for ultrafast solvation response measured by the 3PEPS and DSS experiments have been proposed and relative contributions of the collective and nearest neighbour solvent modes investigated. Relation between the single particle rotation and ultrafast polar solvation in these RTILs has been explored. The analyses suggest 3PEPS and DSS experiments are probably sensitive to different components of the total solvation energy relaxation of a laser-excited dye in a given ionic liquid.

In chapter 6, development of an approximate semi-molecular theory has been described to investigate the composition dependence of Stokes shift dynamics of a fluorescent dye molecule dissolved in binary mixtures of (IL + conventional polar solvent) at different mole fractions. The theory expresses the dynamic Stokes shift as a sum of contributions from the

dye-IL and the dye-polar solvent interactions and suggests substantial solute-cation dipole-dipole interaction contribution to the solvation energy relaxation. The theory, when applied to aqueous mixtures of 1-butyl-3-methylimidazolium hexafluorophosphate ([Bmim][PF_6]) and tetrafluoroborate ([Bmim][BF_4]), and binary mixtures of ([Bmim][BF_4] + acetonitrile), predicts reduction of Stokes shift but acceleration of the dynamics upon increasing the polar solvent concentration for the most part of the mixture composition. The decrease in dynamic Stokes shift values has been found to occur due to decrease of the dye-IL interaction in presence of the added polar solvent. For aqueous binary mixtures of IL, the predicted results are in semi-quantitative agreement with the available experimental results.[131-134] However, the calculated dynamics suggest much weaker composition dependence than that observed in experiments. In addition, the theory predicts a turnaround for dynamic Stokes shift in its composition dependence for ([Bmim][BF_4] + acetonitrile) mixtures at higher dilutions of the IL.

The theory for studying the Stokes shift dynamics of a fluorescent probe in the binary mixture of (IL + common dipolar solvent) in previous chapter has been modified in chapter 7, and applied for a couple of mixtures and then compared the theoretical results with the recent experiments.[135,136] The theoretical calculation has been done using two different approaches, separate and effective medium calculations, in order to find out the better approach for explaining the experimental Stokes shift dynamics. Whereas the effective medium approach has been seen to be more suitable for predicting the Stokes shift, separate medium approach reproduces the dynamics much better. Composition independence of experimental Stokes shift[135,136] has been seen to be well explained by the theory in terms of mutual cancellation of solute – solvent dipole – dipole interaction and solute – solvent dipole – ion interaction contributions. The present theory is able to explain most of the interesting dynamical features observed in experiments.

Chapter 8 describes a semi molecular theory for studying the dielectric relaxation dynamics in IL. This theory predicts triphasic relaxation of generalized orientation correlation. The dielectric relaxation process picks up contributions from dipole-dipole and ion-dipole interactions in pure ILs. The ion-dipole interaction produces an extremely large dielectric relaxation time constant which has not been observed in DR experiments. Hence, ion-dipole

interaction contribution is considered to be absent in experimentally measured dielectric relaxation of these liquids. The theory investigates relations among single particle rotational, collective rotational and dielectric relaxation times. The predicted dielectric relaxation time is seen to be large compared to the experimental values in case of IL, although the dipolar liquids show a very good agreement with the experiments. This difference has been understood in terms of microscopic heterogeneity in IL. Temperature dependence study has been carried out to assess the effects of temperature on relaxation time constants and heterogeneity in the system. The reason of the difference between theoretical and experimental time constants is explained by the difference of effective rotational volume and the actual volume of the dipolar component in the ILs investigated.

It has been discussed earlier that the reaction dynamics study demands a clear understanding on the structure and dynamics of solvent. The molecular dynamics simulation is one of the computer simulation techniques that provides a detailed understanding on static and dynamical features of solvents. Chapter 9 describes the study of molecular dynamics simulations of model liquids interacting via Lennard-Jones (L-J) and Stockmayer (SM) interactions, exploring the effects of the longer-ranged dipole-dipole interaction on solvent viscosity and diffusion. Switching on of the dipolar interaction at a fixed density and temperature has been found to increase the viscosity over that of the LJ liquid, the extent of increase being a few percent to as large as ~60% depending upon the magnitude of the solvent dipole moment used in the SM potential. The simulated translational and rotational diffusion coefficients show strong dipole moment and temperature dependences, eventhough effects of these parameters on solvent-solvent radial distribution function are moderate. Interestingly, a partial solute-solvent decoupling is observed when the simulated translational and rotational diffusion coefficients are connected to the simulated viscosity coefficients via the Stokes-Einstein (SE)[137] and Stokes-Einstein-Debye (SED)[138] relations. In the limit of large dipole moment, simulated self-part of the van Hove correlation function at intermediate times reveals a departure from the Gaussian distribution with particle displacement. This suggests that dynamic heterogeneity is one of the reasons for the departure of centre-of-mass diffusion from the SE relation in these model systems.

Chapter 10 describes the molecular dynamics simulations of binary mixture of model asymmetric liquids interacting via Gay-Berne potential[139]. This simulation has been carried out to explore the effects of composition on solution structure and transport properties. The simulated spatial distribution function shows a hump at a distance approximately 75% of the effective diameter from the central particle which becomes prominent upon increasing the concentration of more asymmetric particle in binary mixture. Non-ideality in the mixture composition dependence of diffusion and pressure has been observed in the entire mole fraction range, although simulated viscosity remains largely insensitive to the composition variation. Average rotational correlation times (τ_l) related to ranks 1 and 2 (that is, l=1 and 2) have been estimated from the simulated reorientational correlation functions and found to be nearly composition independent. The ratio between these time constants, τ_1/τ_2, varies between 1.46 and 1.55, indicating a strong deviation from the Debye law which predicts $\tau_1/\tau_2 = 3$ for rotation in normal liquids. The product of the translational diffusion coefficient (D_T) and τ_l remains nearly constant to the composition variation and, more interestingly, lies near but above the hydrodynamic stick limit, newly defined here for binary mixture of ellipsoids.

A brief concluding remark of this thesis is presented in chapter 11. In addition, a few more research problems are discussed in this chapter which may be studied in future.

References

1. Hynes, J. T. *Ann. Rev. Phys.*, **1985**, *36*, 573.
2. Hynes, J. T.; Klinman, J. P.; Limbach, H.-H.; Schowen, R. L. *Hydrogen Transfer Reactions*, Wiley-VCH: Weinheim, Germany, 2007.
3. Jones, R. A. Y. *Physical and Mechanistic Organic Chemistry*; Cambridge Univ. Press: London, 1979.
4. Reichardt, C. 'Solvent Effects in Organic Chemistry"; VerlagChemie: Weinheim, West Germany, 1979.
5. Yongho, K.; Cramer, C. J.; Truhlar, D. G. *J. Phys. Chem. A* **2009**, *113*, 9109.
6. Gao, J.; Ma, S.; Major, D. T.; Nam, K.; Pu, J.; Truhlar, D. *J. Chem. Rev.* **2006**, *106*, 3188.
7. Hynes, J. T. *Ann. Rev. Phys. Chern.* **1985**, *36*, 573.
8. Steinfeld, J. I.; Francisco, J. S.; Hase, W. L. *Chemical Kinetics and Dynamics*, 2nd ed.; Prentice Hall: Upper Saddle River, NJ, 1999.
9. Laidler, K. J. *Chemical Kinetics*, 3rd ed.; Harper Collins: New York, 1987.
10. Parker, A. *J. Chem. Rev.* **1969**, *69*, 1
11. Tapia, O.; Bertrán, J., Eds.; *Solvent Effects and Chemical Reactivity*; Kluwer: Dordrecht, 1996.
12. Swain, C. G.; Swain, M. S.; Powel, A. L.; Alunni, S. *J. Am. Chem. Soc.* **1983**, *105*, 502.
13. Parsons, A. F. *Keynotes in Organic Chemistry*, Blackwell Science Limited, Oxford, UK, 2003.
14. Richard, J. P.; Toteva, M. M.; Amyes, T. L. *Org. Lett.* **2001**, *3*, 2225.
15. Carey, F. A.; Sundberg, R. J. *Advanced Organic Chemistry*; *Part A & B*, 3rd ed.; Plenum: New York, 1990.
16. March, J. *Advanced Organic Chemistry*, 3rd ed.; John Wiley & Sons: New York, 1985.
17. Johnston, K. P.; Haynes, C. *AIChE Journal*, **1987**, *33*, 2017.
18. Kauppila, T. J.; Kuuranne, T.; Meurer, E. C.; Eberlin, M. N.; Kotiaho, T.; Kostiainen, R. *Anal. Chem.* **2002**, *74*, 5470.
19. Litwinienko, G.; Ingold, K. U. *ACC. Chem Res.* **2007**, *40*, 222
20. Klein, M. T.; Tory, L. A.; Wu, B. C.; Townsend, S. H. *J. Supercrit. Fluids* **1990**, *3*, 222.
21. Catak, S.; Monard, G.; Aviyente, V.; Ruiz-López, M. F. *J. Phys. Chem. A* **2006**, *110*, 8354.
22. Nelson, K. V.; Benjamin, I. *J. Chem. Phys.* **2009**, *130*, 194502.

23. Chandrasekhar, J.; Shariffskul, S. Jorgensen, W. L. *J. Phys. Chem. B*, **2002**, *106*, 8078.
24. Trautz, M. *Zeitschrift für anorganische und allgemeine Chemie*, **1916**, *96*, 1.
25. Fenimore, P.W. Frauenfelder, H.; McMahon, B. H.; Parak, F. G. *Proc. Natl. Acad. Sci. USA* **2002**, *99*, 16047.
26. Fenimore, P. W.; Frauenfelder, H.; McMahon, B. H.; Young, R. D. *Proc. Natl. Acad. Sci. USA* **2004**, *101*, 14408.
27. Lucent, D.; Vishal, V.; Pande, V. S. *Proc. Natl. Acad. Sci. USA* **2007**, *104*, 10430.
28. Frauenfelder, H.; Fenimore, P. W.; Chen, G.; McMahon, B. H. *Proc. Natl. Acad. Sci. USA* **2006**, *103*, 15469.
29. Vaiana, S. M.; Manno, M.; Emanuele, A.; Palma-Vittorelli, M. B.; Palma, M. U. *J. Biol. Phys.* **2001**, *27*, 133.
30. García, A. E.; Hillson, N.; Onuchic, J. N. *Prog. Theor. Phys. Supplement* **2000**, *138*, 282.
31. Xu, Z.; Lazim, R.; Sun, T.; Mei, Y.; Zhang, D. *J. Chem. Phys.* **2012**, *136*, 135102.
32. Bandyopadhyay, S.; Chakraborty, S.; Balasubramanian S.; Pal, S.; Bagchi, B. *J. Phys. Chem. B*, **2004**, *108*, 12608.
33. Nandi, N.; Bagchi, B. *J. Phys. Chem. B*, **1997**, *101*, 10954.
34. Bhattacharyya, K.; Bagchi, B. *J. Phys. Chem. A*, **2000**, *104*, 10603.
35. Jana, B.; Pal, S.; Maiti, P. K.; Lin, S. –T.; Hynes, J. T.; Bagchi, B. *J. Phys. Chem. B*, **2006**, *110*, 19611.
36. Mukherjee, A.; Lavery, R.; Bagchi, B.; Hynes, J. T. *J. Am. Chem. Soc.* **2008**, *130*, 9747.
37. Gazi, H. A. R; Biswas, R. *Journal of Physical Chemistry A*, **2011**, *115*, 2447.
38. Gazi, H. A. R.; Biswas, R. *Journal of Chemical Sciences*, **2011**, *123*, 265.
39. Pradhan, T.; Ghoshal, P.; Biswas, R. *Journal of Physical Chemistry A* **2008**, *112*, 915.
40. Pradhan, T.; Ghoshal, P.; Biswas, R.; *Journal of Chemical Sciences*, **2008**, *120*, 275.
41. Daschakraborty, S.; Biswas, R. Transport Properties of Binary Mixtures of Asymmetric Particles: A Simulation Study. In *Concepts and Methods in Modern Theoretical Chemistry (Vol-2)*; Ghosh, S. K., Chattaraj, P. K. Eds.; CRC Press; Taylor & Francis Group: London, UK, 2013; pp 21-35.
42. Walden, P. *Bull. Acad. Imper. Sci.* (St. Petersburg) 1914, page 1800.
43. Earle, M. J.; Esperança, J. M. S. S.; Gilea, M. A.; Lopes, J. N. C.; Rebelo, L. P. N.; Magee, J. W.; Seddon, K. R.; Widegren, J. A. *Nature*, **2006**, *439*, 831.
44. Huddleston, J. G.; Visser, A. E.; Reichert, W. M.; Willauer, H. D.; Broker, G. A.; Rogers, R. D. *Green Chem.* **2001**, *3*, 156.

45. Rogers, R. D.; Seddon, K. R. *Science*, **2003**, *302*, 792.
46. Chiappe, C.; Pieraccini, D. *J. Phys. Org. Chem.* **2005**, *18*, 275.
47. Leys, J.; Wübbenhorst, M,; Menon, C. P.; Rajesh, R.; Theon, J.; Glorieux, C.; Nockemann, P.; Thijs, B.; Binnemans, K.; Longuemart, S. *J. Chem. Phys.* **2008**, *128*, 064509.
48. Rogers, R. D.; Seddon, K. R. Eds. *Ionic Liquids: Industrial Applications for Green Chemistry*; ACS Symp. Ser. 818, American Chemical Society, Washington, DC, 2002.
49. Weyershausen, B.; Lehmann, K. *Green Chem.* **2005**, *7*, 15.
50. Earle, J. M.; Plechkova, N. V.; Seddon, K. R. *Pure Appl. Chem.* **2009**, *81,* 2045.
51. Heinze, T.; Schwikal, K.; Barthel, S. *Macromol. Biosci.* **2005**, *5*, 520.
52. Ranu, B. C.; Banerjee, S. *Org. Lett.* **2005**, *7*, 3049.
53. Rosa, J. N.; Afonso, C. A. M.; Santos, A. G. *Tetrahedron*, **2001**, *57*, 4189.
54. Liu, C. F.; Sun, R. C.; Zhang, A. P.; Ren, J. L.; Wang, X. A.; Qin, M. H.; Chao, Z. N.; Luo, W. Carbohydr. Res. **2007**, *342*, 919.
55. Sheldon, R. *Chem .Commun.* **2001**, *2399*.
56. Dash, J.; Satapathy, R.; Upadhyay, S. K. *Tetrahedron Lett*. **2004**, *45*, 3055.
57. Weingartner, H. *Angew. Chem., Int. Ed.* **2008**, *47*, 654.
58. Kobrak, M. N. *Advances in Chemical Physics;* John Wiley & Sons, Inc.: New York, **2008**, *139*, 83.
59. Chiappe, C.; Pieraccini, D. *J. Phys. Org. Chem.* **2005**, *18*, 275.
60. Hanke, C. G.; Lynden-Bell, R. M. *J. Phys. Chem. B* **2003**, *107*, 10873.
61. Hanke, C. G.; Atamas, N. A.; Lynden-Bell, R. M. *Green Chem.* **2002**, *4*, 107.
62. Lynden-Bell, R. M.; Atamas, N. A.; Vasilyuk, A.; Hanke, C. G.Mol. Phys. **2002**, *100*, 3225.
63. Wang, Y.; Voth, G. A. *J. Am. Chem. Soc.* **2005**, *127*, 12192.
64. Turton, D. A.; Hunger, J.; Stoppa, A.; Hefter, G.; Thoman, A.; Walther, M.; Buchner, R.; Wynne, K. *J. Am. Chem. Soc.* **2009**, *131*, 11140.
65. Huang, M. M.; Bulut, S.; Crossing, I.; Weingertner, H. *J. Chem. Phys*. **2010**, *133*, 101101.
66. Muramatsu, M.; Nagasawa, Y.; Miyasaka, H. *J. Phys. Chem. A* **2011**, *115*, 3886.
67. Kashyap, H. K.; Biswas, R. *J. Phys. Chem. B* **2010**, *114*, 16811.
68. Kashyap, H. K.; Biswas, R. *J. Phys. Chem. B* **2010**, *114*, 254.
69. Daschakraborty, S.; Biswas, R. *J. Chem. Phys*. **2012**, *137*, 114501.

70. Daschakraborty, S.; Biswas, R. *Chem. Phys. Lett*. **2011**, *510*, 210.
71. Daschakraborty, S.; Biswas, R. *J. Phys. Chem. B* **2011**, *115*, 4011.
72. Daschakraborty, S.; Biswas, R. *Chem. Phys. Lett*. **2012,** *545*, 54.
73. Samanta, A. *J. Phys. Chem. B* **2006**, *110*, 13704.
74. Mandal, P. K.; Saha, S.; Karmakar, R.; Samanta, A. *Curr. Sci*. **2006**, *90*, 301.
75. Samanta, A. *J. Phys. Chem. Lett*. **2010**, *1*, 1557.
76. Samanta, A. *J. Phys. Chem. B* **2006**, *110*, 13704.
77. Arzhantsev, S.; Jin, H.; Baker, G. A.; Maroncelli, M. *J. Phys. Chem. B* **2007**, *111*, 4978.
78. Zhang, X. X.; Liang, M.; Ernsting, N. P.; Maroncelli, M. *J. Phys. Chem. B* **2013**, *117*, 4291.
79. Mandal, P. K.; Sarkar, M.; Samanta, A. *J. Phys. Chem. A* **2004**, *108*, 9048.
80. Sasmal, D. K.; Mandal, A. K.; Mondal, T.; Bhattacharyya, K. *J. Phys. Chem. B* **2011**, *115*, 7781.
81. Roy, D. and Maroncelli, M. *J. Phys. Chem. B* **2012**, *116***,** 5951.
82. Maroncelli, M.; Zhang, X. X.; Liang, M.; Roy, D. and Ernsting, N.P. *Faraday Discuss. Chem. Soc.* **2012**, *154*, 409.
83. Roy, D. and Maroncelli, M. *J. Phys. Chem. B* **2010**, *114*, 12629.
84. Roy, D.; Patel, N.; Conte, S. and Maroncelli, M. *J. Phys. Chem. B* **2010**, *114*, 8410.
85. Zhang, X. X.; Liang, M.; Ernsting, N. P. and Maroncelli, M. *J. Phys. Chem. Lett*. **2013**, *4*, 1205.
86. Shah, J. K.; Brennecke, J. F.; Maginn, E. J. *Green Chem*. **2001**, *4*, 112.
87. Lopes, J. N. C.; Deschamps, J.; Padua, A. A. H. *J. Phys. Chem. B* **2004**, *108*, 2038.
88. Liu, Z.; Huang, S.; Wang, W. *J. Phys. Chem. B* **2004**, *108*, 12978.
89. Triolo, A.; Russina, O.; Fazio, B.; Appetecchi, G. B.; Carewska, M.; Passerini, S. *J. Chem. Phys.* **2009**, *130*, 164521.
90. Santos, C. S.; Murthy, N. S.; Baker, G. A.; Castner, E. W. Jr. *J. Chem. Phys*. **2011**, *134*, 121101.
91. Kashyap, H. K.; Santos, C. S.; Annapureddy, H. V. R.; Murthy, N. S.; Margulis, C. J.; Castner, E. W. Jr. *Faraday Discuss* **2012**, *154*, 133.
92. Liu, Z.; Wu, X.; Wang, W. *Phys Chem Chem Phys* **2006**, *8*, 1096.
93. Bhargava, B. L.; Balasubramanian, S. *J. Chem. Phys*. **2007**, *127*, 114510.
94. Morrow, T. I.; Maginn, E. J. *J. Phys. Chem. B* **2002**, *106*, 12807.
95. Margulis, C. J.; Stern, H. A.; Berne, B. J. *J. Phys. Chem. B* **2002**, *106*, 12017.

96. Sarangi, S. S.; Zhao, W.; Muller-Plathe, F.; Balasubramanian, S. *Chem. Phys. Chem.* **2010**, *11*, 2001.
97. Pal, T.; Biswas, R. *Theo. Chem. Acc.* **2012**, *132*, 1348.
98. Schröder, C.; Haberler, M.; Steinhauser, O. *J. Chem Phys.* **2008**, *128*, 134501.
99. Schröder, C.; Rudas, T. and Steinhauser, O. *J. Chem. Phys*. **2006**, ***125***, 244506.
100. Schröder, C.; Wakai, C.; Weingärtner, H. and Steinhauser, O. *J. Chem. Phys.* **2007**, ***126***, 084511.
101. Schröder, C.; Rudas, T.; Neumayr, G.; Benkner, S. and Steinhauser, O. *J. Chem. Phys*. **2007**, ***127***, 234503.
102. Schröder, C.; Haberler, M. and Steinhauser, O. *J. Chem. Phys*. **2008**, *128*, 134501.
103. Schröder, C. and Steinhauser, O. *J. Chem. Phys.* **2008**, ***128***, 224503.
104. Weingärtner, H. *Angew. Chem. Int. Ed.* **2008**, *47*, 654.
105. Stoppa, A.; Hunger, J.; Buchner, R.; Hefter, G.; Thoman, A.; Helm, H. *J. Phys. Chem. B* **2008**, *112*, 4854.
106. Hunger, J.; Stoppa, A.; Schrodle, S.; Hefter, G.; Buchner, R. *ChemPhysChem* **2009**, *10*, 723.
107. Stoppa, A.; Hunger, J.; Buchner, R. *J. Chem. Eng. Data.* **2009**, *54*, 472.
108. Bester-Rogac, M.; Hunger, J.; Stoppa, A.; Buchner, R. *J. Chem. Eng. Data.* **2010**, *55*, 1799.
109. Bulut, S.; Klose, P.; Huang, M.-M.; Weingartner, H.; Dyson, P. J.; Laurenczy, G.; Friedrich, C.; Menz, J.; Kummerer, K.; Crossing, I. *Chem. Eur. J*. **2010**, *16*, 13139.
110. Huang, M.-M.; Bulut, S.; Crossing, I.; Weingartner, H. *J. Chem. Phys*. **2010**, *133*, 101101.
111. Zech, O.; Kellermeir, M.; Thomaier, S.; Maurer, E.; Klein, R.; Schreiner, C.; Kunz, W. *Chem. Eur. J.* **2009**, *15*, 1341.
112. Zech, O.; Hunger, J.; Sangoro, J. R.; Iacob, C.; Kremer, F.; Kunz, W.; Buchner, R. *Phys. Chem. Chem. Phys*. **2010**, *12*, 14341.
113. Jeong, D.; Shim, Y.; Choi, M. Y.; Kim, H. J. *J. Phys. Chem. B* **2007**, *111*, 4920.
114. Shim, Y.; Choi, M. Y.; Kim, H. J. *J. Chem. Phys.* **2005,** *122*, 044511.
115. Shim, Y.; Duan, J.; Choi, M. Y.; Kim, H. J. *J. Chem. Phys*. **2003**, *119*, 6411.
116. Shim, Y.; Kim, H. J. *J. Phys. Chem. B* **2008**, *112*, 11028.
117. Shim Y.; Kim, H. J. *J. Phys. Chem. B* **2009**, *113*, 12964.
118. Shim Y.; Kim, H. J. *J. Phys. Chem. B* **2007**, *111*, 4510.

119. Shim, Y.; Jeong, D.; Choi, M. Y.; Kim, H. J. *J. Chem. Phys.* **2006**, *125*, 061102.

120. Streeter, I.; Lynden-Bell, R. M.; Compton, R. G. *J. Phys. Chem. C* **2008**, *112*, 14538.

121. Bhargava, B. L.; Balasubramanian, S. *J. Chem. Phys.* **2005**, *123*, 144505.

122. Kobrak, M. N.; Znamenskiy, V. *Chem. Phys. Lett.* **2004**, *395*, 127.

123. Kobrak, M. N. *J. Chem. Phys.* **2006**, *125*, 064502.

124. Kobrak, M. N. *J. Chem. Phys.* **2007**, *127*, 184507.

125. Li, W.; Zhang, Z.; Han, B.; Hu, S.; Xie, Y.; Yang, G. *J. Phys. Chem. B* **2007**, *111*, 6452.

126. Zhang, X. X.; Liang, M.; Ernsting, N. P. and Maroncelli, M. *J. Phys. Chem. B* **2013**, *117*, 4291.

127. Chakraborty, A.; Inagaki, T.; Banno, M.; Mochida, T.; Tominaga, K. *J. Phys. Chem. A* **2011**, *115*, 1313.

128. Balucani, U. and Zoppi, M. *Dynamics of the Liquid State* (Clarendon Press: Oxoford 1994).

129. Bagchi, B. and Bhattacharyya, S. Adv. Chem. Phys., **2007**, *116*, 67**.**

130. Biswas, R.; Bhattacharyya, S. and Bagchi, B. *J. Chem. Phys*. **1998**, *108*, 4963**.**

131. Chakrabarty, D.; Chakraborty, A.; Seth, D.; Hazra, P.; Sarkar, N. *Chem. Phys. Lett.* **2004**, *397*, 469.

132. Chakrabarty, D.; Chakraborty, A.; Seth, D.; Sarkar, N. *J. Phys. Chem. A* **2005**, *109*, 1764.

133. Sarkar, S.; Pramanik, R.; Ghatak, C.; Setua, P.; Sarkar, N. *J. Phys. Chem. B* **2010,** *114*, 2779.

134. Baker, S. N.; Baker, G. A.; Munson, C. A.; Chen, F.; Bukwoski, E. J.; Cartwright, A. N.; Bright, F. V. *Ind. Eng. Chem. Res.* **2003**, *42*, 6457.

135. Liang, M. *Solvation and Electron transfer in Ionic Liquids. Ph.D. Thesis*, The Pennsylvania State University, August 2012.

136. Zhang, X. –X.; Liang, M.; Hunger, J.; Buchner, R.; Maroncelli, M. *J. Phys. Chem. B*, DOI: 10.1021/jp4043528, in press

137. Hansen, J. P. and McDonald, I. R. *Theory of Simple Liquids*, Academic Press: London, 1986.

138. Lakowicz, J. R. *Principles of Fluorescence Spectroscopy* Kluwar Academic, Plenum: New York, 1999.

139. Gay, J. G. and Berne, B. J. *J. Chem. Phys*. **1981**, ***74***, 3316.

Chapter 2

Stokes Shift Dynamics in Alkylimidazolium Aluminate Ionic Liquids: Domination of Solute-IL Dipole-Dipole Interaction

2.1 Introduction

Recently, a new class of ionic liquids (ILs) based on alkylimidazolium cations and the weakly coordinating anion, tetra(hexafluoroisopropoxy)aluminate has been synthesized and their important physical properties measured[1]. These ILs are low viscous solvents compared to other ionic liquids[2] and, most interestingly, the change in viscosity upon variation of the alkyl group attached to imidazolium cation is very small ($\eta = 9\text{-}12$ cP at 343 K). Subsequently, the validity of hydrodynamic relations for these ILs have been verified by carrying out dielectric relaxation (DR) measurements covering a frequency range up to 20 GHz at a temperature (~343 K) well above their respective melting temperatures[3]. These measurements have indicated strongly stretched relaxation dynamics reminiscent of that observed in highly viscous heterogeneous media approaching glass transition[4]. Because of the chemical structures of the cations and the anion (shown in Scheme 2.1), extended hydrophobic and hydrophilic domains may form and lead to microscopic phase segregation[5,6] in these low viscous ILs. This might be the reason for the observed strongly stretched relaxation dynamics[3].

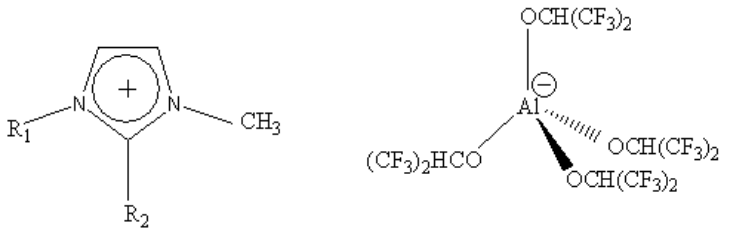

Aluminate ILs studied (R1 = allyl, n-butyl, ethyl, n-hexyl; R2 = H, methyl)

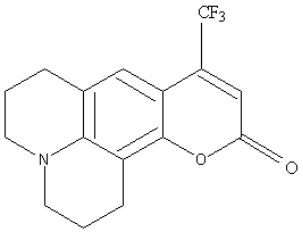

Coumarin 153 (C153)

Scheme 2.1: Chemical structures of aluminate ILs and the dipolar probe.

Apart from the stretched DR dynamics which directly affects solvation energy relaxation of a dissolved laser-excited solute, the static dielectric constant (ε_0) and ion diameter (σ_+ and σ_-) are two important factors which affects the magnitude of the calculated dynamic Stokes shift[7,8]. Furthermore, if the solvent dipole moment required as input for such calculations is obtained from either the mean spherical approximation (MSA)[9] or the Cavell's equation[10], ions with heavier molecular weight lead to a larger value of effective dipole moment (μ_{eff}) for an ionic liquid. Larger values of ε_0 or the slowest dispersion magnitude ($\Delta\varepsilon$) also lead to larger μ_{eff} and this, in turn, increases the relative contribution from the solute-IL dipole-dipole interaction contribution to the calculated total dynamic Stokes shift[7-8,11-12]. In contrast, larger ε_0 decreases the solute-IL dipole-ion interaction contribution via decreasing the ion-solute interaction. Larger size of ions can substantially reduce the collective mode (long wavelength) contributions via the excluded volume effect. These factors naturally motivates one to perform calculations for model ILs characterized by larger values of ε_0 (or $\Delta\varepsilon$), μ_{eff}, $\sigma_{+/-}$(ion diameter) and larger ion molecular weight in order to explore whether solute-IL dipole-dipole interaction indeed dominate the dynamic Stokes shift in IL where ion-ion interaction govern physicochemical properties of these liquids. This is an interesting scenario

as one expects the solute-IL dipole-ion interaction should determine much of the shift and the related dynamics. ILs based on alkylimidazolium cations and weakly coordinating anion, tetra(hexafluoroisopropoxy)aluminate, are such model ionic liquids which contain a large anion (much larger than studied so far[7,8]) and characterized by higher ε_0 values[3] than others[13,14] at comparable temperature.

In this work, we report calculated dynamic Stokes shifts and solvation response functions at 343 K for a dipolar solute probe, C153, dissolved in six different ionic liquids containing a fixed anion, tetra(hexafluoroisopropoxy)aluminate ($[Al(hfip)_4]^-$), and the following cations: 1-ethyl-3-methylimidazolium ($[C2\text{-}mim]^+$), 1-butyl-3-methylimidazolium ($[C4\text{-}mim]^+$), 1-hexyl-3-methylimidazolium ($[C6\text{-}mim]^+$), 1-allyl-3-methylimidazolium ($[allyl\text{-}mim]^+$), 1-ethyl-2,3-dimethylimidazolium ($[C2\text{-}mmim]^+$) and 1-butyl-2,3-dimethylimidazolium ($[C4\text{-}mmim]^+$). Because of variation in the alkyl chain length attached to the imidazolium cation, σ_+ ranges[3] between 6.58 Å and 7.76 Å. σ_-, on the other hand, is 12.5 Å[15], making the ratio between the ion-sizes ($P = \sigma_+/\sigma_-$) vary between ~0.53 and ~0.62. Note that molecular dynamics simulation studies have already suggested substantial effects of ion-size disparity on transport properties in model ILs[16]. In that study, however, cation was considered to be larger than the anion (size held constant) and P was varied between 1 and 5. For the present set of ILs, P obviously falls in the different regime, and the situation is somewhat reverse in the sense that the anion is larger roughly by a factor of 2 than the cations. Interestingly, a systematic study on the effects of P on Stokes shift dynamics in ILs has not yet been reported. This and the dominating contribution of the dipole-dipole interaction to the total dynamic Stokes shift constitute the main focus of the work described in this chapter.

2.2 Theoretical Formulation and Calculation Details

Since the molecular theory used here has already been developed and discussed in detail elsewhere[7-8,11-12,17-18], we only mention the necessary equations along with a brief outline for the calculations. The use of the classical density functional theory[19-21] provides the following

expression for the position ($\mathbf{r}$), orientation ($\mathbf{\Omega}$) and time (t) dependent total fluctuating solvation energy for a mobile dipolar solute with distribution function $\rho_s(\mathbf{r},\mathbf{\Omega};t)$

$$\Delta E_{total}(\mathbf{r},\mathbf{\Omega};t) = -k_B T \rho_s(\mathbf{r},\mathbf{\Omega};t)\left[\int d\mathbf{r}' d\mathbf{\Omega}' c_{sd}(\mathbf{r},\mathbf{\Omega};\mathbf{r}',\mathbf{\Omega}')\delta\rho_d(\mathbf{r}',\mathbf{\Omega}';t) + \sum_{\alpha=1}^{2}\int d\mathbf{r}' c_{s\alpha}(\mathbf{r},\mathbf{\Omega};\mathbf{r}')\delta n_\alpha(\mathbf{r}';t)\right]$$
$$= \Delta E_{sd}(\mathbf{r},\mathbf{\Omega};t) + \Delta E_{si}(\mathbf{r},\mathbf{\Omega};t) \qquad (2.1)$$

$c_{sd}(\mathbf{r},\mathbf{\Omega};\mathbf{r}',\mathbf{\Omega}')$ and $c_{s\alpha}(\mathbf{r},\mathbf{\Omega};\mathbf{r}')$ are respectively the position and orientation dependent solute dipole-solvent dipole (dipole-dipole) and solute dipole-ion (dipole-ion) direct correlation functions and α denotes the type of ions (cation and anion). The fluctuations in dipolar density ($\delta\rho_d$) and ion density (δn_α) from the respective bulk values are: $\delta\rho_d(\mathbf{r},\mathbf{\Omega}) = \rho_d(\mathbf{r},\mathbf{\Omega}) - \rho_d^0/4\pi$ and $\delta n_\alpha(\mathbf{r}) = n_\alpha(\mathbf{r}) - n_\alpha^0$. The solvation energy-energy correlation function averaged over space ($\mathbf{r}$) and orientation ($\mathbf{\Omega}$) is then written as

$$C_E(t) = C_{sd}(t) + C_{si}(t), \qquad (2.2)$$

where the dipole-dipole interaction contribution given as

$$C_{sd}(t) = <\Delta E_{sd}(t)\Delta E_{sd}(0)> = 2\rho_d^0\left(\frac{k_B T}{2\pi}\right)^2 [\int_0^\infty dk k^2 S_{solute}^{10}(k,t)\left|c_{sd}^{10}(k)\right|^2 S_{solvent}^{10}(k;t) + 2\int_0^\infty dk k^2 S_{solute}^{11}(k;t)\left|c_{sd}^{11}(k)\right|^2 S_{solvent}^{11}(k,t)], \qquad (2.3)$$

and the dipole-ion interaction term as

$$C_{si}(t) = <\Delta E_{si}(t)\Delta E_{si}(0)> = 2\left(\frac{k_B T}{2\pi}\right)^2 \sum_{\alpha,\beta}\sqrt{n_\alpha^0 n_\beta^0}\int_0^\infty dk k^2 S_{solute}^{10}(k;t) c_{s\alpha}^{10}(k) c_{s\beta}^{10}(-k) S_{\alpha\beta}^{ion}(k,t), \qquad (2.4)$$

Note in writing Eq. 2.2 the cross-correlation between fluctuating energies has been assumed to vanish due to separation of time-scales involved in fluctuations of dipolar solvent and ion densities. $c_{sd}^{lm}(k)$ represents the wave-number (k) dependent (l, m) component of the static correlation function between the solute and dipolar ion, and $S_{solvent}^{lm}(k,t)$ is the same component of the orientational dynamic structure factor of the dipolar species. While $c_{sd}^{lm}(k)$ has been obtained from the MSA, $S_{solvent}^{lm}(k,t)$ has been calculated, as before[7-8,11-12], by using the experimentally measured[3] frequency dependent dielectric function, $\varepsilon(z)$, summarized in

Table A1 (Appendix A). The solute self-dynamic structure factor, $S^{lm}_{solute}(k,t)$, has been approximated by its diffusive limit where the rotational and translational diffusion coefficients for a spherical solute with a volume of C153 have been obtained from the IL viscosity using the stick boundary condition.

The longitudinal component of the wave-number dependent direct correlation function between the dipolar solute and ions, $c^{10}_{s\alpha}(k)$, is taken as[7,8],

$$c^{10}_{s\alpha}(k) = -\sqrt{\frac{4\pi}{3}}\left(\frac{4\pi i\mu_1 q_\alpha}{k_B T\varepsilon_0 k}\right)\frac{\sin(kr_c)}{kr_c} = -\sqrt{\frac{4\pi}{3}}\left(\frac{4\pi i\mu_1 q_\alpha}{k_B T\varepsilon_0 k}\right)\frac{\sin[k\sigma_{IL}(1+R)/2]}{k\sigma_{IL}(1+R)/2}, \qquad (2.5)$$

where μ_1 is the dipole-moment of the dipolar solute, q_α the charge of α^{th} type ion, ε_0 the static dielectric constant and r_c the distance of the closest approach between the solute dipole and the ionic species. R denotes the solute-IL size-ratio, $\frac{\sigma_{solute}}{\sigma_{IL}}$, σ_{IL} being the effective diameter of an IL determined from the ionic sizes. $S^{ion}_{\alpha\beta}(k,t)$, the isotropic ion dynamic structure factor, has been obtained from known results[22,23] (Appendix B).

Subsequently, the normalized solvation energy-energy correlation function due to the dipole-dipole interaction is given by

$$S_{sd}(t) = \frac{C_{sd}(t)}{C_{sd}(t=0)}, \qquad (2.7)$$

and that due to dipole-ion interaction

$$S_{si}(t) = \frac{C_{si}(t)}{C_{si}(t=0)}. \qquad (2.8)$$

The individual response functions given by Eq. 2.7 and Eq. 2.8 constitute the solvation response function measured in experiments. The total solvation response function (S_{ss}) and the average solvation time ($<\tau_{ss}>$) are calculated as follows: $S_{ss}(t) = (1-f)S_{sd}(t) + fS_{si}(t)$ and $<\tau_{ss}> = \int_0^\infty dt\, S_{ss}(t)$. Based on experimental observations in electrolyte solutions[24] and

earlier success of the present theory for several ILs[7,8], we have set $f = 0.2$, although a small variation does not alter the qualitative feature of the predicted results. Furthermore, the dipole-dipole and ion-dipole interaction contributions to dynamic Stokes shift have been calculated[7-8,11-12] respectively from Eq. 2.3 and Eq. 2.4. Other necessary parameters are provided in Tables A2 and A3 (Appendix A).

2.3 Numerical Results and Discussion

The calculated dynamic Stokes shifts summarized in Table 2.1 indicates that the total shifts predicted for C153 in these ILs are much larger than those obtained with the same probe in more common imidazolium and phosphonium ILs[7,8].

Table 2.1: Calculated dynamic Stokes shifts for C153 in aluminate ILs at 343 K.[a]

Cation Anion = $Al(hfip)_4]^-$	Dipole-dipole contribution, $\Delta\upsilon_{sd}^t$ (cm^{-1})	Ion-dipole contribution, $\Delta\upsilon_{si}^t$ (cm^{-1})	Total[c] $\Delta\upsilon_{total}^t$ (cm^{-1})	% of total Stokes shift from Dipole-
$[allyl\text{-}mim]^+$	2894 (2162)[b]	495	3389 (2657)	85 (81)
$[C4\text{-}mim]^+$	2014 (1650)	577	2691 (2227)	77 (74)
$[C2\text{-}mim]^+$	2151 (1888)	686	2837 (2574)	76 (73)
$[C6\text{-}mim]^+$	1860 (1457)	452	2312 (1909)	80 (76)
$[C2\text{-}mmim]^+$	3231 (2143)	469	3700 (2612)	87 (82)
$[C4\text{-}mmim]^+$	2804 (1829)	433	3237 (2262)	87 (81)

a) Shift calculated using effective dipole moment (μ_{eff}^{Cavell}) obtained from Cavell's equation.

b) Values in parenthesis calculated by using the effective dipole moment (μ_{eff}^{MSA}) from the MSA. μ_{eff}^{Cavell} and μ_{eff}^{MSA} for these ILs are summarized in Table A3 (Appendix A).

c) $\Delta\upsilon_{total}^t = \Delta\upsilon_{sd}^t + \Delta\upsilon_{si}^t$

These shift values have been obtained by using the effective dipole moment (μ_{eff}^{Cavell})[10] determined via Cavell's equation where the magnitude (ΔS) of the slowest dielectric dispersion is used as input. Strikingly, the dipolar interaction between the solute and dipolar imidazolium cation is found to contribute ~75-85% of the total predicted shift ($\Delta\nu_{tot}^{t}$) for each of these $[Al(hfip)_4]^-$ containing ILs. The scenario remains the same even if the shift values are calculated (shown in parenthesis) by using the effective dipole moment (μ_{eff}^{MSA}) from ε_0 via the MSA[9]. This is in sharp contrast to the normal belief that Stokes shift in ILs should be dominated by the dipole-ion ($1/r^2$) interaction between the solute and the constituent ions of the ILs. In addition, this domination of dipole-dipole ($1/r^3$) interaction contribution is different from the calculations[7,8] for the same solute in imidazolium ILs with anions other than $[Al(hfip)_4]^-$ where ~40-50% dipolar contribution ($\Delta\nu_{sd}^{t}$) to the total shift was predicted. Eventhough a role for solute-cation dipolar interaction in determining the shift in ILs was hinted at in earlier reports[25,26], such an overwhelming contribution from the solute-IL dipolar interaction was never anticipated before. A closer inspection of Table 2.1 also indicates while the ion-dipole interaction contribution ($\Delta\nu_{si}^{t}$) increase as ε_0 decreases, $\Delta\nu_{sd}^{t}$ attains the largest value for that IL in which the combined effects of ε_0 and σ_+ (see Table A2) becomes the maximum. Effects of ion-size on $\Delta\nu_{sd}^{t}$ and $\Delta\nu_{si}^{t}$ are best illustrated as follows. $\Delta\nu_{sd}^{t}$ for $[allyl\text{-}mim]^+[Al(hfip)_4]^-$ is larger than that for $[C6\text{-}mim]^+$ $[Al(hfip)_4]^-$ because of smaller σ_+ for the former (6.84 Å) than the latter (7.76 Å) although ε_0 values are quite similar for these ILs (see Table S1). Again, $\Delta\nu_{si}^{t}$ for $[C2\text{-}mim]^+$ $[Al(hfip)_4]^-$ is nearly half of that calculated for $[bmim]^+[BF_4]^-$ because $[Al(hfip)_4]^-$ is ~2.5 times larger in size than that of $[BF_4]^-$ eventhough σ_+ for $[C2\text{-}mim]^+$ and $[bmim]^+$ are similar and ε_0 values of these ILs comparable at comparable temperatures[3,14] (but not the densities[8]). The difference in $\Delta\nu_{sd}^{t}$ values between these two ILs can be attributed largely to the difference in corresponding liquid densities[27].

The ion-size effect on dynamic Stokes shift is further explored in Fig. 2.1 where shift values measured and calculated for C153 in other ILs along with the calculated total shifts ($\Delta\nu_{total}^{t}$)

for these ILs are shown as a function of size-ratio, $P = \sigma_+ / \sigma_-$. Fig. 2.1 indicates a substantial correlation between $\Delta\nu^t_{total}$ and P, and the predicted monotonic decrease of $\Delta\nu^t_{total}$ with P arises from the reduced solute-ion interactions at increased P.

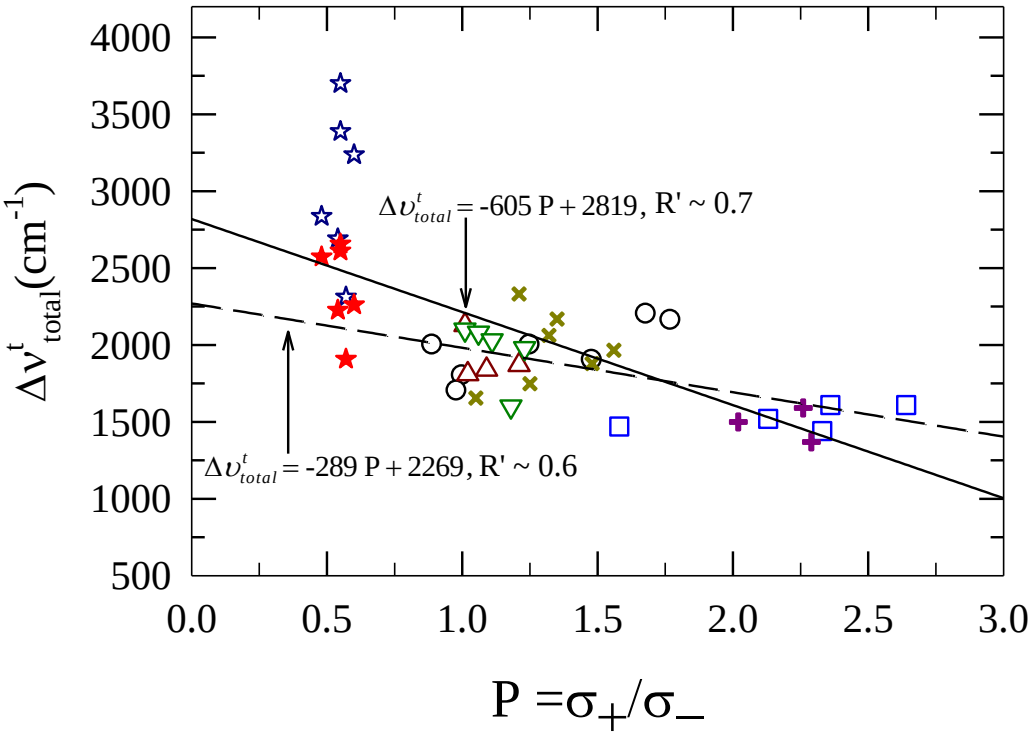

Fig. 2.1: Correlation between the total dynamic Stokes shift and the ratio between the ion diameters, $P = \sigma_+ / \sigma_-$ for C153 in various ILs. Black circles, dark red triangles, dark green inverted triangles, and blue squares denote measured shifts for imidazolium, pyrrolidinium, ammonium and phosphonium ILs respectively. Dark yellow crosses and dark pink pluses denote respectively the calculated shifts for imidazolium, and phosphonium ILs. Dark blue stars denote the predicted shifts for the aluminate ILs considered where effective dipole-moment values used are those obtained from Cavell's equation. Red filled stars are predicted shifts obtained using dipole moment from the MSA. Note while the dashed lines describes a correlation without including the predicted shifts for the aluminate ILs, the solid line is obtained after including both sets of the predicted shifts for these ILs. R' denotes correlation coefficient. References from which shift data taken are provided in Table A4 (Appendix A).

Note the degree of correlation does not significantly alter upon non-inclusion (broken lines, $R' \sim 0.6$) or inclusion (solid line, $R' \sim 0.7$) of the calculated shift values for these aluminate

ILs in the fit. The fact that the calculated shifts for these ILs follow the same linear correlation with P as observed for other ILs suggests that these predictions are qualitatively correct and should therefore be reexamined in experiments. Since $\mu_{eff}^{Cavell} > \mu_{eff}^{MSA}$ for these liquids (see Table S3), the predicted shifts are larger when μ_{eff}^{Cavell} is used in calculations. However, this was not the case for other ionic liquids as $\mu_{eff}^{Cavell} \approx \mu_{eff}^{MSA}$ for them (Table A3).

Calculated decays of the solvation response function, $S_{ss}(t)$, are shown in Fig. 2.2 for two representative ILs, $[C2\text{-mim}]^+[Al(hfip)_4]^-$ and $[C6\text{-mim}]^+[Al(hfip)_4]^-$ as several properties of them, for example, cation-size (σ_+), dielectric relaxation time constant (τ) and the associated stretching exponent (α) are widely different.

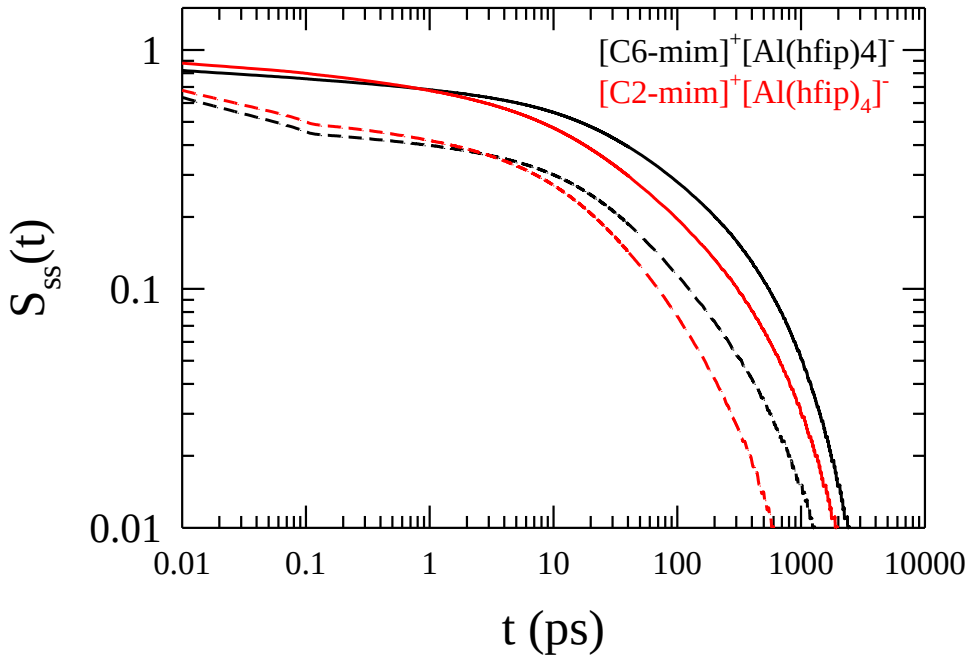

Fig. 2.2: Effects of librational band (~100 cm^{-1}) on calculated normalized solvation response functions for C153 in two representative aluminate ionic liquids, $[C6\text{-mim}]^+[Al(hfp)_4]^-$ (black lines) and $[C2\text{-mim}]^+[Al(hfp)_4]^-$ (red lines) at 343 K. While the solid lines represent calculations without considering the libration contribution, the dashed lines the calculations after incorporating the libration mode. Eq. 5 of Ref. 17 has been used to incorporate the libration contribution.

Fig. 2.2 clearly indicates that the decays are bimodal, which is the case for the other aluminate ILs also. As observed earlier[7-8,32], the bimodal decays have been found to consist of a fast exponential and a slow stretched exponential components. When a libration band centered around 100 cm^{-1} is assigned to carry out the remaining dispersion[28-31],

$[(\varepsilon_0 - S) - n^2]$ (n^2 being the square of the refractive index and fixed at 2) and incorporated in calculations, the bimodal decays become only faster (broken lines) keeping the qualitative features intact. This was also observed previously for solvation dynamics of C153 in liquid amides[33,34]. Parameters obtained from fitting the solvation response functions calculated for these aluminate ILs in the absence and presence of the libration band are summarized in Table 2.2. Table 2.2 indicates that the initial fast component of all the predicted decays is characterized by a time-constant (τ_1) ≤ 20 fs even after using the available DR data[3] measured with "limited" frequency coverage. Interestingly, the amplitude of the ultrafast component (a_1) increases up to ~50% of the total decay with time-constant as fast as ~5 fs when one includes the libration contribution in the solvation energy relaxation. Note such a fast component was not observed in experiments[32] or simulations[35-40] with ILs at room temperature but a simulation study of $[Im_{11}]^+[Cl]^-$ at elevated temperature (425 K) [41] reported a large fast component (~75%) with a time-constant of ~70 fs. The slow time-constant (τ_2), which also does not change appreciably upon inclusion of the libration contribution, appears very similar to the predictions for other imidazolium ILs at ~338 K.[8] Similarities in the amplitude of the slow component (a_2) and the solvation stretching exponent (β) coupled with the closeness in τ_2 then make the calculated average solvation times ($<\tau_{ss}>$) for these aluminate ILs comparable to those predicted for other imidazolium ILs with similar viscosities at elevated temperature.[8]

Table 2.2: Parameters obtained from fitting the calculated solvation response functions for C153 in aluminate ILs at 343 K with and without the libration contribution.[a]

ILs		a_1	τ_1 (fs)	a_2	τ_2 (ps)	β	$\langle\tau_{ss}\rangle$ (ps)
$[allyl\text{-}mim]^+$ $[Al(hfip)_4]^-$	Without libration	0.04	5	0.96	38.0	0.44	95.0
	With libration	0.39	5	0.61	33.7	0.49	20.6
$[C4\text{-}mim]^+$ $[Al(hfip)_4]^-$	Without libration	0.18	9	0.82	48.0	0.41	121.0
	With libration	0.52	6	0.48	30.5	0.51	14.7
$[C2\text{-}mim]^+$ $[Al(hfip)_4]^-$	Without libration	0.11	10	0.89	32.0	0.38	108.0
	With libration	0.48	6	0.52	23.8	0.49	12.4
$[C6\text{-}mim]^+$ $[Al(hfip)_4]^-$	Without libration	0.21	8	0.79	94.0	0.45	181.0
	With libration	0.54	6	0.46	50.8	0.52	23.4
$[C2\text{-}mmim]^+$ $[Al(hfip)_4]^-$	Without libration	0.17	20	0.83	28.0	0.38	89.0
	With libration	0.35	6	0.65	29.5	0.44	19.2
$[C4\text{-}mmim]^+$ $[Al(hfip)_4]^-$	Without libration	0.28	10	0.72	46.0	0.42	96.0
	With libration	0.41	6	0.59	44.7	0.46	26.4

a) DR data and other parameters necessary for the above calculations are summarized in Tables A1 & A2 (Appendix A).

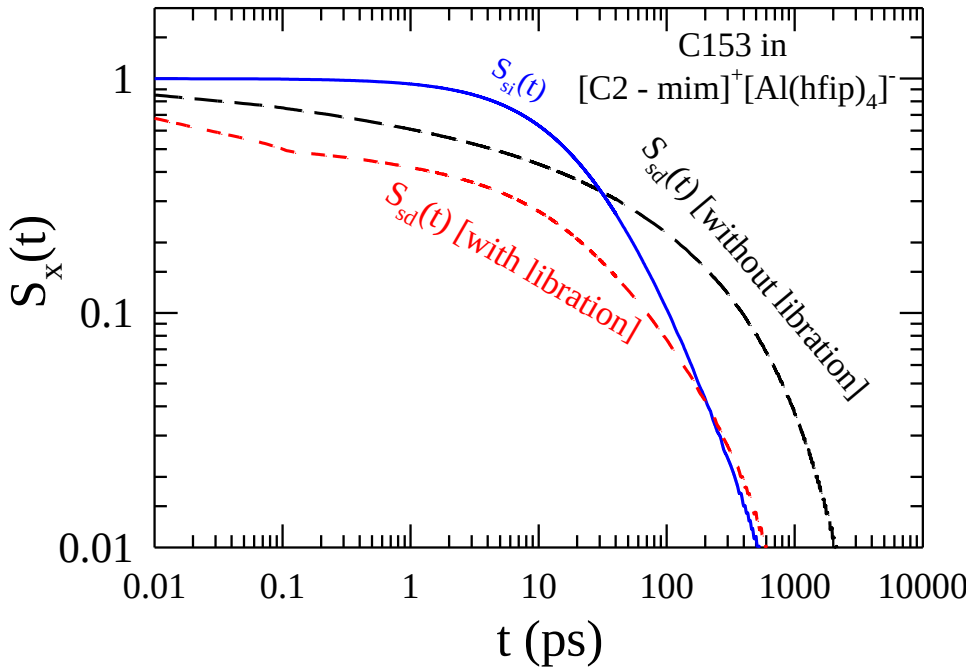

Fig. 2.3: Individual interaction components, $S_{sd}(t)$ and $S_{si}(t)$, of the solvation response functions and importance of high frequency coverage for DR measurements in aluminate ILs. The dipole-dipole interaction component $S_{sd}(t)$ is shown by the broken lines and the ion-dipole component by the solid line, while the red lines denote calculations with the libration mode and black lines without the libration mode.

The predictions that a_1 becomes as large as 50% and $< \tau_{ss} >$ reduces by a factor of ~4-9 upon inclusion of libration originate from assigning whole of the undetected[3] high frequency dispersion ($[(\varepsilon_0 - S) - n^2]$) to the libration band because this dispersion magnitude critically determines the amplitude of the ultrafast polar solvation response.[33] This strongly suggests the importance of the high frequency coverage and accurate description of the dielectric relaxation data for a better performance of the present theory, which is further demonstrated in Fig. 2.3 where decays of $S_{sd}(t)$ with and without libration contribution, and $S_{si}(t)$ are shown for [C2-mim]$^+$[Al(hfip)$_4$]$^-$. Fig. 2.3 suggests that the decay of $S_{sd}(t)$, which in the absence of libration is slower than that of $S_{si}(t)$ at long time ($t > 30$ ps), becomes faster after inclusion of libration contribution. The interesting point here is that because centre-of-mass diffusion of the particles govern the decay of $S_{si}(t)$ as opposed to the much faster

orientational readjustment of dipolar species for $S_{sd}(t)$, the decay of $S_{si}(t)$ is expected to be slower than that of $S_{sd}(t)$. Our best fits to $S_{si}(t)$ (bi-exponential) and $S_{sd}(t)$ (fast exponential followed by a slow stretched one) have produced comparable τ_2 (~50 ps and ~40 ps respectively) but a β value of 0.32 makes the decay of $S_{sd}(t)$ in the absence of libration slower than that of $S_{si}(t)$. Subsequent inclusion of libration considerably reduces τ_2 (17 ps) for $S_{sd}(t)$ but β remains unchanged and consequently $S_{sd}(t)$ decays at a rate faster than the previous case. The same is observed for other ILs considered here as well, stressing the need for a complete DR measurements with wider frequency coverage to better understand the dynamic solvation response in these newly synthesized ILs.

We next investigate to what extent the dynamic continuum model by Rips, Klafter and Jortner (RKJ)[42] is valid in predicting the dynamics in these ILs and explore the origin of the calculated sub-50 fs solvation response. The RKJ theory is one of the simplest theories that directly connects the polar solvation response to the measured DR data but neglects completely the solute-solvent and solvent-solvent static structural correlations. We therefore compare in Fig. 2.4 the decay of $S_{sd}(t)$, calculated without libration contribution, in the long wavelength ($k \to 0$) limit for $[C2\text{-mim}]^+[Al(hfip)_4]^-$ with the corresponding RKJ predictions. A good agreement between $S_{sd}(t, k \to 0)$ and RKJ predictions indicates a simple theory like the RKJ can qualitatively predict the dipolar part of the solvation response in these ILs as it did earlier for common polar solvents.[43] However, the RKJ theory predicts a slower decay than that of $S_{sd}(t, k \to 0)$ at later times because of the neglect of the static solvent structural correlations in the long wavelength limit.

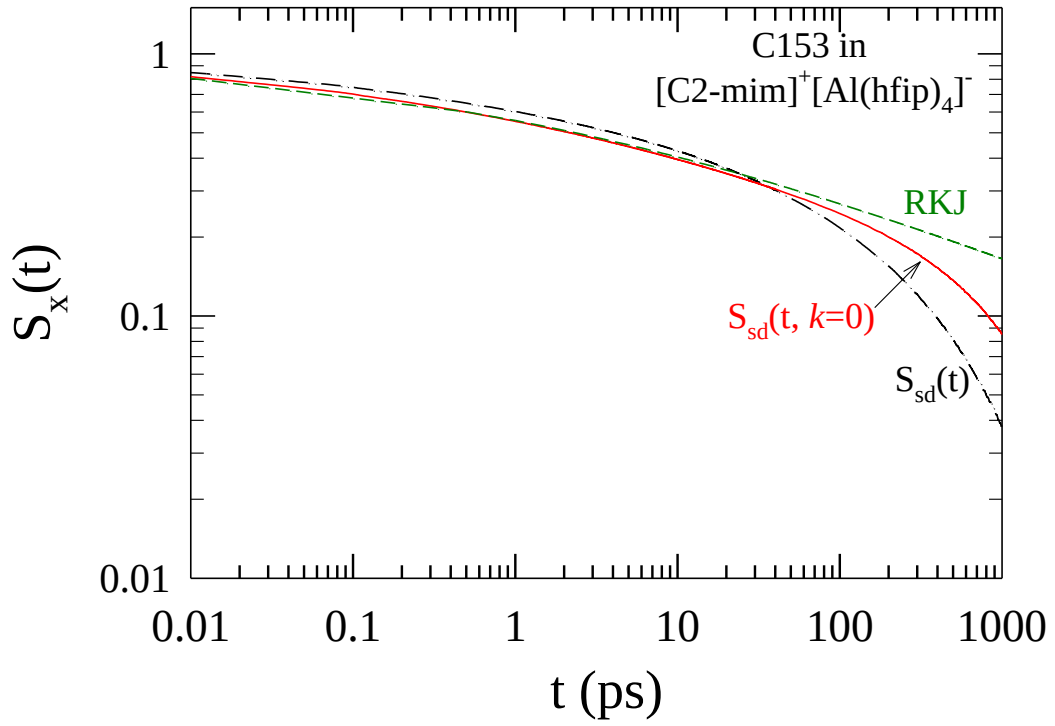

Fig. 2.4: Performance of a dynamic continuum model (RKJ theory here) and the domination of the orientational relaxation in producing the ultrafast component. Tagged symbols denote predictions from the RKJ model and the present theory.

In this time regime, $S_{sd}(t)$ decays faster because of participation of both the solute and solvent translational modes.[18-21] The dramatic break-down for the RKJ theory occurs because of its inability to account for the much slower diffusive relaxation of the ion-dipole interaction component, $S_{si}(t)$, in ILs.

The decay of $S_{sd}(t, k \to 0)$ calculated for [C2-mim]$^+$[Al(hfip)$_4$]$^-$ in the absence of libration contribution, upon fitting, produces a fast time-constant of ~10 fs (a_1 ~30%) and a slow time constant of ~60 ps with $\beta \approx 0.3$. The IL, [C2-mim]$^+$[Al(hfip)$_4$]$^-$, here serves as a representative example as qualitatively similar results have been obtained for other aluminate ILs as well. This observation clearly indicates that the sub-50 fs response in $S_{ss}(t)$ arises solely from the collective orientational response of the dipolar ions in these ILs. Note our earlier calculations for room temperature imidazolium ILs[17] has already shown that, like in

common polar solvents, the ultrafast response in dipolar ILs originates also from the collective orientational relaxation. This argument is further supported by recent simulations of ILs[44,45] and molten NaCl[46] which find no evidence for translational contributions in $\varepsilon(z)$ obtained at the microwave regime (300 MHz – 300 GHz). With such a current understanding of the microwave dielectric relaxation data, the dominating role for the collective orientational polarization relaxation in producing the ultrafast solvation response in dipolar ILs becomes even more evident.

We now present in the upper panel of Fig. 2.5 the results of our model calculations on solute-IL size-ratio dependence of interaction contributions to the total shift for C153 in [C4-mim]$^+$[Al(hfip)$_4$]$^-$. Calculated total shift decreases, as evidenced in the upper panel, with the increase in size ratio ($R = \sigma_{solute}/\sigma_{IL}$), the total decrease for changing R from 1 to 10 being only ~25%. This is because of the dominance of the dipole-dipole interaction contribution which reduces only by ~3% in this range of size-ratio variation. In contrast, the ion-solute ion-dipole interaction contribution reduces by ~80%. Such a strong size-effect on ion-dipole contribution arises from the inverse dependence of $c_{s\alpha}^{10}(k)$ on $(1+R)$ (see Eq. 2.5). The dependence of dipolar contribution is weaker because size-effect in dipole-dipole direct correlation function enters only via the solute number density[9] which is present at infinite dilution. In the limit of extremely large solute (R=50) where solute packing fraction becomes substantial, however, the dipolar contribution becomes nearly one-fifth of that at R=1, and the ion-dipole contribution vanishingly small. Note data in Table A5 (Appendix A) reveals measured shifts in normal solvents of comparable polarity (ε_0) are less than those in ILs. Moreover, the measured shifts in non-dipolar ILs are smaller than those in dipolar counter-parts. These observations probably constitute an indirect experimental evidence in favor of the relative importance of solute-IL dipole-ion and dipole-dipole interaction contributions to the total shift.

The relative importance of translational and rotational modes in the decay of dipolar interaction contribution is shown in the last two panels of Fig. 2.5 where average relaxation time obtained for different values of $p\,(= D_T/D_R\sigma_{IL}^2)$ from the decay of the normalized dipolar dynamic structure factor, $S_{solvent}^{10}(k,t)$, are shown as a function of wave-vector. As observed for dipolar liquids[49], participation of the translational modes shortens the

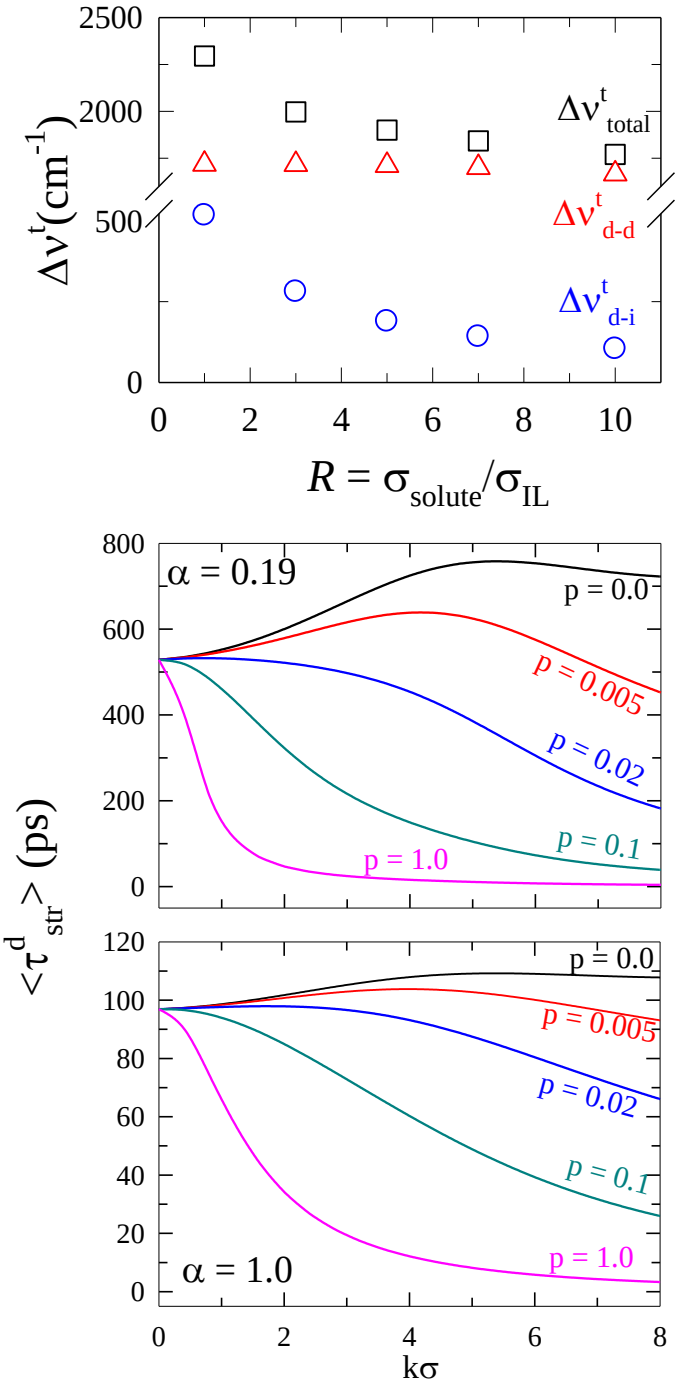

Fig. 2.5: Solute size dependence of dynamic Stokes shift (upper panel) and relative importance of solvent rotational and translational modes for solvation energy relaxation in ILs (middle and lower panels). Various interaction contributions to the calculated total shift (squares) are labeled as follows: triangles denote the solute-IL size ratio (R) dependence of dipole-dipole interaction contribution, and circles the ion-dipole contribution. Note the size of an IL molecule has been kept fixed. The calculations are for C153 in $[C4\text{-mim}]^+$ $[Al(hfip)_4]^-$ at 343 K. The role of solvent translation is quantified for both heterogeneous (middle panel) and homogeneous liquids (lower panel). Note the results shown in the lower panel have been obtained with the same dielectric relaxation data as used for results in the middle panel but with $\alpha = 1.0$.

relaxation time ($< \tau_{str}^{d} >$) considerably, the wavevector dependence of $< \tau_{str}^{d} >$ being more pronounced for inhomogeneous liquid (middle panel, $\alpha = 0.19$) than that for homogeneous one (lower panel, $\alpha = 1.0$) (see also Fig. C1, Appendix C). Interestingly however, the rotation dominates the over-all relaxation because too much efficiency of translation at large wavevectors makes the latter insignificant.

2.4 Conclusion

The present work shows that there could be dipolar ILs such as the present ones where the solvation energy for an excited dipolar solute molecule might be dominated by the solute-IL dipolar interaction rather than the anticipated solute-IL dipole-ion interaction. A weak solute-size dependence is predicted to arise from the domination of the dipole-dipole interaction contribution to the total shift. More importantly, the ultrafast response in dipolar ILs has been found to originate from the collective orientational response of the ILs. A number of new results have been predicted for these fascinating ILs which should be experimentally verified. Once done, the proposed measurements are likely to provide resolutions to the ongoing debate over the interpretation of Stokes shift dynamics[47,48] in these completely new class of solvents.

References

1. Bulut, S.; Klose, P.; Huang, M.-M.; Weingartner, H.; Dyson, P. J.; Laurenczy, G.; Friedrich, C.; Menz, J.; Kummerer, K.; Crossing, I. *Chem. Eur. J.* **2010**, *16*, 13139.
2. Jin, H.; O'Hare, B.; Dong, J.; Arzhantsev, S.; Baker, G. A.; Wishart, J. F.; Benesi, A.; Maroncelli, M. *J. Phys. Chem. B* **2008**, *112*, 81.
3. Huang, M.-M.; Bulut, S.; Crossing, I.; Weingartner, H. *J. Chem. Phys.* **2010**, *133*, 101101.
4. Ediger, M. *Annu. Rev. Phys. Chem.* **2009**, *51*, 99.
5. Triolo, A.; Russina, O.; Bleif, H.-J.; Di Cola, E. *J. Phys. Chem. B* **2007**, *111*, 4641.
6. Canongia Lopes, J. N. A.; Padua, A. A. H. *J. Phys. Chem. B* **2006**, *110*, 3330.
7. Kashyap, H. K.; Biswas, R. *J. Phys. Chem. B* **2010**, *114*, 254.
8. Kashyap, H. K.; Biswas, R. *J. Phys. Chem. B* **2010**, *114*, 16811.
9. Gray, C. G.; Gubbins, K. E. *Theory of Molecular Fluids*, Clarendon: Oxford, 1984, Vol. I.
10. Cavell, E. A. S.; Knight, P. C.; Sheikh, M. A. *J. Chem. Soc. Faraday Trans.* **1971**, *67*, 2225.
11. Guchhait, B.; Gazi, H. A. R.; Kashyap, H. K.; Biswas, R. *J. Phys. Chem. B* **2010**, *114*, 5066.
12. Gazi, H. A. R.; Guchhait, B.; Daschakraborty, S.; Biswas, R. *Chem. Phys. Lett.* **2011**, *501*, 358.
13. Stoppa, A.; Hunger, J.; Buchner, R.; Hefter, G.; Thoman, A.; Helm, H. *J. Phys. Chem. B* **2008**, *112*, 4854.
14. Hunger, J.; Stoppa, A.; Schrodle, S.; Hefter, G.; Buchner, R. *Chem. Phys. Chem.* **2009**, *10*, 723.
15. Crossing, I.; Raabe, I.; *Angew. Chem. Int. Ed.* **2004**, *43*, 2066.
16. Spohr, H. V.; Patey, G. N. *J. Chem. Phys.* **2008**, *129*, 064517.
17. Kashyap, H. K.; Biswas, R. *J. Phys. Chem. B* **2008**, *112*, 12431.
18. Kashyap, H. K.; Biswas, R. *Ind. J. Chem.* **2010**, *49A*, 685.
19. Bagchi, B. *Annu. Rev. Phys. Chem.* **1989**, *40*, 115.
20. Bagchi, B.; Biswas, R. *Adv. Chem. Phys.* **1990**, *109*, 207.
21. Bagchi, B.; Chandra, A. *Adv. Chem. Phys.* **1991**, *80*, 1.
22. Attard, P. *Phys. Rev. E.* **1993**, *48*, 3604.

23. Chandra, A.; Bagchi, B. *J. Chem. Phys.* **1990**, *110*, 10024.
24. Chapman, C. F.; Maroncelli, M. *J. Phys. Chem.* **1991**, *95*, 9095.
25. Castner, Jr., E. W.; Wishart, J. F.; Shirota, H. *Acc. Chem. Res.* B **2007**, *40*, 1217.
26. Arzhantsev, S.; Ito, N.; Heitz, M.; Maroncelli, M. *Chem. Phys. Lett.* **2003**, *381*, 278.
27. Daschakraborty, S.; Biswas, R. *J. Phys. Chem. B* **2011**, *115*, 4011.
28. Turton, D. A.; Hunger, J.; Stoppa, A.; Hefter, G.; Thoman, A.; Walther, M.; Buchner, R.; Wynne, K. *J. Am. Chem. Soc.* **2009**, *131*, 11140.
29. Giraud, G.; Gordon, C. M.; Dunkin, I. R.; Wynne, K. *J. Chem. Phys.* **2003**, *119*, 464.
30. Shirota, H.; Castner, Jr., E. W. *J. Phys. Chem. B* **2005**, *109*, 21576.
31. Hyun, B.-R.; Dzyuba, S. V.; Bartsch, R. A.; Quitevis, E. L. *J. Phys. Chem. A* **2002**, *106*, 7579.
32. Arzhantsev, S.; Jin, H.; Baker, G. A.; Maroncelli, M. *J. Phys. Chem. B* **2007**, *111*, 4978.
33. Biswas, R.; Bagchi, B. *J. Phys. Chem.* **1996**, *100*, 1238.
34. Kashyap, H. K.; Biswas, R. *J. Chem. Phys.* **2006**, *125*, 174506.
35. Shim, Y.; Duan, J.; Choi, M. Y.; Kim, H. J. *J. Chem. Phys.* **2003**, *119*, 6411.
36. Shim, Y.; Duan, J.; Choi, M. Y.; Kim, H. J. *J. Chem. Phys.* **2005**, *122*, 044511.
37. Kobrak, M. N.; Znamenskiy, V. *Chem. Phys. Lett.* **2004**, *395*, 127.
38. Kobrak, M. N. *J. Chem. Phys.* **2006**, *123*, 064502.
39. Margulis, C. J. *Mol. Phys.* **2004**, *102*, 829.
40. Hu, Z.; Margulis, C. J. *J. Phys. Chem. B* **2006**, *110*, 11025.
41. Bhargava, B. L.; Balasubramanian, S. *J. Chem. Phys.* **2005**, *123*, 144505.
42. Rips, I.; Klafter, J.; Jortner, J. *J. Chem. Phys.* **1988**, *88*, 3246.
43. Horng, M. L.; Gardecki, J. A.; Papazyan, A.; Maroncelli, M. *J. Phys. Chem.* **1995**, *99*, 17311.
44. Schroder, C.; Wakai, C.; Weingartner, H.; Steinhauser, O. *J. Chem. Phys.* **2007**, *126*, 084511.
45. Schroder, C.; Haberler, M.; Steinhauser, O. *J. Chem. Phys.* **2009**, *131*, 114504.
46. Song, X. *J. Chem. Phys.* **2009**, *131*,044503.
47. Samanta, A. *J. Phys. Chem. Lett.* **2010**, *1*, 1557.
48. Samanta, A. *J. Phys. Chem. B* **2006**, *110*, 13704.
49. Chandra, A.; Bagchi, B. *J. Chem. Phys.* **1989**, *91*, 1829.

Chapter 3

Stokes shift dynamics of [Na][TOTO] - a new class of ionic liquids: A comparative study with more common imidazolium analogs

3.1 Introduction

A new class of ionic liquids (ILs) based on singly charged alkali metal cation and 2,5,8,11-tetraoxatridecan-13-oate ([TOTO]) anion have been synthesized and characterized by various physicochemical measurements.[1] Among them the IL with Na^+, that is, [Na][TOTO], is particularly interesting because of its strongly reduced cytotoxicity compared to many imidazolium ILs. These properties, coupled with wide liquidous range, enhanced electrochemical stability and large viscosity variation ($2.86\text{x}10^9 \geq \eta/(\text{P}) \geq 14$ in the temperature window $254 \leq \text{T}/(\text{K}) \leq 344$) make [Na][TOTO] an interesting medium for possible biochemical and electrochemical applications.[1] Temperature dependent dielectric relaxation (DR) measurements in the frequency range, $10^{-1} \leq \nu/Hz \leq 10^7$, have also been performed with this IL[2] in order to ascertain the liquid structure with a particular emphasis on the interaction between the alkali metal ion and the oxygen atoms belonging to the ether and carboxylate moieties of the anion, [TOTO]. The measured static dielectric constant ($\varepsilon_0 \sim 20$) has been found to be larger than that in common imidazolium ILs ($\varepsilon_0 \sim 12$)[3,4] but smaller than protic ILs.[5,6] These measurements have also indicated stretched relaxation dynamics for [Na][TOTO] which is common in highly viscous heterogeneous media approaching glass transition.[7] The chemical structure of the large anion (shown in Scheme 3.1) may induce microscopic phase segregation into hydrophobic and hydrophilic domains. This can lead to spatial heterogeneity in the solution structure that can give rise to the observed stretched dynamics.

Eventhough the above DR measurements suggested a single relaxation time constant with a strong stretching exponent, presence of a much faster relaxation mode was indicated for [Na][TOTO] at higher temperature.[2] A faster second relaxation component in the dielectric response is naturally expected for these liquids as the existing DR measurements could not probe

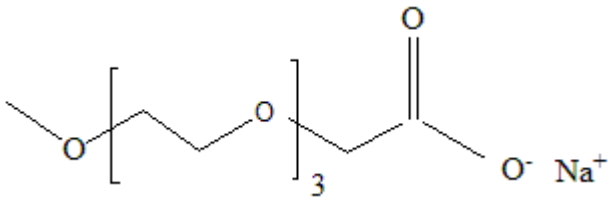

Sodium 2,5,8,11-tetraoxatridecan-13-oate

Scheme 3.1: Chemical structures of Sodium 2,5,8,11-tetraoxatridecan-13-oate ([Na][TOTO])

a significant portion in the higher frequency regime because large viscosity prevented the available techniques to extend the measurements into the higher frequency domain. Subsequently, replacement of the alkali cations by tetraalkylammonium ions were carried out to gain further insight into the structure of ILs containing [TOTO] anion which revealed significant reduction of liquid viscosity and enhanced polarity.[8] An indirect way of gaining insight into the liquid structure is to follow the Stokes shift dynamics of a given liquid where emergence of timescales may be interpreted in terms of structural complexity of the participating liquid particles. However, a comparison between theory and experiments is crucial for such model answers, particularly for ionic liquids where complications arise not only from the longer-ranged electrostatic interactions but from the structural heterogeneity also.[9,10] In addition, cation and anion sizes are important factors for determining the size of the dynamic shift and the timescale of the solvation energy relaxation.[11-14]

Apart from the structural complexity of this oligoethercarboxylate anion based IL and the consequent implications on its physicochemical properties, there exist several factors that

further motivate the study of solvation dynamics in this IL. For example, [Na][TOTO] represents an IL with a monatomic cation (Na^+) that possesses no permanent dipole moment and thus differs qualitatively from the more common imidazolium cation based ionic liquids where the cation is both polyatomic and strongly dipolar.[15,16] Therefore, the cation in [Na][TOTO], owing to its lighter mass, is expected to couple to the early part of the total solvation energy relaxation via its inertial motion[17,18], while the polar response should originate from the orientational readjustment of the oligoethercarboxylate ([TOTO]) anion. In contrast, for imidazolium ILs with relatively lighter non-dipolar anions, particularly with monatomic anions such as Cl^- or Br^-, it is the anionic inertial motion that should couple to the early part of the dynamics, and rearrangement of the bulky dipolar cation to the polar solvation response. This provides a potential source for a possible difference in the qualitative nature of the solvation energy relaxation in these two kinds of ILs. In addition, the polarity of [Na][TOTO], in both $E_T(30)$ and π^* scales, is significantly lower than that of the imidazolium ILs, although ε_0 is larger for [Na][TOTO].[8] This reflects a substantial difference in the solute-medium interaction between these ILs. In such a scenario, it is natural to ask how much of the above disparities translate, after accounting for the viscosity effects, to the dynamic response level and how a simple chemical reaction gets differently affected in them.[19]

In this chapter, we report the predicted dynamic Stokes shift and solvation response functions in [Na][TOTO] using a probe similar to C153 in the temperature range, $254 \leq T/(K) \leq 344$. The diameter of the anion (σ_-), estimated from the space filling model, is ~8.3 Å which is much larger than the cation, $\sigma_+ \approx 2.3$ Å[20]. Since the anion of the present IL possesses dipole moment whereas the cation is a nondipolar species, the solute-solvent dipole - dipole interaction arises solely from the solute - anion interaction. Calculated average solvation times indicate a near-perfect validity of the Stokes-Einstein relationship in this highly viscous IL and suggest Arrhenius type of temperature dependence. Calculated activation energy correlates well with those predicted earlier for imidazolium ILs.[12] Relatively larger value of ε_0 is found to reduce the dipole-ion (solute-ion) interaction contribution to the total dynamic Stokes shift.

3.2 Theoretical Formulation and Calculation Details

The theory has been developed and discussed in detail earlier[11-14,21-24] and thus we provide here the main equations. The position ($\mathbf{r}$), orientation ($\mathbf{\Omega}$) and time (t) dependent total fluctuating solvation energy for a mobile dipolar solute with solute distribution function $\rho_s(\mathbf{r},\mathbf{\Omega};t)$ is written in Eq. 2.1 of Chapter 2, where $c_{sd}(\mathbf{r},\mathbf{\Omega};\mathbf{r}',\mathbf{\Omega}')$ and $c_{s\alpha}(\mathbf{r},\mathbf{\Omega};\mathbf{r}')$ being respectively the position and orientation dependent solute dipole-solvent dipole (dipole-dipole) and solute dipole-ion (dipole-ion) direct correlation functions and α denoting the type of ions (cation and anion). $\delta\rho_d$ and δn_α are respectively the fluctuations in dipolar and ion densities from bulk values: $\delta\rho_d(\mathbf{r},\mathbf{\Omega}) = \rho_d(\mathbf{r},\mathbf{\Omega}) - \rho_d^0/4\pi$ and $\delta n_\alpha(\mathbf{r}) = n_\alpha(\mathbf{r}) - n_\alpha^0$. The solvation energy-energy time correlation function averaged over space ($\mathbf{r}$) and orientation ($\mathbf{\Omega}$) is given by

$$C_E(t) = C_{sd}(t) + C_{si}(t), \qquad (3.1)$$

where the solute-IL dipole-dipole and dipole-ion interaction contribution have been expressed in Eq. 2.3 and 2.4 in Chapter 2 respectively.

Note, Eq. 3.1 can be written only when the cross-correlations between fluctuating energies are assumed to be zero due to separation of time-scales of the fluctuating dipolar and ion densities. $c_{sd}^{lm}(k)$ represents the wave-number (k) dependent (l, m) component of the static correlation function between the solute and dipolar ion, and $S_{solvent}^{lm}(k,t)$ is the same component of the orientational dynamic structure factor of the dipolar species. $c_{sd}^{lm}(k)$ has been obtained from the dipolar mean spherical approximation (MSA) theory[25]. As before[11-14,21-24], $S_{solvent}^{lm}(k,t)$ is calculated by using the experimental[2] frequency dependent dielectric function, $\varepsilon(z)$, summarized in Table A6 (Appendix A). $S_{solute}^{lm}(k,t)$, solute self-dynamic structure factor, has been approximated by its diffusive limit where the rotational and translational diffusion coefficients for a spherical solute with a volume of C153 have been obtained from the IL viscosity using the stick boundary condition.

$c_{s\alpha}^{10}(k)$ and $c_{s\beta}^{10}(k)$ are the longitudinal component of the direct correlation function between the dipolar solute and ions α and β respectively.[11-14] The dipole moment used (14 D) to

calculate these quantities is that of excited C153.[11] $S_{\alpha\beta}^{ion}(k,t)$, the isotropic ion dynamic structure factor, has been obtained from known results.[11-14] The normalized solvation energy-energy correlation function due to the solute-IL dipolar interaction is then given by,

$$S_{sd}(t) = \frac{C_{sd}(t)}{C_{sd}(t=0)}, \tag{3.2}$$

and that due to solute-IL dipole-ion interaction

$$S_{si}(t) = \frac{C_{si}(t)}{C_{si}(t=0)}. \tag{3.3}$$

The total solvation response function (S_{ss}) and the average solvation time ($<\tau_{ss}>$) are then calculated as follows: $S_{ss}(t) = (1-f)S_{sd}(t) + fS_{si}(t)$ and $<\tau_{ss}> = \int_0^\infty dt\, S_{ss}(t)$. Based on experimental observations in electrolyte solutions[26] and earlier success of the present theory[11-13], we have set $f = 0.1$, although a small variation in f is not expected to induce any qualitative change in the predicted results. In addition, Eq. 2.3 and Eq. 2.4 (Chapter 2) provide the dipole-dipole and ion-dipole interaction contributions to dynamic Stokes shift. Other necessary input parameters like measured density [Na][TOTO] (ρ_{IL}), its effective dipole moment (μ_{eff}) and experimental viscosity (η) etc. are provided in Table A7 (Appendix A).

3.3 Numerical Results and Discussion

Table 3.1 summarizes the calculated dynamic Stokes shifts for a C153-like probe in [Na][TOTO] in the temperature range, $254 \le T/(K) \le 344$. The dipole-dipole and dipole-ion interaction contributions ($\Delta\nu_{sd}^t$ and $\Delta\nu_{si}^t$ respectively) are also tabulated. The predicted total shift ($\Delta\nu_{total}^t = \Delta\nu_{sd}^t + \Delta\nu_{si}^t$) decreases with temperature and ranges between 1257 and 1337 cm^{-1}. This range (1257-1337 cm^{-1}) is considerably smaller than the predicted shifts (~1600-2500 cm^{-1}) for C153 in imidazolium ILs[11] eventhough ε_0 for [Na][TOTO] is much larger than that of the latter ILs. As the solute-ion direct correlation function varies inversely as ε_0

($c_{s\alpha}^{10}(k) \propto 1/\varepsilon_0$)[11], larger ε_0 reduces the solute-ion interaction contribution to the total shift via drastically decreasing the magnitude of $\left|c_{s\alpha}^{10}(k)\right|^2$. This is shown in Fig. C2 (Appendix C) for a model IL at 304 K where all other parameters remained the same as those for [Na][TOTO] but with ε_0 =12. Consequently, $\Delta\nu_{si}^t$ for this model IL nearly doubles relative to that for [Na][TOTO], suggesting a strong dependence of $\Delta\nu_{si}^t$ on ε_0. The small variation (~6%) in $\Delta\nu_{total}^t$ for a temperature change of ~100 K is a direct consequence of a small (~10%) change in

Table 3.1: Calculated dynamic Stokes shifts for C153 in [Na][TOTO] at various temperatures

T(K)	$\Delta\upsilon_{sd}^t$ (cm^{-1})	$\Delta\upsilon_{si}^t$ (cm^{-1})	$\Delta\upsilon_{total}^t$ (cm^{-1})
254	587	750	1337
264	612	683	1295
274	618	666	1284
284	619	662	1281
294	618	658	1276
304	615	659	1274
314	613	657	1270
324	614	650	1264
334	616	643	1259
344	613	644	1257

experimental ε_0 for the same temperature range and the opposite temperature dependencies of $\Delta\nu_{sd}^t$ and $\Delta\nu_{si}^t$. Note both these contributions are nearly equal for total shift in

[Na][TOTO] which is in over-all agreement with earlier findings for imidazolium[11] and aluminate[14] ILs.

Fig. 3.1 depicts the time-dependent solvation response due to solute-IL dipolar interaction ($S_{sd}(t)$) and solute-ion dipole-ion interaction ($S_{si}(t)$) for a C153-like solute in [Na][TOTO] at three representative temperatures - 254 K, 294 K, and 344 K. Because of large viscosity, the decays for [Na][TOTO] are very slow, covering an average time-scale for these individual contributions from a few seconds to a few nanoseconds. Decay parameters obtained from fits to these calculated individual response functions are provided in Table A8 (Appendix A) which indicate a strong stretched exponential relaxation for the dipole-dipole interaction energy (S_{sd}) and a bi-exponential decay for the dipole-ion part. The stretched exponential decay for the S_{sd} part originates from the use of experimental DR data (as inputs in the present theory) which which reflects medium heterogeneity through the fit parameters, α' and β', shown in Table A6 (Appendix A). As already stated in the Introduction, microscopic phase segregation due to different types of interactions present in the molecular anion of [Na][TOTO] can produce such micro-heterogeneity. Note that a slightly better description can be achieved if a sum of an exponential and a stretched exponential is used for fitting the calculated S_{sd} decays but in that case the two time constants become too closer to be meaningful, particularly at higher temperatures. This is shown in Fig. C3 (Appendix C) and Table A8 (Appendix A). Considering this and given that the present calculations could be regarded only suggestive because of the use of semi-quantitative experimental DR data (due to both missing of the high frequency response and the consequent complexity in fitting the experimental data [2]), the use of single stretched exponential appears logical as it requires fewer number of fit parameters for $S_{sd}(t)$.

A complete neglect of the spatial heterogeneity in calculating the static correlation functions ($c_{s\alpha}^{10}(k)$), on the other hand, has led to the predicted decay of $S_{si}(t)$ as bi-exponential instead of stretched exponential. The suitability of bi-exponential fit function to describe the calculated $S_{si}(t)$ is demonstrated in Fig. C4 (Appendix C) where the applicability of single exponential function is also shown for a comparison. The bi-exponential character of $S_{si}(t)$

emerges from the different relaxation rates of the ion dynamic structure factor (see Eq. 2.4 (Chapter 2)) at the nearest

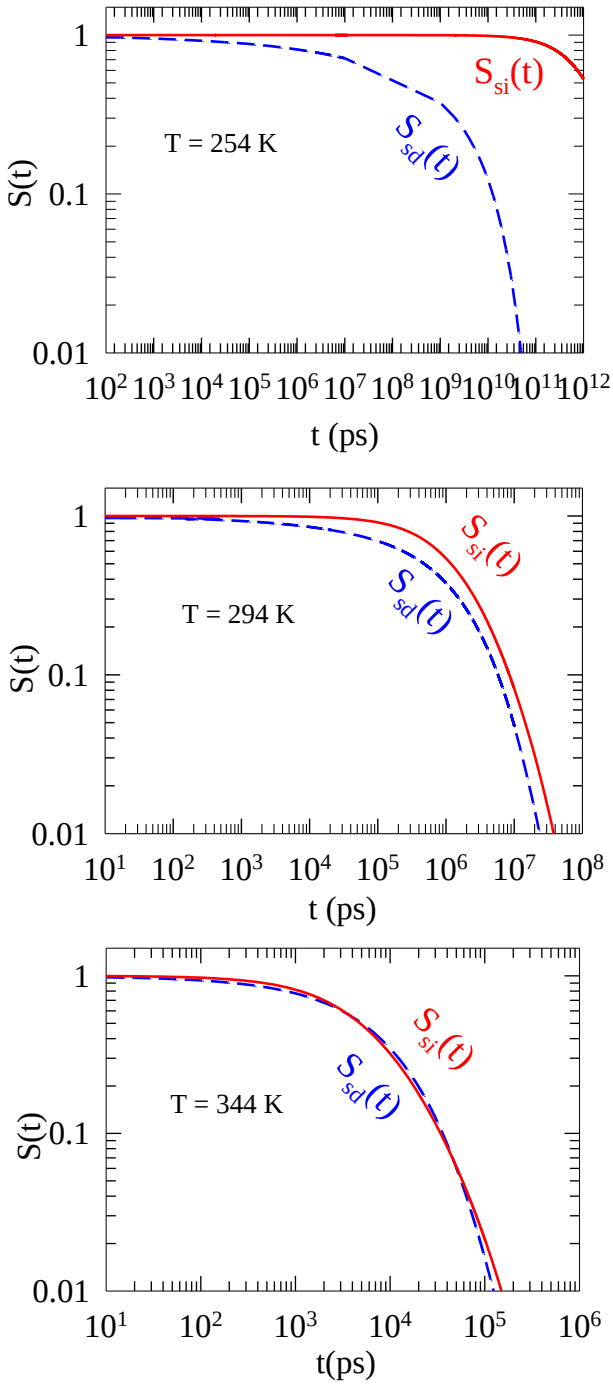

Fig. 3.1: Plot for solute- IL dipole-dipole interaction ($S_{sd}(t)$, blue) and solute-IL dipole - ion interaction ($S_{si}(t)$, red) contributions to the calculated total solvation response function at three different temperatures: 254 K (upper panel), 294 K (middle panel), and 344 K (lower panel).

neighbor ($k\sigma \to 2\pi$) and collective ($k\sigma \to 0$) modes of the ion density fluctuations. Since the ion dynamic structure factor relaxation has been assumed to be proportional to $\exp[-D_T k^2/S(k)]$, the contribution from the $k\sigma \to 2\pi$ modes becomes insignificant because of too much relaxation efficiency at these wavenumbers, particularly more so at higher temperatures where particle diffusion is larger. The numerical closeness between the two time constants for $S_{si}(t)$ at 344 K (see Table A8) is a reflection of the above aspect. Because the polar solvation energy relaxation is governed by collective density fluctuations (that is, involving many molecules together)[27], effects due to local heterogeneity around an excited polar solute becomes secondary. Therefore, neglect of spatial heterogeneity in calculating fluorescence dynamics in this IL is not expected to lead to serious disagreement with experimental results. Because of the predicted decay time constants cover a range between several seconds to several nanoseconds, use of a phosphorescent dye is suggested to examine the present results in experiments.

Next, temperature dependence of polar solvation response in [Na][TOTO] is shown in Fig. 3.2 where the calculated $S_{ss}(t)$ at ten different temperatures are presented. A comparison indicates a complete difference in the early part of the dynamics between imidazolium ILs and [Na][TOTO]. This can be attributed to the faster of the two times scales revealed by DR measurements for these imidazolium ILs.[3] It is evident from this figure that the predicted decays systematically become faster upon increasing the solution temperature and they are well spread-out in timescale. Table 3.2 lists the parameters obtained from fit of these decays to a stretched exponential, $S(t) = a_1 \exp\left(-(t/\tau_1)^{\alpha}\right)$ eventhough fit to a sum of an exponential and a stretched exponential has been found to produce equally good description. Fig. C5 (Appendix C) demonstrates this aspect at two representative temperatures. The reasons for preferring the single stretched exponential over the other have already been described in connection to $S_{sd}(t)$ decays. Note the single decay time constant (τ_1) ranges between a few milli-second to ~10 ns where the stretching exponent, α, increases from 0.19 at 254 K to 0.61 at 344 K. The temperature-induced increase of α roughly follows the trend of β' observed in DR experiments[2] and indicates temperature-assisted homogenization of the liquid structure. It is interesting to note that eventhough the solvation time-scales are much

slower than those in imidazolium ILs (mainly because of much larger viscosity), the stretching exponent (α) falls in the same range as that found for imidazolium ILs.[28,29] However, these calculations do not predict any ultrafast component in the total solvation response of [Na][TOTO] because the experimental DR data[2], which have been used as input, do not cover the dielectric response of this IL beyond 10 MHz. As a result, the dielectric dispersion resulting from faster reorientational motions encompassing the GHz (10^9 Hz) regime has remained unexplored, effecting the non-prediction of a faster solvation component[30]. We have done a representative calculation at 304 K where the missing high frequency dispersion, $\varepsilon_\infty - n^2 = 6.78 - 3.12$ (n being the refractive index), has been attributed to a relaxation time of ~4 ns. This time constant has been modeled in accordance with the available DR data for liquid try(ethylene)glycol[31] at 298 K but only after appropriate

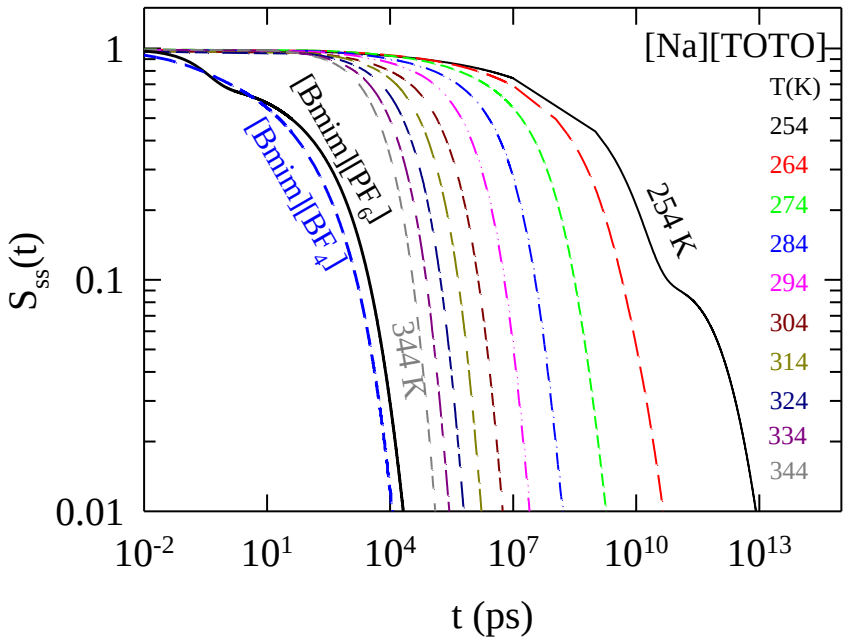

Fig. 3.2: Plot of the calculated total solvation response function ($S_{ss}(t)$) as a function of time at temperatures ranging from 254 K to 344 K. Different curves are color-coded. Note the calculated $S_{ss}(t)$ consists of 90% contributions from $S_{sd}(t)$ and the rest from $S_{si}(t)$. $S_{ss}(t)$ calculated using C153 as solute in two common imidazolium ILs, $[Bmim][BF_4]$ and $[Bmim][PF_6]$ at T = 304 K, are also shown for comparison.

\

Table 3.2: Parameters obtained from fitting the calculated solvation response functions for C153 in [Na][TOTO] at various temperatures.

T (K)	a_1	τ_1 (ps)	α	$\langle\tau_{ss}\rangle$ (s)
254	1	2.9×10^{9}	0.19	3.5×10^{-1}
264	1	2.7×10^{8}	0.29	2.8×10^{-3}
274	1	3.9×10^{7}	0.37	1.3×10^{-4}
284	1	5.9×10^{6}	0.40	1.5×10^{-5}
294	1	1.0×10^{6}	0.46	2.4×10^{-6}
304	1	2.5×10^{5}	0.47	5.3×10^{-7}
314	1	9.7×10^{4}	0.53	1.7×10^{-7}
324	1	3.9×10^{4}	0.56	6.5×10^{-8}
334	1	1.8×10^{4}	0.58	2.5×10^{-8}
344	1	9.2×10^{3}	0.61	1.5×10^{-8}

viscosity[32] scaling. Fits of the calculated response functions obtained after incorporating these model DR data are shown in Fig. C6 (Appendix C) and fit parameters summarized in Table A9 (Appendix A). These data suggest presence of a faster component with time-constant of ~2 ns at 304 K. This time-constant might become even faster if accurate DR data covering the GHz and THz (10^{12} Hz) response of [Na][TOTO] could be included. In spite of the crudeness in the approximation involved, the above calculations do suggest presence of a biphasic dynamics in [Na][TOTO] which has already been hinted by the representative DR measurements exhibiting 'split dynamics' with a dominating slow mode.[2]

The origin of extremely slow solvation in [Na][TOTO] can be traced to the huge frictional response in this liquid. This is demonstrated in Fig. 3.3 for two different temperatures where the frequency (z) dependent collective rotational frictional kernel, $\Gamma_R(z)$, has been calculated by using the relation[30,33]: $\Gamma_R(z) = \left[2k_BTf_L(0)\{\varepsilon_0 - \varepsilon(z)\}/zI\varepsilon_0\{\varepsilon(z) - \varepsilon_\infty\}\right] - z$, with I being the moment of inertia of a rotating dipolar solvent particle, and $f_L(0) = 4\pi\mu^2\rho_d^0/3k_BT(1-\varepsilon_0^{-1})$. Note $\Gamma_R(z)$, an integral part of the orientational solvent dynamic structure factor , largely dictates the rotational rearrangement timescale of the

solvent molecules and is related to $\varepsilon(z)$.[27,30] The upper panel of Fig. 3.3 clearly shows that absence of any faster timescale in the experimental DR data leads to a very large friction in the $z \to 0$ limit at both these temperatures. In addition, $\Gamma_R(z)$ depicts a non-exponential character (derived from the experimental $\varepsilon(z)$) and

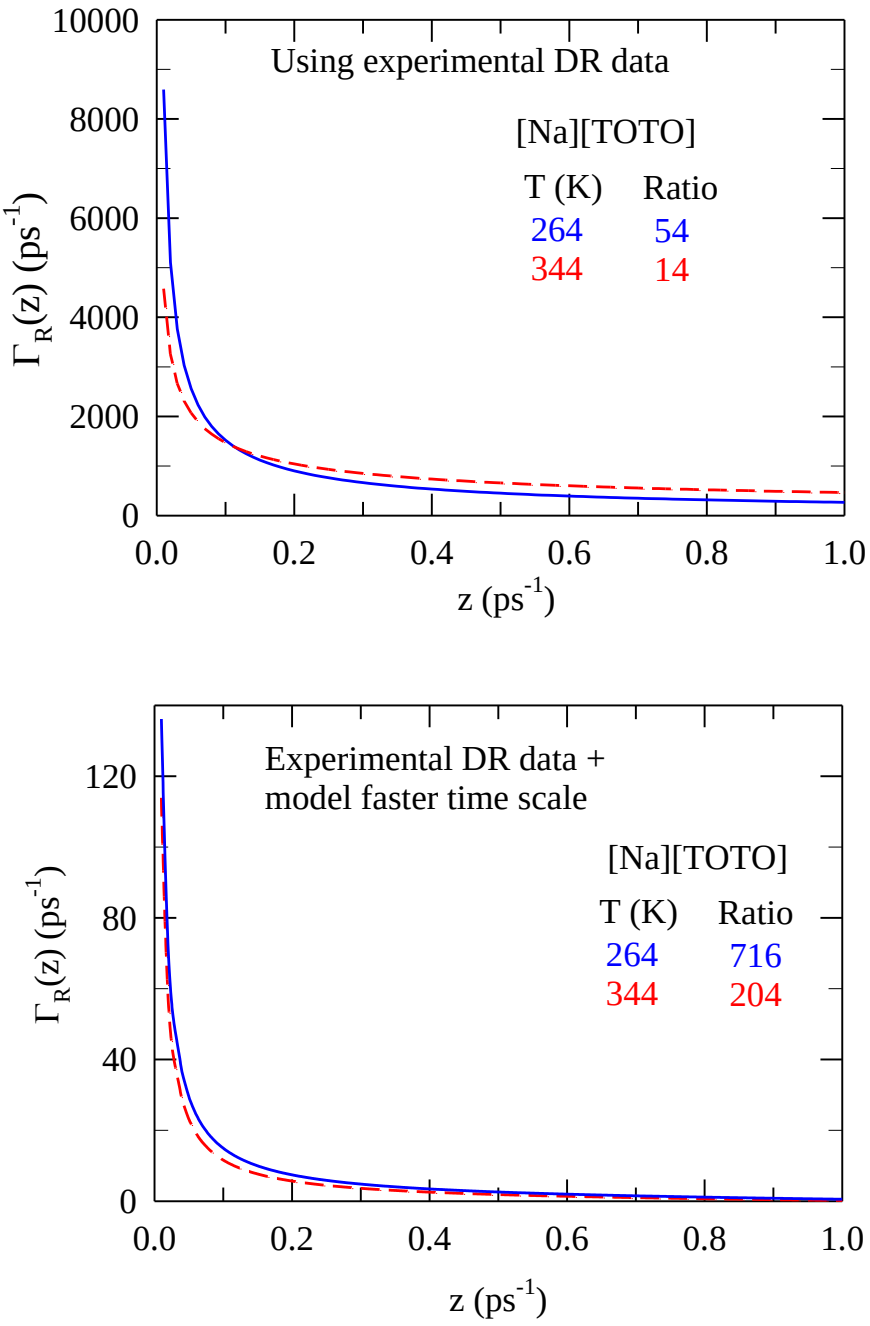

Fig. 3.3: The frequency dependent collective rotational friction kernel, $\Gamma_R(z)$, for neat [Na][TOTO] at two temperatures using the experimental DR data (upper panel) and experimental DR data + model faster time scale (lower panel).

becomes clearly biphasic when a model faster timescale is also considered in addition to the experimental $\varepsilon(z)$. The strength of this biphasic character or the extent of separation between the timescales in a given liquid would, of course, depend upon the ratio between the values of $\Gamma_R(z)$ at the $z \to 0$ and $z \to \infty$ limits. The values of this ratio for [Na][TOTO] at 264 K and 344 K are ~55 and ~15, respectively, which sharply rise to ~700 and ~200, upon inclusion of the model faster dynamics. This could be even more pronounced if extended $\varepsilon(z)$ measurements find faster timescale than the incorporated model ones.

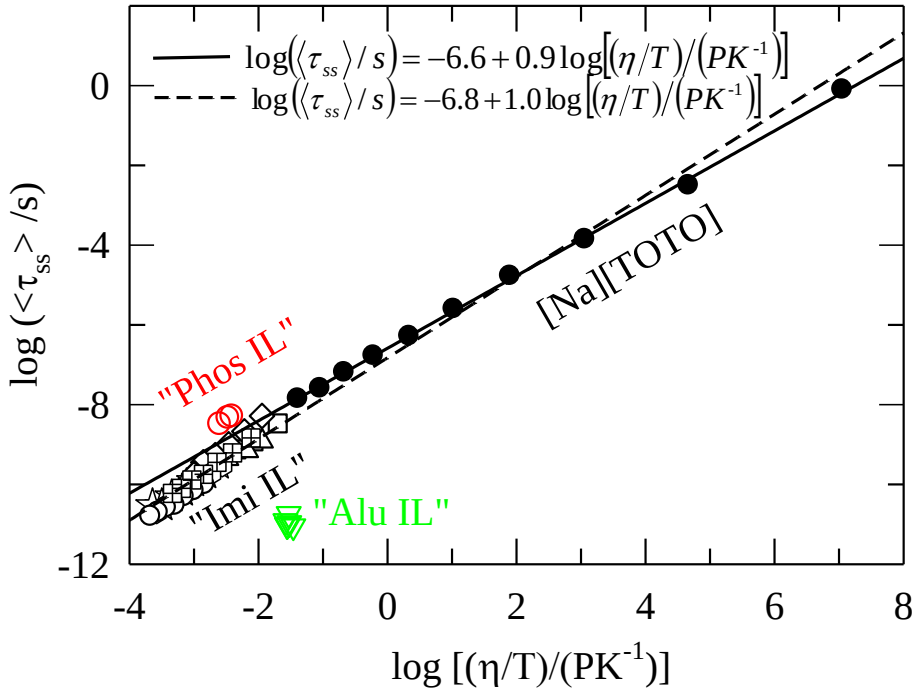

Fig. 3.4: Temperature-scaled viscosity (η/T) dependence of predicted average solvation time ($\langle\tau_{ss}\rangle$) for the present IL. The solid line is a linear fit to the calculated $\langle\tau_{ss}\rangle$ values (filled circles) for [Na][TOTO]. Calculated $\langle\tau_{ss}\rangle$ for phosphonium ("Phos IL") and aluminate ("Alu IL") ILs are also shown by red circles and green inverted triangles, respectively. Other black symbols represent $\langle\tau_{ss}\rangle$ for imidazolium ILs. ("Imi IL"). where the dashed line represents the linear fit to the $\langle\tau_{ss}\rangle$ values for [Na][TOTO] and imidazolium ILs. The dashed lines denote a fit through the calculated $\langle\tau_{ss}\rangle$ for imidazolium and [Na][TOTO] ILs. Note $\langle\tau_{ss}\rangle$ for phosphonium and aluminate ILs have not been included in this correlation.

Additionally, the fact that the inclusion of faster dynamics inducing bimodal character in solvation energy relaxation renders dynamical similarity between [Na][TOTO] and slow conventional polar liquids. However, the quantitative difference would arise from the difference in ε_0 values because the collective solvent orientational correlation is governed by that.

Fig. 3.4 shows the dependence of calculated average solvation times, $\langle \tau_{ss} \rangle$, on the temperature-scaled viscosity, η/T, in a log-log plot for [Na][TOTO], which shows a linear relationship, $\log(\langle \tau_{ss} \rangle) = -6.58 + 0.91 \log(\eta/T)$. In other words, $\langle \tau_{ss} \rangle$ shows a power law dependence on η/T ($\langle \tau_{ss} \rangle = a(\eta/T)^p$) with p = 0.91. This value of the power, $p \approx 1$, is interesting because this indicates validity of the conventional hydrodynamics for motions of solvating particles in [Na][TOTO] although the DR measurements suggest presence of strong micro-heterogeneity. This is of course not new and has already been observed in experimental studies of temperature dependent solvation dynamics in imidazolium and phosphonium ILs.[34-39] The calculated $\langle \tau_{ss} \rangle$ for imidazolium[11,12], phosphonium[11] and aluminate[14] ILs are also shown in the same figure for a comparison. It is interesting to note that while the calculated $\langle \tau_{ss} \rangle$ for imidazolium and phosphonium ILs follow nearly the same correlation as found for [Na][TOTO], those for aluminate ILs deviate strongly. The reasons for such a deviation are not known yet, although a temperature dependence of viscosity for aluminate ILs different from those of imidazolium and phosphonium ILs could be a possibility. This therefore warrants further study.

When the average solvation rates are plotted as a function of inverse temperature in a semi-logarithmic fashion, as done in the upper panel of Fig. 3.5, an approximate linear dependence emerges which closely follows that for the DR relaxation rate. The deviation from linearity for average solvation rate may have arisen from the inaccuracy in the description of the frequency dependent dielectric response of this IL. Since in the present theory the solvation response arises from the coupling between the natural dielectric response of the liquid and the spatial correlations (solute-solvent and solvent-solvent static correlations), inaccuracy

present in experimental DR data may get accentuated in the final prediction of the decay dynamics. The estimated activation energy (from the slope) for $\langle \tau_{ss} \rangle$, is ~134 kJ/mol. whereas the same

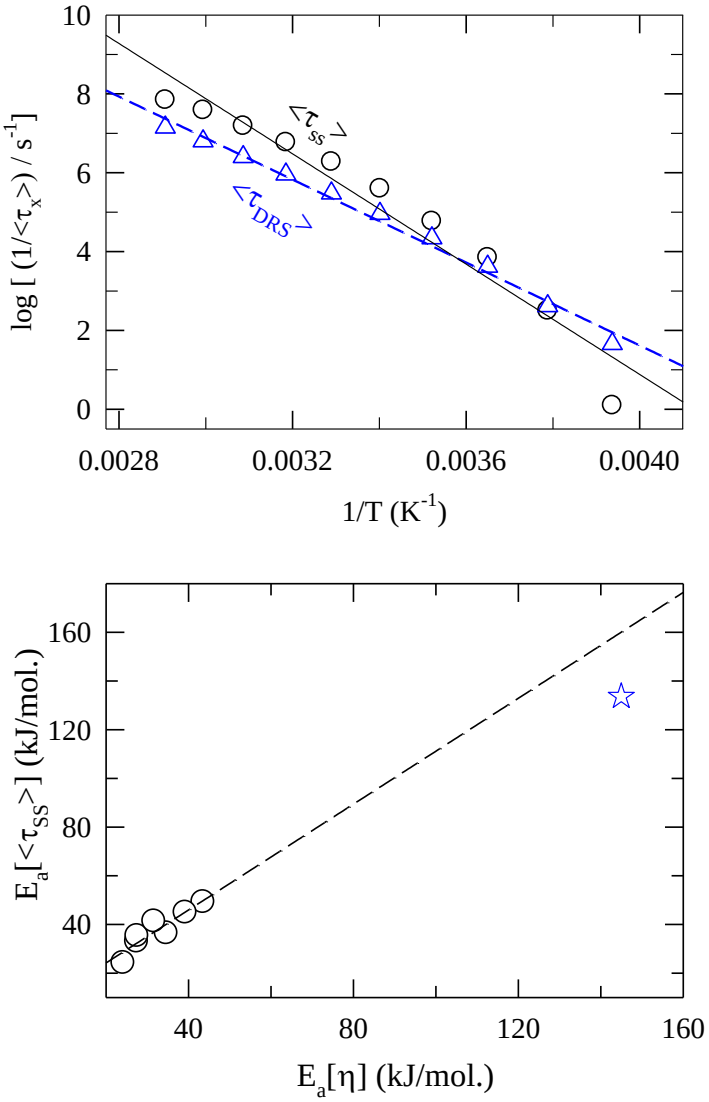

Fig. 3.5: Upper panel: Check for the Arrhenius-type of temperature dependence of average solvation time, $\langle \tau_s \rangle$. Logarithm of inverse dielectric relaxation time (triangle) and average solvation time (circle) have been plotted as a function of the inverse temperature, $1/T$. Lower panel: Plot for activation energy for solvation time ($E_a[\langle \tau_{ss} \rangle]$ kJ/mol.) against that for viscosity ($E_a[\eta]$ kJ/mol.), where black circles represent imidazolium ILs (consisting of $[Bmim]^+$,$[Emim]^+$, and $[Hmim]^+$ cations, and $[BF_4]^-$,$[PF_6]^-$,$[DCA]^-$, and $[NTf_2]^-$ anions), and the blue star represents [Na][TOTO].

determined from DR relaxation time is ~ 101 kJ/mol. This suggests that the temperature dependence of these two relaxation rates in [Na][TOTO] is essentially that of the IL viscosity. In the lower panel of Fig. 3.5, estimated activation energy from predicted solvation time is shown as a function of the activation energy estimated from the temperature dependent measurements of viscosity for both [Na][TOTO] and imidazolium ILs.[3,11] Interestingly, although the activation energy from average solvation rate for [Na][TOTO] is nearly double of that found for imidazolium ILs, it shares approximately the same linear correlation as that found between the activation energies from solvation and DR experiments for imidazolium ILs. This is expected from the correlation depicted in Fig. 3.4.

3.4 Conclusion

The present work shows that [Na][TOTO], although designated as a member of a new class of ionic liquids, exhibits many interesting features which are similar to already well-studied imidazolium ILs. Although the magnitude of the calculated total dynamic Stokes shift is somewhat less and the temperature dependence is weaker than those in imidazolium ILs, the relative contributions of dipole-dipole and ion-dipole interactions are comparable. Expectedly, solvation response in [Na][TOTO] is much slower because of very large viscosity, and experimental detection based on phosphorescence is suggested for examining the predictions discussed here. The absence of a faster timescale in the predicted solvation response in this IL is attributed to the missing of high frequency dispersion in the measured DR data. As in imidazolium ILs, validity of conventional hydrodynamics has also been predicted for the calculated $\langle \tau_{ss} \rangle$ in [Na][TOTO] where solvation activation energy proportionate to that from viscosity has been estimated. In addition, $\langle \tau_{ss} \rangle$ in [Na][TOTO] has been found to be well-correlated with those for imidazolium and phosphonium ILs but not with those calculated for aluminate ILs. These results are suggested to be re-examined via solvation measurements.

References

1. Zech, O.; Kellermeir, M.; Thomaier, S.; Maurer, E.; Klein, R.; Schreiner, C.; Kunz, W. *Chem. Eur. J.* **2009**, *15*, 1341.
2. Zech, O.; Hunger, J.; Sangoro, J. R.; Iacob, C.; Kremer, F.; Kunz, W.; Buchner, R. *Phys. Chem. Chem. Phys.* **2010**, *12*, 14341.
3. Hunger, J.; Stoppa, A.; Schrödle, S.; Hefter, G.; Buchner, R. *Chem. Phys. Chem.* **2009**, *10*, 723.
4. Weingärtner, H. *Z. Phys. Chem.* **2006**, *220*, 1395.
5. Krüger, M.; Bründermann, E.; Funker, S.; Weingärtner, H.; Havenith, M. *J. Chem. Phys.* **2010**, *132*, 101101.
6. Huang, M. M.; Weingärtner, H. *Chem. Phys. Chem.* **2008**, *9*, 2172.
7. Ediger, M. *Annu. Rev. Phys. Chem.* **2000**, *51*, 99.
8. Klein, R.; Zech, O.; Maurer, E.; Kellermeier, M.; Kunz, W. *J. Phys. Chem. B* **2011**, *115*, 8961.
9. Wang, Y.; Voth, G. A. *J. Am. Chem. Soc.* **2005**, *127*, 12192.
10. Triolo, A.; Russina, O.; Fazio, B.; Triolo, R.; Cola, E. D. *Chem. Phys. Lett.* **2008**, *467*, 362.
11. Kashyap, H. K.; Biswas, R. *J. Phys. Chem. B* **2010**, *114*, 254.
12. Kashyap, H. K.; Biswas, R. *J. Phys. Chem. B* **2010**, *114*, 16811.
13. Daschakraborty, S.; Biswas, R. *J. Phys. Chem. B* **2011**, 115, 4011.
14. Daschakraborty, S.; Biswas, R. *Chem. Phys. Lett.* **2011**, 510, 202.
15. Jin, H.; O'Hare, B.; Dong, J.; Arzhantsev, S.; Baker, G. A.; Wishart, J. F.; Benesi, A. J.; Maroncelli, M. *J. Phys. Chem. B* **2008**, *112*, 81.
16. Bhargava, B. L.; Balasubramanian, S. *J. Phys. Chem. B* **2007**, *111*, 4477.
17. Muramatsu, M.; Nagasawa, Y.; Miyasaka, H. *J. Phys. Chem. A* **2011**, *115*, 3886.
18. Roy, D.; Maroncelli, M. *J. Phys. Chem. B* **2012**, *116*, 5951.
19. Pradhan, T.; Biswas, R. *J. Phys. Chem. A* **2007**, *111*, 11524.
20. Shannon, R. D. *Acta Cryst.* **1976**, *A32*, 751.
21. Kashyap, H. K.; Biswas, R. *J. Phys. Chem. B* **2008**, *112*, 12431.
22. Kashyap, H. K.; Biswas, R. *Ind. J. Chem.* **2010**, *49A*, 685.
23. Guchhait, B.; Gazi, H. A. R.; Kashyap, H. K.; Biswas, R. *J. Phys. Chem. B* **2010**, *114*, 5066.

24. Gazi, H. A. R.; Guchhait, B.; Daschakraborty, S.; Biswas, R. *Chem. Phys. Lett.* **2011**, *501*, 358.
25. Gray, C. G.; Gubbins, K. E. *Theory of Molecular Fluids, Vol. I*, Clarendon: Oxford, 1984.
26. Chapman, C. F.; Maroncelli, M. *J. Phys. Chem.* **1991**, *95*, 9095.
27. Bagchi, B.; Biswas, R. *Adv. Chem. Phys.* **1999**, *109*, 207.
28. Arzhantsev, S.; Jin, H.; Baker, G. A.; Maroncelli, M. *J. Phys. Chem. B* **2007**, *111*, 4978.
29. Arzhantsev, S.; Jin, H.; Ito, N.; Maroncelli, M. *Chem. Phys. Lett.* **2006**, 417, 524.
30. Biswas, R.; Bagchi, B. *J. Phys. Chem.* **1996**, *100*, 1238.
31. Schrodle, S.; Buchner, R.; Kunz, W. *J. Phys. Chem. B* **2004**, *108*, 6281.
32. Lee, R-J.; Teja, A. S. *J. Chem. Eng. Data* **1990**, *35*, 385.
33. Biswas, R.; Bagchi, B. *J. Phys. Chem. A* **1999**, *103*, 2495.
34. Jin, H.; Baker, G. A.; Arzhantsev, S.; Dong, J.; Maroncelli, M. *J. Phys. Chem. B.* **2007**, *111*, 7291.
35. Arzhantsev, S.; Ito, N.; Heitz, M.; Maroncelli, M. *Chem. Phys. Lett.* **2003**, *381*, 278.
36. Ito, N.; Arzhantsev, S.; Maroncelli, M. *Chem. Phys. Lett.* **2004**, *396*, 83.
37. Ito, N.; Arzhantsev, S.; Heitz, M.; Maroncelli, M. *J. Phys. Chem. B.* **2004**, *108*, 5771.
38. Samanta, A. *J. Phys. Chem. Lett.* **2010**, *1*, 1557.
39. Samanta, A. *J. Phys. Chem. B* **2006**, *110*, 13704.

Chapter 4

Stokes shift Dynamics of Ionic Liquids: Solute Probe Dependence, Effects of Dielectric Relaxation Window and Solvent Librations

4.1 Introduction

As discussed in the previous chapters, dynamics of ionic liquids (ILs) have intensely been studied by experiments, theory, and computer simulations.[1-26] A number of interesting features of the dynamics have been observed and found markedly different from those observed for conventional polar solvents. Recently, Stokes shift dynamics of a number of ILs using C153 as a probe has been explored via a combination of two techniques - broad-band fluorescence up-conversion (FLUPS) having ~80 fs resolution and time-correlated single photon counting (TCSPC) providing ~25 ps resolution.[1] The obtained response functions are bimodal consisting of an ultrafast Gaussian and a slow stretched exponential components. Depending on the identity of the IL, the ultrafast sub-picosecond component varies between ~10-40% of the total response, followed by a much slower component with time constant ranging between 10 ps and 1 ns. It is also found that the ultrafast time constants correlate with ion mass and the slow time constants with IL viscosity. Consequently, ultrafast response has been attributed to the inertial solvent motions and the slower response to the medium structural relaxation. Solvation response in ILs measured via three pulse photo echo peak shift (3PEPS)[14] technique using Oxazine-4 has been found to be even faster, and fast time constants have been found to be correlated to the anion mass. Interestingly, a recent theoretical study has attempted to explain these 3PEPS results in terms of non-dipolar solute-IL interactions.[13]

A comparison between the above (FLUPS + TCSPC) C153 data and those obtained previously by using DCS (trans-4-dimethylamino-4'-cyanostilbene) via combining Kerr-gated emission (KGE) and TCSPC techniques[2] reveals the following interesting differences:

(i) in contrast to C153 data, the solvation response obtained with DCS is expressed as a sum of a fast exponential and a slow stretched exponential contributions. In both the cases, however, complete detection of the total response has been reported. This immediately raises the following question: does this different description of the measured initial fast dynamics (Gaussian versus exponential) relate to different solutes used or originate from the difference in experimental techniques employed for detecting the initial fast solvation response? This is an important issue as Gaussian response is connected to non-diffusive solvation mechanism whereas exponential description suggests diffusive reorganization of solvent molecules at the early stage. The fitted relaxation time constants and amplitudes obtained from these two different measurements are presented in Table 4.1, where one can see that the amplitudes and time constants differ significantly.

Table 4.1: Time constants and amplitudes of the solvation energy relaxation of three probes, C153, DCS, and Oxazine-4 in three ILs ($[Im_{41}][BF_4]$, $[Im_{41}][PF_6]$, $[Im_{41}][Tf_2N]$) obtained from Stokes shift dynamics[1,2] and 3-PEPS[14] measurements.

ILs	Expt.	Probe	Fit[a] Eq.	a_1	τ_1 (fs)	a_2	τ_2 (ps)	β	τ_3 (ps)
$[Im_{41}][BF_4]$	(FLUPS+ TCSPC)	C153	Gau.+Str. Exp	0.34	200	0.66	170	0.48	
	(KGE+ TCSPC)	DCS	Exp.+ Str. Exp.	0.19	320	0.81	130	0.31	
	3-PEPS	Oxazine-4	Sum of Exp.		110		1.10		21
$[Im_{41}][PF_6]$	(FLUPS+ TCSPC)	C153	Gau.+Str. Exp.	0.33	240	0.67	450	0.50	
	(KGE+ TCSPC)	DCS	Exp.+ Str. Exp.	0.19	330	0.81	140	0.41	
	3-PEPS	Oxazine-4	Sum of Exp.		150		2.2		64
$[Im_{41}][TF_2N]$	(FLUPS + TCSPC)	C153	Gau.+Str. Exp	0.39	340	0.61	190	0.60	
	(KGE+ TCSPC)	DCS	Exp.+ Str. Exp.	0.10	740	0.90	78	0.46	
	3-PEPS	Oxazine-4	Sum of Exp. + Osc.		26		0.54		

a) 'Gau.' refers to *Gaussian*, 'Exp.' to *exponential*, 'Str. Exp.' to *stretched exponential*, 'Sum of Exp. + Osc.' to *sum of exponentials and oscillations* as described in the respective references.

A closer inspection of the above table indicates that the (FLUPS + TCSPC) measurements not only reveal larger amplitudes of fast relaxation with shorter fast time constants (τ_1) than those observed in (KGE+TCSPC) measurements but also report longer slow time constants (τ_2) and larger stretching exponents (β). In making the above comparison it should be kept in mind that the FLUPS technique[1] was employed with a resolution nearly 6 times sharper than that provided by the KGE technique (~450 fs).[2] It may therefore be argued that a technique with sharper resolution detects fast components more accurately and thus the

observed differences reflect merely the effects of difference in time resolutions. This argument, however, does not provide any answer to the question that how use of different solutes affect results accessed by these different measurement techniques. This is one of the questions that we would like to investigate by employing a semi-molecular theory which has been found successful in describing experimental Stokes shift dynamics in various ILs[8,9,11-13] and (IL + polar solvent) mixtures.[10]

The above discussion further leads to the following point: if the ultrafast component arises from the solute-IL nearest neighbor interactions then a difference in τ_1 may originate either from a difference in solute size or from a change in IL density.[13] This is not the case here as the experiments have been carried out in the same IL using different solutes of very similar sizes.[2] The slowing down of τ_2 for C153 by a factor of ~1.3-3.2 is also surprising as this timescale is believed to originate from the structural relaxation (coupled to viscosity) of the IL under study and thus should not be sensitive to solute size. However, solute motion during measurements can modify the relaxation rate.[27-29] It should be mentioned here that solute dependence is not expected polar solvent response where collective polarization density relaxation dominates the ultrafast part of the solvation energy relaxation.[27] Also, within such a framework, difference in solute dipole moments should not modify solvation timescales provided solvent response induced by solute's sudden excitation remains in the linear response regime.[27] C153 and DCS are dipolar molecules with larger excited state dipole moments[8-10] and fluorescence Stokes shift dynamics of dipolar ILs (ILs with one of the ions possessing dipole moment) measured by these probes is expected to contain a large solute-IL dipolar contribution. This consideration suggests that Stokes shift dynamics in dipolar ILs would be significantly coupled to frequency dependent dielectric function, $\varepsilon(\omega)$, accessed by dielectric relaxation (DR) measurements. In such a scenario, one would like to investigate the effects of frequency range covered (frequency window) in dielectric relaxation (DR) measurements on the calculated solvation response because variation in frequency window accessed in different experiments[30-35] is likely to induce variations in fitted dielectric dispersion amplitudes (ΔS_i) and relaxation time constants ($\tau_{i,DR}$). For example, relaxation parameters obtained from experimental $\varepsilon(\omega)$ in 1MHz-20GHz window[31] show some differences with those obtained from measurements using the frequency coverage, 0.2-89

GHz.[30] When the frequency range has been further broadened up to 3000 GHz,[33] cation librations appear. DR parameters also differ even when $\varepsilon(\omega)$ in the same frequency range but reported by different groups[31,32,34] are considered. Since $\varepsilon(\omega)$ has been shown earlier[8] to be connected to polar solvation response in ILs as well, the variation in DR parameters will have impacts on predicted shifts and dynamics.

As a comparison between calculated response using ΔS_i and $\tau_{i,DR}$ as inputs from various experiments and measured solvation response function ($S(t)$) can assist in estimating the spread of the calculated response (and probably the accuracy of available DR data),[30-35] the issue of solvent libration contributions to $S(t)$ requires attention. This is because one would like to assess what roles the low frequency collective (libration) solvent modes play for solvation energy relaxation in ILs. These libration modes are known to be important for ultrafast solvation in polar H-bonded liquids such as water,[36-38] and amides,[29,39] and may also determine the rate of initial fast solvation energy relaxation in ILs. Eleven different ILs have been considered here for studying probe dependence and effects of variations in experimental $\varepsilon(\omega)$. The probes are C153 and DCS and incorporated in the calculations via their diameters and excited state dipole moments. The ILs are 1-ethyl-3-methylimidazolium dicyanamide ($[Im_{21}][DCA]$), 1-ethyl-3-methylimidazolium tetrafluoroborate ($[Im_{21}][BF_4]$), 1-ethyl-3-methylimidazolium bis (trifluoromethylsulfonyl) imide ($[Im_{21}][TF_2N]$), 1-butyl-3-methylimidazolium dicyanamide ($[Im_{41}][DCA]$),1-butyl-3-methylimidazolium tetrafluoroborate ($[Im_{41}][BF_4]$), 1-butyl-3-methylimidazolium hexafluorophosphate ($[Im_{41}][PF_6]$), 1-butyl-3-methylimidazolium bis(trifluoromethylsulfonyl)imide ($[Im_{41}][TF_2N]$), 1-hexyl-3-methylimidazolium (trifluoromethylsulfonyl)imide ($[Im_{61}][TF_2N]$), 1-methyl-3-octylimidazolium bis(triflluoromethylsulfonyl)imide ($[Im_{81}][TF_2N]$), 1-butyl-1-methylpyrrolidinium bis(trifluoromethanesulfonyl)imide ($[Pr_{41}][TF_2N]$), triethylsulfonium bis(trifluoromethylsulfonyl)imide ($[S_{222}][TF_2N]$). Note several of these ILs have been considered before[8,9] for predicting Stokes shift dynamics but we reconsider them again along with a few more new ones in order to test the generality of the present theoretical scheme and its predictive ability. The theoretical results have been

compared with experimental data[1-7,14] to explore the (i) possible reasons behind differences in Stokes shift dynamics data provided by different experimental techniques, (ii) effects due to solute variation, (iii) effects of frequency range covered in experimental $\varepsilon(\omega)$, and (iv) contributions of IL librations on measured $S(t)$.

4.2 Theoretical Formulation and Calculation Details

Since the molecular theory used here has already been discussed in detail elsewhere [8-13], we briefly outline the equations necessary for subsequent calculations. The expression[8-13,40] for the position ($\mathbf{r}$), orientation ($\mathbf{\Omega}$) and time (t) dependent total fluctuating solvation energy for a mobile dipolar solute with distribution function $\rho_s(\mathbf{r},\mathbf{\Omega};t)$ has been given in Eq. 2.1 of Chapter 2, where $c_{sd}(\mathbf{r},\mathbf{\Omega};\mathbf{r}',\mathbf{\Omega}')$ and $c_{s\alpha}(\mathbf{r},\mathbf{\Omega};\mathbf{r}')$ are respectively the position and orientation dependent solute dipole-solvent dipole (dipole-dipole) and solute dipole-ion (dipole-ion) direct correlation functions and α denotes the type of ions (cation and anion). $\delta\rho_d$ and δn_α represent respectively fluctuations in dipolar density and ion density from bulk values: $\delta\rho_d(\mathbf{r},\mathbf{\Omega}) = \rho_d(\mathbf{r},\mathbf{\Omega}) - \rho_d^0/4\pi$ and $\delta n_\alpha(\mathbf{r}) = n_\alpha(\mathbf{r}) - n_\alpha^0$. The solvation energy-energy correlation function averaged over space ($\mathbf{r}$) and orientation ($\mathbf{\Omega}$) is then written as

$$C_E(t) = C_{sd}(t) + C_{si}(t), \qquad (4.1)$$

with $C_{sd}(t)$ and $C_{si}(t)$ respectively are the contributions from solute-IL dipole-dipole and dipole-ion interactions, assuming the cross-correlations between fluctuating dipolar and ion densities do not survive due to widely different timescales.[8-10] The dipole-dipole and ion-dipole interaction terms are given in Eq. 2.3 and 2.4 respectively. In Eq. 2.3 (Chapter 2), $c_{sd}^{lm}(k)$ represents the wave-number (k) dependent (l, m) component of the static correlation function between the solute and dipolar ion, and $S_{solvent}^{lm}(k,t)$ is the same component of the orientational dynamic structure factor of the dipolar species. While $c_{sd}^{lm}(k)$ has been obtained from the mean spherical approximation (MSA) theory, $S_{solvent}^{lm}(k,t)$ has been obtained by using experimental[30-35] $\varepsilon(\omega)$, summarized in Table A10 (Appendix A). The solute self-dynamic structure factor, $S_{solute}^{lm}(k,t)$, has been approximated by its diffusive limit where the

rotational and translational diffusion coefficients for a spherical solute with a volume of C153 and DCS have been obtained from the solution viscosity using the stick boundary condition.

The longitudinal component of the wave-number dependent direct correlation function between the dipolar solute and ions, $c_{s\alpha}^{10}(k)$, is calculated as Eq. 2.5 in Chapter 2,[8-10] where μ_1 is the dipole-moment of the dipolar solute, q_α the charge of α^{th} type ion, ε_0 the static dielectric constant and r_c the distance of the closest approach between the solute dipole and the ionic species. R denotes the solute-IL size-ratio, $\frac{\sigma_{solute}}{\sigma_{IL}}$, σ_{IL} being the effective diameter of ions. $S_{\alpha\beta}^{ion}(k,t)$ is the partial isotropic ion dynamic structure factor, which has been obtained from previous calculation procedure.[8-10] Note that neither the spatial heterogeneity of ionic liquids[41,42] nor shape anisotropy of the constituent ions has been considered while obtaining the spatial correlations. The heterogeneity aspect enters into our calculations via the use of experimental $\varepsilon(\omega)$. In addition, inverse proportionality between $c_{s\alpha}^{10}(k)$ and ε_0 renders ion-dipole contribution to shift more sensitive to small variations in ε_0. Such a dependence of the dipole-dipole contribution is not expected (see Eq. 2.3 of Chapter 2) as $c_{sd}^{lm}(k)$ has been obtained in our calculations by using IL density and dipole moment.

Subsequently, the normalized dipolar contribution is given by

$$S_{sd}(t) = \frac{C_{sd}(t)}{C_{sd}(t=0)}, \qquad (4.2)$$

and that due to dipole-ion interaction

$$S_{si}(t) = \frac{C_{si}(t)}{C_{si}(t=0)}. \qquad (4.3)$$

Note solvation response function measured in experiments is composed of contributions described by Eq. 4.2 and Eq. 4.3. The total solvation response function (S_{ss}) and the average solvation time ($<\tau_{ss}>$) are then calculated as follows: $S_{ss}(t) = (1-f)S_{sd}(t) + fS_{si}(t)$ and

$< \tau_{ss} >= \int_0^\infty dt\, S_{ss}(t)$. Following our earlier works on ILs,[8(b),9,10] we set $f = 0.1$. Note also that the dipole-dipole and ion-dipole interaction contributions to dynamic Stokes shift have been calculated respectively by using Eq. 2.3 (Chapter 2)and Eq. 2.4 (Chapter 2) at $t = 0$, and in all calculations dipole moment values for excited solutes have been used. Other necessary parameters for calculations are presented in Table A11 (Appendix A).

4.3 Results and Discussions

4.3.1 Dynamic Stokes Shift: Probe Dependence

First we present the calculated dynamic Stokes shifts of C153 and DCS in eleven ILs considered above and compare with experiments. Table 4.2 summarizes for C153 the calculated total Stokes shift ($\Delta\nu^t_{total}$), solute-IL dipole-dipole ($\Delta\nu^t_{sd}$) and dipole-ion ($\Delta\nu^t_{si}$) interaction contributions using μ_1=14 D.[8(b)] These calculations have been done by using experimental $\varepsilon(\omega)$ from different sources[30-34] and are mentioned in the table. The experimental Stokes shift values[1] ($\Delta\nu^t_{expt.}$) for the above ILs are also provided in the same table for comparison. The last column of Table 4.2 provides the ratio between the calculated and measured dynamic Stokes shifts for C153 in these ILs. Data in this table clearly indicate a fair agreement between theory and experiments[1] where the deviation between these two are within $\pm$ 20%. This is satisfactory given the complexity of these ILs and the simplicity of the model employed for calculating dynamic Stokes shift in them. In addition, the separated solute-IL dipole-dipole interaction contributes ~40-50% of the total shift in all these ILs, signifying a substantial role for the solute-IL dipolar interaction. Shift values given in parenthesis exhibit sensitivity to ε_0 reported by different measurements using different frequency windows with relatively more dependence for the ion-dipole contribution.

Table 4.3 summarizes the calculated shifts for DCS probe in these ILs and compares with the available experimental data.[2] Shifts have been calculated using different excited state dipole moments as before[8(b)] and use of μ_1 = 28 D produces total shift in 4000 cm^{-1} range observed in experiments for a few ILs. The predictions for other ILs with DCS should be tested in

experiments as too high (~4700 cm^{-1} for $[Im_{21}][DCA]$) and too low values (~2800 cm^{-1} for $[Im_{81}][TF_2N]$) may suggest partial break-down of the present scheme. Such a caveat notwithstanding, the dipole-dipole contribution to shift for this solute is also within ~40-50%, strongly supporting an important role for solute-IL dipolar interactions for Stokes shift dynamics in dipolar ILs. Note that use of $\mu_1 = 14$ D for DCS also predicts, as for C153, dynamic shift in 2000 cm^{-1} range which is nearly half of what has been measured in some of these ILs. Therefore, this solute dependence of shift arises from dependence on μ_1 as their sizes are equal. However, this difference between dynamic shifts does not foretell any difference in Stokes shift dynamics as solute is used merely as a probe for the solvent dynamics and its sudden excitation to create weak perturbation in equilibrium solvent fluctuation. Below we explore this aspect.

Table 4.2: Calculated dynamic Stokes shifts for C153 in various ionic liquids at room temperature

ILs	$\Delta\nu^t_{sd}$ (cm^{-1})	$\Delta\nu^t_{si}$ (cm^{-1})	$\Delta\nu^t_{total}$ (cm^{-1})	$\Delta\nu^t_{expt.}$ (cm^{-1})	$\chi(\Delta\nu^t_{total}/\Delta\nu^t_{expt.})$
$[Im_{21}][DCA]$[a]	876	1473	2349	2080	1.13
$[Im_{21}][BF_4]$[a,b]	850(850)	1136(1217)	1986(2067)	2430	0.82(0.85)
$[Im_{21}][TF_2N]$[c,b]	958(958)	1042(1037)	2000(1995)	2080	0.96(0.96)
$[Im_{41}][DCA]$[a]	821	1330	2151	2070	1.04
$[Im_{41}][BF_4]$[a,d]	822(796)	1085(1315)	1907(2111)	2220	0.86(0.95)
$[Im_{41}][PF_6]$[a]	885	877	1762	2170	0.81
$[Im_{41}][TF_2N]$[b,c]	850(850)	870(950)	1720(1800)	2060	0.83(0.87)
$[Im_{61}][TF_2N]$[a]	750	882	1632	1850	0.88
$[Im_{81}][TF_2N]$[b]	782	620	1402	1790	0.78
$[Pr_{41}][TF_2N]$[e]	800	1006	1806	2080	0.87
$[S_{222}][TF_2N]$[e]	844	939	1783	2070	0.86

a) From Ref. 30; b) From Ref. 31; c) From Ref. 32; d) From Ref. 33; e) From Ref. 34
The shift values in parenthesis have been calculated using the static dielectric constants taken from the second references of the corresponding superscripts.

Table 4.3: Calculated dynamic Stokes shifts for DCS in various ionic liquids at room temperature.

ILs	$\Delta\nu^t_{sd}$ (cm^{-1})			$\Delta\nu^t_{si}$ (cm^{-1})			$\Delta\nu^t_{total}$ (cm^{-1})			$\Delta\nu^t_{expt.}$ (cm^{-1})
	μ_{probe} (D)			μ_{probe} (D)			μ_{probe} (D)			
	14	20	28	14	20	28	14	20	28	
$[Im_{21}][DCA]$ [a]	872	1239	1762	1468	2104	2946	2340	3343	4708	
$[Im_{21}][BF_4]$ [a]	845	1179	1810	1132	1623	2435	1977	2802	4245	
$[Im_{21}][TF_2N]$ [b]	955	1414	2070	1035	1488	2084	1990	2902	4154	
$[Im_{41}][DCA]$ [a]	817 (855)	1032 (1047)	1649 (1658)	1325 (1372)	1900 (1892)	2659 (2649)	2142 (2227)	2932 (2938)	4308 (4307)	
$[Im_{41}][BF_4]$ [a]	820 (760)	1165 (915)	1632 (1629)	1079 (1281)	1549 (1767)	2473 (2473)	1899 (2041)	2514 (2682)	4105 (4102)	4080
$[Im_{41}][PF_6]$ [a]	882 (896)	1240 (1242)	1720 (1736)	874 (1262)	1254 (1740)	1780 (2438)	1756 (2158)	2494 (2982)	3500 (4174)	4240
$[Im_{41}][TF_2N]$ [c]	845	1180	1687	868	1252	1737	1731	2432	3424	3850
$[Im_{61}][TF_2N]$ [a]	750	1088	1510	882	1323	1938	1632	2411	3448	
$[Im_{81}][TF_2N]$ [c]	782	1100	1560	620	870	1235	1402	2335	2795	
$[Pr_{41}][TF_2N]$ [d]	800	1120	1610	1006	1407	2004	1806	2527	3614	
$[S_{222}][TF_2N]$ [d]	844	1180	1682	939	1316	1872	1783	2496	3554	

a) From Ref. 30; b) From Ref. 32; c) From Ref. 31; d) From Ref. 34
The shift values in parenthesis have been taken from Ref. 8(b)

4.3.2 Stokes Shift Dynamics: Probe Dependence

Figure 4.1 presents results on probe size dependence of solvation dynamics in ILs and a comparison between theory and experiments. Experimental results obtained by following the fluorescence shift of C153 via (FLUPS+TCSPC)[1] and that of DCS via (KGE+TCSPC)[2] techniques have been shown, and a comparison between them has been made for one IL for which both measurements exist (but with different solutes).[1,2] Except for $[S_{222}][Tf_2N]$, the calculations have been done by using experimental $\varepsilon(\omega)$ reported in Ref. 30 measured in the frequency window, $0.2 \le \nu/\text{GHz} \le 89$, which did not include any solvent libration contribution to the observed total $\Delta\varepsilon$. For $[S_{222}][Tf_2N]$, we have used $\varepsilon(\omega)$ reported in Ref. 34 and measured in frequency range, 1MHz - 20GHz. A comparison among calculated response functions using three different solutes – C153, DCS and 4-AP (4-aminophthalimide) – has also been made in this panel in order to show to what extent the calculated polar

response is sensitive to size and dipole moment variations. Note diameter of 4-AP (σ_{4-AP} = 6.2 Å)[8(a)] is ~20% shorter and excited state dipole moment (μ_1^{4-AP} = 6.5 D)[8(a)] ~50% smaller than that of C153. A stronger variation in solute size cannot be considered as our earlier study[13] suggests that such a calculation using the present scheme must correspond to a density much lower than the typical IL density. It can be immediately recognized from the right lower panel of Fig. 4.1 that our present calculations do not suggest any significant probe dependence for Stokes shift dynamics in [Im_{41}][PF_6]. The calculated responses for these probes differ slightly at a very later stage of the dynamics when probe translation becomes operational,[28] with no effects from the variation of μ_1. Note this is a general result for ILs where solute-IL dipolar interaction governs the solvation energy relaxation. This insensitivity of the dynamics to the solute variation has also been suggested in experimental results obtained via using a limited number of probes.[1]

It is evident from this figure that the calculated responses using C153 in [Im_{21}][DCA] and [Im_{41}][DCA] are much slower than those obtained via (FLUPS+TCSPC) measurements.[1] Particularly, the ultrafast response seen in (FLUPS+TCSPC) measurements is completely missed. Even consideration of $S_{sd}(t)$ alone, which predicts relaxation due only to the rotation of the IL dipoles, does not reproduce the experimental response functions for these two liquids. Addition of solute-IL dipole-ion contribution ($S_{si}(t)$) to the solute-IL dipole-dipole

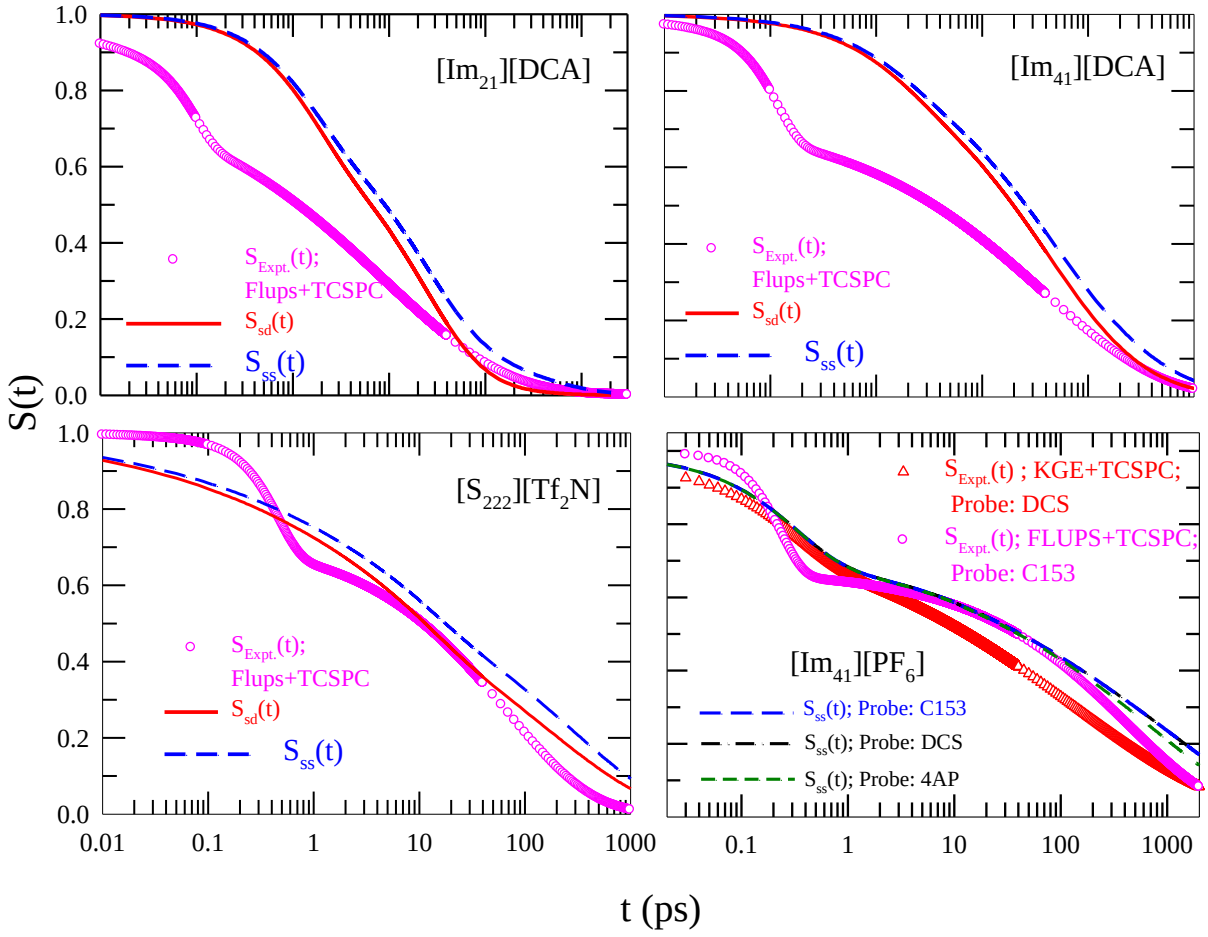

Fig. 4.1: Figure showing the probe dependence of calculated solvation response, and a comparison between calculated dynamics and (FLUPS+TCSPC) data obtained using C153 as solute.

contribution ($S_{sd}(t)$) further slows down the total calculated response ($S_{ss}(t)$). These aspects are described quantitatively in Table 4.4 where the time constants (τ_i) and amplitudes (a_i) have been obtained by fitting the calculated responses to the following form: $S_{sx}(t) = a_1 \exp[-t/\tau_1] + a_2 \exp[-(t/\tau_2)^{\beta}]$, '$x$' denoting '$d$', '$s$'or '$i$' and β being the stretching exponent. For the remaining ILs, the relevant parameters are summarized in Table A12 (Appendix A). Except for $[Im_{41}][PF_6]$, the calculated responses are neither able

to

Table 4.4: Fitting parameters of the solvation response decays of C153 in ionic liquids using experimental dielectric relaxation.

ILs	$S(t)$	a_1	τ_1 (ps)	a_2	τ_2 (ps)	β	$\langle\tau_{solv}\rangle$ (ns)	$\langle\tau_{solv}\rangle^{theo.}$ / $\langle\tau_{solv}\rangle^{expt.}$
$[Im_{21}]$ $[DCA]$	$S_{sd}(t)$	0.27	1.61	0.73	25.7	0.69	0.022	1.48
	$S_{si}(t)$	0.38	90.5	0.62	825	1	0.532	
	$S_{ss}(t)$	0.21	1.77	0.79	32.0	0.59	0.034	
	$S_{expt.}(t)$	0.18	0.10	0.82	9.00	0.34	0.023	
$[Im_{41}]$ $[DCA]$	$S_{sd}(t)$	0.10	2.83	0.90	52.1	0.53	0.081	1.72
	$S_{si}(t)$	0.41	129	0.59	1137	1	0.690	
	$S_{ss}(t)$	0.08	5.37	0.92	72.4	0.48	0.122	
	$S_{expt.}(t)$	0.27	0.12	0.73	40	0.40	0.071	
$[Im_{41}]$ $[BF_4]$	$S_{sd}(t)$	0.30	0.42	0.70	84.8	0.34	0.206	2.06
	$S_{si}(t)$	0.41	336	0.59	3094	1	1.870	
	$S_{ss}(t)$	0.27	0.42	0.73	155	0.34	0.399	
	$S_{expt.}(t)$	0.34	0.20	0.66	170	0.48	0.194	
$[Im_{41}]$ $[PF_6]$	$S_{sd}(t)$	0.27	0.32	0.73	351	0.34	0.903	2.64
	$S_{si}(t)$	0.47	1667	0.53	10000	1	5.899	
	$S_{ss}(t)$	0.26	0.33	0.74	603	0.35	1.467	
	$S_{expt.}(t)$	0.33	0.24	0.67	450	0.50	0.556	
$[Im_{61}]$ $[TF_2N]$	$S_{sd}(t)$	0.07	0.78	0.93	86.4	0.40	0.205	1.38
	$S_{si}(t)$	0.30	308	0.70	3335	1	2.326	
	$S_{ss}(t)$	0.04	0.98	0.96	126	0.36	0.398	
	$S_{expt.}(t)$	0.22	0.30	0.78	250	0.55	0.288	
$[Im_{81}]$ $[TF_2N]$	$S_{sd}(t)$	0.23	24.6	0.77	641	0.63	0.633	1.50
	$S_{si}(t)$	0.38	796	0.62	5243	1	3.396	
	$S_{ss}(t)$	0.21	26.2	0.79	802	0.61	0.839	
	$S_{expt.}(t)$	0.13	0.46	0.87	400	0.52	0.559	
$[Pr_{41}]$ $[TF_2N]$	$S_{sd}(t)$	0.04	0.02	0.96	32.8	0.42	0.073	1.30
	$S_{si}(t)$	0.45	642	0.55	4156	1	2.450	
	$S_{ss}(t)$	0.06	13.9	0.94	56.3	0.34	0.299	
	$S_{expt.}(t)$	0.33	0.43	0.67	210	0.54	0.230	
$[S_{222}]$ $[TF_2N]$	$S_{sd}(t)$			1.0	36.8	0.31	0.187	4.01
	$S_{si}(t)$	0.38	189	0.62	1634	1	1.036	
	$S_{ss}(t)$			1.0	59.3	0.31	0.301	
	$S_{expt.}(t)$	0.28	0.47	0.72	70.0	0.54	0.075	

reproduce the ultrafast timescales nor reflect the distinct biphasic character (via oscillation) of the measured responses for these systems. In addition, the predicted response for $[S_{222}][Tf_2N]$ has been found to be stretched exponential with a single solvation time constant (see Table 4.4). For $[Im_{41}][PF_6]$, the calculations for all three solutes (C153, DCS & 4-AP) show undulation and better agreement with (FLUPS+TCSPC) data. As found earlier for water[36-38] and amides,[29,39] the origin of such a variable agreement between the calculations and experiments arises from the difference between the square of the refractive index (n_D^2) and ε_∞, that is, $\varepsilon_\infty - n_D^2$. The experimentally measured n_D for these ILs lies in the range ~1.4-1.6 (or n_D^2 ~1.96-2.56)[1,43,44] and hence $\varepsilon_\infty - n_D^2$ is appreciable for several of these ILs (see Table A10; Appendix A) indicating a missing faster component inaccessible to the relevant DR measurements.[30] Such an argument can explain the better agreement between theory and experiments for $[Im_{41}][PF_6]$ and the disagreement for other ILs but not for $[S_{222}][Tf_2N]$ as ε_∞ ($\varepsilon_\infty = \varepsilon_0 - \sum_i \Delta S_i$) is reported to be nearly 2 for $[S_{222}][Tf_2N]$. Interestingly, this observation correlates well with the apprehension[34] that the experimental $\varepsilon(\omega)$ for $[S_{222}][Tf_2N]$ may not be accurate due to its high conductivity and thus requires revision. Such an observation notwithstanding, the ratio between calculated and measured average solvation times summarized in the last column of Table 4.4 suggests that, the present theory provides a better description of the experimental dynamics than that by the continuum model[1] for most of the ILs considered here. Note that such an improved description has become possible via allowing molecularity of both the solute and solvent particles through the systematic incorporation of solute-solvent and solvent-solvent static correlations. In addition, the agreement between theory and experiments may be further improved upon by the inclusion of high frequency response in these ILs accounting for the missing dielectric dispersion gap, $\varepsilon_\infty - n_D^2$. Next we present results from such an investigation.

4.3.3 Stokes Shift Dynamics: Effects of IL Libration

Terahertz time-domain spectroscopic measurements involving metallocenium ionic liquid[45] has shown that the librational motion of the cations as well as the inter-ion vibration between the cations and anions are responsible for observed dynamics in THz region. It has also been shown that the bands appear in the frequency range of ~20-50 cm^{-1} show the maximum

amplitude. Moreover, $\varepsilon(\omega)$ measured in the frequency range of $0.1 \le \nu/GHz \le 3000$ contains dispersion contribution from librational modes around ~70-120 cm^{-1} for several imidazolium ILs.[33] Consequently, we have ascribed the missing dispersion, $\varepsilon_\infty - n_D^2$, to a libration mode at 30 cm^{-1} for all the ILs studied here and incorporated in our calculations as follows:[8,33] $\varepsilon(\omega) = \varepsilon_\infty + \sum_i \Delta S_i / [1 + (\omega\tau_i)^{1-\alpha_i}]^{\beta_i} + [\Delta S_{lib}\Omega^2 / (\Omega^2 + \omega^2 + \omega\Gamma)]$ with the damping constant (Γ) being approximately twice as large as the resonating frequency (Ω), and $\Delta S_{lib} = \varepsilon_\infty - n_D^2$. Note a little variation in Ω will not affect the qualitative understanding regarding the role of this collective mode in producing the sub-picosecond response in these ILs.

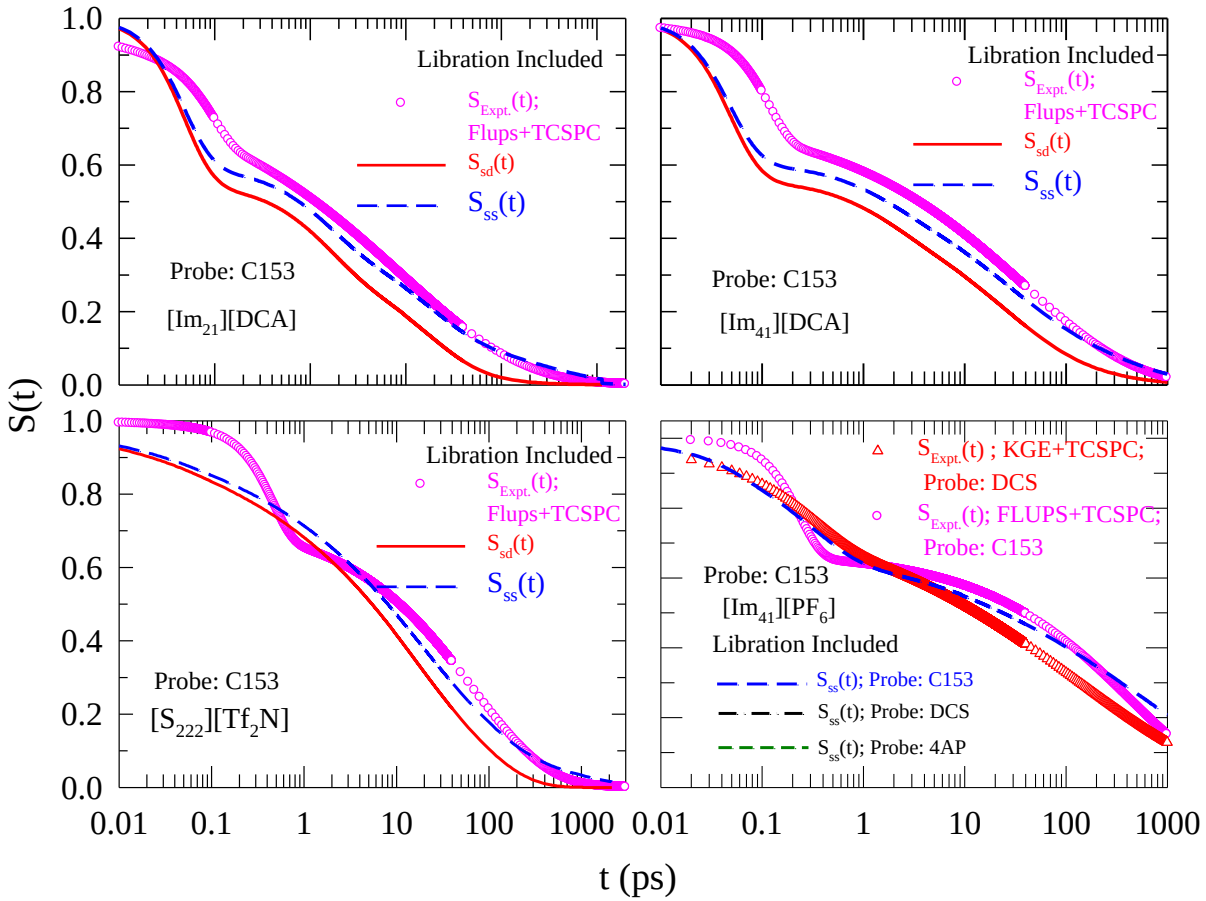

Fig. 4.2: Effect of added librational band on theoretically predicted solvation energy relaxations and comparison with experimentally measured response.

Table 4.5: Fitting parameters of the solvation response decays of C153 in ionic liquids using modified experimental dielectric relaxation.

ILs	$S(t)$	a_1	τ_1 (ps)	a_2	τ_2 (ps)	β	$\langle\tau_{solv}\rangle$ (ns)	$\langle\tau_{solv}\rangle^{theo.}/\langle\tau_{solv}\rangle^{expt.}$
$[Im_{21}]$ $[DCA]$	$S_{sd}(t)$	0.33	0.05	0.67	5.53	0.42	0.008	1.09
	$S_{si}(t)$	0.38	90.5	0.62	825	1	0.532	
	$S_{ss}(t)$	0.27	0.06	0.73	9.54	0.29	0.025	
	$S_{expt.}(t)$	0.18	0.10	0.82	9.00	0.34	0.023	
$[Im_{41}]$ $[DCA]$	$S_{sd}(t)$	0.15	0.10	0.85	35.2	0.49	0.062	1.31
	$S_{si}(t)$	0.41	129	0.59	1137	1	0.691	
	$S_{ss}(t)$	0.13	0.12	0.87	52.0	0.38	0.093	
	$S_{expt.}(t)$	0.27	0.12	0.73	40	0.40	0.071	
$[Im_{41}]$ $[BF_4]$	$S_{sd}(t)$	0.28	0.07	0.72	32.4	0.27	0.165	1.26
	$S_{si}(t)$	0.41	336	0.59	3094	1	1.870	
	$S_{ss}(t)$	0.30	0.08	0.70	86.8	0.29	0.245	
	$S_{expt.}(t)$	0.34	0.20	0.66	170	0.48	0.194	
$[Im_{41}]$ $[PF_6]$	$S_{sd}(t)$	0.31	0.23	0.69	277	0.34	0.674	1.97
	$S_{si}(t)$	0.47	1667	0.53	10000	1	5.899	
	$S_{ss}(t)$	0.29	0.24	0.71	499	0.34	1.095	
	$S_{expt.}(t)$	0.33	0.24	0.67	450	0.50	0.556	
$[Im_{61}]$ $[TF_2N]$	$S_{sd}(t)$	0.15	0.06	0.85	57.6	0.35	0.168	1.16
	$S_{si}(t)$	0.30	308	0.70	3335	1	2.326	
	$S_{ss}(t)$	0.12	0.06	0.88	93.8	0.33	0.334	
	$S_{expt.}(t)$	0.22	0.30	0.78	250	0.55	0.288	
$[Im_{81}]$ $[TF_2N]$	$S_{sd}(t)$	0.19	0.05	0.81	190	0.40	0.382	1.23
	$S_{si}(t)$	0.38	796	0.62	5243	1	3.396	
	$S_{ss}(t)$	0.16	0.04	0.84	293	0.38	0.689	
	$S_{expt.}(t)$	0.13	0.46	0.87	400	0.52	0.559	
$[Pr_{41}]$ $[TF_2N]$	$S_{sd}(t)$	0.11	0.04	0.89	26.9	0.40	0.061	0.60
	$S_{si}(t)$	0.45	642	0.55	4156	1	2.450	
	$S_{ss}(t)$	0.05	0.04	0.95	38.3	0.34	0.139	
	$S_{expt.}(t)$	0.33	0.43	0.67	210	0.54	0.230	
$[S_{222}]$ $[TF_2N]$	$S_{sd}(t)$	0.08	0.03	0.92	16.9	0.43	0.043	1.27
	$S_{si}(t)$	0.38	189	0.62	1634	1	1.036	
	$S_{ss}(t)$	0.02	0.01	0.98	23.1	0.37	0.095	
	$S_{expt.}(t)$	0.28	0.47	0.72	70.0	0.54	0.075	

Fig. 4.2 depicts solvation response calculated after incorporating the libration contribution as discussed above for a few representative ILs and compares with the available C153/(FLUPS+TCSPC) data.[1] Clearly, inclusion of libration contribution leads to better agreement between theory and experiments, particularly, in the time region of sub-picosecond solvation response. In addition, the Gaussian ultrafast response observed in (FLUPS + TCSPC) measurements has been recovered as the calculated response functions fit to the following form: $S_{ss}(t) = a_1 \exp[-(t/\tau_1)^2] + a_2 \exp[-(t/\tau_2)^\beta]$. Note that this (Gaussian + stretched exponential) function fits to both $S_{sd}(t)$ and $S_{ss}(t)$ but not to $S_{si}(t)$ which requires a bi-exponential function. Table 4.5 summarizes the parameters obtained from such fits for eight of the eleven ILs studied here, and similar data for the rest are provided in Table A13 (Appendix A). Evidently, the sub-picosecond response in our calculations originates from the dipole-dipole term, $S_{sd}(t)$, where the libration-included $\varepsilon(\omega)$ has been used as input. In addition, the ratio between the calculated and measured average solvation times, $\langle \tau_{ss} \rangle^{theo} / \langle \tau_{solv} \rangle^{expt.}$, approaches nearer to unity for all the ILs with a marked improvement for [S_{222}][TF_2N] over the calculations without libration contribution. However, β values obtained from the calculated $S_{ss}(t)$ are smaller than those from measurements,[1] suggesting predicted decay kinetics being more inhomogeneous than those observed in experiments. In addition, the predicted ultrafast time constants for several ILs, particularly those with $[TF_2N]^-$ anions, are much shorter than those reported in experiments.[1] This may arise either from inaccuracies in the experimental DR data or from the more complex collective dynamics in THz region than being modelled here for these ILs. This certainly warrants further study.

4.3.4 Stokes Shift Dynamics: Impact of Solute Motion

As the effects of solute motion on its own rate of solvation have been investigated via both calculations[28] and simulations,[6] here we show that the present theory predicts much larger impact of IL libration than solute motion on the ultrafast solvation response in these systems. Fig. 4.3 compares the experimental solvation response obtained for two representative ILs

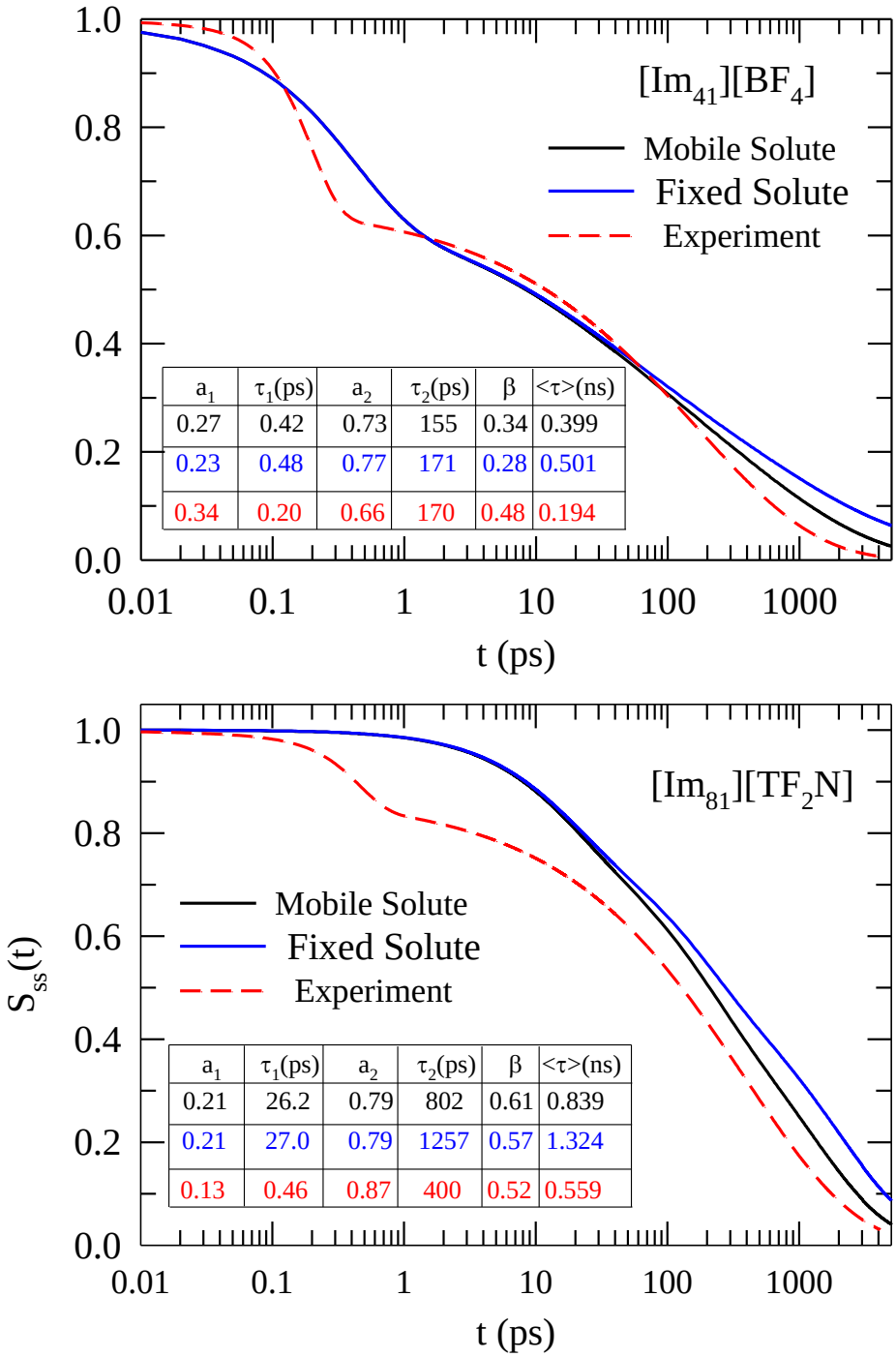

Fig. 4.3: Effect of solute probe-motion on the solvation response of the probe in two ILs.

with those from calculations for fixed and mobile solute cases. Note the fixed solute is motionally frozen with solute translational and rotational diffusion coefficients set to zero

(that is, $D_T = 0$ and $D_R = 0$ in $S^{lm}_{solute}(k,t)$), whereas allowing D_T and D_R to assume values from hydrodynamics (stick conditions used) defined the mobile solute condition. Calculated responses for these ILs have been obtained by using the experimental $\varepsilon(\omega)$ reported in Ref. 30 where libration contributions are not included. The representative calculations shown in this figure demonstrate that solute motion has negligible effects on the initial phase of solvation energy relaxation in both ILs. However, the solute motion accelerates the relaxation at the later stage, bringing in similarity to what has been found for polar solvation dynamics in common dipolar solvents.[27,40] This could be further quantified by considering the weighted amplitudes ($a_i\tau_i$) tabulated in the insets. For example, $a_1\tau_1$ changes by only ~3% for both ILs by allowing solute motion in contrast to ~18% and ~57% change in $a_2\tau_2$ for $[Im_{41}][BF_4]$ and $[Im_{81}][TF_2N]$ ILs, respectively. This change in $a_2\tau_2$ justifies ~26% and ~58% changes (with respect to mobile solute values) in calculated average solvation times in these two ILs. In comparison, incorporation of libration contribution keeping the solute mobile accelerates fast components dramatically (a factor of ~5 for $[Im_{41}][BF_4]$ and ~850 for $[Im_{81}][TF_2N]$!) and slow components by a factor of ~2. Even considering the fact that inaccuracy in experimental DR data may contribute to the unexpectedly large effects of libration, these calculations do show libration regulates the ultrafast solvation timescale and solute motion affects the relatively slower component in these ILs which possess dipolar ion/ions. Moreover, calculated average solvation times becoming faster on allowing solute motion is in general agreement with available simulation results obtained using C153 as probe solute.[6]

4.3.5 Stokes Shift Dynamics: Dependence on Frequency Window of Experimental $\varepsilon(\omega)$

Since the present theory uses experimental $\varepsilon(\omega)$ for determining the solute-IL dipolar interaction contribution to the total dynamics, the calculation scheme becomes naturally sensitive to the DR fit parameters obtained from experimental $\varepsilon(\omega)$ measured in different frequency windows. The accuracy of the fit parameters (and the subsequent assignment to a particular component of the total dielectric response) is largely dependent on the accessible frequency range as information regarding the unobserved dynamics of the medium is gained via extrapolation and fits of the measured response accessed in a limited frequency coverage. This dependency is stronger for conducting media such as the present ILs as accurate

measurements in the low frequency region is severely affected by the inverse-frequency ($1/\omega$) dependence of the generalized polarization response.[46,47] This often leads to spurious determination of ε_0, producing variable estimates for dynamic Stokes shift by the present theory. Non-availability of broader frequency coverage, on the other hand, limits not only the access and interpretation of high frequency response but also affects the mathematical description (Debye, Cole-Cole or Cole-Davidson) of the measured DR for the entire regime. As a result, fit parameters (ΔS_i, τ_i, α and β) representing $\varepsilon(\omega)$ for a given IL differ among measurements employing different frequency windows. This is the source for variation in the calculated solvation response functions (S_{sd} and S_{ss}) for a given IL using $\varepsilon(\omega)$ from different measurements.[30-35]

Fig. 4.4 presents examples of such calculations and subsequent comparison with C153/(FLUPS+TCSPC) data[1] for four ILs, $[Im_{21}][BF_4]$, $[Im_{21}][TF_2N]$, $[Im_{41}][TF_2N]$ and $[Im_{41}][BF_4]$, for which multiple sets of experimental DR data[30-35] are available. Note the calculated responses have been obtained without including the modeled libration contribution to the experimental $\varepsilon(\omega)$.[30-35] As expected, the use of DR data measured in $0.001 \le \nu/GHz \le 20$ window cannot describe the experimental solvation response in $[Im_{21}][BF_4]$, $[Im_{21}][TF_2N]$ and $[Im_{41}][TF_2N]$, particularly at the short-time regime. The agreement improves upon use of $\varepsilon(\omega)$ measured with wider frequency window for these ILs. Inspection of the relevant DR data[30-32,35] given in Table A10 (Appendix A) reveals that the use of broader frequency coverage not only changes the qualitative description of measured $\varepsilon(\omega)$ but also includes faster timescales which affect the over-all agreement between theory and experiments. Also note that the distinct biphasic character of C153/(FLUPS+TCSPC) data is visible only when $\varepsilon(\omega)$ with broader frequency coverage are used. Similar calculations for $[Im_{41}][BF_4]$ and subsequent comparisons with experiments[1] highlights another interesting aspect. For this IL if one uses $\varepsilon(\omega)$ measured in the frequency window of $0.001 \le \nu/GHz \le 3000$,[33] the calculated response becomes much faster than experiments for the entire time-regime. In contrast, a much better agreement is achieved by using $\varepsilon(\omega)$ measured in the frequency range, 0.2-89 GHz.[30] Such a large difference between the

calculations arises because of the presence of libration contribution in $\varepsilon(\omega)$ measured in the wider frequency window[33] but not in the other one. Over-estimation of this high frequency contribution (reflected by the estimated ε_∞ to be much less than n_D^2) in the DR measurements with wider window is one of the possible reasons for the observed difference between experiments and the relevant calculations.

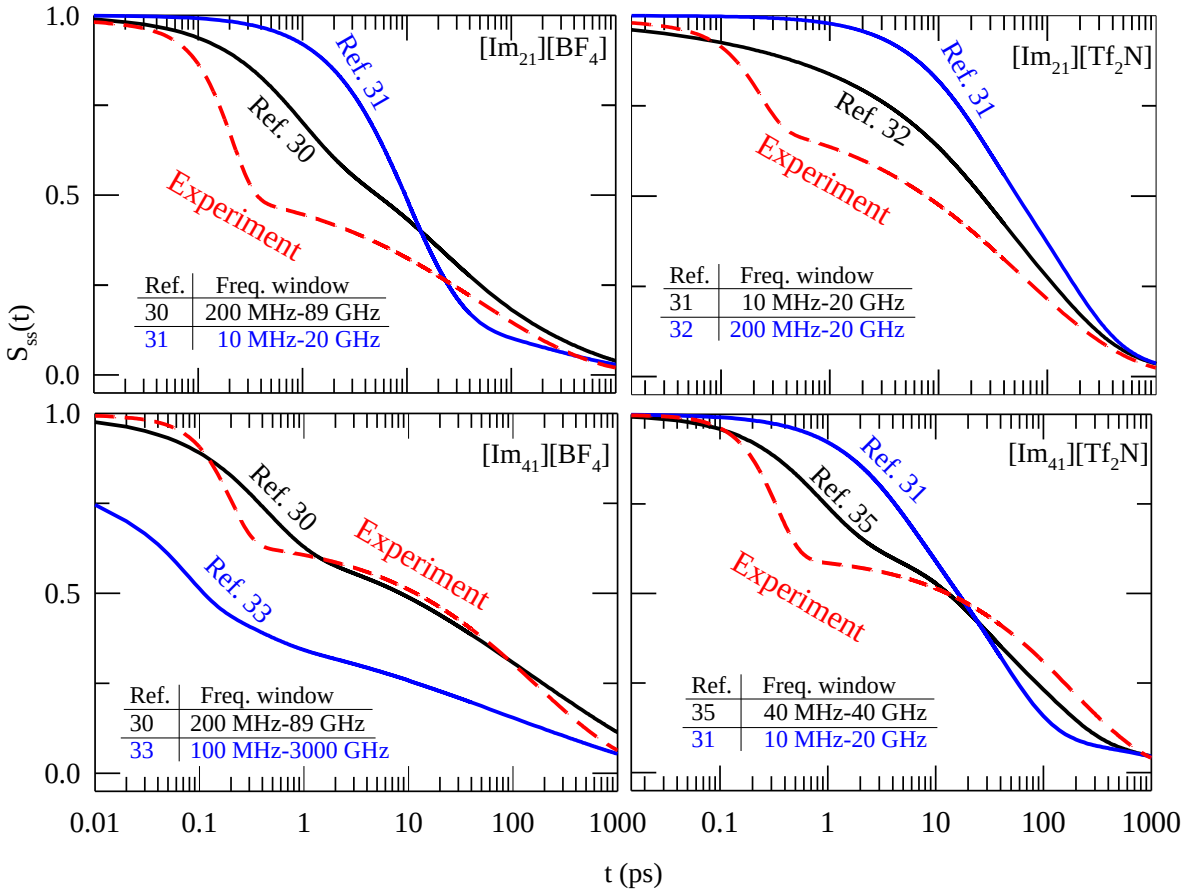

Fig. 4.4: Figure showing the sensitivity of calculated solvation response function to experimental $\varepsilon(\omega)$ measured with different frequency coverage.

4.3.6 Validity of Hydrodynamic Relation

Next we reexamine the agreement between theoretically predicted and (FLUPS/TCSPC) measured average solvation times for C153 in these ILs, and validity of hydrodynamics by

showing in Fig. 4.5 the average times ($<\tau_{ss}>^{theo.}$ and $<\tau_{solv}>^{expt.}$) as a function of temperature-reduced viscosity (η/T). The calculated times (open symbols) have been obtained by using experimental $\varepsilon(\omega)$ having different frequency coverage[30-35] as well as in the absence and presence of the 30 cm^{-1} libration contribution. Note the calculated times using DR data from different sources neither vary widely from each other for a given IL nor deviate much from experiments. This indicates a general validity of these DR data in describing qualitatively correctly the orientational polarization relaxation of these Coulomb fluids. The dominance of the slow timescales in average times suppresses any discrepancies at the initial phase of the solvation energy relaxation, making the agreement between theory and experiments appear better than had the time-profile of the relaxations been compared. The correlation line (short dashed line) constructed after considering experimental and calculated times together provides a $(\eta/T)^p$ dependence for average solvation times with $p = 1.3$ which corroborates well with $p = 1.2 \pm 0.2$ obtained in experiments via correlating the slow structural relaxation timescales to IL viscosity.[1] These values of p are also in good agreement with earlier prediction (p = 1.16) from theoretical study of temperature dependent Stokes shift dynamics in several imidazolium ILs.[9] Note in the present theory the slow timescale arises mainly from the relaxation of the ion dynamic structure factor through centre-of-mass motion and thus coupled to medium viscosity. Interestingly, time-resolved fluorescence measurements using C153 in (amide + electrolyte) deep eutectics[48-52] reveal p values much less than unity although viscosity of these mixtures are comparable to several ILs studied here.

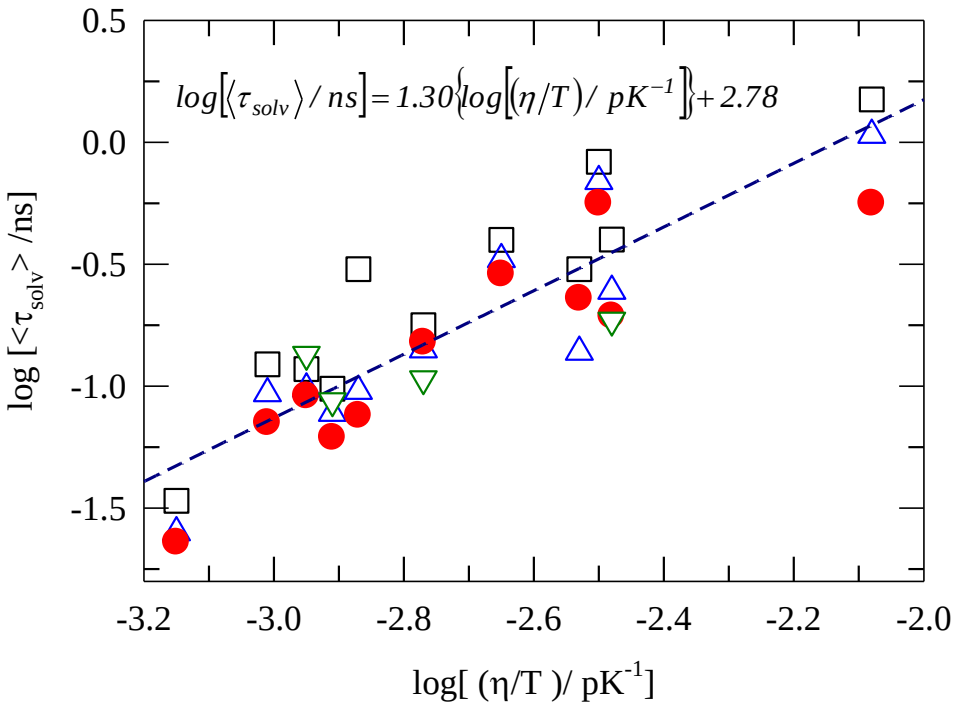

Fig. 4.5: The figure showing the close agreement between the calculated and measured average solvation time and also the validity of hydrodynamical relation.

4.4 Conclusion

Let us first summarize the interesting results of this chapter. First, no significant probe dependence of Stokes shift dynamics in these ILs has been observed while carrying out calculations for probes with the sizes and excited dipole moments of C153, DCS and 4-AP. However, the magnitude of the dynamic shift changes upon changing the excited state dipole moment of the solute considered. Second, the solute motion has been found to affect the long time rate of its own solvation in these liquids, and consideration of self-motion brings the predicted longtime dynamics closer to experiments. Third, inclusion of ultrafast liquid dynamics via assigning a libration contribution to the missing part of measured $\varepsilon(\omega)$ leads to much better agreement between theory and experiments in most of the ILs considered here. Importantly, ultrafast Gaussian component, as observed in experiments, has been recovered only after inclusion of the libration contribution in the calculations. The present calculations also highlight the importance of improved DR measurements for several ILs for which use of existing experimental $\varepsilon(\omega)$ have not been able to successfully track the

C153/(FLUPS+TCSPC) data. Fourth, use of experimental $\varepsilon(\omega)$ measured with different frequency windows in our calculations leads to variations in predicted time-profile of the solvation energy relaxation in a given IL. Quite naturally, $\varepsilon(\omega)$ measured with broader frequency coverage and better description of IL polarization dynamics have led to closer agreement between calculated and measured solvation response functions. Interestingly, average solvation times calculated using experimental $\varepsilon(\omega)$ with different frequency windows vary neither appreciably from each other nor deviate strongly from those measured in experiments. Importantly, incorporation of molecularity in the present theory via solute-solvent and solvent-solvent static correlations has led to better predictions of experimental average solvation times than that produced by the dielectric relaxation based continuum model analyses[1] for these ILs.

The success of the present theory in predicting experimental Stokes shift dynamics does not, however, suggest non-importance of spatial heterogeneity in ILs which have not been considered at all here while obtaining the static correlations.[41-42, 53-54] The present theory models the total solvation energy relaxation in these ILs as a sum of solute-solvent dipole-dipole and ion-dipole interaction contributions with a dominating role for dipole-dipole contribution in the total relaxation. It has already been shown[13] that collective solvent fluctuations (that is, $k\sigma \to 0$ modes) dominate the relaxation of solute-IL dipole-dipole interaction contribution, and the participation of the nearest neighbor ($k\sigma \to 2\pi$) solvent modes comes at a later time. In such a scenario, systematic inclusion of spatial heterogeneity will modify only the later part of the dynamics, leaving the qualitative understanding generated by the present scheme unchanged. Another important issue is the consistent prediction of an extremely slow timescale in ~1-10 ns range by the solute-IL ion-dipole interaction contribution for these ILs which has not been detected by dynamic Stokes shift measurements.[1-4] An indication of such a slow component has been observed in time-resolved fluorescence measurements with ILs at low temperatures,[55] and all-atom simulations of single particle reorientational correlation functions for a room temperature IL[56] have also hinted at the presence of such an extremely slow timescale. Further work is necessary in this direction in order for developing a robust understanding of dynamics in and of ionic liquids.

References

1. Zhang, X. –X.; Liang, M.; Ernsting, N. P.; Maroncelli, M. *J. Phys. Chem. B* **2013**, *117*, 4291.
2. Arzhantsev, S.; Jin, H.; Baker, G. A.; Maroncelli, M. *J. Phys. Chem. B* **2007**, *111*, 4978-4989.
3. Arzhantsev, S.; Jin, H.; Ito, N.; Maroncelli, M. *Chem. Phys. Lett.* **2006**, *417*, 524-529.
4. (a) Samanta, A. *J. Phys. Chem. Lett.* **2010**, *1*, 1557; (b) Samanta, A. *J. Phys. Chem. B* **2006**, *110*, 13704; (c) Mandal, P. K.; Sarkar, M.; Samanta, A. *J. Phys. Chem. A* **2004**, *108*, 9048.
5. (a) Adhikari, A.; Sahu, A. K.; Dey, S.; Ghosh, S.; Mandal, U.; Bhattacharyya, K. *J. Phys. Chem. B* **2007**, *111*, 12809; (b) Sasmal, D. K.; Mandal, A. K. Mandal, T.; Bhattacharyya, K. *J. Phys. Chem. B* **2011**, *115*, 7781.
6. Roy, D.; Maroncelli, M. *J. Phys. Chem. B* **2007**, *116*, 5951.
7. Maroncelli, M.; Zhang, X. –X.; Liang, M.; Roy, D.; Ernsting, N. P. *Faraday Discuss. Chem. Soc.* **2012**, *154*, 409-424.
8. (a) Kashyap, H. K.; Biswas R. *J. Phys. Chem. B* **2008**, *112*, 12431; (b) Kashyap, H. K.; Biswas, R. *J. Phys. Chem. B* **2010**, *114*, 254.
9. Kashyap, H. K.; Biswas, R. *J. Phys. Chem. B* **2010**, *114*, 16811.
10. Daschakraborty, S.; Biswas, R. *J. Phys. Chem. B* **2011**, *115*, 4011.
11. Daschakraborty, S.; Biswas, R. *Chem. Phys. Lett.* **2011**, *510*, 202.
12. Daschakraborty, S.; Biswas, R. *Chem. Phys. Lett.* **2012**, *545*, 54.
13. Daschakraborty, S.; Biswas, R. *J. Chem. Phys.* **2012**, *137*, 114501.
14. Muramatsu, M.; Nagasawa, Y.; Miyasaka, H. *J. Phys. Chem. A* **2011**, *115*, 3886.
15. (a) Das, S. K.; Sahu, P. K.; Sarkar, M. *J. Phys. Chem. B* **2013**, *117*, 636; (b) Das, S. K.; Sarkar, M. *ChemPhysChem*, **2012**, 13,2761.
16. (a) Jeong, D.; Shim, Y.; Choi, M. Y.; Kim, H. J. *J. Phys. Chem. B* **2007**, *111*, 4920; (b) Shim, Y.; Choi, M. Y.; Kim, H. J. *J. Chem. Phys.* **2005,** *122*, 044511.
17. Shim, Y.; Duan, J.; Choi, M. Y.; Kim, H. J. J. Chem. Phys. **2003**, *119*, 6411.
18. Shim, Y.; Kim, H. J. *J. Phys. Chem. B* **2008**, *112*, 11028.
19. Shim Y.; Kim, H. J. *J. Phys. Chem. B* **2009**, *113*, 12964.
20. Shim Y.; Kim, H. J. *J. Phys. Chem. B* **2007**, *111*, 4510.
21. Shim, Y.; Jeong, D.; Choi, M. Y.; Kim, H. J. *J. Chem. Phys.* **2006**, *125*, 061102.

22. Streeter, I.; Lynden-Bell, R. M.; Compton, R. G. *J. Phys. Chem. C* **2008**, *112*, 14538.
23. Bhargava, B. L.; Balasubramanian, S. *J. Chem. Phys.* **2005**, *123*, 144505.
24. Kobrak, M. N.; Znamenskiy, V. *Chem. Phys. Lett.* **2004**, *395*, 127.
25. Kobrak, M. N. *J. Chem. Phys.* **2006**, *125*, 064502.
26. Kobrak, M. N. *J. Chem. Phys.* **2007**, *127*, 184507.
27. Bagchi, B.; Biswas, R. *Adv. Chem. Phys.* **1999**, *109*, 207.
28. Kashyap, H. K.; Biswas R. *Ind. J. Chem.* **2010**, *49A*, 685.
29. Biswas, R.; Bagchi, B. *J. Phys. Chem.* **1996,** *100*, 1238.
30. Hunger, J.; Stoppa, A.; Schrodle, S.; Hefter, G.; Buchner, R. *ChemPhysChem* **2009**, *10*, 723.
31. Nakamura, K.; Shikata, T. *ChemPhysChem* **2010**, *11*, 285.
32. Daguenet, C.; Dyson, P. J.; Krossing, I.; Oleinikova, A.; Slattery, J. M.; Wakai, C.; Weingärtner, H. J. Phys. Chem. B **2006**, *110*, 12682.
33. Stoppa, A.; Hunger, J.; Buchner, R.; Hefter, G.; Thoman, A.; Helm, H. *J. Phys. Chem. B* **2008**, *112*, 4854.
34. Weingärtner, H.; Sasisanker, P.; Daguenet, C.; Dyson, P. J.; Krossing, I.; Slattery, J. M.; Schubert, T. *J. Phys. Chem. B* **2007**, *111*, 4775.
35. Mizoshiri, M.; Nagao, T.; Mizoguchi, Y.; Yao, M. *J. Chem. Phys*. **2010**, *132*, 164510.
36. Roy, S.; Bagchi, B. *J. Chem. Phys.* **1993**, *99*, 9938.
37. Roy, S.; Bagchi, B. *J. Chem. Phys.* **1993**, *99*, 1310.
38. Nandi, N.; Roy, S.; Bagchi, B. *J. Chem. Phys.* **1995**, *102*, 1390.
39. Kashyap, H. K.; Biswas, R. *J. Chem. Phys.* **2006**, *125*, 174506.
40. Biswas, R.; Bagchi, B. *J. Phys. Chem. B* **1996**, *100*, 4261.
41. Triolo, A.; Russina, O.; Bleif, H.; Cola, E. D. *J. Phys. Chem. B* **2007**, *111*, 4641.
42. Wang, Y.; Voth, G. A. *J. Am. Chem. Soc.* **2005**, *127*, 12192.
43. Froba, A. P.; Kremer, H.; Leipertz, A. *J. Phys. Chem. B* **2008**, *112*, 12420.
44. Huddleston, J. G.; Visser, A. E.; Reichert, W. M.; Willauer, H. D.; Broker, G. A.; Rogers, R. D. *Green Chemistry* **2001**, *3*, 156.
45. Chakraborty, A.; Inagaki, T.; Banno, M.; Mochida, T.; Tominaga, K. *J. Phys. Chem. A* **2011**, *115*, 1313.
46. Schroder, C.; Hunger, J.; Stoppa, A.; Buchner, R.; Steinhauser, O. *J. Chem. Phys.* **2008,** *129*, 184501.
47. Caillol, J. M.; Levesque, D.; Weis, J. J. *J. Chem. Phys.* **1989,** *91*, 5555.

48. Guchhait, B.; Gazi, H. A. R.; Kashyap, H. K.; Biswas, R. *J. Phys. Chem. B* **2010**, *114*, 5066.
49. Gazi, H. A. R.; Guchhait, B.; Daschakraborty, S.; Biswas, R. *Chem. Phys. Lett.* **2011**, *501*, 358.
50. Guchhait, B.; Daschakraborty, S.; Biswas, R. *J. Chem. Phys.* **2012,** *136*, 174503.
51. Das, A.; Das, S.; Biswas, R. *Chem. Phys. Lett.* **2013** (in press); doi:j.cplett,2013.07.013.
52. Pal, T.; Biswas, R. *Chem. Phys. Lett.* **2011**, *517*, 180.
53. Castner, E. W. Jr.; Margulis, C. J.; Maroncelli, M.; Wishart, J. F. *Annu. Rev. Phys. Chem.* **62**, 85.
54. Hardacre, C.; Holbrey, J. D.; MacMath, S. E. J.; Bowron, D. T.; Soper, A. K. *J. Chem. Phys.* **2003,** *118*, 273.
55. Funston, A. M.; Fadeeva, T. A.; Wishart, J. F.; Castner, E. W. Jr. *J. Phys. Chem. B* **2007**, *111*, 4963
56. Pal, T.; Biswas, R. *Theo. Chem. Acc.* **2013**, *132*, 1348.

Chapter 5

Ultrafast Solvation Response in Room Temperature Ionic Liquids: Possible Origin, and Importance of the Collective and the Nearest Neighbour Solvent Modes

5.1 Introduction

Recent three pulse photon echo peak shift (3PEPS) measurements[1] using an organic dye, oxazine 4 (Ox4), in a phosphonium and several imidazolium ionic liquids (ILs) at room temperature have revealed multi-exponential solvation response function possessing an ultrafast component (~10-25%) with time constant (τ_1) in 20-220 femtosecond range, followed by a slower component with time constant (τ_2) spreading over nearly a picosecond to a few picoseconds. In some imidazolium ILs another much slower component with time constant in the range, $20 < \tau_3 / ps < 65$, has also been reported. These results are quite striking because of the following reasons: (i) the ultrafast timescale reported by 3PEPS measurements are much faster than those observed in the dynamic Stokes shift (DSS) experiments where complete detection of the dynamics has been performed[2] and (ii) these measurements report, for the first time, sub-hundred femtosecond solvation timescale even for a phosphonium IL which, in earlier complete DSS measurements,[3] showed stretched exponential response with only one relaxation time constant of ~2 ns. Table 5.1 summarizes the solvation time constants reported by the 3PEPS and DSS measurements for some of these RTILS which brings out clearly the differences stated above. Understanding the molecular origin behind such an observation constitutes the central theme of the present work where attempts have been made to ascertain mechanisms for ultrafast solvation revealed by these two different experimental methods.

The above theme then necessitates the following, somewhat detail, discussion of the results obtained by the 3PEPS and DSS measurements. These 3PEPS measurements have used oxazine 4 (Ox4) as a probe molecule which shows steady state Stokes shift values in 200-500 cm^{-1} range for these RTILs. Such a small shift is in fact a characteristic[4] for Ox4 and can

probably be attributed to its weakly polar ground (S_0) and even less polar excited (S_1) states.[5]

Table 5.1: Comparison of solvation time constants reported by 3PEPS and DSS measurements

Ionic Liquid	Route	τ_1 (fs)	τ_2 (ps)	τ_3 (ps)
[Bmim][BF_4]	3PEPS	110	1.1	21
	DSS	320		130
[Bmim][PF_6]	3PEPS	150	2.2	64
	DSS	330		140
[Bmim][TFSI]	3PEPS	26	0.54	
	DSS	740		78
[Phos][Cl]	3PEPS	24	0.53	
	DSS	×	×	1860

Moreover, it has been found that solvent dependence of ultrafast solvation dynamics of Ox4 in conventional molecular liquids cannot be described by dielectric relaxation based theories.[6-10] DSS measurements, on the other hand, have employed dipolar chromophores such as coumarin 153 (C153),[3,11-14] 4-aminophthalimide (4AP)[15] and trans-4-dimethylamino-4'-cyanostilbene (DCS)[2] which undergo large dipole moment changes upon excitation. As a result, Stokes shift values for these probes in phosphonium and imidazolium ionic liquids have been found to be approximately an order of magnitude larger than those with Ox4, and dynamic response explainable by a semi-molecular theory[16-21] that uses experimental dielectric relaxation data[22-25] as inputs. These contrasting results along with those discussed in the above paragraph then give rise to the following question: Do 3PEPS and DSS experiments probe different aspects of solute-solvent interaction while measuring the solvation energy relaxation in these RTILs? The question becomes even more pertinent when one recalls that earlier 3PEPS studies of solvation dynamics in ambient alcohols (albeit with different solutes)[26] produced much faster timescales than those reported by DSS[27] and

transient absorption (TA)[28] measurements, and subsequently, a possible resolution to the debate in terms of solute-solvent nearest neighbour non-polar type interaction was provided.[29] Since peak shift in 3PEPS measurements is related to the line-broadening function[30,31] which is determined by the total solvation energy correlation function and Stokes shift,[26,29] it is quite natural that both polar and non-polar solute-solvent interaction energies contribute to the observed dynamics. Moreover, experimental studies of non-dipolar solvation dynamics in conventional molecular solvents[32-36] have revealed Stokes shift ranging from a few hundred to several hundred cm^{-1}, which is much smaller than those observed in the cases of polar solvation. All these indicate a possible role for non-dipolar solvation dynamics to the timescales measured by the 3PEPS experiments. One therefore needs to investigate the timescales that may arise from interactions which possess spatial dependence shorter-ranged than the dipole-dipole ($u_{id} \propto r^{-3}$) interaction.

What we do next is as follows. Relatively smaller Stokes shift for Ox4 in seven different ILs,[1] namely, [Bmim][Cl], [Bmim][BF_4], [Bmim][PF_6], [Bmim][TFSI], [Emim][TFSI], [Hmim][TFSI] and [Phos][Cl] motivates us to assume solute-IL interaction is primarily non-dipolar in nature. The chemical structures of these RTILs, and probe molecules, Ox4 are shown in Scheme 5.1. C153 molecule has been seen in Scheme 2.1 (Chapter 2). For simplicity, we approximate the non-dipolar interaction as purely a non-polar interaction given by the conventional Lennard-Jones (LJ) 6-12 interaction.[36] The total dynamics is predicted in terms of solute-solvent binary collision and collective structural relaxation through a mode-coupling approach.[37-39] Evidently, the binary collision part describes the initial ultrafast response where solvent distribution around a solute at extremely short time is approximated by the equilibrium radial distribution function.[36] This amounts to stating that the solute is trapped inside a solvent cage at short time where collision against the solvent cage carries out the initial phase of the solvation energy relaxation. The structural relaxation part, governed by the solvent density fluctuations (and hence connected to the medium viscosity), then takes over and accounts for the slower component of the total solvation energy relaxation.[40] In other words, a clear separation between the collisional and density fluctuation timescales are assumed apriori. The timescales associated with the nearest neighbour ($k\sigma \to 2\pi$) and collective ($k\sigma \to 0$) solvent density modes for the structural relaxation part are then explored. Subsequently, the origin for the ultrafast polar solvation response is investigated by testing the relation between solvent rotation (here imidazolium

ILs) and polar solvation energy relaxation. Experimental dielectric relaxation data at the microwave frequency range have been used for such an investigation in order to either minimize or avoid contributions from the solvent translation-rotation coupling (conductivity contribution) which appears at the terahertz (THz) regime.[41-43] Finally, a comparative study between the calculated results and those obtained from 3PEPS, DSS and computer simulations[44-57] is presented which suggests that these different experimental methods probe different aspects of the solute-IL interaction.

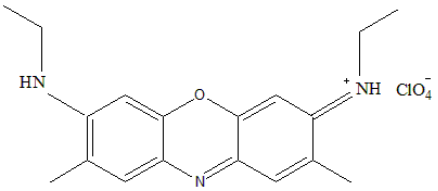

Oxazine 4

Probe molecule

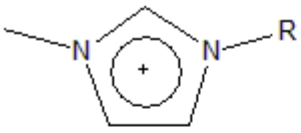

$R = CH_2CH_3$: $[Emim]^+$

$R=(CH_2)_3CH_3$: $[Bmim]^+$

$R=(CH_2)_5CH_3$: $[Hmim]^+$

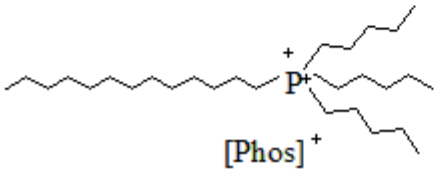

Cl^-

BF_4^-

PF_6^-

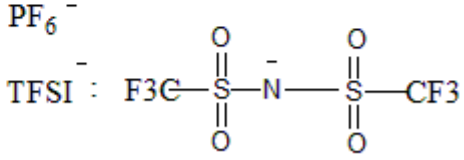

Cations

Anions

Scheme 5.1: Schematic representations of the solute probes and the ions constituting the ionic liquids considered in the present work

5.2 Theory and Calculation Details

The normalized solvation energy-energy time correlation function, $S_{NP}(t)$, for the solute interacting with the solvent molecules via nonpolar interaction can be written as[39]

$$S_{NP}(t) = \frac{C_{EE}^{NP}(t)}{C_{EE}^{NP}(t=0)}, \tag{5.1}$$

where $C_{EE}^{NP}(t)$ is the un-normalized nonpolar solvation energy time correlation function. Following the prescription described earlier,[39] $C_{EE}^{NP}(t)$ can be given by the following expression

$$C_{EE}^{NP}(t) = C_{EE}^{B}(t=0)\exp[-(t/\tau_E^B)^2] + C_{\rho\rho}(t), \tag{5.2}$$

where τ_E^B is the relaxation time of the binary part of the energy-energy correlation function and is given by[39]

$$\tau_E^B = \sqrt{\frac{-2C_{EE}^{B}(t=0)}{\ddot{C}_{EE}^{B}(t=0)}}, \tag{5.3}$$

where $\ddot{C}_{EE}^{B}(t) = \frac{d^2 C_{EE}^{B}(t)}{dt^2}$. At extremely short times, this binary part is determined by the solute-solvent interaction potential ($v_{12}(r)$) where the solvent distribution around the solute can be approximated by the solute-solvent radial distribution function, $g_{12}(r)$, weighted by the solvent density (ρ)[39,58]

$$C_{EE}^{B}(t=0) = 4\pi\rho\int_0^\infty dr\, r^2 [v_{12}(r)]^2 g_{12}(r), \tag{5.4}$$

and

$$\ddot{C}_{EE}^{B}(t=0) = \frac{4\pi\rho}{m^*}\int_0^\infty dr\, r^2 [v_{12}(r)]^2 \nabla_r g_{12}(r) \nabla_r v_{12}(r), \tag{5.5}$$

where m^* denote the reduced mass of the solute-solvent composite system. Note in the above expressions the following equality has been used: $G_{12}(r, t=0) = g_{12}(r)$, where $G_{12}(r,t)$ represent the distinct part of the van Hove correlation function.[36]

The slowly varying, density fluctuation contribution, $C_{\rho\rho}(t)$, is approximated as,[40]

$$C_{\rho\rho}(t) = \frac{(k_B T)^2 \rho}{6\pi^2} \int_0^\infty dk\, k^2 c_{12}^2(k) S(k,t), \tag{5.6}$$

$c_{12}(k)$ being the wave-number (k) dependent solute-solvent direct correlation function and $k_B T$ the Boltzmann constant times the absolute temperature. $c_{12}(k)$ has been obtained by using the Weeks-Chandler-Andersen (WCA) scheme.[59] Subseuqently, the dynamic solvent structure factor, $S(k,t)$, has been calculated by using the relation[37,60]

$$S(k,t) = L^{-1}\left[\frac{S(k)}{z + \left\langle \omega_k^2 \right\rangle \left[z + \Delta_k \left(z + \tau_k^{-1} \right)^{-1} \right]^{-1}} \right], \tag{5.7}$$

where L^{-1} denotes the Laplace inversion operator which is performed numerically by using the Stehfest algorithm.[61] z is the frequency. The static solvent structure factor, $S(k)$, is obtained from the solutions of the Percus-Yevick (PY) equation for binary mixture of hard spheres.[62] $\left\langle \omega_k^2 \right\rangle = \left[k_B T k^2 / m S(k) \right]$, m being the mass of a solvent molecule, $\tau_k^{-1} = 2\sqrt{(\Delta_k / \pi)}$, and $\Delta_k = \omega_l^2(k) - \left\langle \omega_k^2 \right\rangle$. $\omega_l^2(k)$ is the second moment of the longitudinal current correlation function expressed as,[37]

$$\omega_1^2(k) = 3m^{-1}k^2 k_B T + \omega_0^2 + \gamma_d^l(k), \tag{5.8}$$

where the longitudinal component of the vertex function, $\gamma_d^l(k)$, and the Einstein frequency of the solvent, ω_0, can be calculated from the solvent-solvent interaction potential, $v(r)$, and the radial distribution factor, $g(r)$, from the following expressions[37-39]

$$\gamma_d^l(q) = -m^{-1}\rho \int d\boldsymbol{r} \exp(-i\boldsymbol{k}\cdot\boldsymbol{r}) g(r) \frac{\delta^2}{\delta z^2}(v(r)), \tag{5.9}$$

and

$$\omega_0^2 = 3m^{-1}\rho \int d\boldsymbol{r}\, g(r) \nabla^2 v(r). \tag{5.10}$$

It is evident therefore that once the solute-solvent and solvent-solvent interaction potentials (non-polar) are specified, the solvation response function using Eq. 5.1 can be easily evaluated. As already mentioned, we have used the traditional 6-12 LJ potential to represent the solute-solvent and solvent-solvent interactions.

The solute-solvent radial distribution function, $g_{12}(r)$, required in Eqs. (4) and (5), is calculated from partial structure factor.[63,64] The partial structure factors ($S_{ij}(k)$) are the (*i*, *j*) elements of the structure factor matrix ($\mathrm{S}(k)$). For binary mixtures $\mathrm{S}(k)$ is written as following, [63,64]

$$\mathrm{S}(k)=\begin{pmatrix} S_{11} & S_{12} \\ S_{21} & S_{22} \end{pmatrix}. \tag{5.11}$$

Similarly the partial direct correlation function ($c_{ij}(k)$) are the (*i*, *j*) elements of the direct correlation function matrix ($\mathrm{c}(k)$). $\mathrm{S}(k)$, and $\mathrm{c}(k)$ are connected via the following relation

$$\mathrm{S}(q)=[1\text{-}\mathrm{c}(k)]^{-1}, \tag{5.12}$$

where ***1*** denotes the identity matrix.

Hence the partial structure factors can be written as,

$$S_{11}(k)=\left\{1-\rho_1 c_{11}(k)-\frac{\rho_1\rho_2 c_{12}^2(k)}{1-\rho_{22}c_{22}(k)}\right\}^{-1}, \tag{5.13}$$

$$S_{22}(k)=\left\{1-\rho_2 c_{22}(k)-\frac{\rho_1\rho_2 c_{12}^2(k)}{1-\rho_{11}c_{11}(k)}\right\}^{-1}, \tag{5.14}$$

$$S_{12}(k)=(\rho_1\rho_2)^{1/2}c_{12}(k)\{[1-\rho_1 c_{11}(k)][1-\rho_2 c_{22}(k)]-\rho_1\rho_2 c_{12}^2(k)\}^{-1}. \tag{5.15}$$

We have calculated the direct correlation functions, $c_{ij}(k)$, by using the method mentioned earlier [62] via the WCA scheme.

If one considers the ion-ion interaction in addition to the LJ potential for solvent-solvent interaction, solvent-solvent direct correlation functions can be approximated by the pair correlation function ($h_{\alpha\beta}(k)$)[65,66]

$$h_{\alpha\beta}(k)=-\frac{4\pi\, q_\alpha q_\beta}{\varepsilon_0 k_B T(1+\kappa\sigma)}\frac{\kappa^2}{\kappa_D^2(k^2+\kappa^2)}\times\left[\cos k\sigma+\frac{\kappa}{k}\sin k\sigma\right], \tag{5.16}$$

where σ is the ionic diameter, and κ is related to the Debye screening parameter κ_D by

$$\kappa = \frac{\kappa_D}{\left[1-(\kappa_D\sigma)^2/2+(\kappa_D\sigma)^3/6\right]^{1/2}}, \tag{5.17}$$

with

$$\kappa_D = \left(\frac{4\pi}{\varepsilon_0 k_B T}\sum_\alpha \rho_\alpha q_\alpha^2\right)^{1/2}, \tag{5.18}$$

where ε_0 is the static dielectric constant of the medium, ρ_α the density of and q_α the charge on the α^{th} species. Note the Debye screening length, κ_D^{-1}, for these RTILs is even less than 1 A^0 and thus unrealistic as a screening length for these molecular systems.[67,68] In addition, Eq. 5.16 describes static correlations in ionic solutions at the long wavelength (that is, $k\sigma \to 0$) limit. As a result, correlations calculated using Eq. 5.16 is likely to be inaccurate for dynamical events that are regulated by correlations at the molecular length scales. This may lead to improper predictions of RTIL dynamics.

5.3 Numerical Results and Discussions

5.3.1 Ultrafast Solvation Response Measured by 3PEPS Experiments: Possible Origin

Calculated decays of the nonpolar solvation response function, $S_{NP}(t)$, are shown in Fig. 5.1 for five representative RTILs, [Bmim][Cl], [Bmim][BF_4], [Bmim][PF_6], [Bmim][TFSI] and [Phos][Cl]. These calculations are done with solute-IL size ratio, $R = \sigma_{solute}/\sigma_{IL} = 1$, σ being the molecular diameter[2,3,69], and at the respective RTIL densities.[70] Note that fixing the solute-IL size ratio at unity for these calculations may not be quite unphysical as Ox4 (size unavailable) is structurally very similar to C153 whose molecular diameter is known.[27] Data on size ratio provided in Table A14 (Appendix A)[71] suggest that imidazolium ILs, particularly those with non-TFSI anions, possess a size ratio nearly unity against a solute similar to the size of C153. Other parameters necessary for calculations are provided in Table A15 (Appendix A).[71] The calculated decays exhibit an anion dependence which has already been reported by the 3PEPS measurements.[1] A closer inspection of Fig. 5.1 also reveals an anion sequence in terms of non-polar solvation energy decay rate in imidazolium ILs

($Cl^- > BF_4^- > PF_6^-$) which is the same as observed in experiments.[1] However, the decay predicted for [Phos][Cl] is the slowest and thus completely different from the 3PEPS results. Calculated decays shown here are bimodal and nicely fit to a sum of Gaussian and exponential components having the following form: $S_{NP}^{fit}(t) = a_1 \exp\left(-(t/\tau_1)^2\right) + a_2 \exp\left(-t/\tau_2\right)$. Parameters obtained from such fits summarized in Table 5.2 indicate overwhelming dominance (~90%) of the Gaussian component with a time constant (τ_1) in ~100-250 fs range. The slow, exponential component with a time constant (τ_2) of 2-3 ps then carries out the remaining part of the $S_{NP}(t)$ decays in these RTILs. Time constants obtained from 3PEPS measurements are also shown in Table 5.2, and a comparison reveals semi-quantitative agreement between the predicted and measured τ_1 and τ_2 except for [Phos][Cl]. Interestingly, the slowest time constant from 3PEPS measurements (τ_2 = 0.53 ps) for [Phos][Cl] is quite close to τ_1 from theory but the predicted slower time constant (~6 ps) has not been detected in experiments with this RTIL. We have found that equally good description of the calculated decays could be obtained by fitting to a function consisting of a Gaussian and two exponentials producing a third but negligibly small component (~1%) with a time constant (τ_3) in 20-60 ps range (τ_1 and τ_2 remaining more or less unchanged). Although this third time constant is in the same range as found in 3PEPS measurements with some of the imidazolium ILs, the smallness of the associated amplitude does not confidently suggest its real presence in our calculated $S_{NP}(t)$.

The time constants and amplitudes obtained from fits to the $S_{NP}(t)$ decays bear some similarities with those from the simulated solvation response functions for many different ILs with a variety of solutes.[44-57] For example, a very recent simulation study of solvation dynamics in a model IL mimicking [Bmim][PF_6] at 350 K have reported, depending upon solute size and type of solute electronic perturbation, ultrafast Gaussian solvation response characterized by a time scale in ~200-400 fs range with ~30-65% amplitude.[44] Simulation studies of solvation dynamics using model diatomic solutes in [Emim][PF_6] and [Emim][Cl] at 400 K have reported ultrafast Gaussian component (~30-70%) with timescale in ~60-200 fs range.[46-48] This extremely fast timescale with an overwhelming amplitude (80-90%) has also been found in the simulated solvation response for an ionic solute in another IL, [Dmim][PF_6] at 450 K.[52] Simulated solvation response for ions and dipole in [Dmim][Cl] at

425 K suggests an ultrafast Gaussian component with a time constant ~50-60 fs that accounts for nearly 80% of the total solvation energy relaxation.[53] Simulations of solvation dynamics using
realistic solutes, such as betaine-30 and C153, in [Bmim][PF_6] at 300 K has revealed, on the other hand, a much less pronounced Gaussian component (~10-30%) with a time constant of ~200 fs.[54,55] Subsequent simulations involving pyrrolidinium ILs and C153 at 400 K have reported the ultrafast component to be approximately 20% with time constant in ~200-300 fs range.[56,57]

In all the above simulations, the origin of the ultrafast solvation has been attributed to the nearest-neighbour solute-IL interaction. Interestingly, in the present calculations too the ultrafast timescale emerges from the binary interaction of the solute with the molecules in the first solvation shell via the convolution of spatially dependent solute-solvent interaction with solute-solvent radial distribution function (see Eqs. 5.4 and 5.5). According to these equations, it is the solute-solvent radial distribution function at contact (that is, $g_{12}(\sigma)$) that determines the ultrafast collisional timescale at a given liquid density and temperature. Therefore, this description for the ultrafast solvation is equivalent to what is already pointed out by simulations[44-56] and envisaged in Ref. 1 while explaining the 3PEPS results. However, there exists a subtle difference in the sense that the sub-picosecond response in almost all of these simulation studies[44,46-48,53-57] arises from the *electrostatic* solute-IL interaction, whereas the present calculations and the simulation works reported in Ref. 52 suggest non-polar solute-IL interaction as a source for such an initial ultrafast decay. This simulation study[52]

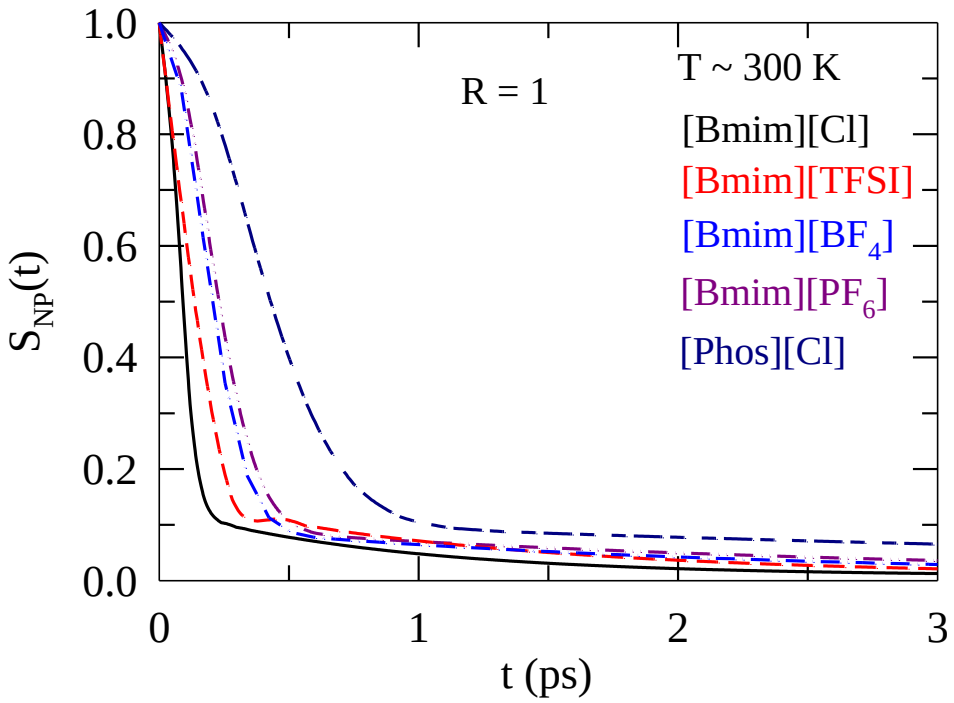

Fig. 5.1: Calculated decays of the nonpolar solvation response function in five different ionic liquids, [Bmim][Cl], [Bmim][TFSI], [Bmim][BF_4], [Bmim][PF_6], and [Phos][Cl] at ~300 K. The solute-solvent size-ratio has been considered to be unity for each of the cases. Note the curves are color coded.

Table 5.2: Comparison between the solvation time constants obtained from the calculated non-polar solvation energy relaxation and those from 3PEPS measurements

Ionic Liquid	Route	a_1	τ_1 (fs)	a_2	τ_2 (ps)	a_3	τ_3 (ps)	$\langle\tau\rangle$ (ps)
[Bmim][Cl]	3PEPS		26		0.54			
	Calculation	0.93	99	0.07	1.99			0.23
[Bmim][BF_4]	3PEPS		110		1.10		21	
	Calculation	0.92	232	0.08	3.01			0.45
[Bmim][PF_6]	3PEPS		150		2.2		64	
	Calculation	0.89	225	0.11	2.76			0.52
[Bmim][TFSI]	3PEPS		210		3.10		52	
	Calculation	0.87	148	0.13	1.62			0.34
[Emim][TFSI]	3PEPS		220		2.70		20	
	Calculation	0.89	183	0.11	2.12			0.40
[Hmim][TFSI]	3PEPS		200		3.30		37	
	Calculation	0.89	210	0.11	2.44			0.46
[Phos][Cl]	3PEPS		24		0.53			
	Calculation			0.89	0.48	0.11	5.75	0.71

monitored fluctuations in both electrostatic and LJ parts of the solute-IL interaction energy and found that equilibrium correlation functions constructed from these individual fluctuating components are characterized by damped oscillations with similar time periods (~350 – 500 fs). The striking resemblance between the calculated and simulated ultrafast timescales and the simulation finding that *the sub-picosecond response is due to changes in the nearest neighbour repulsion*[52] therefore indicate that the solute-IL nearest neighbour non-polar interaction can be one of the possible origins for the ultrafast solvation timescales revealed by the recent 3PEPS measurements[1] for several RTILs.

Before we elaborate further on the role of non-polar solute-solvent interaction in the ultrafast solvation energy relaxation in ILs, let us now explore the region in the density – size ratio ($\rho_N^* - R$) space where the PY approximations[62] for binary hard sphere mixtures provide stable solutions for the direct correlation functions. Here ρ_N denotes the number density of a given IL and $\rho_N^* = \rho_N \sigma_{IL}^3$. Fig. 5.2 demonstrates such a diagram where regions outside the boundary line are inaccessible to the present calculations due to the inability of the existing PY approximations to provide correct solutions for the direct correlation functions. It is evident from this figure that for liquids with densities as high as of these ILs, choice of a solute in the present calculations is rather narrow. For a solute 2-3 times larger than that of an IL molecule, one has to lower the IL density appreciably (from $\rho_N^* \sim 1.3$ to $\rho_N^* \sim 0.7$) in order for the present theory to work. This limitation notwithstanding, the current calculations can be employed to explore the solute size dependence of the ultrafast solvation response in ILs because a significant dependence on solute size has already been predicted for solvation via non-polar mechanism.[40] Such a solute size dependence for [Bmim][Cl] is presented in Fig. 5.3 where in the upper panel the time constants (τ_1 and τ_2) obtained from fits to the $S_{NP}(t)$ decays calculated at $\rho_N^* = 0.7$ are shown as a function of R. Note the fast time constant, τ_1, decreases by about 20% for changing R from 1 to 3 while τ_2 (slower of these two) remains almost insensitive to the size ratio. The origin could be traced in the solute size dependence of the solute-solvent radial distribution function at contact, $g_{12}(\sigma)$, shown in the lower panel of Fig. 5.3, as a function of R. Here also $g_{12}(\sigma)$ increases by ~20% for the same change in R. As $g_{12}(\sigma)$ regulates the solute-solvent interaction via structuring the first

solvation shell, the dependence is more direct and hence the scaling is proportionate. This predicted solute size dependence of ultrafast solvation timescale in ILs may be tested against

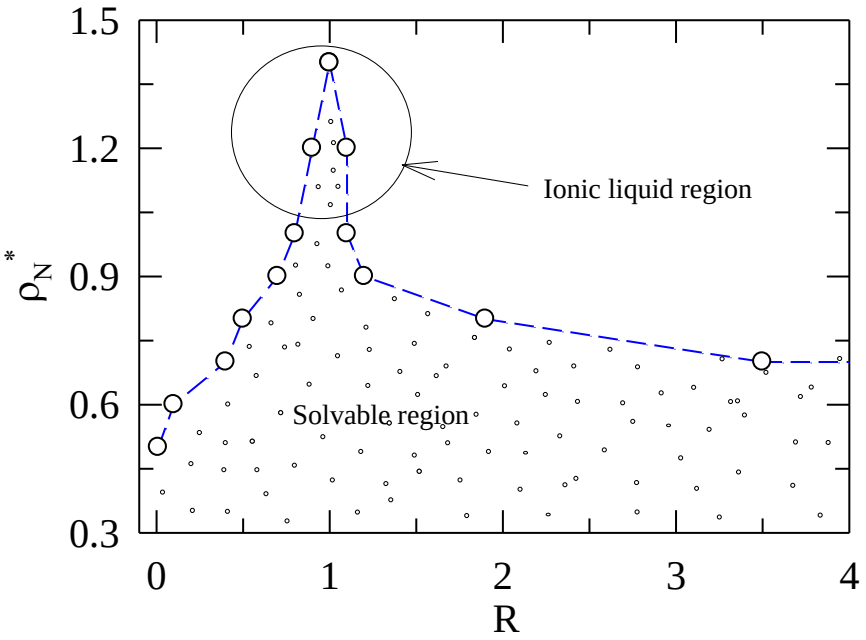

Fig. 5.2: Diagram showing the solvable region in the density – size ratio ($\rho_N^* - R$) space where PY approximations for binary hard sphere mixtures provide stable solutions for the direct correlation functions. R denotes the ratio between the solute and IL sizes. The shaded area is the region where PY approximation works.

3PEPS measurements since the latter can probe more accurately the nearest neighbour ($k\sigma \to 2\pi$) interactions.

The dependence of ultrafast solvation time scale on $g_{12}(\sigma)$ brings into the picture the density dependence of solvation rate since $g_{12}(\sigma)$ is determined by the liquid density at a given temperature via the pressure equation.[36] Fig. 5.4 depicts such a density dependence for R =1 at T = 300 K where both τ_1 and τ_2 are shown as a function of reduced solvent density, ρ_N^*. Note in this figure that while τ_1 decreases steadily with density, τ_2 increases. This can be understood by considering the following physical picture. The increase in liquid density leads to more densely packed solvation structure around the probe solute. This is reflected in the density dependence of $g_{12}(\sigma)$, shown in the upper panel of Fig. C7 (Appendix C).[71] This

'more compact' solvation structure induces accelerated solvation energy relaxation via more effective solute-solvent interaction. This is binary in nature and the origin for τ_1 to become faster with ρ_N^*. The slower timescale (τ_2), on the other hand, becomes even slower with density because τ_2 is controlled by the structural relaxation (see Eq. 5.6) which becomes slower as density increases.

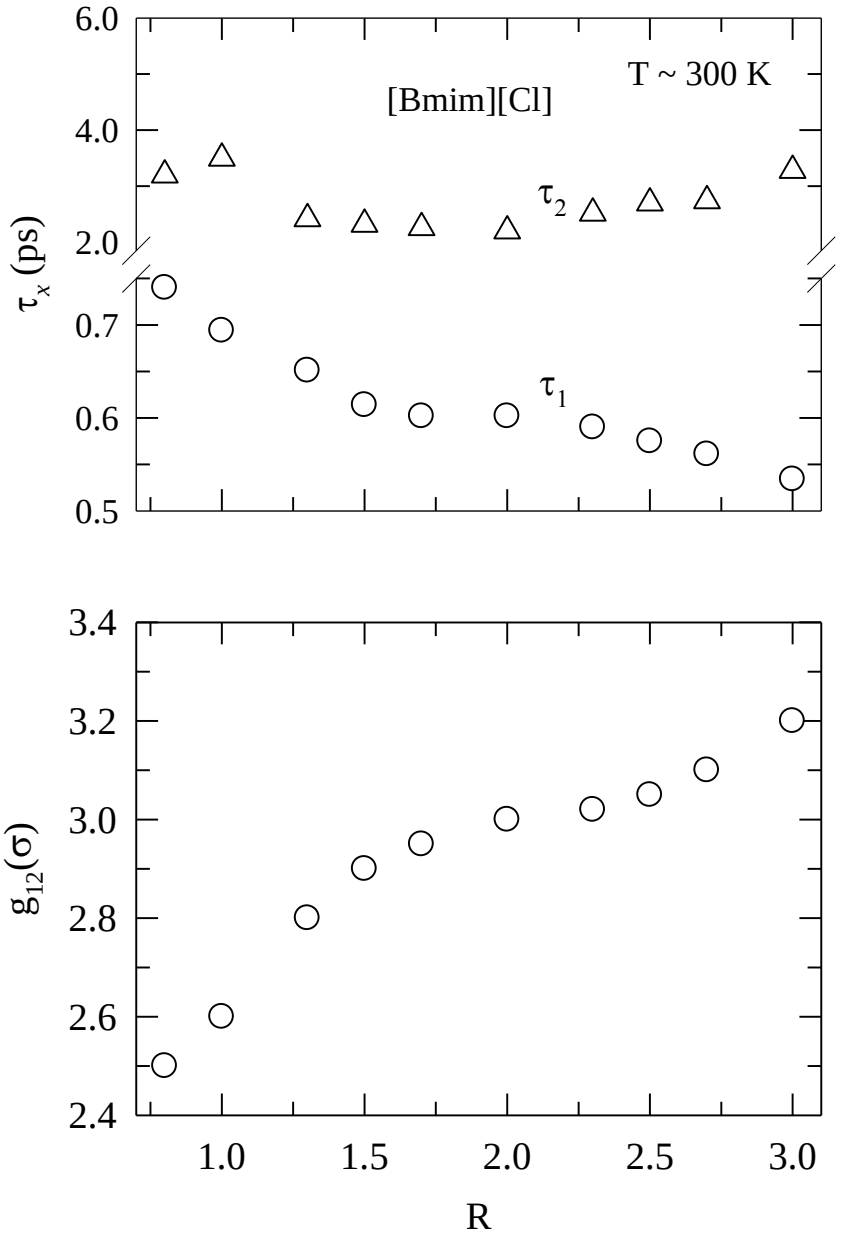

Fig. 5.3: Solute-IL size ratio (R) dependence of the non-polar solvation time constants (upper panel) and the value of the solute – IL radial distribution function at contact, $g_{12}(\sigma)$, for [Bmim][Cl] at ~300 K.

This is shown in the lower panel of Fig. C7 (Appendix C)[71] where decays of the normalized wavenumber dependent solvent dynamic structure factor, $S(k\sigma,t)$, are compared for two different densities at two different wavenumbers. Note here that the decay

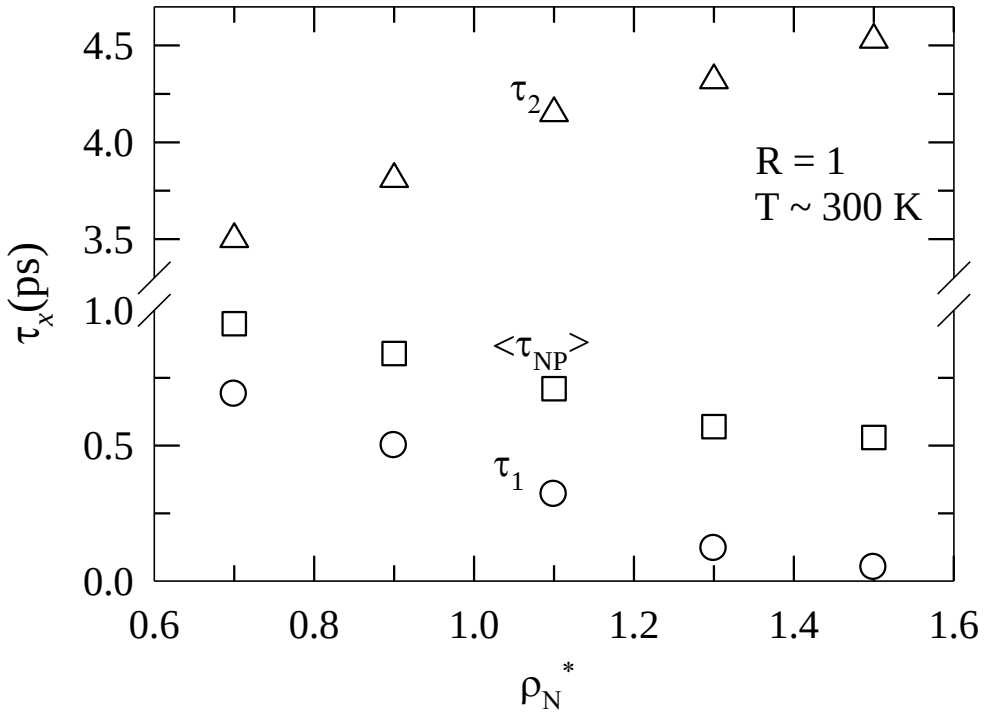

Fig. 5.4: Density dependence of nonpolar solvation time constants, τ_1, τ_2, and the nonpolar average solvation time, $< \tau_{NP} >$, for R =1 at ~300 K.

corresponding to larger wavenumber is faster than that to smaller wavenumber, suggesting the slower timescale is associated with the collective density fluctuations. The average non-polar solvation time, shown also in Fig. 5.4, decreases with density because of the dominant amplitude (~90%) for the calculated ultrafast component. This prediction of solvent density induced fast component becoming faster and slow turning slower, which can be accessed via changing pressure at a fixed temperature, may be cross-examined via experiments and compared between ionic liquids and conventional molecular liquids. It is worth mentioning here that given the solute-solvent size ratio and density dependencies of the solvation timescales and also if one considers the possible change in solute-ion interactions due to

change in conformational structure of larger ion such as TFSI,[72-74] the agreement between the calculated and measured timescales (Table 5.2) may be termed as semi-quantitative. This is interesting as accurate modelling of shorter-ranged interactions in ionic liquids demands more complexity than the simple one presented here because of the heterogeneity inherent to these ILs[75-82] and variations in shape of the constituent ions.

Next we present in Fig. 5.5 the calculated solvation response functions for three different solute-IL size ratios after considering the ion-ion interaction in addition to the LJ interaction

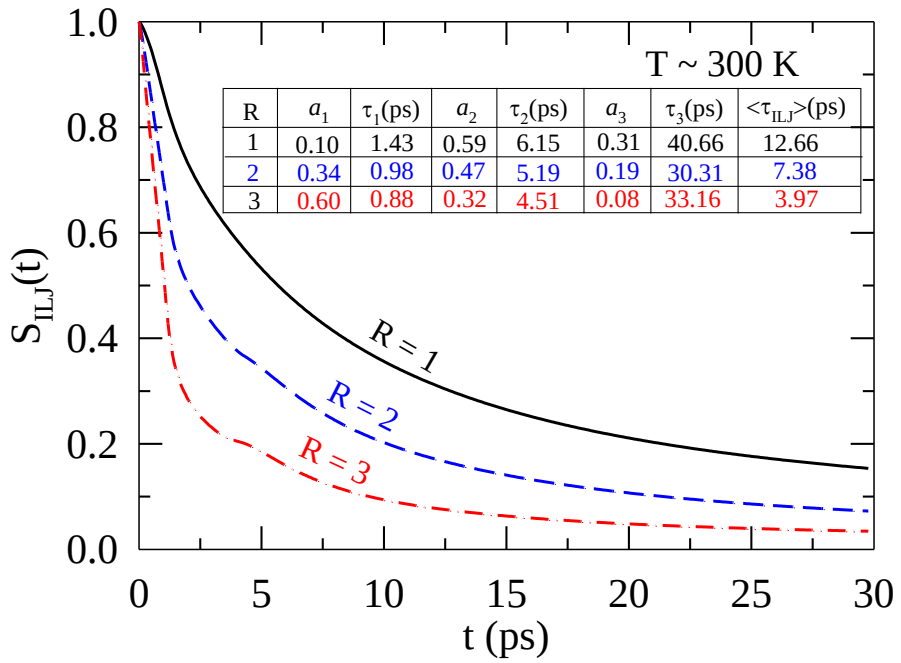

R	a_1	τ_1(ps)	a_2	τ_2(ps)	a_3	τ_3(ps)	$<\tau_{ILJ}>$(ps)
1	0.10	1.43	0.59	6.15	0.31	40.66	12.66
2	0.34	0.98	0.47	5.19	0.19	30.31	7.38
3	0.60	0.88	0.32	4.51	0.08	33.16	3.97

Fig. 5.5: Normalized solvation response for [Bmim][Cl] at ~300 K for three different solute – IL size ratios after considering ion-ion interaction in addition to the nonpolar interaction while obtaining the IL-IL spatial correlations. Fit parameters are shown in the inset.

among IL molecules. This we may term as ionic LJ interaction, and used [Bmim][Cl] as the representative IL for the subsequent calculations. The term that is freshly calculated with this modified interaction is the density fluctuation contribution, $C_{\rho\rho}(t)$. The dissolved solute is, as before, a LJ particle and ρ_N^* = 0.7. Parameters describing the decays of the calculated

response function (denoted as $S_{ILJ}(t)$) are also shown in the inset of this figure. It is evident from this figure that incorporation of the longer-ranged electrostatic interaction in the static ion structure factor ($S(k)$) via Eq. 5.16 leads to much slower relaxation of the solvation energy for a non-polar solute. As already discussed, this may be due to inaccurate description of the ion-ion correlations at the molecular length-scales by Eq. 5.16 which, in turn, has led to the incorrect prediction of the solvation energy relaxation. This is of course expected as Eq. 5.16 is based on continuum model description of systems possessing electrostatic interactions and describes static ion-ion correlations at the long wavelength (that is, $k\sigma \to 0$) limit. Even with this lacuna, the resultant calculations capture the solute size dependence in line with what has already been observed with pure solute-solvent and solvent-solvent non-polar interactions (shown in Fig. 5.3). This is because $g_{12}(r)$ in $C_{EE}^{B}(t)$ is still obtained from solute-IL non-polar interaction and dominates the total solvation energy relaxation via the initial ultrafast component.

5.3.2 Ultrafast Solvation Response Measured by DSS Experiments: Possible Origin

We have already noticed in Table 5.1 that DSS measurements report ultrafast solvation timescale for imidazolium ILs much slower than that by the 3PEPS measurements. Inertial translation of the lighter ions (for these ILs the anions) has been believed to be the origin for the initial fast solvation response detected in DSS experiments.[2,83,84] However, this mechanism fails to explain why DSS measurements do not find any ultrafast component for [Phos][Cl] in which the anion is ~8 times lighter than the anion in [Bmim][TFSI] where DSS experiments report presence of a fast component with time constant ~700 fs. Similar comparison also holds for the other two imidazolium ionic liquids where the anions are 2-4 times heavier than that in the [Phos][Cl]. Subsequently, a semi-molecular theory has successfully described the biphasic solvation energy relaxation in imidazolium ILs observed in DSS measurements by using the experimental dielectric relaxation data as input, and proposed the collective reorientational dynamics of the dipolar ions (for example, imidazolium cation in imidazolium ILs) as the source for the initial fast dynamics.[16-21] In addition, this theory describes the experimental Stokes shift dynamics in these ILs in terms of both solute-IL dipole-dipole and dipole-ion contributions where the slow dynamics at long time has been ascribed to the relaxation of the ion dynamic structure factor via centre-of-mass ion motion. Since the above dielectric relaxation based theory has been discussed in detail

elsewhere,[16-21] we will present here only the necessary equations for stressing the importance of the reorientational motion of the dipolar cations and the lengthscale involved in the orientational density fluctuation that produces the initial fast solvation response measured in these ILs. Later, we explore for an imidazolium IL the validity of the approximate relationship between the single particle orientation and initial solvation response first proposed for explaining the short time dynamics in conventional, strongly polar liquids.[85,86]

The normalized solvation response function due to the fluctuating solute-IL dipole-dipole interaction energy (ΔE_{sd}) is given in Eq. 2.3 in Chapter 2. ($S^{lm}_{solvent}(k,t)$) provides an approximate description of the solvent's frictional response and consists of the rotational ($\Gamma_R(k,z)$) and translational ($\Gamma_T(k,z)$) memory kernels.[10] If one assumes diffusive relaxation for the isotropic dynamic structure factor, $\Gamma_T(k,z)$ can be obtained rather trivially from the centre-of-mass diffusion calculated using the medium viscosity and a suitable hydrodynamic boundary condition. However, one can include the inertial effects in the translational motion via a more accurate ion dynamic structure factor (see Eq. 10 of Ref. 18) but we have not done so as the subsequent calculations avoids direct inclusion of the inertial motions (both rotation and translation). Calculation of $\Gamma_R(k,z)$ is rather difficult and is usually obtained via the following connection to the experimental frequency dependent dielectric relaxation ($\varepsilon(z)$) in the collective limit:[86-89]

$$\frac{2k_BT}{I\left[z+\Gamma_R(k\sigma\to 0,z)\right]}=\frac{z\varepsilon_0\left[\varepsilon(z)-\varepsilon_\infty\right]}{f(110,k\sigma\to 0)\varepsilon_\infty\left[\varepsilon_0-\varepsilon(z)\right]}, \tag{5.19}$$

where ε_0 and ε_∞ are respectively the static and infinite frequency dielectric constants of the medium, I the moment of inertia of the rotating species. $f(110,k\sigma\to 0)=1-(\rho_d^0/4\pi)c(110,k\sigma\to 0)$.

It is clear from Eq. 5.19 that the experimental nature of $\varepsilon(z)$ (multi-exponential or stretched) will be transferred to the calculated polar solvation energy relaxation. This also means that any solvent dynamics, either pure rotational or collisional in character which can impart a time-dependent change in the collective dipole moment autocorrelation function and thus contribute to $\varepsilon(z)$, will be included in the subsequent calculations of polar energy relaxation using Eq. 2.7 of Chapter 2. While the pure rotational contribution to $\varepsilon(z)$ falls in the

microwave frequency regime (300 MHz – 300 GHz)[90-93], the collisional or the translation-rotation coupling contribution emerges in the terahertz (1 THz = 10^3 GHz) range.[41,42] Dielectric relaxation measurements in the frequency range, $0.2 \le \nu/GHz \le 89$, of several of the RTILs studied here have reported $\varepsilon(z)$ in the following form:[23]

$$\varepsilon(z) = \varepsilon_\infty + \frac{S_1}{\left[1+(z\tau_1)^{1-\alpha_1}\right]^{\beta_1}} + \frac{S_2}{\left[1+z\tau_2\right]}, \qquad (5.20)$$

with $\alpha_1 < 1$ and $\beta_1 = 1$ and τ_i being the relaxation time constant associated with the dispersion S_i. For [Bmim][BF_4] and [Bmim][PF_6] at ~298 K, τ_1 and τ_2 have been found to be 284 ps and 620 fs, and 1178 ps and 470 fs, with α_1 as 0.52 and 0.57, respectively. While the slower time constant (τ_1) has been ascribed to the exclusive reorientation of the cation dipole of these ILs, the faster one has been suspected to have contributions also from intermolecular vibration and other high frequency modes such as collision and translation-rotation coupling.[23] In what follows next, we use these two ILs as representative examples to show that ultrafast solvation timescale observed in DSS experiments can indeed arise in the present theory from the measured slowest dielectric relaxation step of these liquids in which ion translation or libration does not contribute at all.

Fig. 5.6 depicts the decays of the predicted solvation response function due to solute-IL dipole-dipole interaction, $S_{sd}(t)$, for [Bmim][BF_4] and [Bmim][PF_6] at ~298 K in the limits of the collective ($k\sigma \to 0$) and the nearest neighbour ($k\sigma \to 2\pi$) modes of the orientational solvent polarization density fluctuation. These decays have been calculated by considering only the slowest step of the experimental dielectric relaxation[23] in Eq. 2.7 of Chapter 2 for the solute DCS.[18] Experimental results[2] are also shown in the same figure for a comparison. Parameters obtained from fits of these decays to a function, $S_{fit}(t) = a_1 \exp(-t/\tau_1) + a_2 \exp\left(-(t/\tau_2)^{\alpha}\right)$, have also been shown in the insets. Analytical works described in the Appendix D[71] provides the necessary logic for suitability of the above fit function for the calculated solvation response functions in the $k\sigma \to 0$ and $k\sigma \to 2\pi$ limits even when one considers only the slowest but stretched component of the full experimental dielectric response. Both visual and numerical comparisons with experimental results strongly suggest that the pure reorientational dynamics of the dipolar cation can indeed generate an ultrafast polar solvation response in the collective limit with a

time constant and amplitude very similar to those observed in the corresponding DSS experiments.[2] Interestingly, the calculated solvation response at $k\sigma \to 0$ limit also predicts the stretching exponent (α) very close and the slow

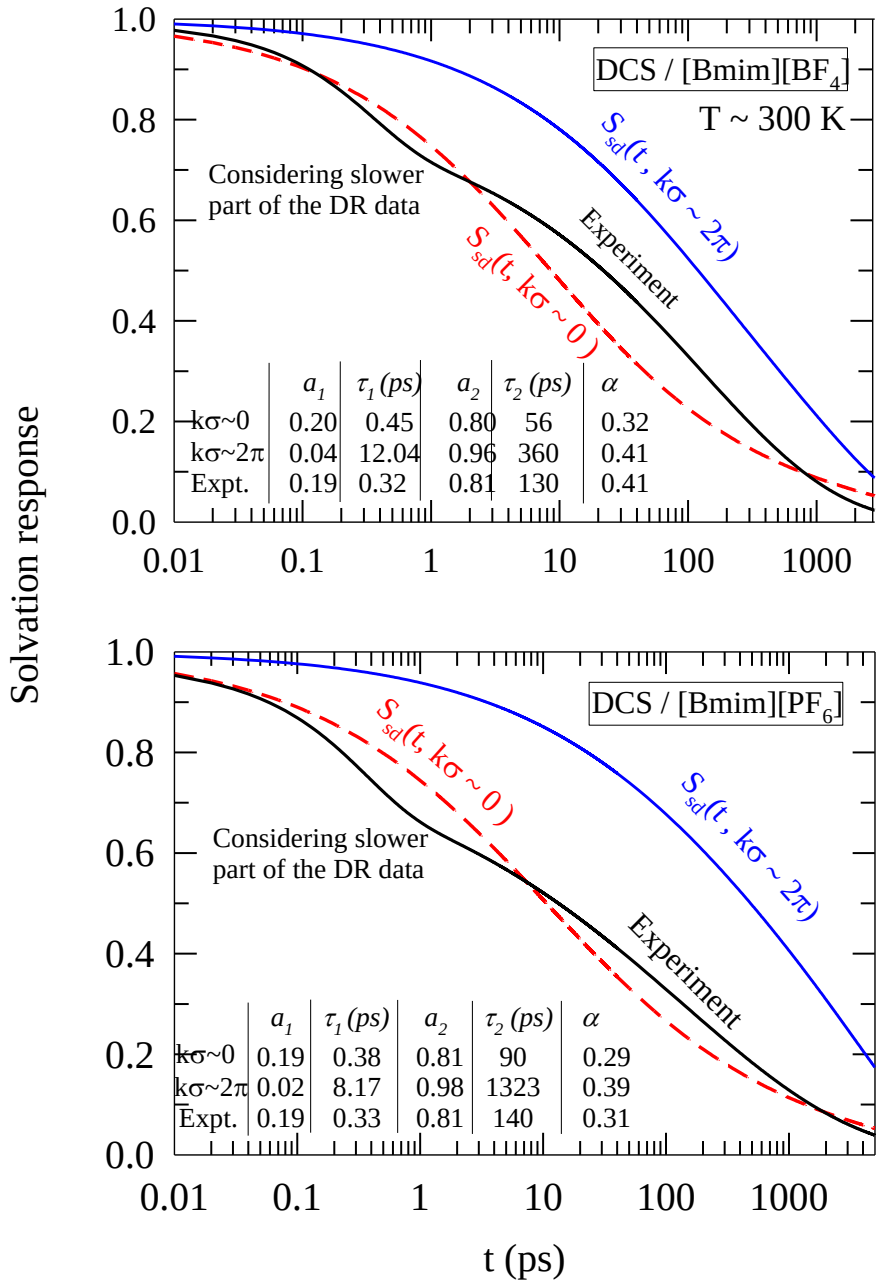

Fig. 5.6: Comparison between the calculated dipole-dipole part of the solvation energy relaxation and the experimental response for DCS in [Bmim][BF_4] (upper panel) and [Bmim][PF_6] (lower panel) at ~300 K in the limits of the collective ($k\sigma \to 0$) and the nearest neighbour ($k\sigma \to 2\pi$) modes of the orientational solvent polarization density fluctuations. Note in calculations, only the slowest part of the experimental dielectric relaxation has been used as input.

time constant (τ_2) within a factor of 2 to those reported by the DSS experiments. The solvation response predicted at $k\sigma \to 2\pi$ limit is, on the other hand, is much slower and suggests overwhelming domination by the slow component (96-98%) even-though the stretched exponential character of the dynamics has been reproduced qualitatively. The incorporation of the full experimental $\varepsilon(z)$[23] in the calculations leads to much faster decay of $S_{sd}(t)$ at the collective limit but brings the nearest neighbour response much closer to the experiments. This is shown in Fig. C8 of the Appendix C.[71] Interestingly, even with full $\varepsilon(z)$ the time constants associated with $S_{sd}(t)$ decays at $k\sigma \to 2\pi$ limit remain slower than those from experiments for these ILs, signifying the dominance of the collective polarization density fluctuation modes in the polar solvation energy relaxation in these coulomb fluids, particularly at short times. Interestingly, this is very similar to the predictions made earlier for polar solvation energy relaxation in conventional dipolar liquids.[10, 94,95] This, however, does not suggest that the nearest neighbour solvent modes are unimportant. In fact, relaxations of both the orientational polarization density and istropic ion density involving the nearest neighbour modes contribute to the slow long time decay so typical of these liquids.[17,18,21]

The closeness between the calculations at the collective limit and experiments observed in Fig. 5.6 then leads us to explore the relationship between the polar solvation response and the collective reorientational dynamics of dipolar IL species. This is along the line of what has been proposed earlier for short time dynamics in common dipolar solvents based on simulation results[85] and subsequently derived analytically in the limit of collective ($k\sigma \to 0$) dipolar solvent response.[86] Note the dipolar species is executing orientational relaxation in the force field of others and thus acquires a 'collective' character in its single particle orientational motion.[29] For a strongly polar and homogeneous liquid where the polar solvation energy relaxation is much faster than the collective single particle orientation, the short time dynamics at the $k\sigma \to 0$ limit was predicted to be given by[86] $S_p(t) = [C_1(t)]^{\gamma} = \left[\exp(-t/\tau_I)^2\right]^{\gamma}$ where $\gamma = f(110, k\sigma \to 0) = \dfrac{3Y}{1-\varepsilon_0^{-1}}$ and $\tau_I = \sqrt{I/k_BT}$. The polarity parameter ($3Y$) is defined as,[90] $3Y = \dfrac{4\pi\mu_{cation}^2\rho}{3k_BT}$, with μ_{cation} being the dipole moment of the dipolar species (cation here) and ρ the IL number density. Fig. C9 (Appendix C)[71] demonstrates that for [Bmim][BF_4] the relaxation of the polar solvation energy is much

faster than that of the collective single particle orientational correlational function ($C_1(t)$) and thus fulfils one of the approximations made for strongly polar solvents. This is a result representative of other imidazolium ILs as well and thus can be regarded as a general trend. The domination of the collective polarization mode in the early part of the polar solvation dynamics noticed in Fig. 5.6 for imidazolium ILs provides further support for carrying out the proposed analyses for these dipolar ILs. However, a direct comparison between the dipolar solvation response calculated from the present theory and that from $\left[\exp(-t/\tau_I)^2\right]^{\gamma}$ may not be proper for these ILs as inhomogeneity present in these liquids induces large departure of the cation reorientational dynamics from the isotropic rotational diffusion.[23,48,96,97] Anisotropic relaxation with large angle hopping motion[48] can give rise to fast energy relaxation in a way equivalent to that producing larger than the expected centre-of-mass diffusion in supercooled systems.[98-101] Even for these inhomogeneous liquids, we find that the calculated collective polar solvation response, $S_{sd}(t, k\sigma \to 0)$, can be mapped semi-quantitatively by the collective single particle orientational relaxation, $C_1(t)$, with a translation factor, γ. Note $C_1(t)$ is connected to $\varepsilon(z)$ via $\Gamma_R(k,z)$ as follows:[10] $C_1(t) = L^{-1}\left[z + \frac{2k_BT}{I\{z + \Gamma_R(k\sigma \to 0, z)\}}\right]^{-1}$, with Eq. 5.19 describing the relationship between $\varepsilon(z)$ and $\Gamma_R(k\sigma \to 0, z)$. Fig. 5.7 presents such a depiction for DCS in [Bmim][BF_4] where only the slowest step of the experimental $\varepsilon(z)$ has been used for calculations. The near quantitative mapping of polar solvation response by the cation rotation at short times again strongly suggest that the solvent orientational polarization density relaxation can indeed generate the ultrafast response observed in DSS experiments. Note, however, that the value of the translation factor (γ) that has lead to the successful mapping of $S_{sd}(t)$ by $C_1(t)$ is approximately half of that (6.20) obtained from the relation, $\gamma = 3Y/(1-\varepsilon_0^{-1})$, using $\mu_{cation} \approx 3.7$ D.[102] If one uses $\mu_{cation} \approx 2.6$ D,[103] the value of γ turns out to be ~3 which is very close to the value (3.36) found here from mapping. This discrepancy, therefore, is more of a reflection of the non-uniqueness for the definition of the dipole moment of a charged species[104] than the inability of the cation rotational dynamics to describe the solvation energy relaxation in dipolar (here imidazolium) ILs. The comparison shown in Fig. 5.7 then do suggest that ultrafast polar solvation measured in DSS experiments with dipolar ILs can arise from the complex reorientational dynamics of the dipolar ions in these ILs .

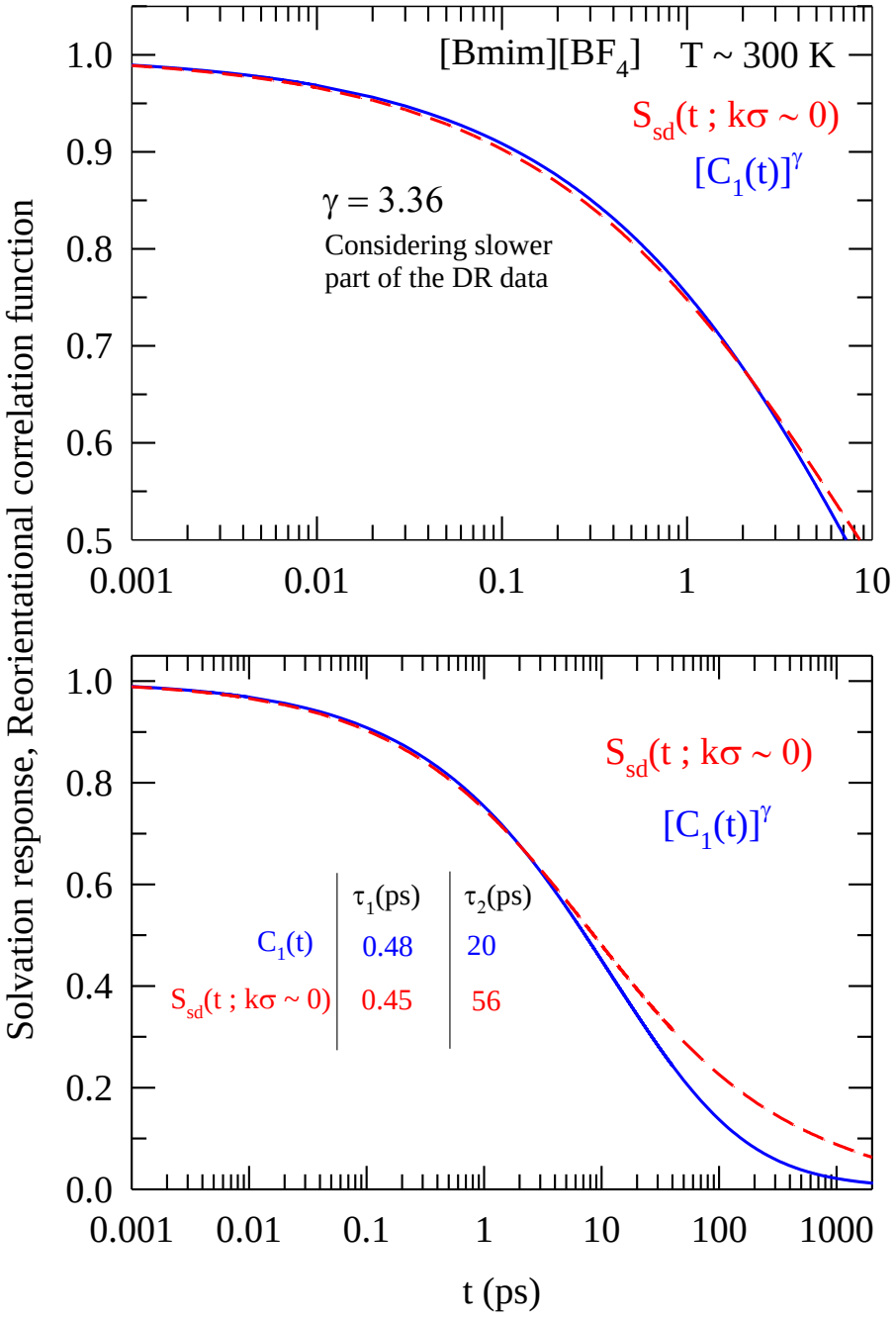

Fig. 5.7: Relation between the calculated polar solvation response, $S_{sd}(t)$, and the collective single particle reorientational correlation function, $C_1(t)$ for a dipolar IL, [Bmim][BF_4], at ~300 K. The calculations of $S_{sd}(t)$ is for the solute, DCS, at the limit of collective solvent polarization density fluctuations and obtained by the slowest part of the experimental dielectric relaxation data. The upper panel shows the mapping of the solvation response by the single particle reorientational correlation function at short times and the lower panel at both short and long times.

5.4 Conclusions

The work described here shows that the ultrafast solvation response in RTILs measured via 3PEPS experiments may have origin in the nearest neighbour solute-solvent non-dipolar interaction. When this non-dipolar interaction and that among solvent molecules are modelled as that given by the traditional LJ potential, the calculated fast time constants have been found to be in very good agreements with 3PEPS experiments for most of the RTILs. The calculated results also agree with the available simulation results and support the picture that sub-hundred femtosecond solvation response in ILs arises mainly from the nearest neighbour solute-IL interaction where solvent (or dipolar cation/anion) rotation plays an insignificant role. The regulatory nature of the nearest neighbour mode for nonpolar solvation energy relaxation forces the Debye-Huckel type description of spatial correlations inaccurate for explaining the 3PEPS and simulation results. A strong solute-solvent size ratio and density dependencies for the binary ultrafast solvation component have been predicted which may be re-examined via suitable experiments. It is, however, to be mentioned here that electrostatic interaction can make the solvent structure around a dipolar solute more compact ('electrostriction'),[105,106] making the binary relaxation timescale much faster through the increased $g_{12}(\sigma)$ values.[107,108] Simulation studies of vibrational energy relaxation in ILs have already found the signature of it.[108] Such an enhancement of solvent density is not expected for a nonpolar solute and present calculations have also not considered this aspect (density enhancement) while predicting the rates for nonpolar solvation energy relaxation of a nonpolar solute in these ILs.

When the solute-IL dipolar solvation response is considered, it turns out to be the reorientational dynamics of the dipolar species (cation or anion) which can successfully describe the calculated polar solvation energy relaxation. Interestingly, the collective polar solvation response has been found to contain an ultrafast component which is very close to that observed in the DSS experiments. The slowest component of the experimental dielectric relaxation data with its stretched exponential character alone is found to generate the ultrafast polar response in the imidazolium ILs in the limit of the collective polarization density relaxation. The calculated dynamics presented here therefore suggest that the 3PEPS and DSS experiments measure the solvation response induced by the different components (non-dipolar and dipolar) of the total solute-IL interaction. However, it should be kept in mind that

such a conclusion has been arrived after comparing the calculated dynamics to those from experiments that have used solutes of different characters – one (OX4) that undergoes small dipole moment change upon excitation and the other (C153 or DCS) undergoes a large dipole moment change. So, the observed difference may partly arise from the difference in this solute character and hence a comparison between the predicted results and those from 3PEPS and DSS measurements using the same solute would make it more rigorous. Applications of the present theory for a wider variety of ILs and comparison with experimental data (obtained using the same solute in 3PEPS and DSS measurements) should therefore be done in future.

References

1. Muramatsu, M.; Nagasawa, Y.; Miyasaka, H. *J. Phys. Chem. A* **2011**, *115*, 3886.
2. Arzhantsev, S.; Jin, H.; Baker, G. A.; Maroncelli, M.; *J. Phys. Chem. B* **2007**, *111*, 4978.
3. Ito, N.; Arzhantsev, S.; Heitz, M.; Maroncelli, M. *J. Phys. Chem. B* **2004**, *108*, 5771.
4. Bardeen, C. J.; Rosenthal, S. J.; Shank, C. V. *J. Phys. Chem. A* **1999**, *103*, 10506.
5. Blanchard, G. *Chem. Phys.* **1989**, *138*, 365.
6. Maroncelli, M.; Fleming, G. R. *J. Chem. Phys.* **1988**, *89*, 5044.
7. Carter, E. A.; Hynes, J. T. *J. Chem. Phys.* **1991**, *94*, 5961.
8. Hsu, C. P.; Song, X.; Marcus, R. A. *J. Phys. Chem. B* **1997**, *101*, 2546.
9. Song, X.; Chandler, D.; *J. Chem. Phys.* **1998**, *108*, 2594.
10. Bagchi, B.; Biswas, R. *Adv. Chem. Phys.* **1999**, *109*, 207.
11. Samanta, A. *J. Phys. Chem. B* **2006**, *110*, 13704.
12. Jin, H.; Baker, G. A.; Arzhantsev, S.; Dong, J.; Maroncelli, M. *J. Phys. Chem. B* **2007**, *111*, 7291.
13. Chowdhury, P. K.; Halder, M.; Sanders, L.; Calhoun, T.; Anderson, J. L.; Armstrong, D. W.; Song, X.; Petrich, J. W. *J. Phys. Chem. B* **2004**, *108*, 10245.
14. Lang, B.; Angulo, G.; Vauthey, E. *J. Phys. Chem. A* **2006**, *110*, 7028.
15. Ingram, J. A.; Moog, R. S.; Ito, N.; Biswas, R.; Maroncelli, M. *J. Phys. Chem. B.* **2003**, *107*, 5926.
16. Kashyap, H. K.; Biswas, R. *J. Phys. Chem. B* **2008**, *112*, 12431.
17. Kashyap, H. K.; Biswas, J. Phys. Chem. B **2010**, *114*, 16811.
18. Kashyap, H. K.; Biswas, J. Phys. Chem. B **2010**, *114*, 254.
19. Kashyap, H. K.; Biswas, Ind. J. Chem. **2010**, 49A, 685.
20. Daschakraborty, S.; Biswas, R. *J. Phys. Chem. B* **2011**, *115*, 4011.
21. (a) Daschakraborty, S.; Biswas, R. *Chem. Phys. Lett.* **2011**, *510*, 210. (b) Daschakraborty, S.; Biswas, R. *Chem. Phys. Lett.* **2012**, *545*, 54.
22. Stoppa, A.; Hunger, J.; Buchner, R.; Hefter, G.; Thoman, A.; Helm, H. *J. Phys. Chem. B* **2008**, *112*, 4854.
23. Hunger, J.; Stoppa, A.; Schrodle, S.; Hefter, G.; Buchner, R. *Chem. Phys. Chem.* **2009**, *10*, 723.
24. Huang, M.-M.; Bulut, S.; Crossing, I.; Weingertner, H. *J. Chem. Phys.* **2010**, *133*, 101101.

25. Zech, O.; Hunger, J.; Sangoro, J. R.; Iacob, C.; Cremer, F.; Kunz, W.; Buchner, R. *Phys. Chem. Chem. Phys.* **2010**, *12*, 14341.
26. Joo, T.; Jia, Y.; Yu, J.-Y.; Lang, M. J.; Fleming, G. R.; *J. Chem. Phys.* **1996**, *104*, 6089.
27. Horng, M. L.; Gardecki, J. A.; Papazyan, A.; Maroncelli, M. *J. Phys. Chem.* **1995**, *99*, 17311**.**
28. Bingemann, D.; Ernsting, N. P. *J. Chem. Phys.* **1995**, *102*, 2691.
29. Biswas, R.; Nandi, N.; Bagchi, B. *J. Phys. Chem. B* **1997**, *101*, 2968.
30. Mukamel, S. *Annu. Rev. Phys. Chem.* **1990**, *41*, 647.
31. Yan, Y. J.; Mukamel, S. *J. Chem. Phys.* **1991**, *94*, 179.
32. Reynolds, L.; Gardecki, J. A.; Frankland, S. J. V.; Horng, M. L.; Maroncelli, M. *J. Phys. Chem.* **1996**, *100*, 10337.
33. Ma, J.; Bout, D. V.; Berg, M. *J. Chem. Phys.* **1995**, *103*, 9146.
34. Fourkas, J. T.; Benigno, A.; Berg, M. *J. Chem. Phys.* **1993**, *99*, 8552.
35. Fourkas, J. T.; Berg, M. *J. Chem. Phys.* **1993**, *98*, 7773.
36. Hansen, J. P.; McDonald, I. R. *Theory of Simple Liquids*; Academic Press: London, 1986.
37. Balucani, U.; Zoppi, M.; *Dynamics of the Liquid State*, Clarendon Press: Oxoford 1994.
38. Bagchi, B.; Bhattacharyya, S. *Adv. Chem. Phys.* **2007**, *116*, 67.
39. Biswas, R.; Bhattacharyya, S.; Bagchi, B. *J. Chem. Phys.* **1998**, *108*, 4963.
40. Bagchi, B. *J. Chem. Phys.* **1994**, *100*, 6658.
41. Schroder, C.; Hunger, J.; Stoppa, A.; Buchner, R.; Steinhauser, O. *J. Chem. Phys.* **2008**, *129*, 184501.
42. Schroder, C.; Haberler, M.; Steinhauser, O. *J. Chem. Phys.* **2008**, *128*, 134501.
43. Turton, D. A.; Hunger, J.; Stoppa, A.; Hefter, G.; Thoman, A.; Walther, M.; Buchner, R.; Wynne, K. *J. Am. Chem. Soc.* **2009**, *131*, 11140.
44. Roy, D.; Maroncelli, M. *J. Phys. Chem. B* **2012**, *116*, 5951.
45. Jeong, D.; Shim, Y.; Choi, M. Y.; Kim, H. J. *J. Phys. Chem. B* **2007**, *111*, 4920.
46. Shim, Y.; Choi, M. Y.; Kim, H. *J. Chem. Phys.* **2005**, *122*, 044511.
47. Shim, Y.; Duan, J.; Choi, M. Y.; Kim, H. J. *J. Chem. Phys.* **2003**, *119*, 6411.
48. Shim, Y.; Kim, H. J. *J. Phys. Chem. B* **2008**, *112*, 11028.
49. Shim, Y.; Kim, H. J. *J. Phys. Chem. B* **2009**, *113*, 12964.
50. Shim, Y.; Kim, H. J.; *J. Phys. Chem. B* **2007**, *111*, 4510.
51. Shim, Y.; Jeong, D.; Choi, M. Y.; Kim, H. J. *J. Chem. Phys.* **2006**, *125*, 061102.
52. Streeter, I.; Lynden-Bell, R. M.; Compton, R. G. *J. Phys. Chem. C* **2008**, *112*, 14538.

53. Bhargava, B. L.; Balasubramanian, S. *J. Chem. Phys.* **2005**, *123*, 144505.
54. Kobrak, M. N.; Znamenskiy, V. *Chem. Phys. Lett.* **2004**, *395*, 127.
55. Kobrak, M. N. *J. Chem. Phys.* **2006**, *125*, 064502.
56. Kobrak, M. N. *J. Chem. Phys.* **2007**, *127*, 184507.
57. Kobrak, M. N. *J. Chem. Phys.* **2007**, *127*, 099903.
58. Stephens, M. D.; Saven, J. G.; Skinner, J. L. *J. Chem. Phys.* **1997**, *106*, 2129.
59. Weeks, J. D.; Chandler, D.; Andersen, H. C. *J. Chem. Phys.* **1971**, *54*, 5237.
60. Chandrasekhar, S. *Rev. Mod. Phys.* **1943**, *15*, 1.
61. Stehfest, H. *Commun. ACM* 1970, **13**, 624.
62. Lebowitz, J. L. *Phys. Rev.* **1964**, *133*, A895.
63. Hoshino, K. *J. Phys. F: Met. Phys.* **1983**, *13*, 1981.
64. Rao, R. V. G.; Satpathy, A. *Phys. Rev. B* **1990**, *41*, 11938.
65. Attard, P. *Phys. Rev. E* **1993**, *48*, 3604.
66. Chandra, A.; Bagchi, B. *J. Chem. Phys.* **1999**, *110*, 10024.
67. Glasstone, S. *An Introduction to Electrochemistry*, Litton Educational Publishing: NY, 1942.
68. Chapman, C. F.; Maroncelli, M. *J. Phys. Chem.* **1991**, *95*, 9095.
69. Daguenet, C.; Dyson, P. J.; Krossing, I.; Oleinikova, A.; Slattery, J.; Wakai, Weingärtner, H. *J. Phys. Chem. B* **2007**, *110*, 12682.
70. Huddleston, J. G.; Visser, A. E.; Reichert, W. M.; Willauer, V. G.; Broker, A.; Rogers, R. D. *Green Chem.* **2001**, *3*, 156.
71. See Appendix A, B, C, D for information regarding solute-RTIL size ratio, RTIL densities, ion diameters, density dependence of radial distribution function at contact and structural relaxation, calculated solvation response functions for [Bmim][BF_4] and [Bmim][PF_6] at the collective and nearest neighbor limits, decay of orientational correlation function and polar solvation response function.
72. Fuji, K.; Fujimori, T.; Takamuku, T.; Kanzaki, R.; Umebayashi, Y.; Ishiguro, S. *J. Phys. Chem. B. Letters*, **2006**, *110*, 8179.
73. Santos, C. S.; Annapureddy, H. V. R.; Murthy, N. S.; Kashyap, H. K.; Castner, E. W. Jr.; Margulis, C. *J. Chem. Phys.* **2011**, *134*, 064501.
74. Logotheti, G.-E.; Ramos, J.; Economou, I. C. *J. Phys. Chem. B* **2009**, *113*, 7211.
75. Triolo, A.; Russina, O.; Fazio, B.; Appetecchi, G. B.; Carewska, M.; Passerini, S. *J. Chem. Phys.* **2009**, *130*, 164521.

76. Triolo, A.; Russina, O.; Fazio, B.; Triolo, R.; Cola, E. D. *Chem. Phys. Lett.* **2008**, *467*, 362.
77. Mandal, P. K.; Sarkar, M.; Samanta, A. *J. Phys. Chem. A* **2004**, *108*, 9048.
78. Wang, Y.; Voth, G. A. *J. Am. Chem. Soc.* **2005**, *127*, 12192.
79. Hu, Z.; Margulis, C. J. *Proc. Natl. Acad. Sci. U.S.A.* **2006**, *103*, 831.
80. Adhikari, A.; Sahu, A. K.; Dey, S.; Ghosh, S.; Mandal, U.; Bhattacharyya, K. *J. Phys. Chem. B* **2007**, *111*, 12809.
81. Jin, H.; Li, X.; Maroncelli, M. *J. Phys. Chem. B* **2007**, *111*, 13473.
82. Sasmal, D. K.; Mandal, A. K.; Mondal, T.; Bhattacharyya, K. *J. Phys. Chem. B* **2011**, *115*, 7781.
83. Samanta, A. *J. Phys. Chem. Lett.* **1970**, *1*, 1557.
84. Maroncelli, M.; Zhang, X. -X.; Liang, M.; Roy, D.; Ernsting, N. P. *Faraday Discuss. Chem. Soc.* **2012**, *154*, 409.
85. Maroncelli, M.; Kumar, V. P.; Papazyan, A. *J. Phys. Chem.* **1993**, *97*, 13.
86. Roy, S.; Bagchi, B. *Chem. Phys.* **1994**, *183*, 207.
87. Roy, S.; Bagchi, B. *J. Chem. Phys.* **1993**, *99*, 9938.
88. Roy, S.; Bagchi, B. *J. Chem. Phys.* **1993**, *99*, 1310.
89. Nandi, N.; Roy, S.; Bagchi, B. *J. Chem. Phys.* **1995**, *102*, 1390.
90. Gray, C. G.; Gubbins, K. E. *Theory of Molecular Fluids*; Clarendon: Oxford, 1984. Vol. I
91. Song, X. *J. Chem. Phys.* **2009**, *131*, 044503.
92. Schroder, C.; Haberler, M.; Steinhauser, O. *J. Chem. Phys.* **2009**, *131*, 114504.
93. Schroder, C.; Wakai, C.; Weingartner, H.; Steinhauser, O. *J. Chem. Phys.* **2007**, *136*, 084511.
94. Bagchi. B.; Chandra, A. *Adv. Chem. Phys.* **1991**, *80*, 1.
95. Bagchi, B.; Chandra, A. *J. Chem. Phys.* **1992**, *97*, 5126.
96. Heimer, N. E.; Wilkes, J. S.; Wahlbeck, P. C.; Carper, W. R. *J. Phys. Chem. A* **2006**, *110*, 868.
97. Koddermann, T.; Ludwig, R.; Paschek, D. *ChemPhysChem*, **2008**, *9*, 1851.
98. Habasaki, J.; Ngai, K. L. *J. Chem. Phys.* **2008**, *129*, 194501.
99. Pal, T.; Biswas, R. *Chem. Phys. Lett.* **2011**, *517*, 180.
100. Guchhait, B.; Daschakraborty, S.; Biswas, R. *J. Chem. Phys.* **2012**, *136*, 174503.
101. Guchhait, B.; Gazi, H. A. R.; Kashyap, H. K.; Biswas, R. *J. Phys. Chem. B* **2010**, *114*, 5066.

102. Jin, H.; O'Hare, B.; Dong, J.; Arzhantsev, S.; Baker, G. A.; Wishart, J. F.; Benesi, A. J.; Maroncelli, M. *J. Phys. Chem. B.* **2008**, *112*, 81.
103. Bhargava, B. L.; Balasubramanian, S. *J. Phys. Chem. B* **2007**, *111*, 4477.
104. Kobrak, M. N.; Sandalow, N. *Molten Salts XIV* ; Eds. A. Mantz and P. Trulove, The Electrochemical Society, Pennington: NJ, 2006.
105. Papazyan, A.; Maroncelli, M. *J. Chem. Phys.* **1995**, *102*, 2888.
106. Kumar, P. V.; Maroncelli, M. *J. Chem. Phys.* **2000**, *112*, 5370.
107. Daschakraborty, S.; Biswas, R. *J. Chem. Sci.* **2012**, *124*, 763.
108. Shim, Y.; Kim, H. J. *J. Chem. Phys.* **2006**, *125*, 024507.

Chapter 6

Stokes Shift Dynamics in (Ionic Liquid + Polar Solvent) Binary Mixtures

6.1 Introduction

Binary mixtures of ionic liquids (ILs) with dipolar solvents offer a new class of media for chemical processing because addition of cosolvents greatly expands the utility of ionic liquids as reaction media via suitably tuning their physicochemical properties. Addition of polar solvents strongly influences viscosities and electrical conductivities of the parent ILs which may make these mixtures better media for certain chemical and electrochemical applications.[1-18] Miscibility of ILs in water is a serious environmental concern as it may irreversibly damage the ecosystem via entering into the food-chain. Consequently, the number of studies - both experimental[19-37] and computer simulations[38-46] investigating interactions between water and IL molecules – is much larger than those performed using binary mixtures of ILs with non-aqueous organic solvents,[47-51] supercritical fluids[52-53] and with another IL.[54-60] Liquid solvent engineering for a desired reaction or extraction requires clear understanding of the solubility behavior[61-75] in which medium polarity plays an important role. These studies provide crucial knowledge for the liquid-liquid extraction of reaction products and thus very relevant to chemical industry. Moreover, successful tailoring of a reaction requires a thorough knowledge of the medium polarity and dynamics as solvent rearrangement often dictate the formation of a suitable reaction intermediate or a desired product through solvent stabilization.

Several spectroscopic studies in the last few years have reported local polarity around a dissolved solute for a number of (IL + dipolar solvent) binary mixtures and the issue of preferential solvation discussed.[19-23, 50-52] Non-ideality in solution dynamics of (IL + dipolar solvent) and (IL + IL) binary mixtures has been explored via dielectric relaxation (DR) measurements[32,45,49,56] and time-resolved optical Kerr effect (OKE) spectroscopic techniques.[59-60] Terahertz time domain measurements of aqueous mixtures of 1-butyl-3-methylimidazolium tetrafluoroborate ([Bmim][BF_4]) have revealed moderate non-ideal

mixture composition dependence in relaxation parameters.[32] However, the slow IL-type time scales are missing in these experiments because of non-coverage of the dispersions occurring at the low frequency regime. Dielectric relaxation measurements of the same mixtures in the water-rich regime covering a frequency range $0.2 \le \nu / GHz \le 89$ ($\omega = 2\pi\nu$) have, on the other hand, revealed a drastic reduction in the bulk static dielectric constant (ε_0) of pure water in presence of as low as 0.2 mole fraction of [Bmim][BF_4] and four different relaxation timescales ranging between approximately a nanosecond and a few picoseconds.[45] Most interestingly, computer simulation studies of aqueous mixtures of [Bmim][BF_4] have suggested negligible contribution to the solution ε_0 from the dipole cross correlation between imidazolium cation and water.[44] Available time-resolved fluorescence Stokes shift data for (IL + dipolar solvent) binary mixtures reveal acceleration of the average rate of solvation in presence of a cosolvent[33-36,47] over the values observed in pure ILs.[76-81] Subsequent computer simulation studies with aqueous mixtures of 1-hexyl—3-methylimidazolium hexafluorphosphate ([Hmim][PF_6])[43] suggest that rotational and translational motions of the ions become faster in presence of water, which, in turn, enhances the rate of solvation. Note, however, that the existing measurements with (IL + dipolar solvent) binary mixtures[33-36,47] could not access the faster part of the solvation energy relaxation at early times due to broader time resolution employed and, therefore, the nature of the initial part of the dynamics has remained completely unknown.

Further review of the existing Stokes shift data measured with different solutes - such as coumarin 153 (C153) or 6-propionyl-2-(N,N-dimethylamino)naphthalene (PRODAN) - in binary mixtures of ionic liquids with molecular solvents reveal several interesting aspects. For example, while addition of water, alcohol or acetonitrile in any of the following ionic liquids - [Bmim][PF_6], [Hmim][PF_6], 1-ethyl-3-methylimidazolium ethyl sulfate ([Emim][$EtSO_4$]) and N,N,N-Trimethyl-N-propyl Ammonium Bis(trifluoromethanesulfonyl) Imide ([N_{3111}][Tf_2N]) - has been found to induce red-shift in the steady state fluorescence emission spectrum of a dissolved solute,[33-36,47] no such effects were observed when toluene or dioxane was added to [Bmim][PF_6].[48] What is even more interesting is that the time-zero fluorescence emission spectrum blueshifts upon addition of toluene or dioxane in [Bmim][PF_6] compared to that in the neat IL, producing a larger dynamic Stokes shift. Note that toluene and dioxane are non-dipolar solvents[82] and addition of either of them in an ionic

liquid probably reduces ε_0 of the resultant mixture.[83] The decrease in ε_0 then enhances the solute-ion interaction[83-84] leading to larger Stokes shift values in (IL + nondipolar solvent) binary mixtures. Computer simulation studies of ([Bmim][BF_4] + TIP3P water)[44] and ([Hmim][PF_6] + SPC water)[43] binary mixtures, on the other hand, suggest screening of ion-ion interactions in presence of water molecules. One then wonders what would be the possible consequences of this screening effect on Stokesshift dynamics as ion-solute interactions considerably influences the Stokes shift dynamics in ionic liquids.[84-87]

Here a semi-molecular theory for studying the Stokes shift dynamics in binary mixtures of (IL + common dipolar solvent) has been developed where the effects of cosolvent have been incorporated via the solute-solvent interactions. As before,[84-90] we have used the classical density functional theory (DFT) to express the fluctuating solvation energy of a dissolved dipolar solute in (IL + dipolar solvent) binary mixtures. In this theory, a restriction up to the linear order in fluctuating density ($\delta\rho$) then leads to the total fluctuating solvation energy separating into contributions from the interactions between the dipolar solute and ionic liquid, and that between the dipolar solute and added cosolvent molecules. The time-dependent progress of solvation of a dipolar solute in such mixtures is then followed in terms of solvation energy-energy time correlation function. Subsequently, the theory is applied to predict the Stokes shift dynamics for a few (IL + dipolar solvent) binary mixtures for which experimental results exist. Subsequently, the calculated results have been compared with those from measurements and plausible molecular level explanations offered for the experimentally observed composition dependence of the Stokes shift dynamics of a dipolar solute dissolved in such mixtures. In addition, effective medium calculations for ([Bmim][BF4] + dichloromethane) binary mixtures using the experimental solution dielectric relaxation data have been carried out in order to explore the non-ideality in composition dependence of Stokes shift dynamics in such binary mixtures.

The organization of the rest of the chapter is a follows. Next section contains the theoretical formulation and calculation details. Numerical results and comparison with experiments are given in Sec. III. The chapter then ends with a discussion in section 6.4.

6.2 Theoretical Formulation and Calculation Details

6.2.1 Derivation of microscopic expressions

The derivation of the microscopic expressions for the total time dependent fluctuating solvation energy for dipolar solute in (IL + dipole solvent) binary mixtures closely follows the framework described in our earlier works.[84-87] It is first assumed that a given ionic liquid is completely dissociated in the presence of a strongly polar solvent. This assumption is perhaps justifiable for some mixtures as experimental studies have found either small or negligible ion-pair formation in binary mixtures of some ionic liquids with strongly polar solvents.[3,91] As in dynamic Stokes shift experiments, a very dilute solution of a dipolar probe in such (IL + dipolar solvent) mixture is considered for the present study. Note that such a solution is a multi-component mixture consisting of the added dipolar solvent and the dipolar solute molecules, and the ions from the dissociated ionic liquid molecules. Moreover, either or both of the ions could be dipolar in character.[49,92-94] In such a multi-component mixture, the Stokes shift is principally governed by the following interactions: (i) the dipolar solute-dipolar ion (dipole-dipole) interactions, (ii) the dipolar solute – ion (dipole – ion) interactions and (iii) dipolar solute – dipolar solvent (dipole - dipole) interactions. The dynamics of Stokes shift, however, involves, in addition to the above interactions, the dipolar and ionic interactions among the ions, and the dipole-dipole interactions among the added dipolar solvent molecules. The present theory neither incorporates separately the cross-interactions such as the ion-solvent and ion-ion "ion-dipole" interactions nor considers the interactions due to the presence of ion-pair and higher ion aggregates.[95-96] While the ion-solvent and ion-ion ion-dipole interactions are neglected assuming that the timescales associated with the fluctuations of dipolar density and ion density are widely different and thus dynamically completely decoupled, the latter (interactions due to ion-pair and higher aggregates) is ignored in order to preserve the analytical simplicity of the present theory. Note that the neglect of the cross correlations between the ion and dipole density fluctuations based on separation of timescales is purely an approximation because of the motions of the ionic and dipolar species in such mixtures are adiabatically coupled.[97-102] Dynamic Stokes shift measurements of electrolyte solutions, on the other hand, reveals that ion-motions affect the dynamics at longer times.[103] It is therefore evident from the above discussion that the present

formalism provides an approximate theoretical framework for studying the Stokes shift dynamics in binary mixtures of ionic liquids with strongly polar solvents.

We next use the classical density functional theory (DFT) to write down the expression for the interaction part of the free energy functional ($\Delta\beta F_{\text{int}}$, with $\beta = 1/k_B T$) in terms of position ($\mathbf{r}$) and orientation ($\mathbf{\Omega}$) dependent densities of dipolar ion, dipolar solute, dipolar solvent molecules, and position dependent ion in the solution.[104-106] Then equating the functional derivative of $\Delta\beta F_{\text{int}}$ with respect to the solute density to zero (equilibrium property) provides the expression for the average solvation energy for a dipolar solute immersed in such a mixture (see Appendix E for derivation). Subsequent extension into the time domain allows one to derive the following expression for the time (t), position and orientation dependent solvation energy for a mobile dipolar solute

$$\begin{aligned}\Delta E_{total}(\mathrm{r},\Omega,t) = -k_B T\rho_s(\mathrm{r},\Omega,t)\Big[&\int d\mathbf{r}'d\mathbf{\Omega}' c_{sd}(\mathbf{r},\mathbf{\Omega};\mathbf{r}',\mathbf{\Omega}')\delta\rho_d(\mathbf{r}',\mathbf{\Omega}';t) \\ &+ \int d\mathbf{r}'d\mathbf{\Omega}' c_{sp}(\mathbf{r},\mathbf{\Omega};\mathbf{r}',\mathbf{\Omega}')\delta\rho_p(\mathbf{r}',\mathbf{\Omega}';t) \\ &+ \sum_{\alpha=1}^{2}\int d\mathbf{r}' c_{s\alpha}(\mathbf{r},\mathbf{\Omega};\mathbf{r}')\delta n_\alpha(\mathbf{r}',t)\Big] \\ = \Delta E_{sd}(\mathbf{r},\mathbf{\Omega},t) &+ \Delta E_{sp}(\mathbf{r},\mathbf{\Omega},t) + \Delta E_{si}(\mathbf{r},\mathbf{\Omega},t) \qquad (6.1)\end{aligned}$$

where $\rho_s(\mathbf{r},\mathbf{\Omega};t)$ is the position ($\mathbf{r}$), orientation ($\mathbf{\Omega}$), and time (t)-dependent number density of the dissolved solute. In the above equation, while $c_{sd}(\mathbf{r},\mathbf{\Omega};\mathbf{r}',\mathbf{\Omega}')$ denotes the direct correlation function (DCF) between a dipolar solute at position $\mathbf{r}$ with orientation $\mathbf{\Omega}$ and a dipolar ion at $\mathbf{r}'$ with $\mathbf{\Omega}'$, $c_{sp}(\mathbf{r},\mathbf{\Omega};\mathbf{r}',\mathbf{\Omega}')$ represents the DCF between the dipolar solute at position $\mathbf{r}$ with orientation $\mathbf{\Omega}$ and the dipolar solvent at $\mathbf{r}'$ with $\mathbf{\Omega}'$. $c_{s\alpha}(\mathbf{r},\mathbf{\Omega};\mathbf{r}')$ represents that between a dipolar solute placed at $\mathbf{r}$ with orientation $\mathbf{\Omega}$ and a charged species (ion) located at $\mathbf{r}'$. α denotes the type of ions (positively charged and negatively charged ions) that are interacting with the solute. The fluctuations in dipolar ion and added polar solvent densities ($\delta\rho_d$ and $\delta\rho_p$), and ion density (δn_α) from the respective equilibrium bulk values are then defined as follows: $\delta\rho_d(\mathbf{r},\mathbf{\Omega}) = \rho_d(\mathbf{r},\mathbf{\Omega}) - \rho_d^0/4\pi$, $\delta\rho_p(\mathbf{r},\mathbf{\Omega}) = \rho_p(\mathbf{r},\mathbf{\Omega}) - \rho_p^0/4\pi$ and $\delta n_\alpha(\mathbf{r}) = n_\alpha(\mathbf{r}) - n_\alpha^0$. Note that the time dependence in the fluctuating total solvation energy, $\Delta E_{total}(\mathbf{r},\mathbf{\Omega},t)$ is introduced through the temporal modulation of the fluctuating

dipolar ($\delta\rho_d(\mathbf{r},\mathbf{\Omega},t)$ and $\delta\rho_p(\mathbf{r},\mathbf{\Omega},t)$) and ion ($\delta n_\alpha(\mathbf{r},t)$) densities. Since the linear response approximation allows one to consider the fluctuation in densities either from the initial ($t=0$) or final ($t=\infty$) state, the time dependent fluctuating total solvation energy $\Delta E_{total}(\mathbf{r},\mathbf{\Omega},t)$ for a solute in (IL + dipolar solvent) binary mixture may be expressed as Eq. 6.1.

Note that Eq. 6.1 expresses the total fluctuating solvation energy $\Delta E_{total}(\mathbf{r},\mathbf{\Omega};t)$ as a sum of three distinct contributions: dipolar contributions from interactions of the solute with the dipolar cations ($\Delta E_{sd}(\mathbf{r},\mathbf{\Omega};t)$) and with the dipolar solvent molecules (($\Delta E_{sp}(\mathbf{r},\mathbf{\Omega};t)$), and the dipole-ion contributions from the interactions of the solute with the charged species ($\Delta E_{si}(\mathbf{r},\mathbf{\Omega};t)$). Such a summation of three separate contributions arises from the linearization $\Delta\beta F_{\text{int}}$ in terms of dipolar and ionic density fluctuations ($\delta\rho_d$, $\delta\rho_p$ and δn_α). We will see later that this approximate description of $\Delta E_{total}(\mathbf{r},\mathbf{\Omega};t)$ and the neglect of cross-correlations among the ΔE_{sj} (with *j=d, p* or *i*) terms while forming the time correlation functions lead to an expression for the total dynamic Stokes shift where these interactions contribute in a mole-fraction weighted manner. This ideal composition dependent description of fluctuating total solvation energy might be different from that in real solution but we consider this as an approximation in order to develop a semi-molecular picture for qualitatively describing the measured Stokes shift dynamics in such complex multi-component mixtures. Since Stokes shift dynamics in (IL + dipolar solvent) binary mixtures is expected to be governed by the long wavelength density fluctuations, the intricate details of the solvent composition around a dissolve solute should play a minor role. This dominance of the collective solvent modes is probably the factor which nullifies inaccuracies associated with a number of approximations while developing a simple theory such as the present one and renders the ability to qualitatively describe the experimental Stokes shift dynamics of such extremely complex systems.

We next form the total (fluctuating) solvation energy auto-correlation function as follows,

$$< \Delta E_{total}(t)\Delta E_{total}(t') > = < \Delta E_{sd}(t)\Delta E_{sd}(t') > + < \Delta E_{sp}(t)\Delta E_{sp}(t') > + < \Delta E_{si}(t)\Delta E_{si}(t') >$$
$$+ < \Delta E_{sd}(t)\Delta E_{si}(t') > + < \Delta E_{si}(t)\Delta E_{sd}(t') >$$

$$+ < \Delta E_{si}(t)\Delta E_{sp}(t') > + < \Delta E_{sp}(t)\Delta E_{si}(t') >$$

$$+ < \Delta E_{sd}(t)\Delta E_{sp}(t') > + < \Delta E_{sp}(t)\Delta E_{sd}(t') >$$

$$= < \Delta E_{sd}(t)\Delta E_{sd}(t') > + < \Delta E_{sp}(t)\Delta E_{sp}(t') > + < \Delta E_{si}(t)\Delta E_{si}(t') >, \quad (6.2)$$

where the position and orientation dependencies of ΔE_{sj} are not shown explicitly in order to avoid crowding. The following comments are in order for the second equality in Eq. 6.2. Because of wide difference in timescales, the cross-correlations between the time dependent fluctuating dipole-dipole interaction energy (ΔE_{sd} or ΔE_{sp}) term and the dipole-ion interaction energy term (ΔE_{si}) are assumed to decouple completely from each other and thus vanish. Moreover, the simulation finding[44] of negligible contribution to solution dielectric constant from the cross-correlations of fluctuating dipoles of different polar species (dipolar ion and dipolar added solvent) suggests that contributions from $< \Delta E_{sd}(t)\Delta E_{sp}(t') >$ terms may be completely ignored. In other words, we set $\left\langle \Delta E_{sd}(t)\Delta E_{sp}(t') \right\rangle = 0 = \left\langle \Delta E_{sp}(t)\Delta E_{sd}(t') \right\rangle$, leading to the final form of Eq. 6.2.

The time dependence of the solvation energy relaxation is then followed in terms of the normalized solvation energy autocorrelation function

$$S_E(t) = \frac{\left\langle |\Delta E_{sd}(0)|^2 \right\rangle S_{sd}(t)}{\left\langle |\Delta E_{sd}(0)|^2 \right\rangle + \left\langle |\Delta E_{sp}(0)|^2 \right\rangle + \left\langle |\Delta E_{si}(0)|^2 \right\rangle} + \frac{\left\langle |\Delta E_{sp}(0)|^2 \right\rangle S_{sp}(t)}{\left\langle |\Delta E_{sd}(0)|^2 \right\rangle + \left\langle |\Delta E_{sp}(0)|^2 \right\rangle + \left\langle |\Delta E_{si}(0)|^2 \right\rangle} + \frac{\left\langle |\Delta E_{si}(0)|^2 \right\rangle S_{si}(t)}{\left\langle |\Delta E_{sd}(0)|^2 \right\rangle + \left\langle |\Delta E_{sp}(0)|^2 \right\rangle + \left\langle |\Delta E_{si}(0)|^2 \right\rangle},$$

(6.3)

where S_{sd}, S_{sp} and S_{si} are the individual normalized solvation energy autocorrelation functions due respectively to solute–dipolar ion (dipole-dipole), solute– added solvent (dipole-dipole) and solute – ion (dipole-ion) interactions. These three distinct interaction components, depending upon the average rate, contribute to constitute the total decay $S_E(t)$. Needless to mention, while the total decay is dominated by the fastest component, the average rate is determined by the slowest of these three separate relaxation channels.

6.2.2 Calculation of the Normalized Solvation Energy Autocorrelation Function Due to Solute-Dipolar Ion (Dipole-Dipole) Interaction, $S_{sd}(t)$

The normalized solvation energy autocorrelation function arising from the dipolar solute – dipolar ion interaction, $S_{sd}(t)$, is defined as follows:

$$S_{sd}(t) = \frac{<\Delta E_{sd}(t)\Delta E_{sd}(0)>}{<\left|\Delta E_{sd}(0)\right|^2>}$$

$$= \frac{A\int_0^\infty dk k^2 S^{10}_{solute}(k,t)\left|c^{10}_{sd}(k)\right|^2 S^{10}_{solvent}(k,t) + 2A\int_0^\infty dk k^2 S^{11}_{solute}(k,t)\left|c^{11}_{sd}(k)\right|^2 S^{11}_{solvent}(k,t)}{A\int_0^\infty dk k^2 S^{10}_{solute}(k)\left|c^{10}_{sd}(k)\right|^2 S^{10}_{solvent}(k) + 2A\int_0^\infty dk k^2 S^{11}_{solute}(k)\left|c^{11}_{sd}(k)\right|^2 S^{11}_{solvent}(k)}, \quad (6.4)$$

where A is a prefactor given by $2\rho_d^0 k_B T/(2\pi)^2$. $c^{lm}_{sd}(k)$ in Eq. 6.4 denotes the Fourier transform of the (l,m) component of the static correlation function between the solute and a dipolar ion, and $S^{lm}_{solvent}(k,t)$ is the same component of the orientational dynamic structure factor of the dipolar ions. $S^{lm}_{solute}(k,t)$ denotes the (l,m) component of solute dynamic structure factor. $c^{lm}_{sd}(k)$ has been obtained by using the mean spherical approximation (MSA) theory for binary dipolar mixtures with one of the components (dipolar solute) at limiting concentration.[107-108] Note that eventhough the real solution is a multi-component mixture, the use of the classical DFT and the subsequent treatment split the total solvation energy relaxation into relaxations of three distinct interaction contributions. These individual contributions then could be obtained by treating as those for binary mixtures with dipolar solute being present at infinite dilution. Note the dipole moment of the dipolar solute in its first excited state has been used while calculating $c^{lm}_{sd}(k)$ and other relevant quantities.

6.2.2.1 Calculation of the wavevector and time dependent orientational dynamic structure factor, $S^{lm}_{solvent}(k,t)$

As before,[84-88] the longitudinal ($S^{10}_{solvent}$) and transverse ($S^{11}_{solvent}$) components of the solvent (dipolar ion or added dipolar cosolvent) orientational dynamic structure factor (or, in other words, orinetational dipolar dynamic structure factor) have been obtained from the experimental dielectric relaxation data. These are given by the following relations,

$$S^{10}_{solvent}(k,t) = \frac{1}{4\pi 3Y}\left[1 - \frac{1}{\varepsilon_L(k)}\right] L^{-1}[z + \Sigma_{10}(k,z)]^{-1} \ , \qquad (6.5)$$

and $$S^{11}_{solvent}(k,t) = \frac{1}{4\pi 3Y}\left[\varepsilon_T(k) - 1\right] L^{-1}[z + \Sigma_{11}(k,z)]^{-1} \ , \qquad (6.6)$$

where the polarity parameter, $3Y = (4\pi/3k_BT)\mu^2\rho^0_d$ with μ and ρ^0_d being the dipole moment and density of the medium. $\varepsilon_L(k)$ and $\varepsilon_T(k)$ are the longitudinal and transverse components of the wave number dependent dielectric function and can be obtained from the orientational static structural correlations as follows:[88,89,104] $[1 - \varepsilon^{-1}_L(k)] = 3Yf^{-1}_{110}(k)$, and $[\varepsilon_T(k) - 1] = 3Yf^{-1}_{111}(k)$ with $f_{llm}(k) = 1 - (\rho^0_d/4\pi)(-1)^m c(llm,k)$. $f_{llm}(k)$ describes the wave number dependent (1,1,0), (1,1,1), and (1,1,-1) components of the orientational static structure of the dipolar particles (dipolar ions or dipolar solvents). In the present calculations, these static structural components have been obtained from the MSA theory[104-105] for (solute + solvent) binary dipolar mixtures with solute present at limiting concentration. L^{-1} represents the Laplace inversion and z is the frequency. $\Sigma_{lm}(k,z)$ is the $(l,m)^{\text{th}}$ component of the generalized rate of the orientational solvent polarization density relaxation. Calculation of $\Sigma_{lm}(k,z)$ is quite non-trivial[88,106-109] and a brief outline is provided in Appendix F.

6.2.2.1 Calculation of the Solute Dynamic Structure factor, $S^{lm}_{solute}(k,t)$

The solute dynamic structure factor is assumed to be diffusive (both rotational and translational) only and is given by[84-88]

$$S^{lm}_{solute}(k,t) = \frac{1}{4\pi}\exp\left[-\left(l(l+1)D^s_R + \mathrm{k}^2 D^s_T\right)t\right]. \qquad (6.7)$$

The rotational (D^s_R) and translational (D^s_T) diffusion coefficients of the solute (assumed spherical) have been obtained from the medium viscosity using the *stick* boundary condition. Eventhough the solute motion was introduced earlier in somewhat arbitrary manner in the expression for the time dependent fluctuating solvation energy of a dipolar solute,[108,110] the effects of the solute-motions were predicted to be quite significant for highly viscous non-dipolar ionic liquids.[87] The normalizing factor, $1/4\pi$, in Eq. 6.7 arises from the time averaging of all possible orientations for the solute dipole. This factor does not enter into the

calculations of dipole-dipole contribution to the Stokes shift because the magnitude of the shift should be the same for both fixed and mobile solute cases.

Following our earlier works,[85-86,111-112] we have calculated the solute-dipolar ion interaction contribution to the total dynamic Stokes shift from the square root of the denominator of Eq. 6.4. That is, $\Delta\nu_{sd}^{t} = \sqrt{\left\langle \left| E_{sd}(0) \right|^2 \right\rangle}$. This is because $\left\langle \left| \Delta E_{sd}(t=0) \right|^2 \right\rangle$ represents the square of the excess solvation energy due to solute-dipolar ion interactions evaluated at time zero immediately after laser excitation of a solute from its non-polar ground state to polar excited state. The equivalence between the calculated and experimental shifts is then drawn by assuming that pure solvent structure (and dynamics) does not change in presence of a solute (dipolar or non-polar) or sudden alteration of polarity of it upon excitation. This is essentially the linear response approximation and each comparison between theory and experiments presented here has been performed within the purview of this approximation.

6.2.3 Calculation of the Normalized Solvation Energy Autocorrelation Function due to Dipolar Solute-Added Dipolar Solvent (Dipole-Dipole) Interaction, $S_{sp}(t)$

The expression for the normalized solvation energy autocorrelation function due to dipolar solute-dipolar added solvent (dipole-dipole) interaction is, in fact, very similar to Eq. 6.4, and can be given by

$$S_{sp}(t) = \frac{< \Delta E_{sp}(t) \Delta E_{sp}(0) >}{< \left| \Delta E_{sp}(0) \right|^2 >}$$

$$= \frac{A\int_0^\infty dk k^2 S^{10}_{solute}(k,t) \left| c^{10}_{sp}(k) \right|^2 S^{10}_{p}(k,t) + 2A\int_0^\infty dk k^2 S^{11}_{solute}(k,t) \left| c^{11}_{sp}(k) \right|^2 S^{11}_{p}(k,t)}{A\int_0^\infty dk k^2 S^{10}_{solute}(k) \left| c^{10}_{sp}(k) \right|^2 S^{10}_{p}(k) + 2A\int_0^\infty dk k^2 S^{11}_{solute}(k) \left| c^{11}_{sp}(k) \right|^2 S^{11}_{p}(k)}, \quad (6.8)$$

where $c_{sp}(k)$ denote the wave number dependent solute-cosolvent (added dipolar solvent) static correlations and $S_p(k,t)$ the orientational dynamic structure factor of the dipolar cosolvent added to prepare the binary mixtures. As before, $c_{sp}(k)$ has been obtained from the dipolar MSA for binary mixtures with solute at infinite dilution, and $S_p(k,t)$ from the

measured dielectric relaxation function of the added cosolvent. The other quantities required for the calculation of $S_{sp}(t)$ have been obtained exactly in the same manner as followed for $S_{sd}(t)$ by using Eq. 6.4. Again, the dynamic Stokes shift due to the interaction between the dipolar solute and polar cosolvent molecules are approximated as, $\Delta\nu_{sp}^{t} = \sqrt{\left\langle \left| E_{sp}(0) \right|^2 \right\rangle}$.

6.2.4 Calculation of the Normalized Solvation Energy Autocorrelation Function due to Dipolar Solute – Ion (Dipole - Ion) Interaction, $S_{si}(t)$

The expression for the normalized solvation energy auto-correlation function due to solute dipole - ion (dipole-ion) interaction can be written as

$$S_{si}(t) = \frac{\left\langle \Delta E_{si}(t)\Delta E_{si}(0) \right\rangle}{\left\langle \left| \Delta E_{si}(0) \right|^2 \right\rangle} = \frac{B\sum_{\alpha,\beta}\sqrt{n_\alpha^0 n_\beta^0}\int_0^\infty dk k^2 S_{solute}^{10}(k,t)c_{s\alpha}^{10}(k)c_{s\beta}^{10}(-k)S_{\alpha\beta}^{ion}(k,t)}{B\sum_{\alpha,\beta}\sqrt{n_\alpha^0 n_\beta^0}\int_0^\infty dk k^2 S_{solute}^{10}(k)c_{s\alpha}^{10}(k)c_{s\beta}^{10}(-k)S_{\alpha\beta}^{ion}(k)}, \qquad (6.9)$$

where $B = 2(k_B T/2\pi)^2$ and $c_{s\alpha}^{10}(k)$ denote the (1,0) component of the wave number dependent static structural correlations between the dipolar solute and an ion of type α. $S_{\alpha\beta}^{ion}(k,t)$ is the partial isotropic ion dynamic structure factor. Note the derivation of Eq. 6.9 and calculation procedure of $S_{si}(t)$ have already been discussed in detail elsewhere[85,86] and thus not repeated here. For completeness, we would like to mention that a diffusive form[113] for $S_{\alpha\beta}^{ion}(k,t)$ has been used in our calculations where the diffusion coefficient of the ions (D_α) have been obtained from the medium viscosity by using the Stokes-Einstein relation with stick boundary condition. The relevant part of the isotropic ion static structure factor, $S_{\alpha\alpha}(k)$, has been approximated by the Percus-Yevick (P-Y) solution for binary mixtures[114] of singly charged hard spheres of equal radii and used the expressions derived elsewhere[115,116] for the calculation of ion static structure factor, $S_{\alpha\beta}^{ion}(k)$. The longitudinal component of the wavenumber dependent direct correlation function between the dipolar solute and ions, $c_{s\alpha}^{10}(k)$, is taken as, $c_{s\alpha}^{10}(k) = -\sqrt{\frac{4\pi}{3}}\left(\frac{4\pi i\mu_1 q_\alpha}{k_B T\varepsilon_0 k}\right)\frac{\sin(kr_c)}{kr_c}$, where μ_1 is the excited state dipole-moment of the dipolar solute, q_α the charge of α^{th} type ion, r_c the distance of the closest approach between the solute dipole and the ionic species. Note that the above calculation

schemes for the ion-dipole and ion-ion static correlations do not consider at all the static heterogeneity that may be present in these mixtures. As described in our earlier works,[85-86,111-112] the ion-solute contribution to the dynamical Stokes shift is given by $\sqrt{<|\Delta E_{si}(0)|^2>}$ which can be calculated easily from the denominator of Eq. 6.9. That is, $\Delta\nu_{si}^{t} = \sqrt{\left\langle |E_{si}(0)|^2 \right\rangle}$. Subsequently, the total dynamic Stokes shift is approximated as, $\Delta\nu_{tot}^{t} = \Delta\nu_{sd}^{t} + \Delta\nu_{si}^{t} + \Delta\nu_{sp}^{t} = \sqrt{\left\langle |\Delta E_{sd}(0)|^2 \right\rangle} + \sqrt{\left\langle |\Delta E_{si}(0)|^2 \right\rangle} + \sqrt{\left\langle |\Delta E_{sp}(0)|^2 \right\rangle}$. In addition, Stehfest algorithm[117] has been used to perform the Laplace inversion whenever required.

6.3 Numerical Results and Comparison with Experiments

In this section we shall first present the theoretical predictions on dynamic Stokes shift in several (IL + polar solvent) binary mixtures and its mixture composition dependence. Next the predicted mole fraction dependent Stokes shift dynamics for these mixtures are discussed. The solute considered in the calculations is coumarin 153 (C153) for which experimental results for a few (IL+ polar solvent) binary mixtures are available. Subsequently, the calculated results have been compared with experimental data in order to test the validity of the present theory and provide molecular level explanation for the experimental observations.

6.3.1 Dynamic Stokes Shift in Binary Mixtures: Composition Dependence

6.3.1.1 Binary Mixtures of ([Bmim][PF_6] + Water)

Table 6.1 summarizes the predicted and measured values of the dynamic Stokes shift for ([Bmim][PF_6] + water) binary mixtures at four water mole fractions (x_w) along with that for dry [Bmim][PF_6]. Experimental densities[6] at various water concentrations shown in this table indicate decrease (small though) in solution density with successive addition of water. While the dielectric relaxation data for pure ionic liquids reported in Ref. 94 and for pure water in Ref. 118 have been used in the present work for calculations of dynamic Stokes shift, the values in parentheses have been obtained by using the dielectric relaxation data reported in Ref. 119. It is interesting to note that relatively smaller ε_0 value (~12) for pure [Bmim][PF_6] reported in Ref. 119 significantly enhances the ion-dipole contribution to the total shift,[85,86] leading to an almost quantitative agreement between theory and experiments for the neat

ionic liquid.[81] This, in fact, shows the sensitivity of the present calculation scheme to a small variation in the description of experimental dielectric relaxation data for the same liquid.

Table 6.1: Comparison between the composition dependent predicted and experimental dynamic Stokes shift for C153 in ([Bmim] [PF_6] + water) binary mixtures

a) From Ref. 81
b) From Ref. 33

Mole fraction of water, x_w	Density (g/cm^3)	solute-dipolar cation (dipole-dipole) interaction contribution, $\Delta\nu_{sd}^t$ (cm^{-1})	solute-ion (dipole-ion) interaction contribution, $\Delta\nu_{si}^t$ (cm^{-1})	solute-water (dipole-dipole) interaction contribution $\Delta\nu_{sp}^t$ (cm^{-1})	Total $\Delta\nu_{tot}^t$ (cm^{-1})	Experiment (cm^{-1})
0.00	1.368	871 (861)	877 (1219)	0	1748(2080)	2000[a]
0.03	1.363	720 (714)	869 (1214)	9	1598 (1937)	1492[b]
0.10	1.359	684 (680)	831 (1160)	18	1533 (1858)	1494
0.18	1.355	644 (641)	785 (1098)	26	1455 (1765)	1493
0.22	1.353	625 (622)	763 (1066)	30	1418 (1718)	1506

However, the difference between the shift obtained for the neat ionic liquid and that in presence of water, $\Delta\Delta\nu_x^t = \Delta\nu_x^t(w=0) - \Delta\nu_x^t(w)$ (x being "sd", "si" or "tot"), remains approximately the same regardless of which dielectric relaxation data (from Ref. 94 or from Ref. 119) for [Bmim][PF_6] were used in the calculations. Interestingly, a comparison between the present calculations and experimental[33] shifts for aqueous binary mixtures of [Bmim][PF_6] reveals a close agreement, suggesting that the interactions of the dipolar solute with the anions and dipolar cations govern the dynamic Stokes shift in this binary mixture at the water-deficient regime. A closer inspection of Table 6.1 further reveals that the calculated total Stokes shift ($\Delta\nu_{tot}^t$) decreases with water concentration as both the solute-cation (diplole-dipole) and solute-ion (dipole-ion) interaction contributions decrease. The solute-water (dipole-dipole) interaction contribution to $\Delta\nu_{tot}^t$, on the other hand, increases with water concentration but remains very small ($\leq 2\%$) at this water-deficient regime. Note that upon

addition of ~0.22 mole fraction (1.8% w/w) of water in pure [Bmim][PF_6], the solute-cation dipolar interaction contribution, $\Delta\nu_{sd}^{t}$, decreases by ~250 cm^{-1} whereas the solute-ion (dipole-ion) contribution, $\Delta\nu_{si}^{t}$, registers a decrease[120] of approximately 100 cm^{-1}. The present calculations therefore suggest an over-all decrease of ~350 cm^{-1} in total dynamic Stokes shift upon addition of ~0.22 mole fraction of water in dry [Bmim][PF_6]. This is somewhat different from what has been found in experiments[33] where the estimated experimental shift was found to be ~1500 cm^{-1} and showed no dependence on x_w. In addition, measurements described in Ref. 33 do not report the estimated true shift for dry [Bmim][PF_6], which prohibits further analyses. However, experimental study by the same research group reported true dynamic Stokes shift of ~1400 cm^{-1} and ~1600 cm^{-1} for C153 in dry [Hmim][PF_6][34] and [Emim][$EtSO_4$],[35] respectively. Interestingly, several other measurements[79,81,121] using C153 in ionic liquids containing imidazolium cations reported true estimated shift of ~2000 cm^{-1}. All these observations indicate that the true estimated shifts reported for C153 in ([Bmim][PF_6] + water) binary mixtures[33] might be ~300-500 cm^{-1} less than the expected "true" shift for this mixture. One of the most likely reasons could be imperfect drying of the ionic liquids and the presence of additional moisture might have led to smaller shift due to reduced ion-solute interaction because of decreased ion-density upon dilution. In fact, the present theory suggests that the calculated shift decreases with water concentration because of dilution effects. A more quantitative description of these dilution effects will be provided when the mixture composition dependence of dynamic Stokes shift in ([Bmim][BF_4] + water) binary mixtures are presented.

6.3.1.2 Binary Mixtures of ([Bmim][BF_4] + Water)

Table 6.2 summarizes the calculated dynamic Stokes shift values for C153 in ([Bmim][BF_4] + water) binary mixtures at various mole fractions of water. As before, the values in parentheses have been calculated by using the dielectric relaxation data reported in Ref. 119 and the predicted shift for the neat [Bmim][BF_4] matches well with the experimental estimate (~1900 cm^{-1}).[79] Note here that higher solubility of water in [Bmim][BF_4] than in its hydrophobic counterpart [Bmim][PF_6] allows one to study the dynamic Stokes shift even in very dilute aqueous solution of [Bmim][BF_4]. Consequently, the present calculations have

been extended from the neat ionic liquid to aqueous binary mixture with 0.9 mole fraction of water. Data in Table 6.2 indicates

that except the water-solute dipolar interaction contribution ($\Delta\nu_{sp}^{t}$), other individual interaction contributions as well as the total calculated shift decrease upon increasing the water concentration in ([Bmim][BF_4] + water) binary mixture. The decrease in calculated total shift is quite large (~1100 cm^{-1}) for changing the water concentration from $x_w = 0$ to $x_w = 0.9$.

According to the present theory, such a substantial reduction in dynamic Stokes shift originates mainly from the following two sources. First, successive addition of water reduces the individual (anion and dipolar cation) as well as the total number densities in the mixture (see Fig. C10, Appendix C). This dilution significantly reduces the value at the collective ($k\sigma \to 0$) limit of the wave number dependent solute-cation static orientational structural correlation function ($\sqrt{\left|c_{sd}^{10}(k)\right|^2}$). This is shown in the upper panel of Fig. 6.1. The transverse component, $\sqrt{\left|c_{sd}^{11}(k)\right|^2}$, on the other hand, increases with water concentration in binary mixture but the extent of increase is much smaller (lower panel, Fig. 6.1) than the

Table 6.2: Composition dependence of the predicted dynamic Stokes shift for C153 in ([Bmim] [BF_4] + water) binary mixtures

Mole fraction of water, x_w	Density (g/cm^3)	solute-dipolar cation (dipole-dipole) interaction contribution, $\Delta\nu_{sd}^t$ (cm^{-1})	solute-ion (dipole-ion) interaction contribution, $\Delta\nu_{si}^t$ (cm^{-1})	solute-water (dipole-dipole) interaction contribution $\Delta\nu_{sp}^t$ (cm^{-1})	Total $\Delta\nu_{tot}^t$ (cm^{-1})
0.0	1.182	695 (690)	1033 (1253)	0	1728 (1943)
0.1	1.179	671 (665)	970 (1177)	18	1659 (1860)
0.2	1.176	630 (625)	916 (1112)	26	1572 (1753)
0.3	1.172	583 (578)	849 (1030)	35	1467 (1643)
0.4	1.166	527 (520)	761 (924)	47	1335 (1491)
0.5	1.161	485 (480)	693 (843)	59	1237 (1382)
0.6	1.153	443 (440)	612 (745)	76	1131 (1261)
0.7	1.141	391 (381)	510 (622)	108	1009 (1111)
0.8	1.125	332 (328)	400 (488)	166	898 (982)
0.9	1.093	245 (240)	265 (335)	263	773 (838)

decrease in $\sqrt{\left|c_{sd}^{10}(k)\right|^2}$. The cation-cation dipolar orientational static structural correlation function, $S_{solvent}^{lm}(k)$, also decreases with successive lowering of dipolar cation density (see Fig. C11, Appendix C). The decrease in dipolar cation density and the consequent reduction in solute-cation and cation-cation orientational static structural correlations are responsible for the lowering of the predicted value of solute-cation dipole-dipole contribution ($\Delta\nu_{sd}^t$) from 695 cm^{-1} at x_w = 0 to 245 cm^{-1} at x_w = 0.9 in ([Bmim][BF_4] + water) binary mixture. Second, the solute-ion dipole-ion interaction contribution, $\Delta\nu_{si}^t$, decreases by ~750 cm^{-1} for increasing x_w from 0 to 0.9 mainly because of the concomitant decrease in ion number densities. Note that the approximate expression used here to obtain the ion-dipole direct correlation function, $c_{s\alpha}^{10}(k)$, does not depend on density. Moreover, the density-induced changes in the ion-ion static structural correlations, $S_{\alpha\beta}^{10}(k)$ (for both $\alpha = \beta$ and $\alpha \neq \beta$), are

small (see Fig. C12, Appendix C). Therefore, the decrease in $\Delta\nu_{si}^{t}$ upon increasing x_w arises almost entirely from the presence of the density term as a multiplicative factor in Eq. 6.9. Note also that at x_w = 0.9, the calculated value of the shift ($\Delta\nu_{sp}^{t}$) due to solute-water dipole-dipole

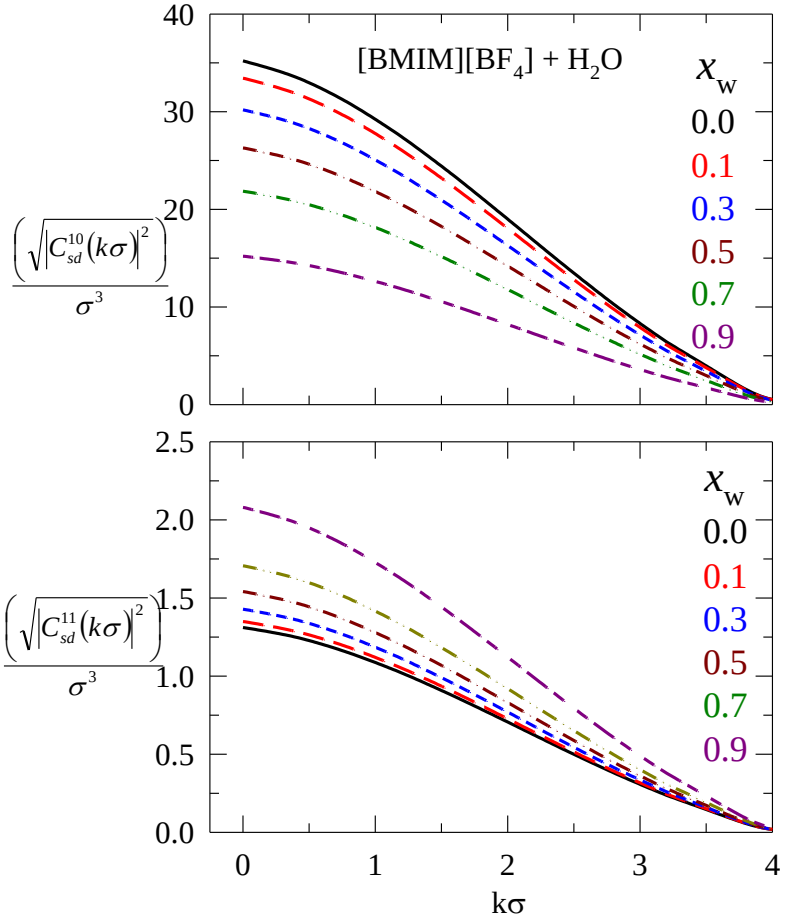

Fig. 6.1: A plot of longitudinal (10) and transverse (11) components of the wave number dependent dipolar solute-dipolar cation (dipole-dipole) static direct correlation function for aqueous mixtures of the ionic liquid, [Bmim][BF_4] at six different mole fractions (x_w) of water. The curves are color-coded and x_w increases from black to dark pink. The solute is C153 and the dipole moment of excited solute has been used in these calculations at T = 298 K.

Note also that, at x_w = 0.9, the calculated value of the shift ($\Delta\nu_{sp}$ (t)) due to solute water dipole dipoleinteraction is only about 250 cm^{-1} which is much smaller than expected[123] for a

dipolar solute like C153. This is because of using ~1.9 D as dipole moment for water[124] in the present calculations. However, the predicted shift becomes ~2000 cm^{-1} for a C153-like probe in pure water (C153 is sparingly soluble in pure water) if one uses ~2.5 D as water dipole moment.[125]

6.3.1.3 Binary Mixtures of ([Bmim][BF_4] + Acetonitrile)

Next we present the numerical results on composition dependent dynamic Stokes shift for C153 in ([Bmim][BF_4] + acetonitrile) binary mixture. This mixture is a relatively less complicated system than the corresponding aqueous mixture because of the non-associative nature of acetonitrile. In addition, one expects a dominance of $\Delta\nu_{sp}^{t}$ contribution over the other two ($\Delta\nu_{sd}^{t}$ and $\Delta\nu_{si}^{t}$) at sufficiently higher concentration of acetonitrile. Since the dipole moment of acetonitrile is larger (~3.9 D)[126] than that of water, the present theory should predict larger Stokes shift values in acetonitrile than water. The calculated shift values at various mole fractions of acetonitrile (x_{AN}) are summarized in Table 6.3.

Table 6.3: Composition dependence of predicted dynamic Stokes shift for C153 in ([Bmim][BF_4] + acetonitrile) binary mixtures

Mole fraction of acetonitrile, x_{AN}	Density (g/cm^3)	solute-dipolar cation (dipole-dipole) interaction contribution, $\Delta\nu_{sd}^{t}$ (cm^{-1})	solute-ion (dipole-ion) interaction contribution, $\Delta\nu_{si}^{t}$ (cm^{-1})	solute-water (dipole-dipole) interaction contribution $\Delta\nu_{sp}^{t}$ (cm^{-1})	Total $\Delta\nu_{tot}^{t}$ (cm^{-1})
0.0	1.182	695 (690)	1033 (1253)	0	1728 (1943)
0.1	1.160	641 (632)	972 (1180)	41	1654 (1853)
0.2	1.117	595 (592)	908 (1102)	75	1578 (1769)
0.3	1.075	537 (532)	840 (1020)	123	1500 (1675)
0.4	1.032	475 (470)	768 (933)	187	1430 (1590)
0.5	0.990	409 (401)	689 (838)	273	1371 (1512)
0.6	0.947	337 (332)	604 (735)	384	1325 (1451)
0.7	0.905	260 (254)	508 (619)	529	1297 (1402)
0.8	0.862	179 (176)	396 (484)	725	1300 (1385)
0.9	0.820	95 (90)	258 (315)	1011	1364 (1416)

Dielectric relaxation data necessary for the calculation of $\Delta\nu_{sp}^{t}$ were taken from the existing literature.[126,127] It is interesting to note here that eventhough the magnitudes of reduction in $\Delta\nu_{sd}^{t}$ and $\Delta\nu_{si}^{t}$ for increasing x_{AN} from zero to 0.9 in ([Bmim][BF_4] + acetonitrile) binary mixture are comparable with those predicted for ([Bmim][BF_4] + water) binary mixture, the decrease in total shift ($\Delta\nu_{tot}^{t}$) for ([Bmim][BF_4] + acetonitrile) mixture is roughly one-third of that obtained for the corresponding aqueous mixture. This is because of relatively larger positive contribution of $\Delta\nu_{sp}^{t}$ to the total shift due to its larger dipole moment of acetonitrile. In fact, $\Delta\nu_{sp}^{t}$ becomes larger than $(\Delta\nu_{sd}^{t}+\Delta\nu_{si}^{t})$ at x_{AN} = 0.8 and a turn around in composition dependence of $\Delta\nu_{tot}^{t}$ occurs at this acetonitrile concentration. This prediction should be tested against experiments. However, the predicted shifts at higher values of x_{AN} might be less accurate because the use of dipolar MSA for strongly polar solvents is known to produce partially incorrect solute-solvent and solvent-solvent static correlations.[104] The fact that the calculated shift for C153 in pure acetonitrile is ~1500 cm^{-1} – a value ~700 cm^{-1} less than what has been observed in experiments[128]- reflects this non-quantitativeness of a theory that uses static correlations as input from the MSA.

6.3.2 Composition Dependent Stokes Shift Dynamics in (IL + Polar Solvent) Binary Mixtures

In this subsection theoretically predicted composition dependent Stokes shift dynamics for C153 in three binary mixtures - ([Bmim][PF_6] + water), ([Bmim][BF_4] + water) and ([Bmim][BF_4] + acetonitrile) will be presented. Since experimentally measured dynamics is incomplete for ([Bmim][PF_6] + water) mixtures and no experimental data exist for the other two mixtures, a direct comparison of dynamics between the predicted dynamics and measurements could not be done. Therefore, experimental reexamination is necessary to test the validity of the predicted dynamics for these binary mixtures. Note our earlier works[85,86] have suggested a contribution of ~10-15% to the total dynamics from the solute-ion (dipole-ion) interaction and the rest from the dipolar interaction between the solute and dipolar cations. In this work also the contribution from the solute-ion interaction (S_{si}) has been fixed

to 10% and the effects of added dipolar solvent on solvation energy relaxation have been investigated via constructing the following normalized correlation function,

$$S_{ss}(t) = 0.9\left[fS_{sd}(t) + (1-f)S_{sp}(t)\right] + 0.1S_{si}(t), \qquad (6.10)$$

where $S_{sd}(t)$, $S_{sp}(t)$ and $S_{si}(t)$ have been obtained by using Eq. 6.4, Eq. 6.8 and Eq. 6.9, respectively. The relative contribution to the total dynamics arising from solute-cosolvent dipolar interaction can then be investigated by varying the value of f in Eq. 6.10. As usual, the average solvation time is obtained via time integration as follows: $\langle \tau_x \rangle = \int_0^\infty dt S_x(t)$, where x represent "sd", "sp","si"and "ss". It is obvious then the inclusion of larger contribution from $S_{si}(t)$ will lead to larger value of $\langle \tau_{ss} \rangle$ as the decay of $S_{si}(t)$ is solely governed by the centre-of-mass motion of the ions.

6.3.2.1 Binary Mixtures of ([Bmim][PF_6] + Water)

Fig. 6.2 displays the decay of the solvation response function, $S_{ss}(t)$, calculated at four different mole fractions of water (x_w) for a fixed value of f = 0.9. Composition dependent viscosities for these mixtures are summarized in Table A16 (Appendix A). For comparison, the calculated decay for the neat IL is also shown in the same figure. As observed in experiments, the calculated decays are bimodal both for the neat IL[77] and its aqueous mixtures.[33] Addition of water accelerates the average decay rate over that in the neat IL, the enhancement factor between the neat IL and aqueous mixture at x_w=0.22 ($\langle \tau_{ss} \rangle^{IL} / \langle \tau_{ss} \rangle^{mixture} \approx 2.2$) being roughly proportional to the change in medium viscosity[6] ($\eta^{IL} / \eta^{mixture} \approx 2.9$). The theory also predicts an insensitivity of the decay rate to x_w after the first addition of water in the neat IL for an initial period of ~50 ps and then branches out showing the effects of medium viscosity. This initial insensitivity to medium viscosity in the present theory stresses the importance of rapid angular readjustment of the dipolar particles present in the system which has been incorporated in the theory by using the experimental measured frequency dependent dielectric function, $\varepsilon(z)$. Note that ~50% of the decay is complete within this initial period, and experiments unable to capture this initial fast dynamics might lead to a different conclusion. In fact, existing measurements with limited time resolution (~85 ps)[33] report setady increase in decay rate upon addition of water in

[Bmim][PF_6]. Interestingly, the measured average solvation time changes by a factor of ~2.5 for changing x_w from ~0.1 to ~0.22, the calculated average times differ by a factor of ~1.6 for the same variation of x_w. Since these experiments report a missing of ~30-40% of the initial fast dynamics which tallies well with the prediction of half of the dynamics being complete in the first 50 ps, it is

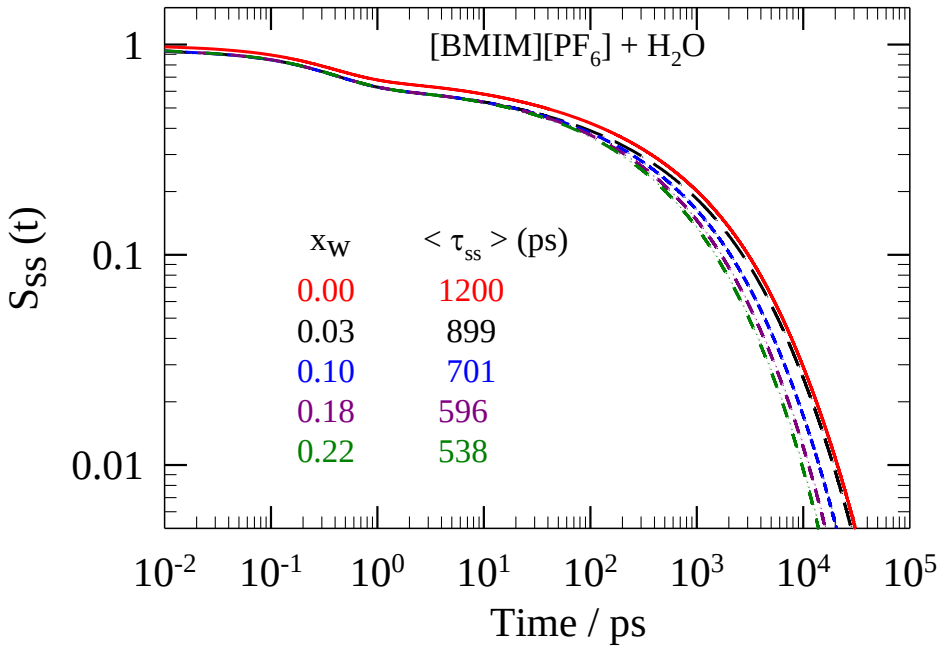

Fig. 6.2: Decay of the constructed solvation response function, $S_{ss}(t)$, as a function of time (log-log scale) for the laser-excited solute, C153, in binary mixtures of ([Bmim][PF_6] + water) at five different values of x_w at 298 K. The curves are color-coded where x_w increases from red to dark green. Note x_w values along with the corresponding average solvation times are also quoted explicitly (color-coded). Dielectric relaxation data required for the calculations have been taken from Ref. 94 (IL) and Ref. 118 (water). The dipole moment of the cation used is 4.4 D (Ref. 85) and radii of the cation and anion are 3.39 and 2.72 angstrom, respectively. The dipole moment of water used is 1.85 D and radius 1.425 angstrom (Ref. 126). The radius of C153 used is 3.9 angstrom (Ref. 128). Solution viscosity values used are those reported in Ref. 6.

likely that the experimentally observed more pronounced dependence on x_w is a reflection of incomplete detection rather the actual composition dependence of Stokes shift dynamics in these aqueous binary mixtures.

The difference between theory and experiments becomes more prominent when one compares the amplitudes (a_i) and time constants (τ_i). Table 6.4 summarizes the amplitudes and time constants obtained for ([Bmim][PF_6] + water) binary mixture at x_w=0.10 from fitting the calculated decays to the following general form: $S_{fit}(t) = a_1 \exp[-(t/\tau_1)^{\alpha}] + a_2 \exp[-(t/\tau_2)^{\beta}]$ with α and β as stretching exponents.

Table 6.4: Comparison between the calculated and experimental solvation response function for C153 in aqueous mixture of [Bmim][PF_6] at $x_w = 0.1$

$S_x(t)$	f	a_1	τ_1 (ps)	α	a_2	τ_2 (ps)	β	$\langle\tau_x\rangle$ (ps)
$S_{si}(t)$		0.11	123	1	0.89	2500	1	2240
$S_{sd}(t)$		0.29	0.32	1	0.71	294	0.38	610
$S_{sp}(t)$		0.58	0.005	1	0.42	0.53	1	0.23
$S_{ss}(t)$= 0.90 [f $S_{Sd}(t)$+(1-f) $S_{sp}(t)$] + 0.10$S_{si}(t)$	0.0	0.90	0.16	1	0.10	1972	1	194
	0.1	0.85	0.10	0.40	0.15	1667	0.67	290
	0.2	0.79	0.11	0.42	0.21	1190	0.53	354
	0.3	0.73	0.12	0.43	0.27	897	0.47	405
	0.4	0.66	0.13	0.45	0.34	720	0.44	462
	0.5	0.60	0.15	0.48	0.40	611	0.43	496
	0.6	0.49	0.20	1	0.51	427	0.35	621
	0.7	0.44	0.22	1	0.56	423	0.37	630
	0.8	0.38	0.24	1	0.62	417	0.38	680
	0.9	0.33	0.28	1	0.67	410	0.39	701
	1.0	0.27	0.31	1	0.73	404	0.40	733
Experiment[a]		0.85	648	1	0.15	11010	1	2200

a) From Ref. 33

Similar fit parameters for other values of x_w are provided in the Supporting Information (Tables A17 – A19, Appendix A). Since the Stokes shift dynamics in water is much faster

than in neat [Bmim][PF_6], progressive inclusion of more contribution from the solute-cation (dipole-dipole) interaction via the factor f renders the dynamics successively slower. Note in Table 6.4 that the time constants associated with the measured[33] bi-exponential solvation response function are much larger than those obtained in the calculations at any contribution (f) of $S_{sd}(t)$. Even the predicted decay of $S_{si}(t)$ - the slowest and the only bi-exponential among all of the components – does not produce a time constant in the range of ~12 ns. In fact, the fastest time constant (τ_1) obtained in experiments at this x_w is much closer to the slowest (τ_2) of the calculated ones. In addition, the calculated decays of $S_{ss}(t)$ at all non-zero values of f are bimodal with a stretched exponential (for $0.1 \le f \le 0.5$ with $0.4 \le \alpha \le 0.5$) or exponential (for $f \ge 0.6$) fast component, followed by a stretched-exponential slow component with β ranging between 0.66 and 0.37. Attempt to simple exponential fit to the calculated fast component for f ranging between 0.1 and 0.5 at all water mole fractions studied here has led to inaccurate description of the relevant decays. Interestingly, average solvation time measured[33] at x_w=0.1 is ~3 ns which is approximately three times larger than even the value for neat [Bmim][PF_6] measured in experiments with sophisticated technique and/or better time resolution.[77,81] A further comparison among the data for the neat IL reported by these authors[129] and other researchers[36, 130, 131] strongly suggests that the measured[33] average solvation times for ([Bmim][PF_6] + water) binary mixtures have been uniformly overestimated by a factor of ~3 over the 'true' values. This has led us to believe that the 'true' average solvation time at x_w=0.1 should be less than a nanosecond. The present theory predicts such a value at x_w=0.1 with $f = 0.9$ which incorporates ~10% contribution each to the total dynamics from the water-solute (dipole-dipole) and solute-ion (dipole-ion) interactions.

The origin of increase in average rate of solvation with water mole fraction in ([Bmim][PF_6] + water) binary mixtures is further explored in Fig. 6.3 where the decays of the solute-cation dipole-dipole interaction (S_{sd}) and solute-ion dipole-ion interaction (S_{si}) components are shown as a function of time. Note the effects of medium viscosity on both S_{sd} and S_{si} have been incorporated via the translational kernel ($\Gamma_T(k,z)$, see Eq. A2) only. As expected,[89] larger translational diffusion coefficient at higher water concentration (that is, lower

viscosity[6]) facilitates the decay of $S_{sd}(t)$ at longer times, and the decay of $S_{si}(t)$ becomes faster uniformly over the entire time-range. Consequently, the ratio between the average solvation times at x_w=0 and 0.22 calculated from the decay of $S_{si}(t)$ is somewhat closer ($\langle \tau_{si}(x_w = 0) \rangle / \langle \tau_{si}(x_w = 0.22) \rangle \approx 2.6$) to the corresponding viscosity-ratio ($\langle \eta(x_w = 0) \rangle / \langle \eta(x_w = 0.22) \rangle \approx 2.9$) than that ($\approx 2.3$) for the average times obtained from

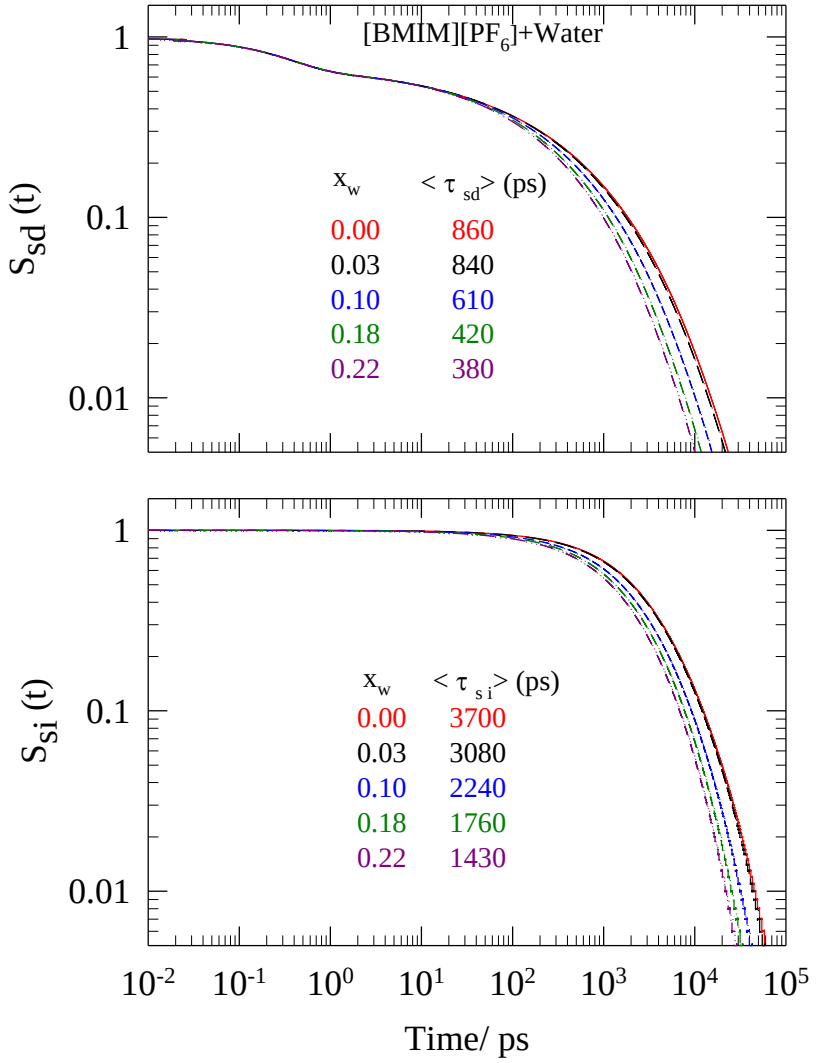

Fig. 6.3: Decay of the calculated individual response functions at five different compositions for the binary mixture of ([Bmim][PF_6] + water) at 298 K. While the upper panel shows the time dependent decay (log-log scale) of the normalized solvation energy due to solute-cation dipole-dipole interaction, the lower panel presents that due to solute-ion dipole-ion interaction. The solute used is C153. The curves are color-coded, and both x_w values and corresponding average solvation times are clearly mentioned in these panels. Note x_w increases from red to dark pink.

$S_{sd}(t)$. The effects of change in solution viscosity are more pronounced for $S_{si}(t)$ because the relevant relaxation occurs only via the translational diffusion of the ionic particles.

6.3.2.2 Binary Mixtures of ([Bmim][BF_4] + Water)

Calculated decays of the solvation response function ($S_{ss}(t)$) for C153 in aqueous solution of [Bmim][BF_4] for five different water mole fractions (x_w) are presented in Fig. 6.4. Note that for $x_w \neq 0$, calculations have been performed with $f = 0.9$. Dielectric relaxation data used in these calculations are those reported in Ref. 94. As observed for ([Bmim][PF_6] + water) binary mixtures, here too the decay becomes increasingly faster upon successive addition of water in [Bmim][BF_4].

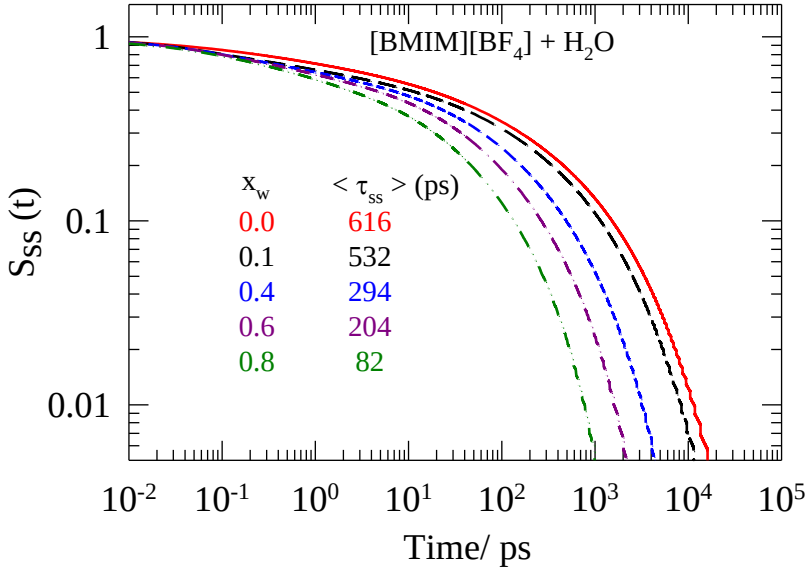

Fig. 6.4: Composition dependence of the constructed solvation response function for C153 in binary mixtures of ([Bmim][BF_4] + water) at 298 K. Time-dependent decays at five different water mole fractions (x_w) are shown using a color code where x_w increases from red to dark green. Numerical values for the x_w considered and the corresponding average solvation times are also shown. The cation and anion radii used are (in angstrom unit) 3.39 and 2.29 respectively and the cation dipole moment 3.7 D (Ref. 85). Dielectric relaxation data required for the calculations have been taken from Ref. 94 (IL). Solution viscosity values used are taken from Ref. 6.

The fit parameters for the calculated decays at various values of x_w are summarized in Table A20 (Appendix A). Following the trend of mixture composition dependent viscosity presented in Table A16 (Appendix A), all measures of the average solvation time ($\langle \tau_{si} \rangle, \langle \tau_{sd} \rangle$

and $\langle \tau_{ss} \rangle$) show a decrease upon increasing x_w in the mixture. Data in this table (Table A20, Appendix A) reveals that $\langle \tau_{ss}(x_w = 0) \rangle / \langle \tau_{ss}(x_w = 0.8) \rangle$ is much smaller (≈ 7.8) than the corresponding viscosity-ratio, $\langle \eta(x_w = 0) \rangle / \langle \eta(x_w = 0.8) \rangle \approx 20)$. Such a relatively weaker viscosity dependence originates in the calculations from the weaker coupling of the $S_{sd}(t)$ to medium viscosity which produces, $\langle \tau_{sd}(x_w = 0) \rangle / \langle \tau_{sd}(x_w = 0.8) \rangle \approx 6.3$. This is approximately three times smaller than the corresponding viscosity ratio. The coupling for $S_{si}(t)$ is stronger, producing $\langle \tau_{si}(x_w = 0) \rangle / \langle \tau_{si}(x_w = 0.8) \rangle \approx 12.4$. The fact that $\langle \tau_{ss}(x_w = 0) \rangle / \langle \tau_{ss}(x_w = 0.8) \rangle$ is closer to $\langle \tau_{sd}(x_w = 0) \rangle / \langle \tau_{sd}(x_w = 0.8) \rangle$ than to $\langle \tau_{si}(x_w = 0) \rangle / \langle \tau_{si}(x_w = 0.8) \rangle$ indicates dominance of the solute-cation dipole-dipole interaction contribution in the solvation energy relaxation of a laser-excited polar dye in these binary mixtures. Experimental studies with ([Bmim][BF_4] + water) binary mixtures should be carried out to test whether such a decoupling between average solvation time and viscosity exists for this mixture.

6.3.2.3 Binary Mixtures of ([Bmim][BF_4] + Acetonitrile)

Calculated decays of $S_{ss}(t)$ for C153 in binary mixture of ([Bmim][BF_4] + acetonitrile) for five different acetonitrile mole fractions (x_{AN}) are shown in Fig. 6.5. As before, calculations have been performed with $f = 0.9$ for mixtures at $x_{an} \neq 0$. Decays shown in this figure are clearly bimodal and indicate progressive enhancement of average solvation rate upon successive addition of acetonitrile in this ionic liquid. Time constants and amplitudes obtained from fit of these decays and a few others are provided in Table A21 (Appendix A). As these data indicate, average solvation times obtained from the individual (S_{sd} and S_{si}) and the constructed (S_{ss}) decays decrease steadily upon successive addition of acetonitrile in [Bmim][BF_4]. In fact, $\langle \tau_{ss} \rangle$ decreases so much upon addition of water or acetonitrile in [Bmim][BF_4] that it becomes comparable to the measured average solvation times in 1-butanol or 1-pentanol[128] at 0.8 mole fraction of added dipolar solvent. As seen in ([Bmim][BF_4] + water) binary mixture, the ratio of average solvation times at the lowest and

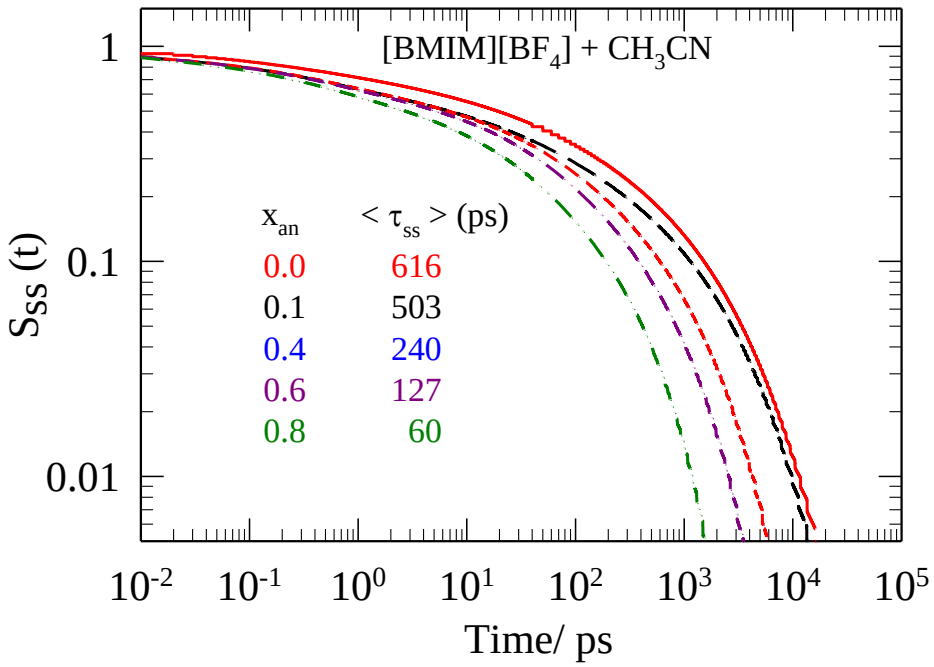

Fig. 6.5: Acetonitrile mole fraction (x_{AN}) dependence of the constructed solvation response function, $S_{ss}(t)$, for binary mixtures of ([Bmim][BF_4] + acetonitrile) at 298 K. As before, curves are color-coded where x_{AN} increases from red to dark green. Average solvation times calculated at these acetonitrile mole fractions are also mentioned (color coded). Dielectric relaxation data for acetonitrile used in the calculations are those from Refs. 126 and 127. Radius of acetonitrile used is 2.24 angstrom (Ref. 88).

highest acetonitrile concentrations, $\langle \tau_{ss}(x_{an}=0)\rangle / \langle \tau_{ss}(x_{an}=0.8)\rangle$, is approximately 10 and much smaller than the corresponding viscosity ratio, $\langle \eta(x_{an}=0)\rangle / \langle \eta(x_{an}=0.8)\rangle \approx 31$. Interestingly, $\langle \tau_{sd}(x_{an}=0)\rangle / \langle \tau_{sd}(x_{an}=0.8)\rangle \approx 7.6$ and $\langle \tau_{si}(x_{an}=0)\rangle / \langle \tau_{si}(x_{an}=0.8)\rangle \approx 11$, which again suggests substantial decoupling of the average solvation rate from medium viscosity and a minor role for the structural relaxation via ion translation.

6.4 Discussion

The theory developed here is a generalized semi-molecular theory for studying Stokes shift dynamics in binary mixtures of ionic liquid with a conventional polar solvent. This theory can also be suitably extended to investigate the fluorescence dynamics in binary mixture of ionic liquids, provided suitable dielectric relaxation data are available. It is to be mentioned that the present treatment neither incorporates the effects of medium heterogeneity nor the shape of the ions while calculating the static correlations. Moreover, a linearized statistical mechanical prescription, such as, the MSA, has been used to calculate the spatial correlations between solute-ion, ion-ion and solvent-solvent particles. These approximations definitely make the theory a less quantitative one because the real mixture is composed of neither spherical particles (ions or solvent molecules) nor completely free of heterogeneity.[131-137] However, this becomes a minor issue as the measured polar solvation response in these systems via fluorescence Stokes shift experiments is primarily a collective response where details of the spatial arrangement assume secondary importance. A more important issue is, however, the systematic incorporation in the theory of the non-ideal composition dependence observed in experiments[20-22] with several (ionic liquid + polar solvent) binary mixtures. Unfortunately, the non-ideality in spatial correlations (that is, solution structure) cannot be incorporated in the theory described here in its present form.

One can, however, partially account for the solution non-ideality via using the experimental dielectric relaxation data of the binary mixture, assuming the mixture an effective dipolar medium where the solution ε_0 determines the dipole moment of the 'fictitious' effective dipolar species.[84] The ions are then assumed to be dispersed in such effective dipolar medium. Dynamic Stokes shift in such an effective medium can then be described as composed of contributions from dipolar solute-dipolar medium(effective) interaction and dipolar solute-ion (dipole-ion) interaction. Subsequently, one calculates Stokes shift and dynamics as before by using Eq. 6.4 and Eq. 6.9. Accordingly, the dynamic Stokes shift may be expressed as, $\Delta\nu^t_{tot,eff} = \Delta\nu^t_{sd,eff} + \Delta\nu^t_{si,eff}$, and the dynamics as, $S_{ss,eff}(t) = 0.9S_{sd,eff}(t) + 0.1S_{si}(t)$. We have already carried out such calculations for binary mixtures of [Bmim][BF_4] and dichloromethane (DCM) for which composition dependent dielectric relaxation data measured over a broad frequency range[91] are available. Mixture

composition dependent effective dipole moment is obtained from solution ε_0 by using Cavell's equation.[91,138] The calculated dynamic Stokes shifts and average solvation times are shown as a function of DCM mole fraction (x_{DCM}) in the first two panels of Fig. 6.6. The bottom panel shows the solution viscosity dependence of calculated average solvation times for ([Bmim][BF_4] + DCM) binary mixtures where the same (viscosity dependence) for experimentally measured solvation times in several pure ionic liquids at different temperatures are also presented. The results are shown for DCM mole fraction up to 0.8 in order to avoid inaccuracy in the calculations due to the presence of complex ionic species in the real mixtures at further higher dilutions of the ionic liquid.[91] Interestingly, the calculated total shift decreases almost *linearly* with increasing x_{DCM} and do not reflect the non-linear composition dependence observed in experiments for ε_0 (Fig. C13, Appendix C). The individual (dipole-dipole and dipole-ion) interaction contributions, also decreasing with increasing x_{DCM}, exhibit a slight non-ideality with opposite trends which cancels each other to produce a linear dependence of the total shift on mixture composition. The dipole-dipole interaction contribution, $\Delta\nu^t_{sd}$ decreases because of reduction in both the effective dipole moment (4.49 D at x_{DCM}=0 to 2.7 D at $x_{DCM} \approx 0.8$) and the dipole density. Note here that the dipole-ion contribution to the shift, $\Delta\nu^t_{si}$, decreases with decreasing static dielectric constant eventhough it was argued earlier[85] that $\Delta\nu^t_{si}$ should increase in such a scenario. The steady decrease in ion density upon successive addition of DCM in the mixture which is shown in the second panel of Fig. S10, is responsible for the decrease of $\Delta\nu^t_{si}$ with DCM mole fraction. The calculated average solvation times also show a weak non-ideal mixture composition dependence because of the weak to moderate non-linear composition dependence of the dielectric relaxation times and solution viscosity (see respectively the third and the fourth panels, Fig. S10). The lower panel of Fig. 6.6 suggests that the composition dependent $\langle\tau_{ss}\rangle$ exhibits a power-law dependence on solution viscosity ($\langle\tau_{ss}\rangle \propto (\eta/T)^a$) with $a = 1.05$. Note this value of power (a) indicates validity of hydrodynamic description ($a = 1$) of motions for solvating particles and resembles the results for neat ionic liquids

($a = 1$).[139] The individual average solvation times ($\langle \tau_{sd,eff} \rangle$ and $\langle \tau_{si} \rangle$), however, show non-linear composition dependence but with opposite trends. A relatively smaller weight of $\langle \tau_{si} \rangle$ in $\langle \tau_{ss} \rangle$ and subsequent mutual cancellation of composition dependence trends produces the linear dependence on solution viscosity for $\langle \tau_{ss} \rangle$. This prediction should be reexamined in experiments.

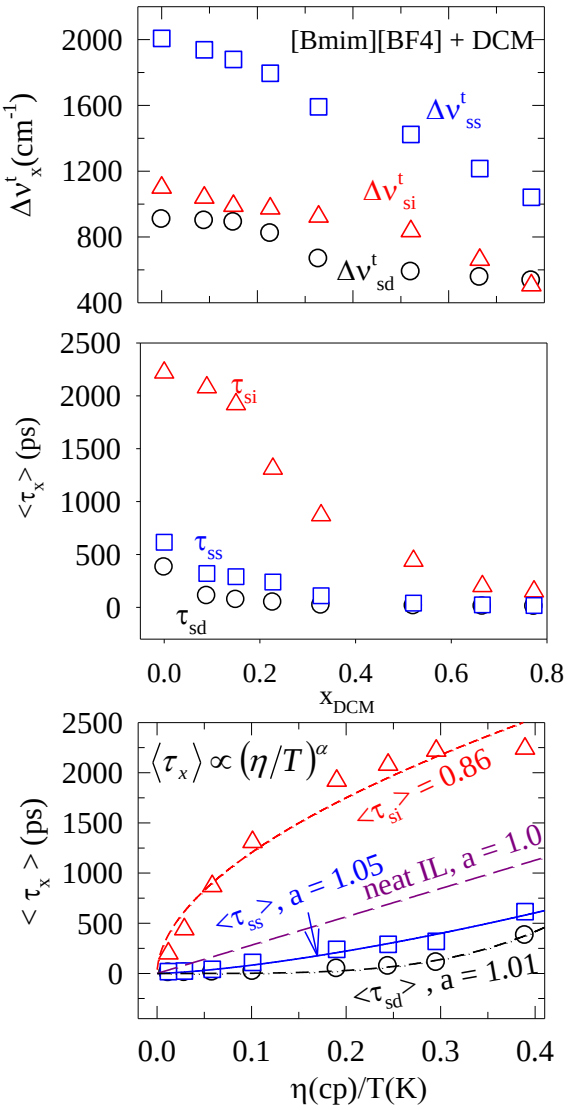

Fig. 6.6: Composition dependence of dynamic Stokes shift and average solvation times, and solution viscosity dependence of average solvation times in binary mixture of ([Bmim][BF_4] + dichloromethane) at 298 K. The calculated values are shown either as a function of dichloromethane mole fraction (x_{DCM}) or temperature-reduced solution viscosity (η/T). The solute is C153. As discussed in the text, calculations have been performed assuming the binary mixture as an effective dipolar medium where the required dielectric relaxation data supplied by Ref. 91. Mixture composition dependent viscosity values are taken from Ref. 6. The radius of a DCM molecule is 2.35 angstrom (Ref. 140). Squares, circles and triangles in all these panels denote calculated results for total shift, dipole-dipole and dipole-ion interaction contributions. The lines going through the symbols in the bottom panel represent fits to a general form, $\langle\tau_x\rangle = B(\eta/T)^a$. The values for a are already indicated. B values for $\langle\tau_{si}\rangle$, $\langle\tau_{sd}\rangle$ and $\langle\tau_{ss}\rangle$ are (in proper unit) 4168, 13838, 2256 respectively. The dark pink broken line (B = 3559) denote the fit through the experimentally measured average solvation times (data not shown to avoid clutter) for a number of neat ILs at various temperatures reported in Ref. 139.

References

1. Seddon, K. R.; Stark, A.; Torres, M-J. *Pure Apply. Chem.* **2000**, *72*, 2275.
2. Rodriguez, H.; Brennecke, J. F. *J. Chem. Eng. Data.* **2006**, *51*, 2145.
3. Stoppa, A.; Hunger, J.; Buchner, R. *J. Chem. Eng. Data.* **2009**, *54*, 472.
4. Bester-Rogac, M.; Hunger, J.; Stoppa, A.; Buchner, R. *J. Chem. Eng. Data.* **2010**, *55*, 1799.
5. Gonzalez, E. J.; Alonso, L.; Dominguez, A. *J. Chem. Eng. Data.* **2006**, *51*, 1446.
6. Li, W.; Zhang, Z.; Han, B.; Hu, S.; Xie, Y.; Yang, G. *J. Phys. Chem. B* **2007**, *111*, 6452.
7. Heinz, A.; Klasen, D.; Lehmann, J. K. *J. Soln. Chem.* **2002**, *31*, 467.
8. Schroder, U.; Wadhawan, J. D.; Compton, R. G.; Marken, F.; Suarez, P. A. Z.; Consorti, C. S.; de Souza, R. F.; Dupont, J. *New. J. Chem.* **2000**, *24*, 1009.
9. Khupse, N. D.; Kumar, A. *J. Soln. Chem.* **2009**, *38*, 589.
10. Tokuda, H.; Baek, S. J.; Watanabe, M. *Electrochemistry* **2005**, *73*, 620.
11. (a) Kanakubo, M.; Umecky, T.; Aizawa, T.; Kurata, Y. *Chem. Lett.* **2005**, *34*, 324; (b) Hayamizu, K.; Tsuzuki, S.; Seki, S.; Fujii, K.; Suenaga, M.; Umebayashi, Y. *J. Chem. Phys.* 2010, *133*, 194505.
12. Jarosik, A.; Krajewski, S. R.; Lewandowski, A.; Radzimski, P. *J. Mol. Liq.* **2006**, *123*, 43.
13. Nishida, T.; Tashiro, Y.; Yamamoto, M. *J. Fluorine Chem.* **2003**, *120*, 135.
14. Widegren, J. A.; Saurer, E. M.; Marsh, K. N.; Magee, J. W. *J. Chem. Thermodyn.* **2005**, *37*, 569.
15. Zhang, Z. M.; Wu, W. Z.; Jiang, T.; Gao, H. X.; Liu, Z. M.; He, J.; Han, B. X. *J. Chem. Eng. Data.* **2003**, *48*, 1315.
16. Xu, H.; Zhao, D.; Xu, P.; Liu, F.; Gao, G. *J. Chem. Eng. Data.* **2005**, *50*, 133.
17. Gomez, E.; Gonzalez, B.; Dominguez A.; Tojo, E.; Tojo, J. *J. Chem. Eng. Data.* **2006**, *51*, 696.
18. Zhou, Q.; Wang, L.-S.; Chen, H. -P. *J. Chem. Eng. Data.* **2006**, *51*, 905.
19. Baker, S. N.; Baker, G. A.; Bright, F. V. *Green Chem.* **2002**, *4*, 165.
20. Fletcher, K. A.; Pandey, S. *Appl. Spectrosc.* **2002**, *56*, 266.
21. Fletcher, K. A.; Pandey, S. *J. Phys. Chem. B* **2003**, *107*, 13532.

22. (a)Harifi-Mood, A. R.; Habibi-Yangjeh, A.; Gholami, M. R. *J. Phys. Chem. B* **2006**, *110*, 7073; (b) Khodadadi-Moghaddam, M.; Habibi-Yangjeh, A.; Gholami, M. R. *Monatsh Chem.* **2009**, *140*, 329.
23. Aparicio, S.; Alcalde, R.; Atilhan, M. *J. Phys. Chem. B* **2010**, *114*, 5795.
24. Masaki, T.; Nishikawa, K.; Shirota, H. *J. Phys. Chem. B* **2010**, *114*, 6323.
25. Cammarata, L.; Kazarian, S. G.; Salter, P. A.; Welton, T. *Phys. Chem. Chem. Phys.* **2001**, *3*, 5192.
26. Jeon, Y.; Sung, J.; Kim, D.; Seo, C.; Cheong, H.; Ouchi, Y.; Ozawa, R.; Hamaguchi, H.-O. *J. Phys. Chem. B* **2008**, *112*, 923.
27. Jeon, Y.; Sung, J.; Seo, C.; Lim, H.; Cheong, H.; Kang, M.; Moon, B.; Ouchi, Y.; Kim, D. *J. Phys. Chem. B* **2008**, *112*, 4735.
28. Danten, Y.; Cabao M. I.; Besnard, M. *J. Phys. Chem. A* **2009**, *113*, 2873.
29. Umebayashi, Y.; Jiang, J.-C.; Shan, Y.-L.; Lin, K.-H.; Fujii, K.; Seki, S.; Ishiguro, S.-I.; Lin, S.H.; Chang, H.-C. *J. Chem. Phys.* **2009**, *130*, 124503.
30. Koddermann, T.; Christiane, W.; Heintz, A.; Ludwig, R. *Angew Chem. Int. Ed. Engl.* **2006**, *45*, 3697.
31. Sando, G. M.; Dahl, K.; Owrutsky, J. C. *J. Phys. Chem. B* **2007,** *111*, 4901.
32. Koeberga, M.; Wu, C.-C.; Kim, D.; Bonn, M. *Chem. Phys. Lett.* **2007**, *439*, 60.
33. Chakrabarty, D.; Chakraborty, A.; Seth, D.; Hazra, P.; Sarkar, N. *Chem. Phys. Lett.* **2004**, *397*, 469.
34. Chakrabarty, D.; Chakraborty, A.; Seth, D.; Sarkar, N. *J. Phys. Chem. A* **2005**, *109*, 1764.
35. Sarkar, S.; Pramanik, R.; Ghatak, C.; Setua, P.; Sarkar, N. *J. Phys. Chem. B* **2010,** *114*, 2779.
36. Baker, S. N.; Baker, G. A.; Munson, C. A.; Chen, F.; Bukwoski, E. J.; Cartwright, A. N.; Bright, F. V. *Ind. Eng. Chem. Res.* **2003**, *42*, 6457.
37. Tran C. D.; Lacerda, S. H. D. P.; Oliveira, D. *Appl. Spectrosc.* **2003**, *57*, 152.
38. Spohr, V. H.; Patey, G. N. *J. Chem. Phys.* **2010**, *132*, 234510.
39. Hanke, C. G.; Lynden-Bell, R. M. *J. Phys. Chem. B* **2003,** *107*, 10873.
40. Hanke, C. G.; Atamas, N. A.; Lynden-Bell, R. M. *Green Chem.* **2002,** *4*, 107. 107.
41. Lynden-Bell, R. M.; Atamas, N. A.; Vasilyuk, A.; Hanke, C. G. *Mol. Phys.*. **2002,** *100*, 3225.

42. (a) Spickermann, C.; Thar, J.; Lehman, S. B. C.; Zahn, S.; Hunger, J.; Buchner, R.; Hunt, P. A.; Welton, T.; Kirchner, B. *J. Chem. Phys.* **2008**, *129*, 104505.; (b) Chang, T. M.; Dang, L. X.; Devanathan, R.; Dupuis, M. *J. Phys. Chem. A* **2010,** *114*, 12764.

43. Annapureddy, H. V. R.; Hu, Z.; Xia, J.; Margulis, C. J. *J. Phys. Chem. B* **2008,** *112*, 1770.

44. Schroder, C.; Rudas, T.; Neumayr, G.; Benkner, S.; Steinhauser, O. *J. Chem. Phys.* **2007**, *127*, 234503.

45. Schroder, C.; Hunger, J.; Stoppa, A.; Buchner, R.; Steinhauser, O. *J. Chem. Phys.* **2008**, *129*, 184501.

46. Schroder, C.; Neumayr, G.; Steinhauser, O. *J. Chem. Phys.* **2009**, *130*, 194503.

47. Pramanik, R.; Rao, V. G.; Sarkar, S.; Ghatak, C.; Setua, P.; Sarkar, N. *J. Phys. Chem. B* **2009,** *113*, 8626.

48. Paul, A.; Samanta, A. *J. Phys. Chem. B* **2008,** *112*, 947.

49. Hunger, J.; Stoppa, A.; Buchner, R.; Hefter, G. *J. Phys. Chem. B* **2009,** *113*, 9527.

50. Fletcher, K. A.; Pandey, S. *Appl. Spectrosc.* **2002**, *56*, 1498.

51. Salari, H.; Khodadadi-Moghaddam, M.; Harifi-Mood, A. R.; Gholami, M. R. *J. Phys. Chem. B* **2010**, *114*, 9586.

52. Baker, S. N.; Baker, G. A.; Kane, M. A.; Bright, F. V. *J. Phys. Chem. B* **2001**, *105*, 9663.

53. Blanchard, L. A.; Hancu, D.; Beckman, E. J.; Brennecke, J. F. *Nature* **1999**, *399*, 28.

54. Fletcher, K. A.; Baker, S. N.; Baker, G. A.; Pandey, S. *New J. Chem.* **2003**, *27*, 1706.

55. Canongia Lopes, J. N.; Cordeiro, T. C.; Esperanca, J. M. S. S.; Guedes, H. J. R.; Huq, S.; Rebelo, L. P. N.; Seddon, K. R. *J. Phys. Chem. B* **2005,** *109*, 3519.

56. Stoppa, A.; Buchner, R.; Hefter, G. *J. Mol. Liq.* **2010**, *153*, 46.

57. Khupse, N. D.; Kurolikar, S. R.; Kumar, A.; *Ind. J. Chem.* **2010**, *49A*, 727.

58. Annat, G.; Macfarlane, D. R.; Forsyth, M. *J. Phys. Chem. B* **2007,** *111*, 9018.

59. Xiao, D.; Rajian, J. R.; Li, S.; Bartsch, R. A.; Quitevis, E. L. *J. Phys. Chem. B* **2006,** *110*, 16174.

60. Xiao, D.; Rajian, J. R.; Hines, L. G. Jr.; Li, S.; Bartsch, R. A.; Quitevis, E. L. *J. Phys. Chem. B* **2008,** *1120*, 13316.

61. Blanchard, L. A.; Brennecke, J. F. *Ind. Eng. Chem. Res.* **2001**, *40*, 287.

62. Huddleston, J. G.; Willauer, H. D.; Swatloski, R. P.; Visser, A. E.; Rogers, R. D. *Chem. Commun.* **1998**, 1765.

63. Wong, D. S. H.; Chen, J. P.; Chang, J. M.; Chou, C. H. *Fluid Phase Equilib.* **2002**, *194-197*, 1089.

64. Anthony, J. L.; Maginn, E. J.; Brennecke, J. F. *J. Phys. Chem. B* **2001,** *105,* 10942.

65. Padua, A. A. H.; Gomes, M. F. C.; J. N. A. Canongia Lopes *Acc. Chem. Res.* **2007**, *40*, 1087.

66. Castner, Jr., E. W.; Wishart, J. F.; Shirota, H. *Acc. Chem. Res.* **2007**, *40*, 1217.

67. Hu, Z.; Margulis, C. *Acc. Chem. Res.* **2007**, *40*, 1097.

68. Turner, M. B.; Spear, S. K.; Holbrey, J. D.; Rogers, R. D. *Biomacromolecules*, **2004**, *5*, 1379.

69. Remsing, R. C.; Swatloski, R. P.; Rogers, R. D.; Moyna, G. *Chem. Commun.* **2006**, 1271.

70. Fort, D. A.; Remsing, R. C.; Swatloski, R. P.; Moyna, P.; Moyna, G.; Rogers, R. D. *Green Chem.* **2007**, *9*, 63.

71. Kumar, A.; Singh, T.; Gardas, R. L.; Coutinho, J. A. P. *J. Chem. Thermodyn.* **2008**, *40*, 32.

72. Singh, T.; Kumar, A.; Kaur, M.; Kaur, G.; Kumar, H. *J. Chem. Thermodyn.* **2009**, *41*, 717.

73. (a) Aerov, A. A.; Khokhlov, A. R.; Potemkin, I. I. *J. Phys. Chem. B*. **2010**, *114*, 15066.; (b) Freire, M. G.; Neves, C. M. S. S.; Shimizu, K.; Bernardes, C. E. S.; Marrucho, I. M.; Coutinho, J. A. P.; Lopes, J. N. C.; Rebelo, L. P. N. *J. Phys. Chem. B*. **2010**, *114*, 15925.; (c)Sadeghi, R.; Mostafa, B.; Parsi, E; Shahebrahimi, Y. *J. Phys. Chem. B*. **2010**, *114*, 16528**.**

74. Makowska, A.; Dyoniziak, E.; Siproska, A.; Szydlowski, J. *J. Phys. Chem. B*. **2010**, *114*, 2504.

75. Klahn, M.; Stuber, C.; Seduraman, A.; Wu, P. *J. Phys. Chem. B*. **2010**, *114*, 2856.

76. Samanta, A. *J. Phys. Chem. B*. **2006**, *110*, 13704.

77. Arzhantsev, S.; Jin, H.; Baker, G. A.; Maroncelli, M. *J. Phys. Chem. B*. **2007**, *111*, 4978.

78. Ingram, J. A.; Moog, R. S.; Ito N.; Biswas, R.; Maroncelli, M. *J. Phys. Chem. B* **2003**, *107*, 5926.

79. Karamkar, R.; Samanta, A. *J. Phys. Chem. A* **2002**, *106*, 4447.

80. Karamkar, R.; Samanta, A. *J. Phys. Chem. A* **2002**, *106*, 6670.

81. Ito, N.; Arzhantsev, S.; Maroncelli, M. *Chem. Phys. Lett.* **2004**, *396*, 83.

82. Reynolds, L.; Gardecki, J. A.; Frankland, S. J. V.; Horng, M. L.; Maroncelli, M. *J. Phys. Chem.* **1996**, *100*, 10337.

83. Eventhough the dielectric relaxation (DR) data for binary mixtures of ionic liquids with nonpolar solvents are not available yet, DR studies with binary mixtures of solvents with different polarities indicate decrease of static dielectric constant (ε_0) of the mixture upon increasing the concentration of the less polar component. Following representative references demonstrate the above observation: (a) Shinyashiki, N.; Sudo, S.; Abe, W.; Yagihara, S. *J. Chem. Phys.* **1998**, *109*, 9843.; (b) Sato, T.; Chiba, A. *J. Chem. Phys.* **2000**, *112*, 2924; (c) Kaatze, U.; Behrends, R.; von Roden, K. *J. Chem. Phys.* **2010,** *133*, 094508; (d) Kaatze, U.; Schumacher, A.; Pottel, R. *Ber. Bunsenges. Phys. Chem.* **1991**, *95*, 585; (e) Patil, S. P.; Chaudhari, A. S.; Lokhande, M. P.; Lande, M. K.; Shankarwar, A. G.; Helambe, S. N.; Arbad, B. R.; Mehrotra, S. C. *J. Chem. Eng. Data*, **1999**, *44*, 875; (f) Shirke, R. M.; Chaudhari, A.; More, N. M.; Patil, P. B. *J. Chem. Eng. Data*, **2000**, *45*, 917; (g) Shirke, R. M.; Chaudhari, A.; More, N. M.; Patil, P. B. *J. Mol. Liq.*, **2001**, *94*, 27; (h) Chaudhari, A.; Shirke, R. M.; Nore, N. M.; Patil, P. B. *J. Solution Chem.* **2002**, *31*, 305; (g) Sengwa, R. J.; Madhvi; Abhilasha. *J. Mol. Liq.* **2006**, *123*, 92; (h) Petong. P.; Pottel, R.; Kaatze, U. *J. Phys. Chem. A* **1999**, *103*, 6114; (i) Sudo, S.; Shimomura, M.; Shinyashiki, N.; Yagihara, S. *J. Non-Cryst. Solids* **2002**, *307-310*, 356; (j) Sato, T.; Chiba, A.; Nozaki, R. *J. Mol. Liq.* **2002**, *96-97*, 327; (k) Sato, T.; Chiba, A.; Nozaki, R. *J. Mol. Liq.* **2002**, *101*(*1-3*), 99; (l) von Hornhardt, S.; Stockhausen, M.; Herba, H.; Jadzyn, J.; Czechowski, G.; Zywucki, B. *J. Mol. Liq.* **1996**, *69*, 201; (m) Sengwa, R. J.; Chaudhary, R.; Mehrotra, S. C. *Mol. Phys.* **2001**, *99*, 1805; (n) Khirade, P. W.; Chaudhari, A.; Shinde, J. B.; Helambe, S. N.; Mehrotra, S. C. *J. Solution Chem.* **1999**, *28*, 1031; (p) Sudo, S.; Shinyashiki, N.; Kitsuki, Y.; Yagihara, S. *J. Phys. Chem. A* **2002**, *106*, 458; (q) Sato, T.; Buchner, R. *J. Chem. Phys.* **2003**, *118*, 4606.

84. Kashyap, H. K.; Biswas R. *J. Phys. Chem. B* **2008**, *112*, 12431.

85. Kashyap, H. K.; Biswas R. *J. Phys. Chem. B* **2010**, *114*, 16811.

86. Kashyap, H. K.; Biswas R. *J. Phys. Chem. B* **2010**, *114*, 254.

87. Kashyap, H. K.; Biswas R. *Ind. J. Chem.* **2010**, *49A*, 685.

88. Bagchi, B.; Biswas, R. *Adv. Chem. Phys.* **1999**, *109*, 207.

89. Bagchi, B.; Chandra, A. *Adv. Chem. Phys.* **1991**, *80*, 1.

90. Bagchi, B. *Annu. Rev. Phys. Chem.* **1989**, *40*, 115.

91. Hunger, J.; Stoppa, A.; Hefter, G.; Buchner, R. *J. Phys. Chem. B* **2008**, *112*, 12913.

92. Jin, H.; O'Hare, B.; Arzhantsev, S.; Baker, G.; Wishart, J. F.; Binesi, A. J.; Maroncelli, M. *J. Phys. Chem. B* **2008**, *112*, 81.

93. Bhargava, B. L.; Balasubramanian, S. *J. Phys. Chem. B* **2007**, *111*, 4477.

94. Hunger, J.; Stoppa, A.; Schrodle, S.; Hefter, G.; Buchner, R. *ChemPhysChem* **2009**, *10*, 723.

95. Tokuda, H.; Tsuzuki, S.; Susan, M. A. B. H.; Hayamizu, K.; Watanabe, M. *J. Phys. Chem. B* **2006**, *110*, 19593.

96. MacFarlane, D. R.; Forsyth, M.; Izgorodina, E. I.; Abbott, A. P.; Annat, G.; Fraser, K. *Phys. Chem. Chem. Phys.* **2009**, *11*, 4962.

97. Chandra, A.; Wei, D. ; Patey, G. N. *J. Chem. Phys.* **1993**, *98*, 4959.

98. Chandra, A.; Wei, D. ; Patey, G. N. *J. Chem. Phys.* **1993**, *99*, 2083.

99. Chandra, A.; Patey, G. N. *J. Chem. Phys.* **1994**, *100*, 1552.

100. Chandra, A. *Chem. Phys. Lett.* **1995**, *244*, 314.

101. Chandra, A.; Jana, D.; Bhattacharjee, S. *J. Chem. Phys.* **1996**, *104*, 8662.

102. Mahajan, K.; Chandra, A. *J. Chem. Phys.* **1997**, *106*, 2360.

103. Chapman, C. F.; Maroncelli, M. *J. Phys. Chem.* **1991**, *95*, 9095.

104. Gray, C. G.; Gubbins, K. E. *Theory of Molecular Fluids*; Clarendon: Oxford, 1984. Vol. I

105. Isbister, D.; Bearman, R. *J. Mol. Phys.* **1974**, *28*, 1297.

106. Roy, S.; Bagchi, B. *J. Chem. Phys.* **1993**, *99*, 9938.

107. Roy, S.; Bagchi, B. *J. Chem. Phys.* **1993**, *99*, 1310.

108. Biswas, R.; Bagchi, B. *J. Phys. Chem.* **1996**, *100*, 4261.

109. Biswas, R.; Bagchi, B. *J. Phys. Chem.* **1996**, *100*, 1238.

110. Indrani, A. V.; Ramaswamy, S. *Phys. Rev. Lett.* **1994**, *73*, 360.

111. Guchhait, B.; Gazi, H. A. R.; Kashyap, H. K.; Biswas, R. *J. Phys. Chem. B* **2010**, *114*, 5066.

112. Gazi, H. A. R.; Guchhait, B.; Daschakraborty, S.; Biswas, R. *Chem. Phys. Lett.* **2011**, *501*, 358..

113. Hansen, J. P.; McDonald, I. R. *Theory of Simple Liquids*; Academic Press: London, 1986.

114. Labowitz, J. L. *Phys. Rev.* **1964**, *133*, A895.

115. Attard, P. *Phys. Rev. E*, **1993**, *48*, 3604.

116. Chandra, A.; Bagchi, B. *J. Chem. Phys.* **1999**, *110*, 10024.

117. Stehfest, H; *Commun. ACM* **1970**, *13*, 624.

118. Kindt, J. T.; Schmuttenmaer, C. A. *J. Phys. Chem.* **1996**, *100*, 10373.

119. Stoppa, A.; Hunger, J.; Buchner, R.; Hefter, G.; Thoman, A.; Helm, H. *J. Phys. Chem. B* **2008**, *112*, 4854.

120. These differences are between shifts calculated by using the dielectric relaxation data described in Ref.94.

121. Paul, A.; Samanta, A. *J. Phys. Chem. B* **2007**, *111*, 4724.

122. Sarkar, N. (*private communication*).

123. Jimenez, R.; Fleming, G. R.; Kumar, P. V.; Maroncelli, M. *Nature* **1994**, *369*, 471.

124. Lovas, F. J. *J. Phys. Chem. Ref. Data* **1978**, *7*, 1445.

125. Measurements using coumarin 343 (C343) – C343, a probe structurally very similar to C153- in pure water indicates a dynamic Stokes shift ~2000 cm^{-1}. Note the sodium salt of this probe was used in Ref. 123 for enhanced solubility.

126. Jellema, R.; Bulthuis, J.; van der Zwan, G. *J. Mol. Liq.* **1997**, *73-74*, 179.

127. Asaki, M. L. T.; Redondo, A.; Zawodzinski, T. A.; Taylor, A. J. *J. Chem. Phys.* **2002**, *116*, 10377.

128. Horng, M. L.; Gardecki, J. A.; Papazyan, A.; Maroncelli, M. *J. Phys. Chem.* **1995**, *99*, 17311.

129. Chakrabarti, D.; Hazra, P.; Chakraborty, A.; Seth, D.; Sarkar, N. *Chem. Phys. Lett.* **2003**, *381*, 697.

130. Chowdhury, P. K.; Halder, M. K.; Sanders, L.; Calhoun, T.; Anderson, J. L.; Armstrong, D. W.; Song, X.; Petrich, J. W. *J. Phys. Chem. B* **2004**, *108*, 10245.

131. Saha, S.; Mandal, P. K.; Samanta, A. *Phys. Chem. Chem. Phys.* **2004**, *6*, 3106.

132. Wang, Y.; Voth, G. A. *J. Am. Chem. Soc*. **2005**, *127*, 12192.

133. Triolo, A.; Russina, O.; Bleif, H.; Cola, E. D.*; J. Phys. Chem. B* **2007**, *111*, 4641.

134. Mandal, P. K.; Sarkar, M.; Samanta,A. *J. Phys. Chem. A* **2004** , *108*, 9048.

135. Jin, H.; Li, X.; Maroncelli, M. *J. Phys. Chem. B* **, 2007** , *111* 13473.

136. Adhikari, A.; Sahu, A. K.; Dey, S.; Ghose, S.; Mandal, U.; Bhattacharyya, K. *J. Phys. Chem. B* **2007** , *111*, 12809.

137. Hu, Z.; Margulis, C. J. *Proc. Natl. Acad. Sci. U. S. A.* **2006**, *103*, 831.

138. Cavell, E. A. S.; Knight, P. C.; Sheikh, M. A.; *Trans. Faraday Soc.* **1971**, *67*, 2225.

139. Jn, H.; Baker, G. A.; Arzhantsev, S.; Dong, J.; Maroncelli, M. *J. Phys. Chem. B* **2007**, *111*, 7291.

140. Zhou, J.; Findley, B. R.; Braun, C. L.; Sutin, N. *J. Chem. Phys.* **2001**, *114*, 10448.

Chapter 7

Composition Dependent Stokes Shift Dynamics in (Ionic Liquid + Dipolar Solvent) Binary Mixtures: Comparison between Theory and Experiments

7.1 Introduction

As we discussed in earlier chapters, recent years have witnessed tremendous growth in experimental[1-10], theoretical[11-19] and simulation studies[20-31] of dynamics of ionic liquids (ILs). These studies have investigated various dynamical features at microscopic level with a focus on understanding the uniqueness of ILs as media and/or materials for various applications. Being environment friendly, ILs can be used as reaction media and employed in various electrochemical applications.[32-50] The binary mixtures of (IL + common dipolar solvent) are interesting systems, because the desired physicochemical properties for a designed application can be tailored via simple tuning of the composition of the binary mixtures. On other hand, the miscibility of ILs in water may be a serious threat to the environment because it may enter to the food chain to affect the entire ecosystem.[51] These possible advantages and disadvantages of these binary mixtures demand a detailed study on the microscopic structural and dynamical aspects of binary mixtures containing ILs so that more intelligent applications are enabled. Moreover, such a study will provide comparative understanding between electrolyte solutions of common polar solvents and (IL + common dipolar solvent) mixtures.

In the past few years, several spectroscopic studies have reported local polarity around a dissolved solute in various binary mixtures of ILs and polar solvents and explained the data in terms of preferential solvation.[52-60] Terahertz time domain measurements of aqueous mixtures of $[\mathrm{Bmim}][\mathrm{BF_4}]$ have revealed moderate non-ideal mixture composition dependence in relaxation parameters.[61] Dielectric relaxation (DR) measurements[62-63] and time-resolved

optical Kerr effect (OKE) spectroscopic techniques[64,65] explored the non-ideality in dynamics. Recently, a detailed investigation of dielectric relaxations of binary mixtures of several ILs and acetonitrile have been done over the entire composition range at room temperature covering a frequency range $0.2 \le \nu / GHz \le 89$ ($\omega = 2\pi\nu$) in order to understand the composition dependence of dielectric properties of these mixtures.[66] It has been seen that experimental dielectric spectra follow two modes of relaxation, Cole-Cole (CC) and Debye, among which, CC mode corresponds to the jump rotation of the imidazolium cation and hindered rotational motion of slow acetonitrile molecule, and Debye mode corresponds to the free rotational motion of acetonitrile molecule with contributions from vibration and libration of ILs. Strong non-ideality has been observed in dielectric relaxation time constants, static dielectric constants, and dielectric dispersion.

Stokes shift dynamics have been measured for various (IL + dipolar solvent) binary mixtures using a number of solute probes.[67-69] These studies have revealed several interesting featuers regarding the mixture dynamics. The measured solvation response functions have been found to be non exponential and the associated relaxation time constants exhibit non-ideality with mixture composition. As these experiments could not capture the full dynamics, the dynamic Stokes shift and the solvation relaxation time constants might not be very accurate, and therefore complete detection of full relaxation dynamics is warranted.

Recent experiments on solvation and rotational dynamics of C153 in binary mixtures of 1-butyl-3-methylimidazolium tetrafluoroborate with acetonitrile ($[\mathrm{Bmim}][\mathrm{BF_4}] + \mathrm{CH_3CN}$)[70], and water ($[\mathrm{Bmim}][\mathrm{BF_4}] + \mathrm{H_2O}$)[71] using a combination of florescence up-conversion spectroscopy (FLUPS) and time-correlated single photon counting (TCSPC), have revealed several interesting aspects. The dynamic Stokes shift has been seen to remain almost constant in the whole composition region of the binary mixtures. This may appear contrary to the intuition that dynamic Stokes shift (determined by solute-solvent interactions) should increase with increasing polarity of the medium, which, in this case, is the static dielectric constant. Mean Spherical Approximation (MSA)[72,73] and Cavell's equation[74] are empirical relations, which connect the static dielectric constant and polarity of the medium. Interestingly, the experimental solvation energy relaxation of C153 probe in binary mixtures

of ($[Bmim][BF_4]+CH_3CN$) required a sum of four-exponentials at all compositions, a sum of Gaussian and stretched exponential functions was needed to fit the measured response in ($[Bmim][BF_4]+H_2O$) binary mixtures. The fastest timescale has been ascribed to the inertial component of the medium and slower part of the solvation explained in terms of the slow diffusive motion of the medium particles. The integral ultrafast solvation time remains almost insensitive to mixture composition, but that associated with the slow decay increases with the increase in IL concentration in the mixture.

An approximate semi-molecular theory has been developed to investigate the composition dependence of Stokes shift dynamics of a dissolved dipolar solute in binary mixtures of ILs with conventional polar solvents.[15] This has been discussed in the previous chapter. The theory predicts decreasing stokes shift with decrease of IL mole fraction and suggests a strong density dependence. Addition of dipolar solvent in the mixture has been found to accelerate the decay of the calculated solvation response function and therefore correlates linearly with viscosity of the medium. Calculated dynamic Stokes shift and response functions show semi-quantitative agreement with the available experimental results.

In the present study, we have carried out a theoretical investigation on the Stokes shift dynamics of C153 in room temperature binary mixtures of ($[Bmim][BF_4]+CH_3CN$) and ($[Bmim][BF_4]+H_2O$) at various compositions. The results obtained have been employed to explain several interesting features observed in recent experiments.[70,71] Note experimental frequency dependent dielectric function, $\varepsilon(\omega)$, at various compositions are now available for these mixtures[66,71] which can be used in our theory as inputs. The comparison between theory and experiments also provides a check for the robustness of the present calculation scheme. Both the effective medium and separate medium calculations have been performed. For effective medium calculation we have assumed that the binary mixture is actually a single component system characterized by an effective dipole moment and mole fraction weighted ion size. The separate medium calculations involve, as before,[15] utilization of experimental $\varepsilon(\omega)$ of individual pure components. Interestingly, effective medium calculations make better predictions for experimental dynamic Stokes shift whereas separate medium

calculations reproduces better the measured composition dependent solvation response. Composition independence of experimental Stokes shift[70,71] can be explained by the present theory in terms of mutual cancellation of same order of increase and decrease of solute – solvent (dipole – dipole) and solute – IL (dipole – ion) interactions, respectively.

The organization of the rest of the chapter is a follows. Next section contains the theoretical formulation and calculation details. Numerical results and comparison with experiments are given in Sec. 7.3. The chapter then ends with a discussion in Sec. 7.4.

7.2 Theory and Calculation Details

As the detailed theory has been discussed elsewhere[15], here we will discuss the theory briefly and present the necessary equations briefly. At first, we have assumed that the IL is fully dissociated even in the absence of any added polar solvent and remains so upon addition of it. Note ion pair formation in IL decreases considerably in presence of a strong dipolar solvent.[38,75] We assume that three types of solute – solvent interactions are mainly responsible for the Stokes shift dynamics in these binary mixtures: (i) dipolar solute-dipolar ion (dipole-dipole) interaction, (ii) the dipolar solute – ion (dipole – ion) interaction and (iii) dipolar solute – dipolar solvent (dipole - dipole) interaction. The cross interactions are not included in the present calculations. In this section we will separately discuss the two approaches, separate medium calculations and effective medium calculations.

7.2.1 Theory for Separate Medium Calculations

The use of the classical density functional theory provides the expression, presented in Eq. 6.1 (Chapter 6) for the position ($\mathbf{r}$), orientation ($\mathbf{\Omega}$) and time (t) dependent total fluctuating solvation energy for a mobile dipolar solute with distribution function $\rho_s(\mathbf{r},\mathbf{\Omega};t)$.

where, $c_{sd}(\mathbf{r},\mathbf{\Omega};\mathbf{r}',\mathbf{\Omega}')$, $c_{sp}(\mathbf{r},\mathbf{\Omega};\mathbf{r}',\mathbf{\Omega}')$, and $c_{s\alpha}(\mathbf{r},\mathbf{\Omega};\mathbf{r}')$ are the position and orientation dependent solute dipole – IL dipole (dipole-dipole), solute dipole – ion (dipole-ion), and solute dipole – dipolar solvent dipole (dipole-dipole) direct correlation functions respectively

and α denotes the type of ions (cation and anion). The fluctuations in dipolar density ($\delta\rho_d$) and ion density (δn_α) from the respective bulk values are: $\delta\rho_d(\mathbf{r},\mathbf{\Omega}) = \rho_d(\mathbf{r},\mathbf{\Omega}) - \rho_d^0/4\pi$, $\delta\rho_p(\mathbf{r},\mathbf{\Omega}) = \rho_p(\mathbf{r},\mathbf{\Omega}) - \rho_p^0/4\pi$ and $\delta n_\alpha(\mathbf{r}) = n_\alpha(\mathbf{r}) - n_\alpha^0$. The solvation energy-energy correlation function averaged over space ($\mathbf{r}$) and orientation ($\mathbf{\Omega}$) is then written as,

$$C_E(t) = C_{sd}(t) + C_{si}(t) + C_{sp}(t), \tag{7.1}$$

We next form the total (fluctuating) solvation energy auto-correlation function which has been given in Eq. 6.2 in Chapter 6. Here we have assumed that the cross correlations are almost zero. This approximation is valid because of the separation of time-scales involved in fluctuations of dipolar solvent and ion densities.

The time dependence of the solvation energy relaxation is then followed in terms of the normalized solvation energy autocorrelation function as Eq. 6.3 of Chapter 6, where S_{sd}, S_{sp} and S_{si} are the individual normalized solvation energy autocorrelation functions due respectively to solute–dipolar ion (dipole-dipole), solute– added solvent (dipole-dipole) and solute – ion (dipole-ion) interactions. The normalized solvation energy autocorrelation function arising from the solute – IL dipole (dipole – dipole) interaction ($S_{sd}(t)$)**,** solute – dipolar solvent dipole (dipole – dipole) ($S_{sp}(t)$)**,** and solute – ion interaction (dipole – ion) ($S_{si}(t)$), are defined respectively in Eqs. 6.4, 6.8, and 6.9 of Chapter 6, where *A* is a pre-factor given by $2\rho_d^0 k_B T/(2\pi)^2$. $c_{sd}^{lm}(k)$ (*l,m=1,0 or 1,1*) in Eq. 6.4 (Chapter 6) and $c_{sp}^{lm}(k)$ (*l,m=1,0 or 1,1*) in Eq. 6.8 (Chapter 6) denote the Fourier transform of the (*l,m*) component of the static correlation function between the solute and a IL dipole and solute and a dipole solvent dipole respectively. $S_{solvent}^{lm}(k,t)$ and $S_p^{lm}(k,t)$ are the same components of the orientational dynamic structure factor of the IL dipole and dipolar solvent dipole. The longitudinal ($S_{solvent}^{10}$) and transverse ($S_{solvent}^{11}$) components have been obtained from the experimental dielectric relaxation data. These are given by Eq. 6.5 and 6.6 of Chapter 6, where the polarity parameter, $3Y = (4\pi/3k_BT)\mu^2\rho_d^0$ with μ and ρ_d^0 being the dipole moment and density of the medium. $\varepsilon_L(k)$ and $\varepsilon_T(k)$ are the longitudinal and transverse components of the wave number dependent dielectric function and can be obtained from the orientational

static structural correlations as follows. $[1-\varepsilon_L^{-1}(k)]=3Yf_{110}^{-1}(k)$, and $[\varepsilon_T(k)-1]=3Yf_{111}^{-1}(k)$ with $f_{llm}(k)=1-(\rho_d^0/4\pi)(-1)^m c(llm,k)$. In the present calculations, these static direct correlation functions have been obtained from the MSA theory[72,73] for binary dipolar mixtures of solute and solvent where the concentration of solute is much less. L^{-1} represents the Laplace inversion and z is the frequency. $\Sigma_{lm}(k,z)$ is the $(l,m)^{\text{th}}$ component of the generalized rate of the orientational solvent polarization density relaxation. Calculation of $\Sigma_{lm}(k,z)$ is done using experimental dielectric relaxation data and the equations are presented elsewhere.[11,12,14,15] Calculation of $S_p^{lm}(k,t)$ is done in the same manner as followed for $S_{solvent}^{lm}(k,t)$.

$S_{solute}^{lm}(k,t)$ denotes the (*l*,*m*) component of solute dynamic structure factor. We have assumed that the solute dynamic structure factor is diffusive (both rotational and translational) and the expression is written in Eq. 6.7[11-19,76] of Chapter 6, where D_R^s and D_T^s are the rotational and translational diffusion coefficients of the solute. We have assumed that solute dynamics follow hydrodynamic relationship in the *stick* boundary limit, and hence can be obtained from medium viscosity using Stokes Einstein Debye relation (SED).

Now the derivation of Eq. 6.9 (Chapter 6) and the method of calculation have been given in previous chapters and elsewhere[12,14], and hence we mention only the important points and equations in the present chapter. In Eq. 6.9 (Chapter 6), *B* is the pre-factor, given by, $B=2(k_BT/2\pi)^2$ and $c_{s\alpha}^{10}(k)$ denotes the longitudinal component of the wave number dependent static structural correlations between the dipolar solute and an ion of type α. $c_{s\alpha}^{10}(k)$ is represented by,

$$c_{s\alpha}^{10}(k)=-\sqrt{\frac{4\pi}{3}}\left(\frac{4\pi i\mu_1 q_\alpha}{k_BT\varepsilon_0 k}\right)\frac{\sin(kr_c)}{kr_c} \qquad (7.2)$$

where μ_1 is the dipole-moment of the dipolar solute in excited state, q_α the charge of α^{th} type ion, ε_0 the static dielectric constant and r_c the distance of the closest approach between the solute dipole and the ionic species. $S_{\alpha\beta}^{ion}(k,t)$, in Eq. 6.9 (Chapter 6), is the partial isotropic ion dynamic structure factor. Diffusive form for $S_{\alpha\beta}^{ion}(k,t)$ has been used in our calculations where the diffusion coefficient of the ions (D_α) have been obtained from the medium viscosity by using the Stokes-Einstein relation with stick boundary condition. The relevant part of the isotropic ion static structure factor, $S_{\alpha\alpha}(k)$, has been approximated by the Percus-Yevick (P-Y) solution for binary mixtures[77] of singly charged hard spheres of equal radii and used the expressions derived elsewhere[78,79] for the calculation of ion static structure factor, $S_{\alpha\beta}^{ion}(k)$. The longitudinal component of the wavenumber dependent direct correlation function between the dipolar solute and ions, $c_{s\alpha}^{10}(k)$, is taken as, $c_{s\alpha}^{10}(k) = -\sqrt{\frac{4\pi}{3}}\left(\frac{4\pi i\mu_1 q_\alpha}{k_B T\varepsilon_0 k}\right)\frac{\sin(kr_c)}{kr_c}$, where μ_1 is the excited state dipole-moment of the dipolar solute, q_α the charge of α^{th} type ion, r_c the distance of the closest approach between the solute dipole and the ionic species. Note that the above calculation schemes for the ion-dipole and ion-ion static correlations do not consider at all the static heterogeneity that may be present in these mixtures.

As described in earlier work[15], the dynamic Stokes shifts for solute – IL dipole (dipole – dipole) interaction ($\Delta\nu_{sd}^t$), solute – dipolar solvent dipole (dipole – dipole) ($\Delta\nu_{sp}^t$), and solute – ion interaction (dipole – ion) ($\Delta\nu_{si}^t$), can be calculated easily from the denominator of Eq. 6.4, 6.8, and 6.9 of Chapter 6 respectively. Subsequently, the total dynamic Stokes shift is approximated as,

$$\Delta\nu_{tot}^t = \Delta\nu_{sd}^t + \Delta\nu_{si}^t + \Delta\nu_{sp}^t = \sqrt{\left\langle\left|\Delta E_{sd}(0)\right|^2\right\rangle} + \sqrt{\left\langle\left|\Delta E_{si}(0)\right|^2\right\rangle} + \sqrt{\left\langle\left|\Delta E_{sp}(0)\right|^2\right\rangle}.$$

7.2.2 Theory for Effective Medium Calculations

The main difference of the effective medium approach from separate medium calculations is that the dipoles of the IL and dipolar solvent molecules are not treated as separate entity, rather, as a single unit characterized by an effective dipole moment, which can be obtained from MSA or Cavell's relation, and mole fraction weighted effective size and molar mass of the dipolar constituents. By virtue of this approximation, the binary mixtures of (IL + dipolar solvent) effectively reduces to a medium consisting of ionic species and an effective dipolar medium. The components that contribute to calculated dynamics are solute-solvent dipole (dipole-dipole) and solute-ion (dipole-ion) interaction contributions. The diameter of the dipolar constituents (σ_d) are calculated from the following relation:

$$\sigma_d = \left(x_{IL}\sigma_{IL}^3 + (1-x_{IL})\sigma_{dip.solv.}^3\right)^{1/3}, \tag{7.3}$$

where x_{IL}, x_{IL}, and x_{IL} are the molefraction of the IL in the mixture, diameter of IL dipole, and diameter of dipolar solvent. The molar mass of the dipolar constitute is also calculated from similar molefraction weighted mean, $M_d = x_{IL}M_{IL} + (1-x_{IL})M_{dip.solv.}$

The main advantage of this theoretical scheme is that experimental dielectric relaxation data for the binary mixture can be used directly as inputs to determine both the Stokes shift values and solvation response function. Consequently, the non-ideality in mole fraction dependence observed in experiments is expected to be reflected in effective medium calculations.

7.3 Result and Discussion

In this section, we first present the calculated dynamic Stokes shift by two approaches, separate medium calculation and effective medium calculation and then compare between these approaches and with the experimental results.

7.3.1 Dynamic Stokes Shift for C153 in Binary Mixtures of ($[Bmim][BF_4] + CH_3CN$): Composition Dependence

A. Separate Medium Calculations: Binary Mixtures of ($[Bmim][BF_4] + CH_3CN$)

First, we present the necessary input parameters, such as density, number density, viscosity and dipole-moments for the calculation in Table A22 (Appendix A). The density (ρ) and viscosity (η) have been taken from the experimental paper.[70] The number density of dipole (ρ_N^d) and ions (ρ_N^i) have been calculated using diameter of $[Bmim]^+$ (6.78 Å)[14], $[BF_4]^-$ (4.58 Å)[14], and CH_3CN (4.48 Å)[80]. The static dielectric constants of $[Bmim][BF_4]$ and CH_3CN are taken from Ref. 71 and 66 respectively. Table 7.1 summarizes the composition dependence of calculated and experimentally measured dynamic Stokes shifts of C153 in the binary mixture of ($[Bmim][BF_4] + CH_3CN$). The table shows the calculated dynamic Stokes shifts originating separately from solute-IL dipole (dipole-dipole) interaction ($\Delta\nu_{sd}^t$), solute-dipolar solvent dipole (dipole-dipole) interaction ($\Delta\nu_{sp}^t$), solute-ion (dipole-ion) interaction ($\Delta\nu_{si}^t$). Total theoretical dynamic Stokes shifts ($\Delta\nu_{tot}^t = \Delta\nu_{sd}^t + \Delta\nu_{si}^t + \Delta\nu_{sp}^t$) and experimental shifts ($\Delta\nu_{\text{expt.}}^t$) are also presented in the same table. It is clearly seen that mixture composition play a considerable role on calculated Stokes shifts in these mixtures, whereas the experimental shift[70] remains almost insensitive toward IL mole fraction. A closer investigation of the table further reveals that calculated total shift, $\Delta\nu_{tot}^t$, shows non-ideal composition dependence. This non-ideality of the calculated total shift can be understood by examining the mixture composition dependence of $\Delta\nu_{sd}^t$, $\Delta\nu_{si}^t$, and

Table 7.1: Composition dependence of dynamic Stokes shift of C153 probe in the binary mixture of ($[Bmim][BF_4] + CH_3CN$) using separate medium calculation approach

Mole fraction of IL, x_{IL}	solute-IL (dipole-dipole) interaction contribution, $\Delta\nu_{sd}^t$ (cm^{-1})	solute-ion (dipole-ion) interaction contribution, $\Delta\nu_{si}^t$ (cm^{-1})	solute-dipolar solvent (dipole-dipole) interaction contribution, $\Delta\nu_{sp}^t$ (cm^{-1})	Total $\Delta\nu_{tot}^t$ (cm^{-1})	Experiment, $\Delta\nu_{expt.}^t$ (cm^{-1})
0.0	0	0	1977	1977	1980
0.1	104	242	1300	1646	
0.2	199	454	730	1383	2100
0.3	254	582	533	1369	2160
0.4	343	691	387	1421	2090
0.5	482	790	274	1546	2100
0.6	570	879	188	1637	2120
0.7	649	955	164	1768	
0.8	734	1041	122	1897	2120
0.9	833	1115	57	2005	2150
1.0	947	1261	0	2208	2160

$\Delta\nu_{sp}^t$. It is seen that while $\Delta\nu_{sd}^t$ and $\Delta\nu_{si}^t$ increase almost linearly with increase in IL concentration (due to increase of density of IL), $\Delta\nu_{sp}^t$ decreases (due to decrease of density of dipolar solvent). This contrasting composition dependence of interaction contributions gives rise to the non-ideality in the calculated total shift. It is seen earlier that with increase in polar solvent concentration, the static solute-IL dipole correlation and solute-ion correlation decrease following a regular trend.[15] This is due to the screening of solute-IL interaction by another dipolar solvent. The decrease of IL density is another reason for decreasing the

solute-IL (dipole-dipole and dipole-ion interaction) interaction contribution of the dynamic Stokes shift in the system. Calculated Stokes shifts at pure $[\mathrm{Bmim}][\mathrm{BF_4}]$ ($x_{IL} = 1.0$) and $\mathrm{CH_3CN}$ ($x_{IL} = 0.0$) are 2208 cm^{-1} and 1977 cm^{-1} respectively, which are in near-quantitative agreement with experimental values.[70] However, Stokes shifts in binary mixtures deviate from the experiments and the deviation is the maximum (~900 cm^{-1}) at $x_{IL} \approx 0.3$. Hence it is clear that separate medium calculations can neither predict the experimental Stokes shifts nor reproduce the experimentally observed insensitivity of dynamic shift to mixture composition for these binary mixtures.

B. Effective Medium Calculations: Binary Mixtures of ($[\mathrm{Bmim}][\mathrm{BF_4}] + \mathrm{CH_3CN}$)

The composition dependent dynamic Stokes shift values for the binary mixtures of ($[\mathrm{Bmim}][\mathrm{BF_4}] + \mathrm{CH_3CN}$), obtained from effective medium calculation for the binary mixtures, have been presented in Table 7.2. Note that the effective dipolemoments for the mixtures, which have been calculated from MSA method using experimental dielectric constant are presented in Table A22 (Appendix A). The dynamic Stokes shifts, originated specifically from solute-solvent dipole (dipole-dipole) ($\Delta\nu^t_{sd}$) and solute-ion (dipole-ion) interaction ($\Delta\nu^t_{si}$) are presented in the same table. $\Delta\nu^t_{\mathrm{expt.}}$ is provided also for a clear comparison. Note that static dielectric constant, used in this calculation, have been taken from the recent dielectric relaxation measurement[66] of the binary mixture of ($[\mathrm{Bmim}][\mathrm{BF_4}] + \mathrm{CH_3CN}$).It is seen from the table that the calculated shift ranges between ~1800 and ~2300 cm^{-1}, which is semi-quantitative to the experimental range (~1900 – 2200 cm^{-1})[70]. More interesting feature is that, $\Delta\nu^t_{tot}$ remains nearly constant with mole

Table 7.2: Composition dependence of dynamic Stokes shift of C153 probe in the binary mixture of ($[Bmim][BF_4] + CH_3CN$) using effective medium calculation approach

Mole fraction of IL, x_{IL}	solute-solvent (dipole-dipole) interaction contribution, $\Delta\nu_{sd}^t$ (cm^{-1})	solute-ion (dipole-ion) interaction contribution, $\Delta\nu_{si}^t$ (cm^{-1})	Total $\Delta\nu_{tot}^t$ (cm^{-1})	Experiment, $\Delta\nu_{expt.}^t$ (cm^{-1})
0.0	1977	0	1977	1980
0.1	1910	138	2048	
0.2	1858	282	2140	2100
0.3	1907	400	2307	2160
0.4	1678	509	2187	2090
0.5	1450	661	2111	2100
0.6	1326	777	2103	2120
0.7	1240	874	2114	
0.8	1162	952	2114	2120
0.9	1021	1063	2084	2150
1.0	822	1085	1907	2160

fraction of IL, which is in close agreement with experiments. The reason of the insensitivity of Stokes shift is understood if one observes the composition dependence of $\Delta\nu_{sd}^t$ and $\Delta\nu_{si}^t$, where $\Delta\nu_{sd}^t$ decreases by nearly the same amount as $\Delta\nu_{si}^t$ increases with IL concentration, making the summation ($\Delta\nu_{tot}^t = \Delta\nu_{sd}^t + \Delta\nu_{si}^t$) almost constant. The reason of increase of $\Delta\nu_{si}^t$ is simply due to gradual increase of ion density with increasing IL concentration (Table A22, Appendix A), but the reason for decrease of $\Delta\nu_{sd}^t$ may appear surprising because of the apparent increase of density upon increase in IL mole fraction in the binary mixtures. But a more detailed investigation reveals that, although mass density of the system increases, the number density of the dipole in the mixture decreases with increase in IL mole fraction (Table A22, Appendix A), and hence $\Delta\nu_{sd}^t$ decreases with increase of IL concentration. Thus

this theoretical approach can effectively explain the insensitivity of total shift on the composition of the binary mixture in terms of mutual cancellation by approximately the same magnitude of decrease and increase of $\Delta\nu_{sd}^{t}$ and $\Delta\nu_{si}^{t}$ respectively with IL mole fraction in binary mixture under investigation.

7.3.2 Dynamic Stokes Shift for C153 in Binary Mixtures of ($[Bmim][BF_4]+H_2O$): Composition Dependence

Similar to the mixture ($[Bmim][BF_4]+CH_3CN$), we have done dynamic Stokes shift calculation of C153 in the binary mixture of ($[Bmim][BF_4]+H_2O$) also using both approaches, separate and effective medium calculation. Here, our target is to choose the better approach for explaining the experimental dynamic Stokes shift[71] values and more specifically, the insensitivity of the shift on the composition of the mixture.

A. Separate Medium Calculations: Binary Mixtures of ($[Bmim][BF_4]+H_2O$)

Table A23 (Appendix A) summarizes the necessary input parameters for the calculations reported below. The density (ρ)[81] and viscosity (η)[71] have been taken from different experiments. The diameter of water molecule is taken as 2.8 Å.[82] Static dielectric constant value for $[Bmim][BF_4]$ has been taken from Ref. 71 and the static dielectric constant of water has been taken from Ref. 83. The use of gas phase dipole moment ($\mu_{H_2O} = 1.8D$)[84] of water molecule in our previous calculation of dynamic Stokes shift for this mixture leads to roughly 2-fold difference between the Stokes shift in water (~800 cm^{-1}) compared to that in $[Bmim][BF_4]$ (2000 cm^{-1}), in contrast to the near composition independence of measured shift[71]. In the present calculations we use the liquid phase dipole moment of water as 2.85 Debye[84,85]. The theory suggests that the effects of using different dipole moments of water will not significantly affect the solvation response of the mixture. We have summarized the composition dependence of calculated and experimentally measured dynamic Stokes shifts of C153 in the binary mixtures of ($[Bmim][BF_4]+H_2O$) in Table 7.3. The table shows the calculated dynamic Stokes shifts, originated separately from solute-IL dipole (dipole-dipole)

interaction ($\Delta\nu_{sd}^{t}$), solute-dipolar solvent dipole (dipole-dipole) interaction ($\Delta\nu_{sp}^{t}$), solute-ion (dipole-ion) interaction ($\Delta\nu_{si}^{t}$). Total theoretical dynamic Stokes shifts ($\Delta\nu_{tot}^{t} = \Delta\nu_{sd}^{t} + \Delta\nu_{si}^{t} + \Delta\nu_{sp}^{t}$) and experimental shifts ($\Delta\nu_{\exp t.}^{t}$) are also presented in the same table.

It is clearly seen from theoretical results that the composition of the binary mixture has a strong influence on total Stokes shift of this system, whereas the experimental shift[71] is seen to be almost insensitive towards IL mole fraction. It is clearly seen in Table 7.3 that the use of dipole moment of water molecule as 2.85 Debye generates a value of Stokes shift for water very close to that observed in experiment[71]. Similar to the case of the previous mixture ($[\mathrm{Bmim}][\mathrm{BF_4}] + \mathrm{CH_3CN}$), here also the theory predicts that the Stokes shifts, near IL and water rich regions, are very close to the experimental values and on the other hand the theory differs from experiment at appreciable amount at ~0.5 mole fraction of IL.

Table 7.3: Composition dependence of dynamic Stokes shift of C153 probe in the binary mixture of ($[\mathrm{Bmim}][\mathrm{BF_4}] + \mathrm{H_2O}$) using separate medium calculation approach

Mole fraction of IL, x_{IL}	solute-IL (dipole-dipole) interaction contribution, $\Delta\nu_{sd}^{t}$ (cm^{-1})	solute-ion (dipole-ion) interaction contribution, $\Delta\nu_{si}^{t}$ (cm^{-1})	solute-dipolar solvent (dipole-dipole) interaction contribution, $\Delta\nu_{sp}^{t}$ (cm^{-1})	Total $\Delta\nu_{tot}^{t}$ (cm^{-1})	Experiment, $\Delta\nu_{\exp t.}^{t}$ (cm^{-1})
0.0	0	0	2310	2310	2452
0.1	300	430	840	1570	2324
0.3	401	670	280	1351	2306
0.5	538	844	130	1512	2306
0.7	696	1027	80	1803	2306
0.9	860	1187	40	2087	2200
1.0	947	1261	0	2208	2240

B. Effective Medium Calculations: Binary Mixtures of ($[Bmim][BF_4]+H_2O$)

The composition dependent dynamic Stokes shift values for the binary mixtures of ($[Bmim][BF_4]+H_2O$), obtained from effective medium calculation for the binary mixtures, have been presented in Table 7.4. The dynamic Stokes shifts, originated from different specific interactions are also presented in the same table. The calculated shifts are also compared with measured values. Note that static dielectric constant, used in this calculation, have been taken from the recent dielectric relaxation measurement[71] of the binary mixture of ($[Bmim][BF_4]+H_2O$). The effective dipole moment has been calculated using MSA from measured static dielectric constant. Table 7.4 shows that the calculated shift ranges between ~1800 and ~2300 cm^{-1}, which is semi-quantitative to the experimental range (~1900 – 2200 cm^{-1})[71]. Like the binary mixture of ($[Bmim][BF_4]+CH_3CN$), here also $\Delta\nu^t_{tot}$ remains almost constant with mole fraction of IL, which is in very much similar with the experiment. The possible reason for composition independence of experimental Stokes shift is thus understood in terms of mutual understanding of the Stokes shifts, originated from specific interactions, broadly speaking the decrease in $\Delta\nu^t_{sd}$ in contrast to increase in $\Delta\nu^t_{si}$ upon gradual rise of IL concentration. This is already observed in the previous binary mixture ($[Bmim][BF_4]+CH_3CN$).

Table 7.4: Composition dependence of dynamic Stokes shift of C153 probe in the binary mixture of ($[Bmim][BF_4]+H_2O$) using effective medium calculation approach

Mole fraction of IL, x_{IL}	solute-solvent dipole (dipole-dipole) interaction contribution, $\Delta\nu^t_{sd}$ (cm^{-1})	solute-ion (dipole-ion) interaction contribution, $\Delta\nu^t_{si}$ (cm^{-1})	Total $\Delta\nu^t_{tot}$ (cm^{-1})	Experiment, $\Delta\nu^t_{expt.}$ (cm^{-1})
0.0	2310	0	2310	2452
0.1	2223	122	2345	2324
0.3	1929	433	2362	2306
0.5	1690	720	2410	2306
0.7	1373	1007	2320	2306
0.9	1053	1217	2270	2200
1.0	947	1261	2208	2240

Fig. 7.1 represents a pictorial comparison between the predicted shifts in these binary mixtures via effective and separate medium calculations and experimental values. Evidently, effective medium calculations reproduce better the observed shifts and its insensitivity to mixture composition.

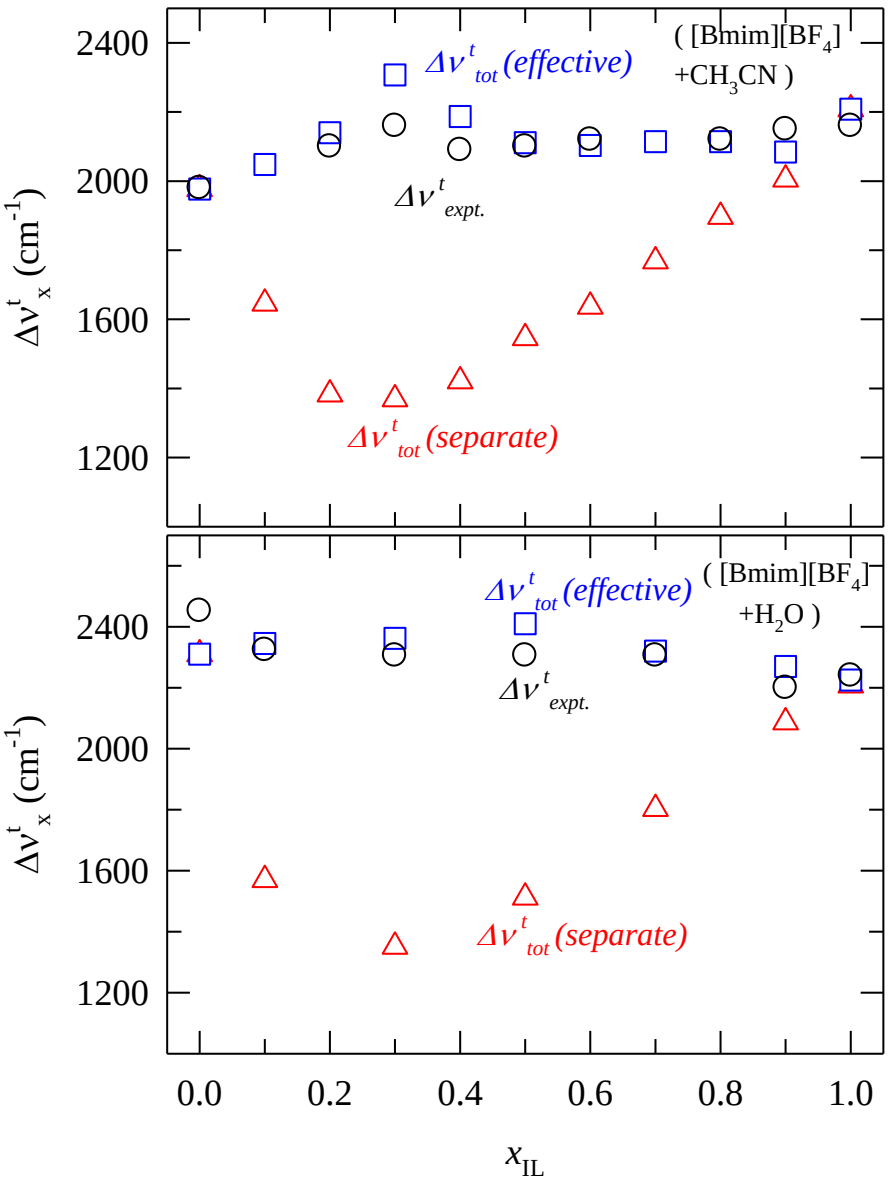

Fig. 7.1: Comparison of composition dependence of theoretical dynamic Stokes shift with observed in experiment (black circle). The shifts, obtained from separate medium calculation approach (red triangle), are also compared with that, obtained from medium calculation approach (blue square). The upper and the lower panel represent the binary mixture of $([Bmim][BF_4]+CH_3CN)$ and $([Bmim][BF_4]+H_2O)$ respectively.

7.3.3 Stokes Shift Dynamics for C153 in Binary Mixtures of ($[Bmim][BF_4]+CH_3CN$): Composition Dependence

Theoretical calculations of Stokes shift dynamics of C153 in the binary mixtures of ($[Bmim][BF_4]+CH_3CN$) and ($[Bmim][BF_4]+H_2O$) have been performed to understand the composition dependence of solvation response of the mixture. Like dynamic Stokes shift calculations, we have obtained the solvation response via two approaches, separate medium and effective medium calculations.

A. Separate Medium Calculations: Binary Mixtures of ($[Bmim][BF_4]+CH_3CN$)

Here, the calculated Stokes shift dynamics for C153 in the binary mixture ($[Bmim][BF_4]+CH_3CN$) using separate medium calculations will be presented and a comparison between theory and experiments will be discussed in details. Note that the dielectric relaxation data for neat $[Bmim][BF_4]$ and CH_3CN have been taken from Ref. 71 and 66 respectively. Earlier theoretical works[12-17] on Stokes shift dynamics of a fluorescent probe in neat IL have already suggested that the solvation response function (S_{sd}), originated from solute-IL dipole-dipole interaction, has dominating contribution (85-90%) over that (S_{si}), originated from solute-IL dipole-ion interaction to the total response. In the binary mixtures of IL and dipolar solvent, the total solvation response function (S_{ss}) is constructed from S_{sd}, S_{sp}, and S_{si} as follows:

$$S_{ss}(t) = (1-0.1x_{IL})\left[x_{IL}\, S_{sd}(t) + (1-x_{IL})\, S_{sp}(t)\right] + 0.1\, x_{IL}\, S_{si}(t), \tag{7.3}$$

where $S_{sd}(t)$, $S_{sp}(t)$, and $S_{si}(t)$ have been obtained by using Eq. 6.5, Eq. 6.8 and Eq. 6.9 of Chapter 6, respectively. The relative contribution to the total dynamics arising from solute-dipolar solvent interaction can then be investigated by varying the value of f in Eq. 7.3. As usual, the average solvation time is obtained via time integration as follows: $\langle \tau_x \rangle = \int_0^\infty dt\, S_x(t)$, where x represents "sd", "sp","si"and "ss". Now we check the equation for S_{ss} at two limiting mole fractions of IL. For pure IL, at $x_{IL} = 1.0$, Eq. 7.3 turns into ,

$$S_{ss}(t) = 0.9\, S_{sd}(t) + 0.1\, S_{si}(t)\ , \tag{7.4}$$

which has already been used in the case of Stokes shift dynamics in neat IL,[12-14, 16,17] whereas for pure dipolar solvent, at $x_{IL} = 1.0$, Eq. 7.3 turns into , $S_{ss}(t) = S_{sp}$. Thus Eq. 7.3 is a general equation and can be used at any composition of the binary mixtures of IL and dipolar solvent.

Fig. 7.2 displays the experimental solvation response[70] and our calculated response for three representative compositions of the binary mixtures of ($[\mathrm{Bmim}][\mathrm{BF_4}] + \mathrm{CH_3CN}$). Here we can see a fairly good agreement of our calculated responses with the experimental ones. it is clear that the solvation response functions are multi-phasic. A more detailed investigation of Fig. 7.2 further revels that our theoretical response becomes faster than the experiment at relatively lower concentrations of IL in the mixture ($x_{IL} < 0.5$). The disagreement becomes even more at sub-picoseconds regime ($t < 1\ ps$). The use of FLUPS technique of ~80 fs time resolution allows the detection of the dynamical response at the initial part of the solvation, while on the other hand, use of the incomplete DR spectra, measured over a range of frequencies ($0.2 \le \nu/GHz \le 89$), in our calculation does not lead to the ultrafast response. Use of this incomplete dielectric relaxation can indeed affect our calculated response and may be one of the reasons for this disagreement.

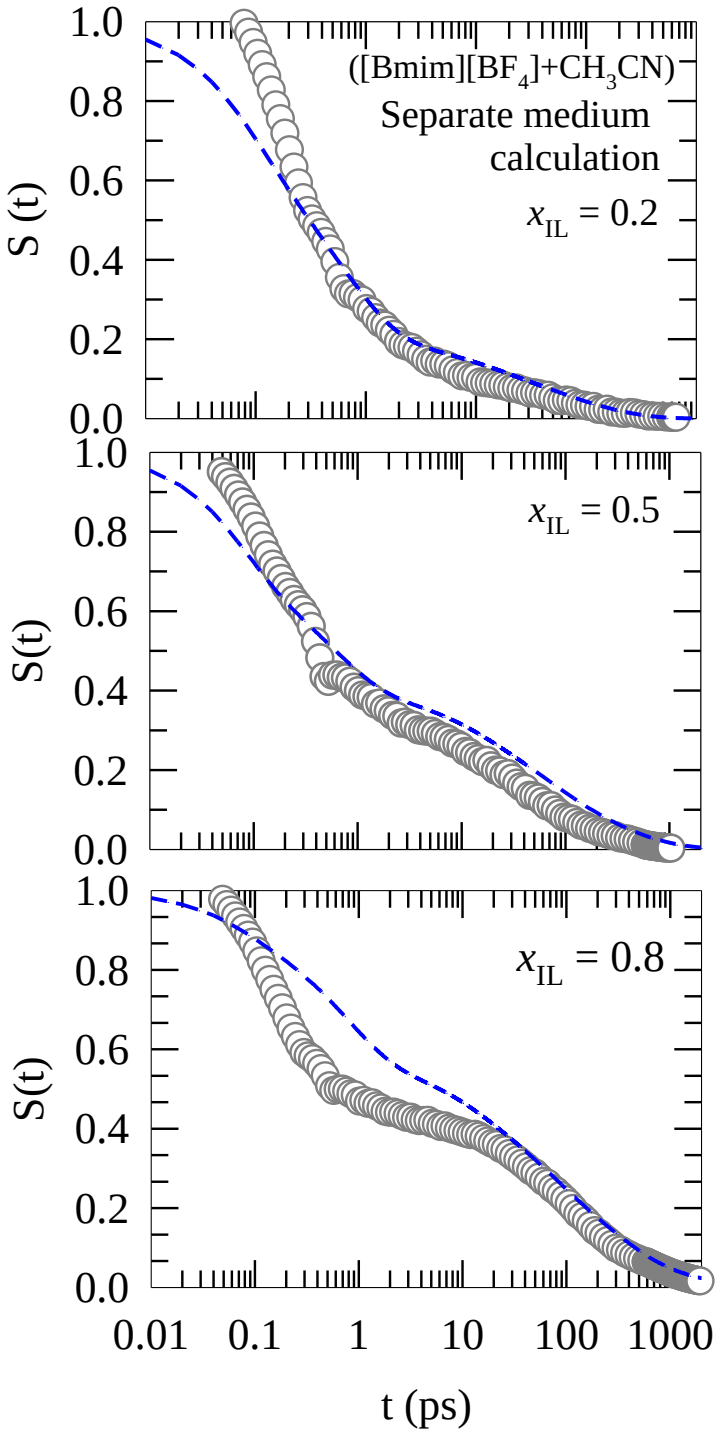

Fig. 7.2: Decay of the calculated (blue short dashed line) and measured (dark grey open circle) solvation response with time of C153 probe in the binary mixture of ($[Bmim][BF_4] + CH_3CN$) at three representative compositions. The calculated solvation response functions have been obtained from separate medium calculation approach.

In Table 7.5, we have summarized the fitting parameters for these theoretically and experimentally obtained solvation response functions for the binary mixtures. It has been seen that at low IL concentration ($x_{IL} \leq 0.3$) our theoretical solvation response function is tri-exponential ($S_{ss}(t) = a_1 exp(-t/\tau_1) + a_2 exp(-t/\tau_2) + a_3 exp(-t/\tau_3)$), while at other compositions it is exponential followed by stretched exponential function ($S_{ss}(t) = a_1 exp(-t/\tau_1) + a_2 exp\left(-(t/\tau_2)^{\beta}\right)$), where τ_1, τ_2, and τ_3 are the time constants, a_1, a_2, and a_3 are the corresponding amplitudes, and β is the stretched exponent. On the other hand experimental response is seen to be composed of Gaussian and tri-exponential functions ($S_{expt.}(t) = f_G exp\left(-(t/\tau_G)^2\right) + f_e[a_1 exp(-t/\tau_1) + a_2 exp(-t/\tau_2) + a_3 exp(-t/\tau_3)]$) at every binary mixture compositions.[70] Table 7.5 shows a semi-quantitative agreement of our theoretical response functions with the experimental ones. The theoretical integral times of ultrafast part ($\langle \tau_f \rangle$) and the slowest part ($\langle \tau_s \rangle$) of the solvation are calculated, shown in the 12th and 13th column respectively, to compare with the experimental values. It is clearly seen that at lower IL concentration ($x_{IL} < 0.3$), theoretical $\langle \tau_f \rangle$ is faster than experimental $\langle \tau_f \rangle$, whereas at higher IL concentration ($x_{IL} \geq 0.5$) the observation is just reversed. Now for $\langle \tau_s \rangle$, the theory agrees very well with experiments and thus the predicted average solvation time ($\langle \tau_{solv} \rangle$) agrees well to experiments at all mole fractions. These comparisons will be clearer in Fig. 7.3, where we have shown the integral times both obtained from our theory and experiments.

Table 7.5: Fitting parameters of solvation responses of C153 probe in the binary mixture of ($[Bmim][BF_4]+CH_3CN$) from experiment and theory, using separate medium calculation approach and *new* DR data of neat $[\mathrm{Bmim}][\mathrm{BF_4}]$. The time constants are in ps.

x_{IL}	Tool	f_1	τ_1	f_2	τ_2	f_3	τ_3	f_4	τ_4	β	$\langle\tau_f\rangle$	$\langle\tau_s\rangle$	$\langle\tau_{solv}\rangle$
0.2	Theo.	0.44	0.12	0.38	0.99	0.18	48.5				0.12	16.3	9.16
	Expt.	0.54	0.26	0.32	1.40	0.07	14.0	0.07	118	1	0.23	22.0	10.0
0.3	Theo.	0.48	0.11	0.33	0.92	0.19	44.2				0.11	16.7	8.75
	Expt.	0.42	0.20	0.32	0.76	0.16	9.00	0.10	90.0	1	0.18	19.0	11.0
0.4	Theo.	0.49	0.22					0.51	15.5	0.31	0.22	124	63.5
	Expt.	0.60	0.26	0.17	2.00	0.16	37.0	0.07	237	1	0.23	56.0	23.0
0.5	Theo.	0.47	0.21					0.53	53.8	0.39	0.21	192	102
	Expt.	0.19	0.15	0.45	0.41	0.19	16.0	0.16	161	1	0.13	37.0	30.0
0.6	Theo.	0.42	0.23					0.58	73.5	0.40	0.23	244	142
	Expt.	0.42	0.17	0.22	0.55	0.17	71.0	0.18	287	1	0.15	112	65.0
0.8	Theo.	0.31	0.51					0.69	97.1	0.41	0.51	302	208
	Expt.	0.34	0.17	0.23	0.65	0.29	86.0	0.14	779	1	0.15	198	131
0.9	Theo.	0.25	0.58					0.75	124	0.42	0.58	362	272
	Expt.	0.08	0.12	0.45	0.26	0.21	39.0	0.26	648	1	0.11	193	243

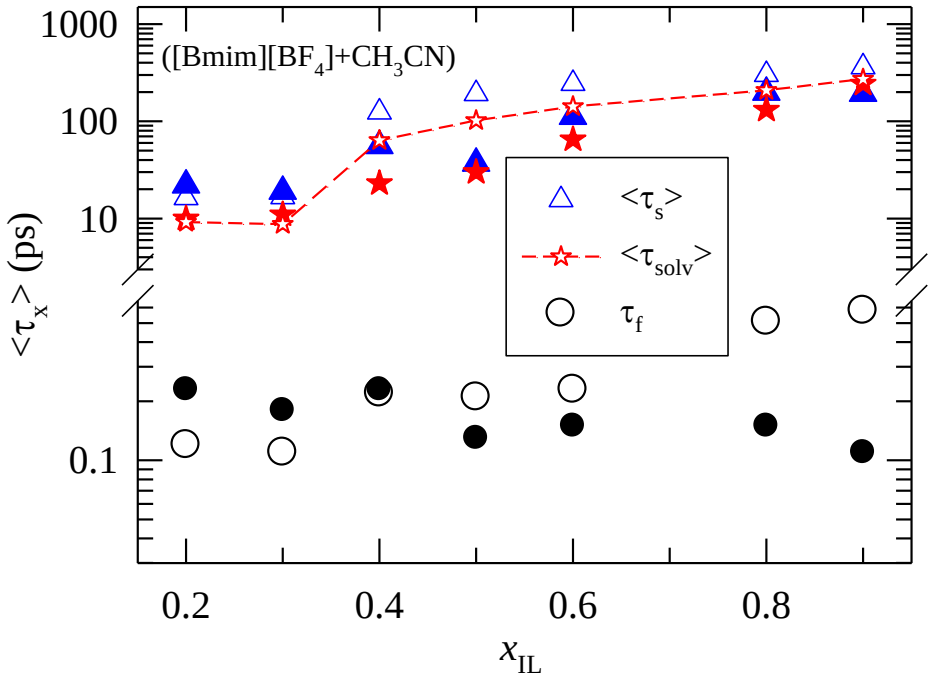

Fig. 7.3: Plot for comparison of the calculated integral times (open symbols) with those measured in experiment (filled symbols) for the binary mixture of ($[Bmim][BF_4]+CH_3CN$).

B. Effective Medium Calculations: Binary Mixtures of ($[Bmim][BF_4]+CH_3CN$)

Here we present our results of Stokes shift dynamics of C153 in binary mixtures of ($[Bmim][BF_4]+CH_3CN$) at a several compositions. Note that in this type of calculations, two different dipoles of the binary mixture (IL dipole and dipolar solvent dipole) are not treated separately, rather they are assumed to be a single dipolar part of the solvent, having an effective dipole moment, diameter, and mass. This assumption leads us into similar calculation like neat IL, done previously.[12,14,16,17] As the ion concentration decreases with decreasing the concentration of IL in the binary mixture, the solute-ion interaction contribution ($S_{si}(t)$) to the total solvation is expected to decrease. Assuming $S_{si}(t)$ to be linearly proportional with the mole fraction of IL, we can write the expression of $S_{ss}(t)$ in terms of $S_{ss}(t)$ and $S_{si}(t)$ as following:

$$S_{ss}^{eff}(t) = (1 - 0.1\,x_{IL})S_{sd} + 0.1\,x_{IL}S_{si}(t) \qquad (7.5)$$

The calculation of solvent dynamic structure factor for the effective dipolar medium has been done using the recent experimental dielectric relaxation data.[66] We have compared $S_{ss}^{eff}(t)$ with $S_{expt.}(t)$ in Fig. C14 (Appendix C) for three representative compositions of the binary mixtures ($[Bmim][BF_4]+CH_3CN$), where, it is seen that the agreement between experiment and theory is poor at initial time, although a fairly good agreement is observed in long time limit. The $S_{ss}^{eff}(t)$ for all the compositions have been fitted with a tri-exponential function and the fitting parameters are summarized in Table A24 (Appendix A). A closer investigation of Table A24 (Appendix A), particularly the comparison of this approach and experiment in the light of $\langle \tau_f \rangle$ and $\langle \tau_s \rangle$, reveals that the ultrafast time constants, obtained from the experimental measurement for the binary mixtures, are absent in the effective medium calculation. Thus this theoretical approach is unable to predict the ultrafast solvation and hence cannot be used for this study. The slower response is probed by this approach much better and thus the $\langle \tau_s \rangle$, predicted by the effective medium calculation, agrees very good with experiment.[70]

7.3.4 Stokes Shift Dynamics for C153 in Binary Mixtures of ($[Bmim][BF_4]+H_2O$): Composition Dependence

A. Separate Medium Calculation: Binary Mixtures of ($[Bmim][BF_4]+H_2O$)

Stokes shift dynamics of C153 in the binary mixture of ($[Bmim][BF_4]+H_2O$) has been done recently using combination of FLUPS and TCSPC techniques to observe the complete solvation response of C153 over the time window from 100 fs to 20 ns.[71] Along with that, dielectric relaxation measurement of the same binary mixtures has also been done over a wide frequency range (100 MHz – 89 GHz). The dielectric relaxation data for the neat IL has been used in our calculation. The water dynamic structure factor ($S_p^{lm}(k,t)$) has been calculated using the dielectric relaxation of water, measured elsewhere[83]. The total solvation response function ($S_{ss}(t)$) has

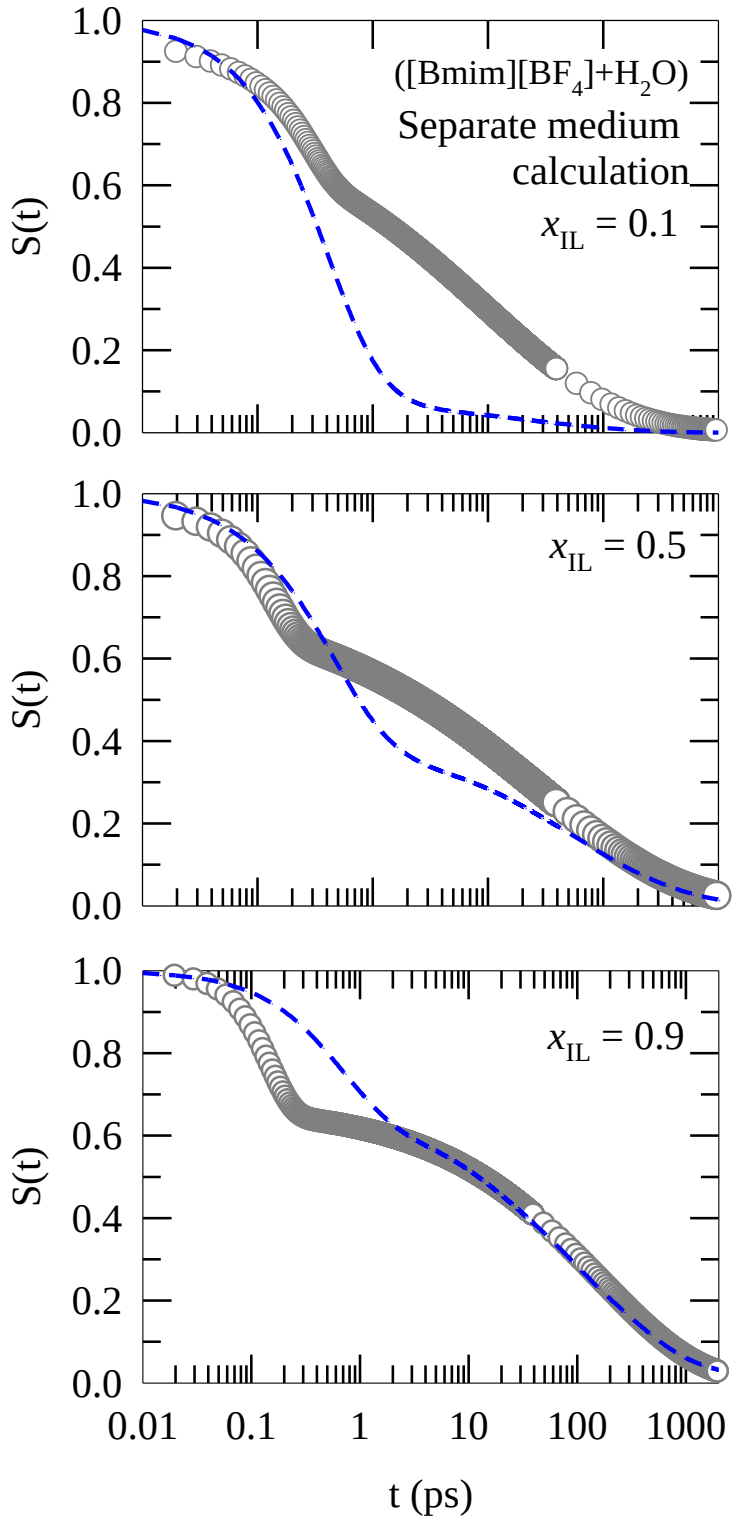

Fig. 7.4: Decay of the calculated (blue short dashed line) and measured (dark grey open circle) solvation response with time of C153 probe in the binary mixture of ($[Bmim][BF_4]+H_2O$) at three representative compositions. Here the calculated solvation response functions are obtained from separate medium calculation approach.

been calculated in the same way as for the previous case ($[\mathrm{Bmim}][\mathrm{BF_4}]+\mathrm{CH_3CN}$) using Eq. 7.3. The necessary input parameters for the calculation of this binary mixture are summarized in Table A23 (Appendix A).

We have plotted the theoretical and experimental solvation response functions for this binary mixture in Fig. 7.4 at three representative mole fraction of IL to see the agreement of our theory with the experiment for this particular mixture. Fig. 7.4 clearly tells that the theoretically predicted response is very much similar to that of the experiment[71]. At lower mole fraction of IL, the predicted response seems to deviate more than at higher mole fraction region in this mixture, which recalls the similar observation in case of ($[\mathrm{Bmim}][\mathrm{BF_4}]+\mathrm{CH_3CN}$). In the water rich region ($x_{IL} < 0.5$), calculated responses is faster than the measured ones, especially at small time limit. At IL rich compositions the calculated response matches very well with experiment. These observations give rise to the question: what makes the difference between theoretical and experimental responses mainly at water rich regime? The question will be more relevant if we fit the calculated response and compare the amplitudes and time scales with those from measured responses. The calculated responses ($S_{ss}(t)$) have been seen to fit by a function, which is a linear combination of exponential and stretched exponential function, mathematically expressed as, $S_{ss}(t) = a_1\, exp(-t/\tau_1) + a_2\, exp\left(-(t/\tau_2)^{\beta}\right)$. The fitting parameters for theoretical and experimental responses are presented in Table 7.6, where it is clearly seen that the theoretical time scales and amplitudes are quantitatively similar to the experimental parameters, which means that our theory is in very good agreement with the experiment especially at higher IL concentration. On the other hand significant differences are observed between theoretical and experimental time scales and associated amplitudes in water rich regime. Whereas the theory predicts larger amplitudes of the ultrafast time scale, the experiment shows relatively small amplitudes, which essentially tells that the experiment does not probe the profound contribution of the ultrafast relaxation to the total solvation response. Closer inspection of the Table 4 further reveals an interesting and surprising feature and that is the almost insensitivity of the amplitudes of the ultrafast solvation (~10-35%), which is not seen in our theoretical values. Instead our theory predicts a steady increase of the amplitude associated to the ultrafast time scale (a_1 = 0.27 to a_1 = 0.86) while the IL molefraction (x_{IL}) decreases from

0.9 to 0.1. One possible reason for this insensitivity of ultrafast relaxation contribution on the composition may be the microscopic inhomogeneity present in the medium, which creates microscopic phase separation and thus

Table 7.6: Fitting parameters of solvation responses of C153 probe in the binary mixture of ($[\mathrm{Bmim}][\mathrm{BF_4}]+\mathrm{H_2O}$) from experiment and theory, using separate medium calculation approach and *new* DR data of $[\mathrm{Bmim}][\mathrm{BF_4}]$

x_{IL}	Mode	a_1	τ_1(ps)	a_2	τ_2(ps)	β	$\langle\tau_f\rangle$ (ps)	$\langle\tau_s\rangle$ (ps)	$\langle\tau_{solv}\rangle$ (ps)
0.1	Theory	0.86	0.45	0.14	6.2	0.31	0.45	49.8	7.40
	Expt.	0.19	0.27	0.81	10.0	0.37	0.27	44.0	36.0
0.3	Theory	0.71	0.46	0.29	31.0	0.40	0.46	103	30.2
	Expt.	0.09	0.15	0.91	12.0	0.31	0.15	89.0	81.0
0.5	Theory	0.55	0.47	0.45	60.2	0.43	0.47	166	74.9
	Expt.	0.25	0.13	0.75	30.0	0.36	0.13	141	106
0.7	Theory	0.40	0.51	0.60	69.4	0.43	0.51	191	115
	Expt.	0.35	0.08	0.65	76	0.41	0.08	231	151
0.9	Theory	0.27	0.72	0.73	115	0.43	0.72	317	232
	Expt.	0.33	0.14	0.67	170	0.48	0.14	362	243

C153 probe, being sparingly soluble in water[86], stays mainly at IL regime. If this happens then the solute cannot probe the fast dynamics of water although mole fraction of water is present in the medium. Now the integral values of the faster time ($\langle\tau_f\rangle$) and slower time ($\langle\tau_s\rangle$) are also tabulated in the 8th and 9th column respectively in Table 4, where it is seen that $\langle\tau_s\rangle$ increases upon increase in x_{IL} although $\langle\tau_f\rangle$ remains almost constant. The increase of

$\langle \tau_s \rangle$ with x_{IL} is actually the effect of gradual rise of viscosity of the medium. Now theoretical values of $\langle \tau_f \rangle$ are always higher than experimental ones[71], while theoretical $\langle \tau_s \rangle$ goes very close to the experimental and thus the theoretical average solvation time ($\langle \tau_{solv} \rangle$) follows the experimental trend much efficiently at all mole fractions of the binary mixtures. Fig. 7.5, represents the mole fraction dependence of the integral times both obtained from our theory and the experiment, where the excellent agreement between theory and experiment has once again reflected.

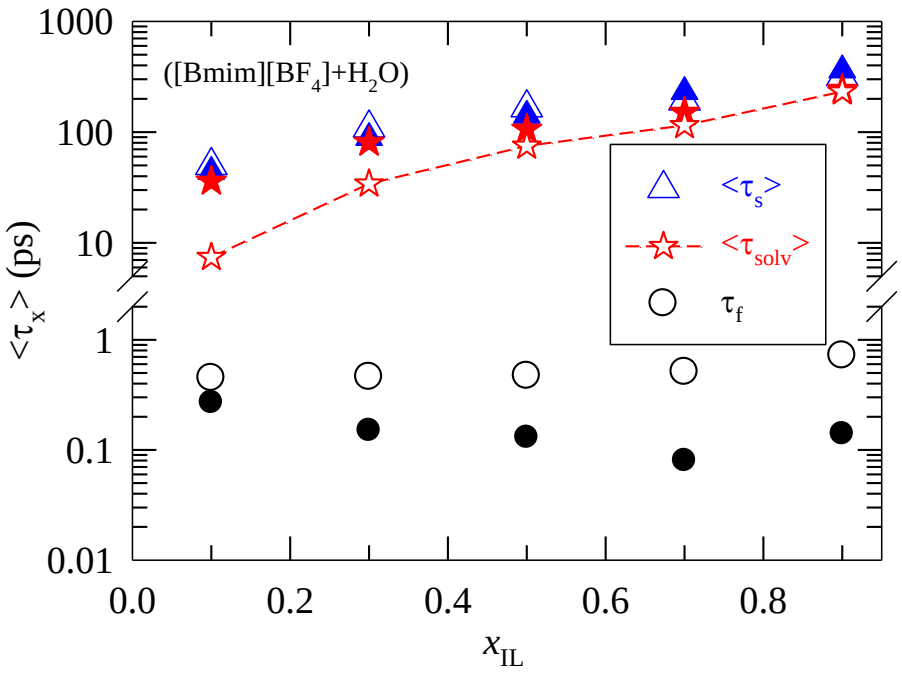

Fig. 7.5: Plot for comparison of the calculated integral times (open symbols) with those measured in experiments (filled symbols) for the binary mixture of ($[\mathrm{Bmim}][\mathrm{BF_4}] + \mathrm{H_2O}$).

The experimental dielectric relaxation data is very much important for our calculation of solvation response functions, because the dielectric relaxation parameters go into the calculation through the solvent dynamic structure factor, which is needed to calculate $S_{sd}(t)$ and $S_{sp}(t)$ (see Eq. 7.5, 7.6, 7.8, 7.9). There are two dielectric relaxation measurements for $[\mathrm{Bmim}][\mathrm{BF_4}]$ IL, of which the first measurement (*old* DR data)[87] has been done in the

frequency range ($0.2 \le \nu / GHz \le 89$) and the second one (*new* DR data)[71] in the frequency range ($0.1 \le \nu / GHz \le 89$). In the *old* case[87] the authors have fitted the dielectric permittivity and loss spectra with (Cole-Cole + Debye) (CC+D) type of function, whereas in the *new* case[71] the spectra have been fitted with 4-Debye (4-D) form. These slight difference in working frequency region and the different fitted forms for these two cases may crucially alter our theoretical solvation response functions. Here we investigate the sensitivity of our theoretical solvation response on these two different measured dielectric relaxation parameters of $[\mathrm{Bmim}][\mathrm{BF_4}]$. Fig. 7.6 represents the comparison of solvation relaxations of the binary mixture of $[\mathrm{Bmim}][\mathrm{BF_4}]+\mathrm{H_2O}$ using two different DR parameters for three representative compositions. We have plotted the experimental response as well to make a clear comparison. It is seen that at

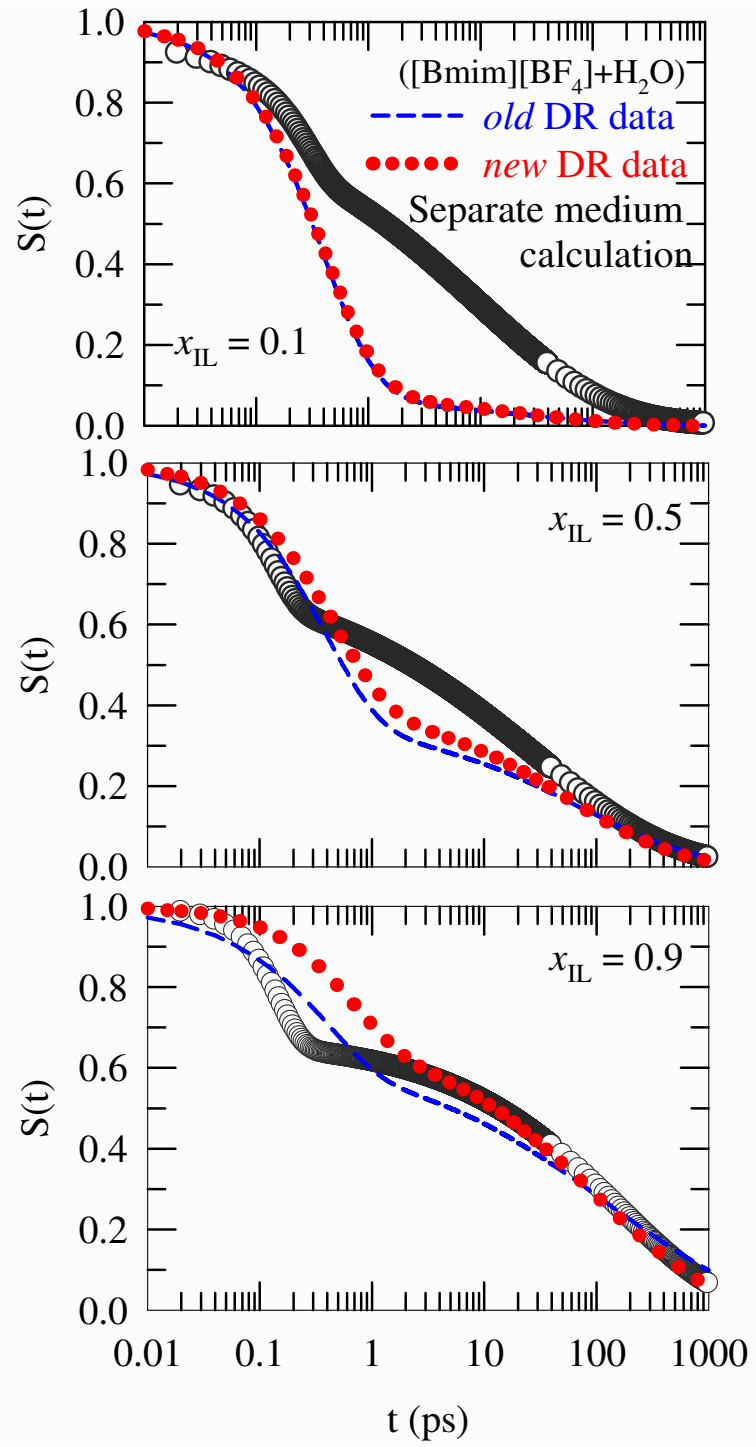

Fig. 7.6: The plots for the study of sensitivity of the calculated solvation response functions upon the experimentally measured DR data, which are used as input to the calculation. While the blue short dashed and red dotted lines represent the solvation response of C153 in the binary mixture of $([Bmim][BF_4]+H_2O)$ using *new* and *old* DR data respectively, measured solvation responses are shown in dark grey open circles. The three panels are for three different compositions of the mixture.

low IL concentrations, two theoretical responses are not much different with one another, because of using the same DR data for water. The fitting parameters for the response functions are summarized in Table A25 (Appendix A), where we can see a clear difference in the relaxation time scales and average solvation time, as we use two different DR data mainly at higher IL concentration region. This proves the sensitivity of our theoretically calculated solvation response function on the frequency region, at which DR spectra have been collected, and on the nature of function (whether CC+D or 4-D) of fitting of the dielectric permittivity and loss spectra.

B. Effective Medium Calculations: Binary Mixtures of ($[Bmim][BF_4]+H_2O$)

Here we present our results of Stokes shift dynamics of C153 probe in binary mixture ($[Bmim][BF_4]+H_2O$) for a number of compositions using effective medium calculation approach. The exactly same approach has been done for ($[Bmim][BF_4]+CH_3CN$) binary mixture. The total solvation response ($S_{ss}^{eff}(t)$) has been calculated using Eq. 7.15. The calculation of solvent dynamic structure factor for the effective dipolar medium has been done using the recent experimental dielectric relaxation data.[71] We have compared $S_{ss}^{eff}(t)$ with $S_{expt.}(t)$ in Fig. C15 (Appendix C) for three representative compositions of the binary mixtures ($[Bmim][BF_4]+CH_3CN$), where, it is seen that the agreement between experiment and theory is poor at initial time, although a fairly good agreement is observed in long time limit. This is similar to the previous binary mixture ($[Bmim][BF_4]+CH_3CN$) studied. The $S_{ss}^{eff}(t)$ for all the compositions have been fitted with a (exponential + stretched exponential) function and the fitting parameters are summarized in Table A26 (Appendix A). A closer investigation of Table A26 (Appendix A), particularly the comparison of this approach with experiment in the light of $\langle \tau_f \rangle$ and $\langle \tau_s \rangle$, reveals that the ultrafast time constants, obtained from the experimental measurement for the binary mixtures, are absent in the effective medium calculation. Thus this theoretical approach is unable to predict the ultrafast solvation and hence cannot be used for this study. The slower response is probed by this approach much better and thus the $\langle \tau_s \rangle$, predicted by the effective medium calculation, agrees very good with experiment.

7.4 Conclusion

We have presented the theoretical calculation for Stokes shift dynamics of a fluorescent probe in two binary mixtures of (IL + common dipolar liquid). The acceptability of this theory lies into the agreement of the theoretical results with the recent experiments. We have employed two different types of theoretical approaches, separate and effective medium calculation, to do a comparative study for choosing the better approach to predict the experimental Stokes shift dynamics. We have seen that while effective medium calculation is better approach for reproducing the experimental shift, separate medium calculation provides more detail information about the solvation response. The mole fraction independence of the experimental Stokes shift is well explained in our theory in terms of mutual cancellation of increase of $\Delta\nu_{sd}^{t}$ (solute dipole -solvent dipole interaction contribution) by the decrease of $\Delta\nu_{si}^{t}$ (solute dipole - ion interaction contribution), making total shift almost insensitive to the composition of the binary mixture. We have modified the form of the total calculated solvation response function (Eq. 7.13) (used in our earlier works) and have become a general equation, applicable for neat IL, neat common dipolar liquid, and binary mixture of (IL + common dipolar liquid). The present form can also qualitatively explain the reason of not describing the behaviors of these mixtures by the relationship between experimental average solvation time and inverse conductivity does not appear to describe the behavior of this mixture, at least not over the entire composition range.[71] The theoretical solvation response function is very close to the experiment although in low concentration of IL region the theoretical response is faster than the experiment. The agreement between theoretical and experimental solvation relaxation time scales is overwhelming and thus proves the validity of our theory. The sensitivity of theoretical solvation response on the experimental dielectric constant, used as input in our calculation, has been studied and seen to be more in IL rich region. This proves the fact that the incapability to explain the experimental solvation phenomena may partly arise from the accuracy of available experimental dielectric relaxation data and partly from various approximations used in our theory..

References

57. Zhang, X. –X.; Liang, M.; Ernsting, N. P.; Maroncelli, M. *J. Phys. Chem. B* **2013**, *117*, 4291.
58. Arzhantsev, S.; Jin, H.; Baker, G. A.; Maroncelli, M. *J. Phys. Chem. B* **2007**, *111*, 4978.
59. Arzhantsev, S.; Jin, H.; Ito, N.; Maroncelli, M. *Chem. Phys. Lett.* **2006**, *417*, 524.
60. Samanta, A. *J. Phys. Chem. Lett.* **2010**, *1*, 1557.
61. Mandal, P. K.; Sarkar, M.; Samanta, A. *J. Phys. Chem. A* **2004**, *108*, 9048.
62. Roy, D.; Maroncelli, M. *J. Phys. Chem. B* **2007**, *116*, 5951–5970.
63. Maroncelli, M.; Zhang, X. –X.; Liang, M.; Roy, D.; Ernsting, N. P. *Faraday Discuss. Chem. Soc.* **2012**, *154*, 409.
64. Muramatsu, M.; Nagasawa, Y.; Miyasaka, H. *J. Phys. Chem. A* **2011**, *115*, 3886.
65. Hunger, J.; Stoppa, A.; Schrodle, S.; Hefter, G.; Buchner, R. *ChemPhysChem* **2009**, *10*, 723.
66. Stoppa, A.; Hunger, J.; Buchner, R.; Hefter, G.; Thoman, A.; Helm, H. *J. Phys. Chem. B* **2008**, *112*, 4854.
67. Kashyap, H. K.; Biswas R. *J. Phys. Chem. B* **2008**, *112*, 12431.
68. Kashyap, H. K.; Biswas, R. *J. Phys. Chem. B* **2010**, *114*, 254.
69. Kashyap, H. K.; Biswas R. *Ind. J. Chem.* **2010**, *49A*, 685.
70. Kashyap, H. K.; Biswas, R. *J. Phys. Chem. B* **2010**, *114*, 16811.
71. Daschakraborty, S.; Biswas, R. *J. Phys. Chem. B* **2011**, *115*, 4011.
72. Daschakraborty, S.; Biswas, R. *Chem. Phys. Lett.* **2011**, *510*, 202.
73. Daschakraborty, S.; Biswas, R. *Chem. Phys. Lett.* **2012**, *545*, 54.
74. Daschakraborty, S.; Biswas, R. *J. Chem Phys.* **2012**, *137*, 114501.
75. Daschakraborty, S.; Biswas, R. *J. Phys. Chem B* **2013**, (Submitted).
76. Jeong, D.; Shim, Y.; Choi, M. Y.; Kim, H. J. *J. Phys. Chem. B* **2007**, *111*, 4920.
77. Shim, Y.; Choi, M. Y.; Kim, H. J. *J. Chem. Phys.* **2005,** *122*, 044511.
78. Shim, Y.; Duan, J.; Choi, M. Y.; Kim, H. J. *J. Chem. Phys.* **2003**, *119*, 6411.
79. Shim, Y.; Kim, H. J. *J. Phys. Chem. B* **2008**, *112*, 11028.
80. Shim Y.; Kim, H. J. *J. Phys. Chem. B* **2009**, *113*, 12964.
81. Shim Y.; Kim, H. J. *J. Phys. Chem. B* **2007**, *111*, 4510.
82. Shim, Y.; Jeong, D.; Choi, M. Y.; Kim, H. J. *J. Chem. Phys.* **2006**, *125*, 061102.
83. Streeter, I.; Lynden-Bell, R. M.; Compton, R. G. *J. Phys. Chem. C* **2008**, *112*, 14538.

84. Bhargava, B. L.; Balasubramanian, S. *J. Chem. Phys.* **2005**, *123*, 144505.
85. Kobrak, M. N.; Znamenskiy, V. *Chem. Phys. Lett.* **2004**, *395*, 127.
86. Kobrak, M. N. *J. Chem. Phys.* **2006**, *125*, 064502.
87. Kobrak, M. N. *J. Chem. Phys.* **2007**, *127*, 184507.
88. Gonzalez, E. J.; Alonso, L.; Dominguez, A. *J. Chem. Eng. Data.* **2006**, *51*, 1446.
89. Li, W.; Zhang, Z.; Han, B.; Hu, S.; Xie, Y.; Yang, G. *J. Phys. Chem. B* **2007**, *111*, 6452.
90. Heinz, A.; Klasen, D.; Lehmann, J. K. *J. Soln. Chem.* **2002**, *31*, 467.
91. Schroder, U.; Wadhawan, J. D.; Compton, R. G.; Marken, F.; Suarez, P. A. Z.; Consorti, C. S.; de Souza, R. F.; Dupont, J. *New. J. Chem.* **2000**, *24*, 1009.
92. Seddon, K. R.; Stark, A.; Torres, M-J. *Pure Apply. Chem.* **2000**, *72*, 2275.
93. Rodriguez, H.; Brennecke, J. F. *J. Chem. Eng. Data.* **2006**, *51*, 2145.
94. Stoppa, A.; Hunger, J.; Buchner, R. *J. Chem. Eng. Data.* **2009**, *54*, 472.
95. Bester-Rogac, M.; Hunger, J.; Stoppa, A.; Buchner, R. *J. Chem. Eng. Data.* **2010**, *55*, 1799.
96. Khupse, N. D.; Kumar, A. *J. Soln. Chem.* **2009**, *38*, 589.
97. Tokuda, H.; Baek, S. J.; Watanabe, M. *Electrochemistry* **2005**, *73*, 620.
98. Zhang, Z. M.; Wu, W. Z.; Jiang, T.; Gao, H. X.; Liu, Z. M.; He, J.; Han, B. X. *J. Chem. Eng. Data.* **2003**, *48*, 1315.
99. Xu, H.; Zhao, D.; Xu, P.; Liu, F.; Gao, G. *J. Chem. Eng. Data.* **2005**, *50*, 133.
100. Gomez, E.; Gonzalez, B.; Dominguez A.; Tojo, E.; Tojo, J. *J. Chem. Eng. Data.* **2006**, *51*, 696.
101. Zhou, Q.; Wang, L.-S.; Chen, H. -P. *J. Chem. Eng. Data.* **2006**, *51*, 905.
102. Kanakubo, M.; Umecky, T.; Aizawa, T.; Kurata, Y. *Chem. Lett.* **2005**, *34*, 324.
103. Hayamizu, K.; Tsuzuki, S.; Seki, S.; Fujii, K.; Suenaga, M.; Umebayashi, Y. *J. Chem. Phys.* **2010**, *133*, 194505.
104. Jarosik, A.; Krajewski, S. R.; Lewandowski, A.; Radzimski, P. *J. Mol. Liq.* **2006**, *123*, 43.
105. Nishida, T.; Tashiro, Y.; Yamamoto, M. *J. Fluorine Chem.* **2003**, *120*, 135.
106. Widegren, J. A.; Saurer, E. M.; Marsh, K. N.; Magee, J. W. *J. Chem. Thermodyn.* **2005**, *37*, 569.
107. Jungnickel, C.; Mrozik, W.; Markiewicz, M.; Luczak, J. *Curr. Org. Chem.***2011**, *15*, 1928.
108. Baker, S.N.; Baker, G. A.; Bright, F. V. *Green Chem.* **2002**, *4*, 165.

109. Fletcher, K. A.; Pandey, S. *Appl. Spectrosc.* **2002**, *56*, 266.

110. Fletcher, K. A.; Pandey, S. *J. Phys. Chem. B* **200**3, *107*, 13532.

111. Harifi-Mood, A. R.; Habibi-Yangjeh, A.; Gholami, M. R. *J. Phys. Chem. B* **2006**, *110*, 7073.

112. Khodadadi-Moghaddam, M.; Habibi-Yangjeh, A.; Gholami, M. R. *Monatsh. Chem.* **2009**, *140*, 329.

113. Aparicio, S.; Alcalde, R.; Atilhan, M. *J. Phys. Chem. B* **2010**, *114*, 5795.

114. Fletcher, K. A.; Pandey, S. *Appl. Spectrosc.* **2002**, *56*, 1498.

115. Salari, H.; Khodadadi-Moghaddam, M.; Harifi-Mood, A. R.; Gholami, M. R. *J. Phys. Chem. B* **2010**, *114*, 9586.

116. Baker, S. N.; Baker, G. A.; Kane, M. A.; Bright, F. V. *J. Phys.Chem. B* **2001**, *105*, 9663.

117. Koeberga, M.; Wu, C.-C.; Kim, D.; Bonn, M. *Chem. Phys. Lett.* **2007**, *439*, 60.

118. Schroder, C.; Hunger, J.; Stoppa, A.; Buchner, R.; Steinhauser, O. *J. Chem. Phys.* **2008**, *129*, 184501.

119. Hunger, J.; Stoppa, A.; Buchner, R.; Hefter, G. *J. Phys. Chem. B* **2009,** *113*, 9527.

120. Xiao, D.; Rajian, J. R.; Li, S.; Bartsch, R. A.; Quitevis, E. L. *J. Phys. Chem. B* **2006,** *110*, 16174.

121. Xiao, D.; Rajian, J. R.; Hines, L. G. Jr.; Li, S.; Bartsch, R. A.; Quitevis, E. L. *J. Phys. Chem. B* **2008**, *1120*, 13316.

122. Stoppa, A.; Hunger, J.; Hefter, G.; Buchner, R. *J. Phys. Chem. B* **2012,** *116*, 7509–7521.

123. Sarkar, S.; Pramanik, R.; Ghatak, C.; Setua, P.; Sarkar, N. **2010**, *114*, 2779–2789.

124. Chakrabarty, D.; Chakraborty, A.; Seth, D.; Sarkar, N. *J. Phys. Chem. A* **2005**, *109*, 1764.

125. Chakrabarty, D.; Chakraborty, A.; Seth, D.; Hazra, P.; Sarkar, N. *Chem. Phys. Lett.* **2004**, *397*, 469.

126. Liang, M. Solvation and Electron transfer in Ionic Liquids. Ph.D. Thesis, The Pennsylvania State University, August 2012.

127. Zhang, X. –X.; Liang, M.; Hunger, J.; Buchner, R.; Maroncelli, M. *J. Phys. Chem. B*, **2013**, DOI: 10.1021/jp4043528.

128. Gray, C. G.; Gubbins, K. E. *Theory of Molecular Fluids*; Clarendon: Oxford, UK, 1984; Vol. I.

129. Hansen, J. P.; McDonald, I. R. *Theory of Simple Liquids*; Academic Press: London, 1986.

130. Cavell, E. A. S.; Knight, P. C.; Sheikh, M. A. *J. Chem. Soc. Faraday Trans.* **1971**, *67*, 2225.

131. Jin, H.; O'Hare, B.; Arzhantsev, S.; Baker, G.; Wishart, J. F.;Binesi, A. J.; Maroncelli, M. *J. Phys. Chem. B* **2008**, *112*, 81.

132. Bagchi, B.; Biswas, R. *Adv. Chem. Phys.* **1999**, *109*, 207.

133. Labowitz, J. L. *Phys. Rev.* **1964**, *133*, A895.

134. Attard, P. Phys. Rev. E **1993**, *48*, 3604.

135. Chandra, A.; Bagchi, B. J. Chem. Phys. **1999**, 110, 10024.

136. Wang, J.; Tian, Y.; Zhao, Y.; Zhuo, K. *Green Chem.* **2003**, *5*, 618.

137. Taib, M. M.; Murugesan, T. *J. Chem. Engg. Data* **2012**, *57*, 120.

138. Jellema, R.; Bulthuis, J.; van der Zwan, G. *J. Mol. Liq.* **1997**, *73-74*, 179.

139. Kindt, J. T.; Schmuttenmaer, C. A. *J. Phys. Chem.* **1996**, *100*, 10373.

140. Kemp, D. D.; Gordon, M. S. *J. Phys. Chem. A* **2008**, *112*, 4885.

141. Gubskaya, A. V.; Kushalik, P. J. *J. Chem. Phys.* **2002**, *117*, 5290.

142. Mandal, U.; Ghosh S.; Das, D. K.; Adhikari, A.; Dey, S.; Bhattacharyya, K. *J. Chem. Sci.* **2009**, *120*, 15.

143. Hunger, J.; Stoppa, A.; Schrodle, S.; Hefter, G.; Buchner, R. *Chem. Phys. Chem.* **2009**, *10*, 723.

Chapter 8

Dielectric Relaxation of Ionic Liquid: Role of Ion-Dipole and Ion-Ion Interactions and Effects of Heterogeneity

8.1 Introduction

Dielectric relaxation (DR) is a well established experimental method and employed substantially to understand the dynamical characteristics of neat ionic liquids (ILs) and (IL + common solvent) binary mixtures.[1-12]. These studies have shown that the DR of ILs follow either Cole-Cole or Cole-Davidson relaxation process supplimented by faster Debye-type relaxation. These studies have investigated about the probable microscopic origins of the DR relaxation timescales and also tested the hydrodynamic models of rotational dynamics in these systems. DR associates with long wave number polarization fluctuations and thus the system's collective response is measured. There exists a macro-micro relation that connects single particle orientation time (τ_u) to the Debye relaxation time (τ_D) measured in experiments[13,14]

$$\tau_u = \frac{n^2 + 2}{\varepsilon_0 + 2}\tau_D \qquad (8.1)$$

where ε_0 is the static dielectric constant and n is the refractive index of the solvent continuum, and assuming that such a continuum is characterized by a single relaxation time constant. For strongly polar solvents, however, medium polarizability is important and a modified expression has been derived[15]

$$\tau_u = \frac{2\varepsilon_0 + \varepsilon_\infty}{3\varepsilon_0}\tau_D \qquad (8.2)$$

where ε_∞ is the infinite-frequency dielectric constant of the solvent continuum. It is expected that for solvents with large ε_0, $\tau_u \approx \tau_D$. Eq. 8.2 is a limiting relation of a more general relation derived by Powel[16,17]

$$\tau_u = \frac{2\varepsilon_0 + \varepsilon_\infty}{3\varepsilon_0}\left(\frac{\tau_D}{g}\right) \qquad (8.3)$$

Note Eq. 8.3 includes molecularity of the solvent through the incorporation of the Kirkwood's g factor[18] which is a measure of short-range solvent-solvent correlations. This is a departure from continuum approximation towards molecular description of liquids. The author showed that there has not much difference between τ_D and τ_u. g can be analytically expressed as the integration over the anisotropic part of the radial distribution function of the dipolar liquid. Madden and Kivelson[19,20] derived a further modified relation by including the dipole moment and a dynamic coupling parameter (g'):

$$\tau_u = \frac{\beta\mu^2\rho_0}{3\varepsilon_0(\varepsilon_0 - 1)} g'\tau_D \qquad (8.4)$$

Where $\beta = 1/k_BT$; k_B is the Boltzmann constant and T is the temperature, μ is the dipole moment of the liquid molecule, and ρ_0 is the equilibrium density of the dipolar liquid.

Chandra and Bagchi[14,21-28] proposed a microscopic theory for DR of normal polar liquids, which is based on generalized Smoluchowski description for the time dependence of the position and orientation dependent density field. They suggested relations among τ_D, τ_u and many body orientation relaxation time, τ_M. Unlike the previous theories,[13,16,17,19,20] the microscopic theory of Chandra and Bagchi was found valid over a large polarity range. The relation between τ_D and τ_u interpolates between Debye relation (Eq. 8.1), valid at low dielectric constant, and Onsagar – Glarum relation (Eq. 8.8.2). The theory also agrees well with the Madden and Kivelson conclusion regarding the relation between τ_D and τ_M, which stated that if the single particle orientation correlation function (C_u) is single exponential, the many body orientation correlation function (C_M) will be bi-exponential. The authors also derived the microscopic form of frequency dependent dielectric function ($\varepsilon(\omega)$) for dipolar liquid and obtained single Debye form for the associated relaxation.

These relations, though important, can be used for correlating the different relaxation times in simple dipolar liquids only. These relations are sometimes even used for ILs to relate the experimentally measured τ_D with τ_u to investigate the validity of hydrodynamics.[29] These relations may not be valid for ILs as the ion-ion and ion-dipole interactions may affect the relaxation processes significantly. A combined computational and experimental study has

explored the validity of the Madden-Kivelson relation between single particle and collective motion in an IL, $[\mathrm{Bmim}][\mathrm{BF_4}]$.[30] Surprisingly, the authors found that the Madden – Kivelson relation is fairy obeyed in long-term simulation studies (> 100 ns), essentially suggesting that the collective rotational time for an IL can be predicted by the single particle orientation time and the static dipolar correlation factor. This finding is important in the sense that the ion-ion and ion-dipole interaction cannot appreciably affect the relation between τ_M and τ_u. This interesting finding has not yet been investigated from a theoretical perspective, and therefore, a microscopic understanding is still lacking.

Moreover it has been established previously that IL consists of appreciable amount of heterogeneity which can substantially affect the relaxation dynamics.[31-40] Researchers have seen that in ILs τ_D is correlated to medium viscosity (η) by conventional hydrodynamic relations (Stokes Einstein Debye (SED)[3,5,7,

$$\tau_u = \frac{3V_{eff}\eta}{k_B T} \tag{8.5}$$

where V_{eff} is the effective rotational volume of the dipolar species and is commonly determined by the molecular volume (V_m), the shape factor (f) of the rotating particle, and a hydrodynamic friction coefficient (C). k_B is the Boltzmann constant and T is the absolute temperature. The importance of SED relation lies in its use for prediction of heterogeneity in liquid system.[46-48] Simulation studies have found that SED relation in ILs may not be valid.[49] It is interesting to note that fluorescence Stokes shift dynamics results have suggested the validity of SED relation in ILs for the viscosity dependence of average solvation time ($<\tau_s>$), which is more collective in nature than τ_u.[50-53] In DR spectroscopy also, researchers have verified the validity of SED relation in ILs by calculating τ_u from experimentally measured τ_D via relations described already. They calculated V_{eff} for a number of ILs, where the value found is considerably less than V_m. Recently for aluminate IL[11,54,55] it has been seen that V_{eff} is only ~ 4 % of V_m and more interestingly for common imidazolium ILs[5] V_{eff} is even less and generally it is only ~ 1 % of their respective V_m. This finding is very important because it hints at either frictionless rotation in ILs or a very few particles participate in DR relaxation. The reason for such anomaly is still not understood

although explained in terms of shape asymmetry and spatial heterogeneity.[5,11] Moreover, the jump-like orientational motion[32,56] is also proposed to explain such a low value for the effective rotational volume in ILs. The non-diffusive jump-like rotation can render such a small value of V_{eff} .

In the present work we have proposed a semi molecular theory for the DR in ILs where we have considered the ion-dipole interaction and its effect towards the DR time scale. We have also derived the relation among τ_D, τ_u, and τ_M for ILs. The present work considers ion-dipole and ion-ion interactions in addition to dipole-dipole interactions while constructing the generalized Smoluchowski description for the time, position and orientation dependent density field. The Smoluchowski equation contains dipole and ion density fluctuation terms and dipole-dipole and ion-dipole correlations and also includes contributions from both the rotational and translational motions. Ion-ion interaction does not enter into the theory and the reason will be explained in details in the next section. In the long wavelength ($k\sigma \to 0$) limit, the translational contribution to the orientation correlation functions disappears, although it is significant at intermediate length-scales. Temperature dependence of DR time has also been studied to explore the effects of temperature on heterogeneity.

Interestingly, the present theory predicts a triphasic C_M where the three time constants originate from longitudinal and transverse components of dipole-dipole interaction and longitudinal component of ion-dipole interaction. Like Chandra – Bagchi theory, we have obtained the same simple Debye form for $\varepsilon(\omega)$ in ILs. Calculated DR time ($\tau_D^{theo.}$) for model IL has been seen to strongly deviate from experimental time ($\tau_D^{expt.}$) if V_{eff} is considered to be equal to V_m. We have included the effects of heterogeneity indirectly in the equation by introducing V_{eff} which is much less than V_m . This provides a way to understand the effects of rotating volume on DR timescales. The study of temperature dependence shows that V_{eff} approaches to V_m with sufficient increase in temperature of the system. This observation is linked to the temperature-induced homogenization of a system possessing heterogeneity at lower temperature.

8.2 Theory and Calculation Details

We will discuss the theoretical details in two subsections. In the first, we derive the Smoluchowski equation for IL and in the next we use that to derive the expressions for orientation relaxation function and microscopic expressions of various relaxation time constants relevant to IL systems.

8.2.1 Derivation of the Smoluchowski equation

The present derivation is motivated by the Chandra-Bagchi approach for dipolar fluids and we assume here that the same observation regarding the fast relaxation of spatial and angular momentum is also valid in ILs. The continuity equation for the number density ($\rho(\mathrm{r},\Omega,t)$)[23,58]

$$\frac{\partial\rho(\boldsymbol{r},\boldsymbol{\Omega},t)}{\partial t} = -\nabla\cdot\boldsymbol{J} - \nabla_{\boldsymbol{\Omega}}\cdot\boldsymbol{J}_{\boldsymbol{\Omega}} \ , \tag{8.6}$$

where $\boldsymbol{r}$, and $\boldsymbol{\Omega}$ denote the spatial position and orientation vector, $\boldsymbol{J}$, and $\boldsymbol{J}_{\boldsymbol{\Omega}}$ are the spatial and angular fluxes respectively. ∇ , and $\nabla_{\boldsymbol{\Omega}}$ are the usual spatial and orientation gradient respectively. In the overdamped limit, these fluxes are calculated from generalized free energy functional which is obtained from density functional theory[55,59-62] and is written by,

$$\begin{aligned}\beta F[\rho(\boldsymbol{r},\boldsymbol{\Omega}),n_\alpha(\boldsymbol{r})] = &\int d\boldsymbol{r}d\boldsymbol{\Omega}\,\delta\rho(\boldsymbol{r},\boldsymbol{\Omega})[\boldsymbol{ln}\,\rho(\boldsymbol{r},\boldsymbol{\Omega})-1]\\ &-\frac{1}{2}\int d\boldsymbol{r}d\boldsymbol{\Omega}d\boldsymbol{r}'d\boldsymbol{\Omega}'\delta\rho(\boldsymbol{r},\boldsymbol{\Omega})\delta\rho(\boldsymbol{r}',\boldsymbol{\Omega}')c(\boldsymbol{r},\boldsymbol{\Omega};\boldsymbol{r}',\boldsymbol{\Omega}')\\ &+\sum_{\alpha=1}^{2}\int d\boldsymbol{r}n_\alpha(\boldsymbol{r})[\boldsymbol{ln}\,n_\alpha(\boldsymbol{r})-1]\\ &-\frac{1}{2}\sum_{\alpha,\beta=1}^{2}d\boldsymbol{r}d\boldsymbol{r}'c_{\alpha\beta}(\boldsymbol{r},\boldsymbol{r}')\delta n_\alpha(\boldsymbol{r})\delta n_\beta(\boldsymbol{r}')\\ &-\sum_{\alpha=1}^{2}\int d\boldsymbol{r}d\boldsymbol{r}'d\boldsymbol{\Omega}\,c_{d\alpha}(\boldsymbol{r},\boldsymbol{\Omega};\boldsymbol{r}')\delta\rho(\boldsymbol{r},\boldsymbol{\Omega})\delta n_\alpha(\boldsymbol{r}')\end{aligned} \ , \tag{8.7}$$

where $n_\alpha(\boldsymbol{r})$ is the ion number density, $c(\boldsymbol{r},\boldsymbol{\Omega};\boldsymbol{r}',\boldsymbol{\Omega}')$, $c_{\alpha\beta}(\boldsymbol{r},\boldsymbol{r}')$, and $c_{d\alpha}(\boldsymbol{r},\boldsymbol{\Omega};\boldsymbol{r}')$ are the two particle dipole-dipole, ion-ion and dipole-ion static correlation respectively, and the term, δ is used to represent the fluctuation over bulk value. $\beta=(k_BT)^{-1}$.

In the overdamped limit, the fluxes can be written as,[63-65]

$$\begin{aligned}\boldsymbol{J} &= -D_T\rho(\boldsymbol{r},\boldsymbol{\Omega},t)\nabla\cdot\frac{\delta F\left[\{\rho(\boldsymbol{r},\boldsymbol{\Omega},t)\}\right]}{\delta\ \ \rho(\boldsymbol{r},\boldsymbol{\Omega},t)}\\ \boldsymbol{J}_{\boldsymbol{\Omega}} &= -D_R\rho(\boldsymbol{r},\boldsymbol{\Omega},t)\nabla\cdot\frac{\delta F\left[\{\rho(\boldsymbol{r},\boldsymbol{\Omega},t)\}\right]}{\delta\ \ \rho(\boldsymbol{r},\boldsymbol{\Omega},t)}\end{aligned}, \tag{8.8}$$

where D_T and D_R are the translational and rotation diffusion coefficients of the dipolar and ionic constituents of a given IL.

From Eq. 8.6, 8.7, and 8.8 we can write,

$$\begin{aligned}\frac{\partial}{\partial t}\left[\delta\rho(\boldsymbol{r},\boldsymbol{\Omega},t)\right] &= D_T\nabla^2\delta\rho(\boldsymbol{r},\boldsymbol{\Omega},t)\\ &- D_T\left(\frac{\rho_0}{4\pi}\right)\nabla^2\int d\boldsymbol{r}'d\boldsymbol{\Omega}'c(\boldsymbol{r},\boldsymbol{\Omega};\boldsymbol{r}',\boldsymbol{\Omega}')\delta\rho(\boldsymbol{r}',\boldsymbol{\Omega}',t)\\ &- D_T\left(\frac{\rho_0}{4\pi}\right)\nabla^2\sum_{\alpha=1}^{2}\int d\boldsymbol{r}'c_{d\alpha}(\boldsymbol{r},\boldsymbol{\Omega};\boldsymbol{r}')\delta n_\alpha(\boldsymbol{r}',t)\\ &+ D_R\nabla_\Omega^2\delta\rho(\boldsymbol{r},\boldsymbol{\Omega},t)\\ &- D_R\left(\frac{\rho_0}{4\pi}\right)\nabla_\Omega^2\int d\boldsymbol{r}'d\boldsymbol{\Omega}'c(\boldsymbol{r},\boldsymbol{\Omega};\boldsymbol{r}',\boldsymbol{\Omega}')\delta\rho(\boldsymbol{r}',\boldsymbol{\Omega}',t)\\ &+ D_R\left(\frac{\rho_0}{4\pi}\right)\nabla_\Omega^2\sum_{\alpha=1}^{2}\int d\boldsymbol{r}'c_{d\alpha}(\boldsymbol{r},\boldsymbol{\Omega};\boldsymbol{r}')\delta n_\alpha(\boldsymbol{r}',t)\end{aligned} \tag{8.9}$$

Since the term containing pure ion-ion interaction is independent of orientation, it vanishes during the construction of functional derivative.

The above equation is Smoluchowski equation for IL system. Here the third and sixth terms are originated from ion-dipole interaction and the remaining ones from dipole-dipole interaction. This is the first derivation of Smoluchowski equation for IL system.

8.2.2 Derivation of Orientation Relaxation Function

Now by Fourier transforming the Smoluchowski equation (Eq. 8.9) we obtain the relation as following,

$$\begin{aligned}\frac{\partial}{\partial t}\left[\delta\rho(\boldsymbol{k},\boldsymbol{\Omega},t)\right] &= -D_T k^2 \delta\rho(\boldsymbol{k},\boldsymbol{\Omega},t) \\ &+ D_T\left(\frac{\rho_0}{4\pi}\right)k^2\int d\boldsymbol{\Omega}' c(\boldsymbol{k},\boldsymbol{\Omega},\boldsymbol{\Omega}')\delta\rho(\boldsymbol{k},\boldsymbol{\Omega}',t) \\ &+ D_T\left(\frac{\rho_0}{4\pi}\right)k^2\sum_{\alpha=1}^{2}\left[c_{d\alpha}(\boldsymbol{k},\boldsymbol{\Omega})\delta n_\alpha(\boldsymbol{k},t)\right] \\ &+ D_R\nabla_\Omega^2\delta\rho(\boldsymbol{k},\boldsymbol{\Omega},t) \\ &- D_R\left(\frac{\rho_0}{4\pi}\right)\nabla_\Omega^2\int d\boldsymbol{\Omega}' c(\boldsymbol{k},\boldsymbol{\Omega},\boldsymbol{\Omega}')\delta\rho(\boldsymbol{k},\boldsymbol{\Omega}',t) \\ &+ D_R\left(\frac{\rho_0}{4\pi}\right)\nabla_\Omega^2\sum_{\alpha=1}^{2}\left[c_{d\alpha}(\boldsymbol{k},\boldsymbol{\Omega}')\delta n_\alpha(\boldsymbol{k},t)\right]\end{aligned} \tag{8.10}$$

Now we expand the dipole and ion density fluctuations and direct correlation functions in terms of spherical harmonics. These are written as follows,

$$\begin{aligned}c_{d\alpha}(k,\Omega) &= \sum_{l,m} c_\alpha(\boldsymbol{lm};\boldsymbol{k})Y_{lm}(\Omega) \\ c(k,\Omega,\Omega') &= \sum_{l_1 l_2 m} c(l_1 l_2 m;\boldsymbol{k})Y_{l_1 m}(\boldsymbol{\Omega})Y_{l_2 m}(\boldsymbol{\Omega}') \\ \delta\rho(k,\Omega',t) &= \sum_{lm} a_{lm}(\boldsymbol{k},t)Y_{lm}(\boldsymbol{\Omega}')\end{aligned} \tag{8.11}$$

By combining Eq. 8.10 and 8.11 we obtain the following relation

$$\begin{aligned}\frac{\partial}{\partial t}\left[\sum_{lm} a_{lm}(\boldsymbol{k},t)Y_{lm}(\boldsymbol{\Omega})\right] &= -D_T k^2\sum_{lm} a_{lm}(\boldsymbol{k},t)Y_{lm}(\boldsymbol{\Omega}) \\ &+ D_T\left(\frac{\rho_0}{4\pi}\right)k^2\int d\boldsymbol{\Omega}'\sum_{l_1 l_2 m} c(l_1 l_2 m;\boldsymbol{k})Y_{l_1 m}(\boldsymbol{\Omega})Y_{l_2 m}(\boldsymbol{\Omega}')\sum_{lm} a_{lm}(\boldsymbol{k},t)Y_{lm}(\boldsymbol{\Omega}') \\ &+ D_T\left(\frac{\rho_0}{4\pi}\right)k^2\sum_{\alpha=1}^{2}\left[\sum_{lm} c_\alpha(lm;\boldsymbol{k})Y_{lm}(\boldsymbol{\Omega})\delta n_\alpha(\boldsymbol{k},t)\right] \\ &+ D_R\nabla_\Omega^2\sum_{lm} a_{lm}(\boldsymbol{k},t)Y_{lm}(\boldsymbol{\Omega}) \\ &- D_R\left(\frac{\rho}{4\pi}\right)\nabla_\Omega^2\int d\boldsymbol{\Omega}'\sum_{l_1 l_2 m} c(l_1 l_2 m;\boldsymbol{k})Y_{l_1 m}(\Omega)Y_{l_2 m}(\Omega')\sum_{lm} a_{lm}(\boldsymbol{k},t)Y_{lm}(\Omega') \\ &- D_R\left(\frac{\rho}{4\pi}\right)\nabla_\Omega^2\sum_{\alpha=1}^{2}\left[\sum_{lm} c_\alpha(lm;\boldsymbol{k})Y_{lm}(\boldsymbol{\Omega})\delta n_\alpha(\boldsymbol{k},t)\right]\end{aligned}$$

(8.12)

Multiplying both side of the above equation by the complex conjugate of the spherical harmonics we get,

$$\begin{aligned}\frac{\partial}{\partial t}\left[\sum_{lm} a_{lm}(k,t)Y_{lm}(\Omega)Y_{lm}^{*}(\Omega)\right] &= -D_T k^2 \sum_{lm} a_{lm}(\boldsymbol{k},t)Y_{lm}(\boldsymbol{\Omega})Y_{lm}^{*}(\boldsymbol{\Omega}) \\ &+ D_T\left(\frac{\rho_0}{4\pi}\right)k^2 \int d\boldsymbol{\Omega}' \sum_{l_1 l_2 m} c(l_1 l_2 m;\boldsymbol{k})Y_{l_1 m}(\boldsymbol{\Omega})Y_{l_2 m}(\boldsymbol{\Omega}')\sum_{lm} a_{lm}(\boldsymbol{k},t)Y_{lm}(\Omega')Y_{lm}^{*}(\boldsymbol{\Omega}) \\ &+ D_T\left(\frac{\rho_0}{4\pi}\right)k^2 \sum_{\alpha=1}^{2}\left[\sum_{lm} c_\alpha(lm;\boldsymbol{k})Y_{lm}(\boldsymbol{\Omega})\delta n_\alpha(\boldsymbol{k},t)Y_{lm}^{*}(\boldsymbol{\Omega})\right] \\ &+ D_R \nabla_\Omega^2 \sum_{lm} a_{lm}(\boldsymbol{k},t)Y_{lm}(\boldsymbol{\Omega})Y_{lm}^{*}(\boldsymbol{\Omega}) \\ &- D_R\left(\frac{\rho_0}{4\pi}\right)\nabla_\Omega^2 \int d\boldsymbol{\Omega}' \sum_{l_1 l_2 m} c(l_1 l_2 m;\boldsymbol{k})Y_{l_1 m}(\boldsymbol{\Omega})Y_{l_2 m}(\boldsymbol{\Omega}')\sum_{lm} a_{lm}(\boldsymbol{k},t)Y_{lm}(\boldsymbol{\Omega}')Y_{lm}^{*}(\boldsymbol{\Omega}) \\ &- D_R\left(\frac{\rho_0}{4\pi}\right)\nabla_\Omega^2 \sum_{\alpha=1}^{2}\left[\sum_{lm} c_\alpha(lm;\boldsymbol{k})Y_{lm}(\boldsymbol{\Omega})\delta n_\alpha(\boldsymbol{k},t)Y_{lm}^{*}(\boldsymbol{\Omega})\right]\end{aligned} \tag{8.13}$$

Integrating both sides of the Eq. 8.13 over orientation space and using the normalization rule of spherical harmonics, we obtain the following equation for the time derivative of $a_{lm}(\boldsymbol{k},t)$.

$$\begin{aligned}\frac{\partial}{\partial t}\left[a_{lm}(\boldsymbol{k},t)\right] &= -D_T k^2 a_{lm}(\boldsymbol{k},t) + D_T k^2\left(\frac{\rho_0}{4\pi}\right)(-1)^m \sum_{l_2} c(ll_2 m;\boldsymbol{k})a_{l_2 m}(\boldsymbol{k},t) \\ &+ D_T k^2\left(\frac{\rho_0}{4\pi}\right)\sum_{\alpha=1}^{2} c_\alpha(lm;\boldsymbol{k})\delta n_\alpha(\boldsymbol{k},t) - D_R l(l+1)a_{lm}(\boldsymbol{k},t) \\ &+ D_R l(l+1)(-1)^m\left(\frac{\rho_0}{4\pi}\right)\sum_{l_2} c(ll_2 m;\boldsymbol{k})a_{l_2 m}(\boldsymbol{k},t) + D_R l(l+1)\left(\frac{\rho_0}{4\pi}\right)\sum_{\alpha=1}^{2} c_\alpha(lm;\boldsymbol{k})\delta n_\alpha(\boldsymbol{k},t)\end{aligned} \tag{8.14}$$

If $l=1$, Eq. 8.14 will be the equation of motion for DR**.** Here we use Mean Spherical Approximation (MSA) for $c(k,\Omega,\Omega')$ which predicts that the only non-vanishing $c(l_1,l_2,m;\boldsymbol{k})$'s are $c(000;\boldsymbol{k})$, $c(110;\boldsymbol{k})$, and $c(111;\boldsymbol{k})$.[66,67] Eq. 8.14 then reduces to a simpler equation of the following,

$$\frac{\partial}{\partial t}\left[a_{lm}(\boldsymbol{k},t)\right] = -\left[D_R l(l+1) + D_T k^2\right] a_{lm}(\boldsymbol{k},t) + \left[D_R l(l+1) + D_T k^2\right](-1)^m \left(\frac{\rho_0}{4\pi}\right) c(llm;\boldsymbol{k}) a_{lm}(\boldsymbol{k},t)\left[\delta_{l,1} + \delta_{l,0}\right] + \left[D_R l(l+1) + D_T k^2\right]\left(\frac{\rho_0}{4\pi}\right)\sum_{\alpha=1}^{2} c_\alpha(lm;\boldsymbol{k})\delta n_\alpha(\boldsymbol{k},t) \tag{8.15}$$

Slight rearrangement of Eq. 8.15 results the following equation,

$$\frac{\partial}{\partial t}\left[a_{lm}(\boldsymbol{k},t)\right] = -\left[D_R l(l+1) + D_T k^2\right] a_{lm}(\boldsymbol{k},t)\left[1 - (-1)^m \left(\frac{\rho_0}{4\pi}\right) c(llm;\boldsymbol{k})\left[\delta_{l,1} + \delta_{l,0}\right]\right] + \left[D_R l(l+1) + D_T k^2\right]\left(\frac{\rho_0}{4\pi}\right)\sum_{\alpha=1}^{2} c_\alpha(lm;\boldsymbol{k})\delta n_\alpha(\boldsymbol{k},t) \tag{8.16}$$

So, the Eq. 8.16 is a first order differential equation with respect to time. This equation can easily be solved to get the wave number dependent, rank, time dependent solution of $a_{lm}(\boldsymbol{k},t)$. Here one important point should be mentioned. The last term of the Eq. 8.16, originated from ion-dipole interaction, contains ion density fluctuation term ($\delta n_\alpha(\boldsymbol{k},t)$), which is also wave number and time dependent. For solving the equation for $a_{lm}(\boldsymbol{k},t)$ we will assume that $\delta n_\alpha(\boldsymbol{k},t)$ is very slow and does not change with time although the time dependent behaviour of $\delta n_\alpha(\boldsymbol{k},t)$ remains same and this nature retains when the correlations are designed. This approximation is not very bad in the sense that $\delta n_\alpha(\boldsymbol{k},t)$ is really very slow in comparison to dipole density fluctuation. Note that the same approximation was used in the theoretical studies of the Stokes shift dynamics of ILs and binary mixture of IL and dipolar solvents, where the theory was successful enough to predict the experimental data. Taking these approximations we can calculate the correlations.

Now let us define a generalized correlation function,

$$\psi(k,t) = \left\langle a_{lm}(\boldsymbol{k},0) a_{lm}(-\boldsymbol{k},t)\right\rangle \tag{8.17}$$

At large wavelength limit ($k \to 0$), $\psi(\boldsymbol{k},t)$ corresponds to C_M , meaning

$$C_M = \underset{k\to 0}{Lt}\left[\psi(\boldsymbol{k},t)\right], \tag{8.18}$$

and at small wavelength limit ($k \to \infty$), $\psi(\boldsymbol{k},t)$ corresponds to C_u , meaning

$$C_u = \underset{k\to \infty}{Lt}\left[\psi(\boldsymbol{k},t)\right], \tag{8.19}$$

Now by solving the Eq. 8.16, we obtain the functional form for $a_{lm}(\boldsymbol{k},t)$, which is written as following,

$$a_{lm}(\boldsymbol{k},t) = \frac{\left[\{Aa_{lm}(\boldsymbol{k},0)+C\}\right]exp(At)-B_t}{A}, \tag{8.20}$$

where $$A = -\left[D_R l(l+1)+D_T k^2\right]\left[1-\left\{(-1)^m\left(\frac{\rho_0}{4\pi}\right)c(llm;\boldsymbol{k})\left[\delta_{l,1}+\delta_{l,0}\right]\right\}\right] \tag{8.21}$$

$$C = \left[D_R l(l+1)+D_T k^2\right]\left[\frac{\rho_0}{4\pi}\right]\left[\sum_{\alpha=1}^{2} c_\alpha(lm;\boldsymbol{k})\delta n_\alpha(\boldsymbol{k},0)\right], \tag{8.22}$$

and $$B_t = \left[D_R l(l+1)+D_T k^2\right]\left[\frac{\rho_0}{4\pi}\right]\left[\sum_{\alpha=1}^{2} c_\alpha(lm;\boldsymbol{k})\delta n_\alpha(\boldsymbol{k},t)\right] \tag{8.23}$$

It is clear that in Eq. 8.23 B_t is still time dependent function.

Now for constructing $\psi(\boldsymbol{k},t)$ (Eq. 8.17), we will define isotropic ion dynamic structure factor ($S_{\alpha\beta}^{ion}(\boldsymbol{k},t)$) by following,

$$S_{\alpha\beta}^{ion}(k,t) = \left\langle \delta n_\alpha(\boldsymbol{k};0)\delta n_\beta(-\boldsymbol{k};t)\right\rangle \tag{8.24}$$

$S_{\alpha\beta}^{ion}(\boldsymbol{k},t)$ is assumed to be given by[67],

$$S_{\alpha\beta}^{ion}(\boldsymbol{k},t) = S_{\alpha\beta}^{ion}(\boldsymbol{k})exp\left[-D_T k^2 t/S_{\alpha\alpha}(\boldsymbol{k})\right] = S_{\alpha\beta}^{ion}(\boldsymbol{k},t)exp\left[-D_T k^2 t/\tau_\alpha(\boldsymbol{k})\right] \quad (8.25)$$

Now from Eq. 8.17, 8.20-8.25 we obtain the equation for $\psi(\boldsymbol{k},t)$ as following,

$$\psi(\boldsymbol{k},t) = X\,exp(-t/\tau_1) + Y\,exp(-t/\tau_2) + Z\,exp(-t/\tau_3) \quad (8.26)$$

Hence the generalized correlation function is tri-exponential. Note that for dipolar liquid the correlation function is bi-exponential. Here the first two terms of the right hand side are originated from dipole-dipole interaction and the last term comes from ion-dipole interaction. Hence the ion-dipole interaction can generate a new time scale. In Eq. 8.25, X , Y ,and Z are the coefficients, which are represented by,

$$X = \frac{\left[2D_R + D_T k^2\right]^2\left[1-\left(\frac{\rho_0}{4\pi}\right)c(110;\boldsymbol{k})\right]\left[1-\left(\frac{\rho_0}{4\pi}\right)c(110;-\boldsymbol{k})\right]\langle a_{10}(\boldsymbol{k},0)a_{10}(-\boldsymbol{k},0)\rangle + \left[2D_R + D_T k^2\right]^2\left(\frac{\rho_0}{4\pi}\right)\sum_{\alpha=1}^{2}\left[c_\alpha(10;\boldsymbol{k})c_\alpha(10;-\boldsymbol{k})\langle\delta n_\alpha(\boldsymbol{k},0)\delta n_\alpha(-\boldsymbol{k},0)\rangle\right]}{\left[2D_R + D_T k^2\right]^2\left[1-\left(\frac{\rho_0}{4\pi}\right)c(110;\boldsymbol{k})\right]\left[1-\left(\frac{\rho_0}{4\pi}\right)c(110;-\boldsymbol{k})\right]}, \quad (8.27)$$

$$Y = \frac{\left[2D_R + D_T k^2\right]^2\left[1+\left(\frac{\rho_0}{4\pi}\right)c(111;\boldsymbol{k})\right]\left[1+\left(\frac{\rho_0}{4\pi}\right)c(111;-\boldsymbol{k})\right]\langle a_{11}(k,0)a_{11}(-k,0)\rangle + \left[2D_R + D_T k^2\right]^2\left(\frac{\rho_0}{4\pi}\right)\sum_{\alpha=1}^{2}\left[c_\alpha(11;\boldsymbol{k})c_\alpha(11;-\boldsymbol{k})\langle\delta n_\alpha(\boldsymbol{k},0)\delta n_\alpha(-\boldsymbol{k},0)\rangle\right]}{\left[2D_R + D_T k^2\right]^2\left[1+\left(\frac{\rho_0}{4\pi}\right)c(111;\boldsymbol{k})\right]\left[1+\left(\frac{\rho_0}{4\pi}\right)c(111;-\boldsymbol{k})\right]}, \quad (8.28)$$

and

$$Z = \frac{\left[2D_R + D_T k^2\right]^2\left(\frac{\rho_0}{4\pi}\right)^2\sum_{\alpha=1}^{2}\left[c_\alpha(10;\boldsymbol{k})c_\alpha(10;-k)S_\alpha^{ion}(\boldsymbol{k})\right]}{\left[2D_R + D_T k^2\right]^2\left[1+\left(\frac{\rho_0}{4\pi}\right)c(111;\boldsymbol{k})\right]\left[1+\left(\frac{\rho_0}{4\pi}\right)c(111;-\boldsymbol{k})\right]}, \quad (8.29)$$

It is very interesting to note that the coefficients are having contributions from both the

dipole-dipole and ion-dipole interactions.

The time scales are represented by,

$$\tau_1 = \left\{\left[2D_R + D_T k^2\right]\left[1 - \left(\frac{\rho_0}{4\pi}\right)c(110;\boldsymbol{k})\right]\right\}^{-1} = (2D_R)^{-1}\left\{\left[1 + p(k\sigma)^2\right]\left[1 - \left(\frac{\rho_0}{4\pi}\right)c(110;\boldsymbol{k})\right]\right\}^{-1}$$

$$\tau_2 = \left\{\left[2D_R + D_T k^2\right]\left[1 + \left(\frac{\rho_0}{4\pi}\right)c(111;\boldsymbol{k})\right]\right\}^{-1} = (2D_R)^{-1}\left\{\left[1 + p(k\sigma)^2\right]\left[1 + \left(\frac{\rho_0}{4\pi}\right)c(111;\boldsymbol{k})\right]\right\}^{-1},$$

$$\tau_3 = \left\{\sum_{\alpha=1}^{2}\left[S_\alpha(k)/D_T k^2\right]\right\}^{-1} = (2D_R)^{-1}\left\{\sum_{\alpha=1}^{2}\left[S_\alpha(k)/p(k\sigma)^2\right]\right\}$$

(8.30)

where σ is the diameter of the IL molecule. $p = D_T/(2D_R\sigma^2)$. Where τ_1 and τ_2 are the longitudinal and transverse time scales respectively, τ_3 is the longitudinal time scale. The time constants, τ_1 and τ_2, have contributions only from dipole-dipole interaction, and the time constant, τ_3 has contribution from ion-dipole interaction.

The relation between τ_D and τ_M has already been established by Chandra-Bagchi for dipolar liquids.[25] Here the relations will not change and that is why we will write only the necessary equations describing the relationships between τ_D and τ_M. It is known that for dipolar liquids, τ_D is equal to the transverse polarization relaxation time and also equal to static dielectric constant multiplied by the longitudinal polarization relaxation time. In ILs, where C_M is tri-exponential and consists of dipole-dipole and ion-dipole interactions, the relation between τ_D and τ_M can be separated into two parts, where one part is related to dipole-dipole interaction and the other part is originated from ion-dipole interaction. Here the relations between τ_D and τ_M are written as following,

$$\tau_D = \tau_{M_2} = \varepsilon_0 \tau_{M_1}$$
$$\tau_D^{di} = \varepsilon_0 \tau_{M_3}$$

where
$$\tau_{M_1} = \underset{k\to 0}{Lt}\ \tau_1(k) \quad , \tag{8.31}$$
$$\tau_{M_2} = \underset{k\to 0}{Lt}\ \tau_2(k)$$
$$\tau_{M_3} = \underset{k\to 0}{Lt}\ \tau_3(k)$$

Hence
$$\tau_D = \underset{k\to 0}{Lt}\left\{(2D_R)^{-1}\left\{\left[1+p(k\sigma)^2\right]\left[1+\left(\frac{\rho_0}{4\pi}\right)c(111;\mathrm{k})\right]\right\}^{-1}\right\}, \tag{8.32}$$

and
$$\tau_D^{di} = \underset{k\to 0}{Lt}\left\{\varepsilon_0(2D_R)^{-1}\left\{\sum_{\alpha=1}^{2}\left[S_\alpha(k)/\,p(k\sigma)^2\right]\right\}\right\} \tag{8.33}$$

Here we have written the two different DR time constants originated from dipole-dipole and ion-dipole interaction.

Now from the definition of τ_u we know,

$$\tau_u = \frac{1}{L(L+1)D_R} \tag{8.34}$$

As for DR,
$$L = 1,\ \tau_u = \frac{1}{2D_R} \tag{8.35}$$

Eq. 8.29-8.33 establishes the relations among τ_D, τ_u, and τ_M.

8.3 Numerical Results and Discussion

Here we have used six ILs as model systems for our theoretical investigation of DR and these are $[\mathrm{Bmim}][\mathrm{BF_4}]$, $[\mathrm{Bmim}][\mathrm{PF_6}]$, $[\mathrm{Emim}][\mathrm{DCA}]$, $[\mathrm{Hmim}][\mathrm{NTf_2}]$, $[\mathrm{Emim}][\mathrm{BF_4}]$, and $[\mathrm{Na}][\mathrm{TOTO}]$. We have chosen particularly these six ILs because of availability of experimental DR data at wide range of temperatures, which is required for verification of our theoretical results. Various physical properties of these ILs, required as input in this calculation, are provided in Table A27 (Appendix A)[68]. We have benchmarked our results using five dipolar liquids, $\mathrm{H_2O}$, $\mathrm{CH_3OH}$, $\mathrm{CH_3CN}$, $\mathrm{CH_3CH_2OH}$, and $\mathrm{CH_3CH_2CH_2OH}$.

We have calculated $\psi(k,t)$ at T = 298 K and plotted the $\psi(k,t)$ against t at $k \sim 0$, $k \sim 2\pi$, and $k \sim 4\pi$ for $[\text{Bmim}][\text{BF}_4]$ as a representative IL in Fig. 1. Note that $\psi(k,t)$ is tri-exponential. In Fig. 1, it is also evident that $\psi(\boldsymbol{k},t)$ becomes faster on increasing the value of k, what essentially tells that the generalized correlation function decays more rapidly in the case of nearest neighbour compared to the bulk. This observation is well understood and seen in simple dipolar liquids also.[21]

The effect of translational diffusion coefficient on the wavelength dependent relaxation time constants τ_1, τ_2, and τ_3 have been shown in Fig. 2 (upper and lower panel) for $[\text{Bmim}][\text{BF}_4]$ as a representative IL, where $\tau_i D_R$ has been plotted against wave number for four representative $p\,(=D_T/D_R)$ values of 0.0, 0.2, 0.4, and 1.0. Note that whereas τ_1 and τ_2 are the relaxation time constants originated from the dipole-dipole interaction, τ_3 is rooted from the ion-dipole interaction. At $k \sim 0$, translational contribution is totally absent on the three time constants although an appreciable contribution comes from translational motion at intermediate k. Now, from Eq. 8.18 it is clear that both τ_{M_1} and τ_{M_2} are independent of p, what tells that collective rotational relaxation process does not couple to translational motion of the molecule at all. From Eq. 8.32, it is noted that also τ_D is independent of p, meaning DR, due to dipole-dipole interaction, does not include translation contribution of the molecules. Fig. 2 also establishes a relation between the relaxation time constants (τ_i), k, and p. It is very interesting to note that when we neglect the translational effect, intermediate values of k slows down the dipole dipole part of the relaxation process. This slowing down of relaxation at intermediate k is similar to well known de Gennes' narrowing[69] of the dynamic structure factor of a dense liquid at intermediate wave vectors. In the latter case, the slowing down occurs at the intermediate wave vectors because of the

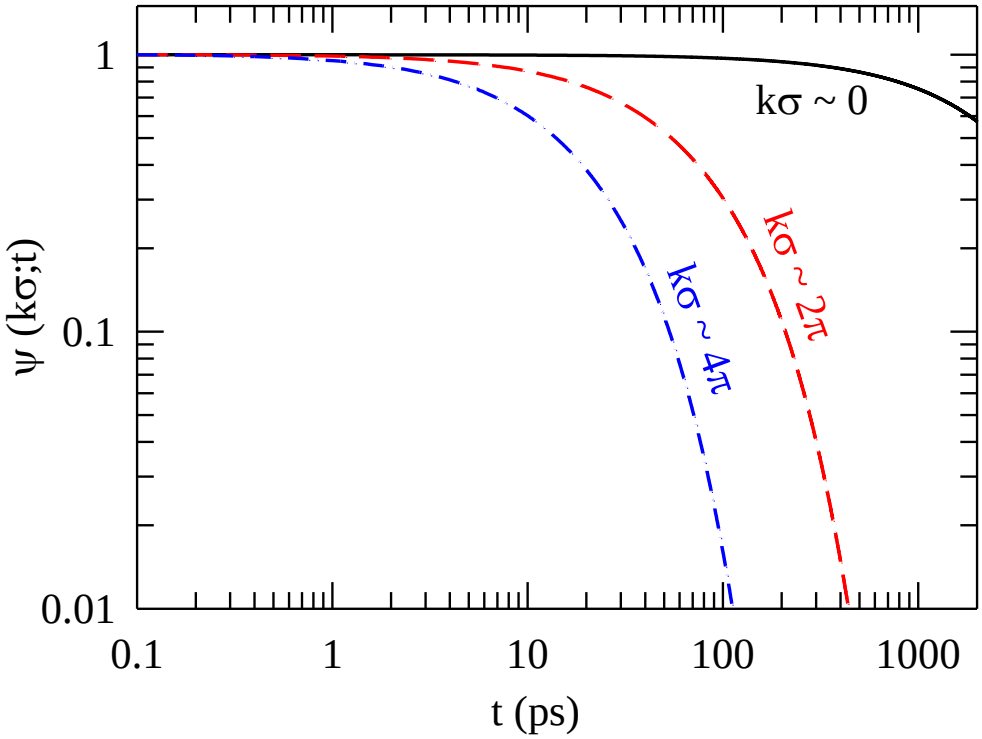

Fig. 8.1: Plot for generalized orientation correlation as a function of time at three magnitudes of wavevectors for $[\mathrm{Bmim}][\mathrm{BF_4}]$ as a representative IL at T = 298 K.

peaks of the static structure factor in dense dipolar liquids. Since this slowing down occurs at intermediate wave vectors where structure is determined largely by the strong repulsive part of the intermolecular potential, such a slowing down in density fluctuations will also occur in the present case of IL. This was previously observed by Chandra-Bagchi in their theoretical calculation of DR in dipolar liquids.[21] This slowing down of the relaxation is more prominent in case of τ_1, longitudinal component of generalized relaxation time. This slowing down of the relaxation effectively becomes weaker when p increases from zero value meaning inclusion of translational contribution. This finding is also similar to that in dipolar liquid.[21] Closer inspection of fig. 2 further reveals that at comparatively large value of k, τ_1 and τ_2 become closer, which means identity of longitudinal and transverse component of the generalized relaxation time at small wavelength.

Now the third relaxation time (τ_3), originated from ion-dipole interaction, behaves quite differently from the other two relaxation times (τ_1 and τ_2), originated from dipole-dipole

interaction. τ_3 starts from very high value. For $[Bmim][BF_4]$ IL, $\tau_{M_3} = \underset{k\to 0}{Lt}[\tau_3(k)] \approx 25000\,\tau_u$. This extremely high value of relaxation time slows down C_M, the collective reorientation correlation function. This slow dynamics should be reflected in ion-dipole contributed DR time (τ_D^{di}). Experimental DR data for the ILs are presented in Table A28 (Appendix A)[68], where no such trace of extremely high value of relaxation time is found. Note that several simulation studies have been done in solution of ion in simple dipolar solvent in order to see the effect of ion concentration on the DR dynamics.[70-73] It is very interesting to note that it has been seen that added electrolyte in a dipolar solvent does not affect the DR dynamics much, for example the relaxation process in electrolyte solution is still single Debye and the relaxation time constants are not very much different from that of simple dipolar solvent.[71] These observation indicates that either the ion density fluctuations are irrelevant in DR dynamics in ILs or the contribution is too small to be detected by the experimental setup. Recently in super cooled molten mixtures, it has been found that collective ion density fluctuation generates an extremely large time scale which has not been measured in the time resolved fluorescence Stokes shift measurement.[74,75] But the ion density fluctuation at nearest neighbour ($k \sim 2\pi$) generates the time scale fascinatingly agrees with the experimental one. This again supports to the fact that ion density fluctuation in IL may be irrelevant or having too small contribution to detect in the DR spectroscopic technique. Note that ion density fluctuation, originated from ion-dipole interaction, can still affect the DR time by altering the medium density, viscosity, polarity etc. Fig. 2 also shows that τ_3 quickly falls to almost zero value as k slightly increases (Eq. 8.30). This relaxation, like the other ones, becomes faster as p increases.

Three collective orientation relaxation time constants (τ_{M_1}, τ_{M_2}, and τ_{M_3}), obtained from the present theory, for six ILs are provided in Table 1. Here it has been seen that the three time constants are widely separated with each other for all the ILs. The fastest time constant is in the order of 0.5-2 ns, whereas the slowest time constant is in the order of 5-30 μs and the intermediate one is in the order of 1-6 ns. All the three time constants obtained for $[\mathrm{Na}][\mathrm{TOTO}]$ are much higher compared to other ones because of extremely high viscosity of the IL. τ_{M_3} in all cases are extremely high and that can be explained by very slow ion density fluctuation, described in the previous paragraph. A closer inspection of Table 1 further reveals

that τ_{M_1}, τ_{M_2}, and τ_{M_3} are coupled to medium viscosity, which is quite expected generally in liquid state of any kind of system. Next we have calculated DR times for the above six ILs by using the relation in Eq. 8.32 and 33. As τ_D is very much high compared to the experimentally found time scales, we assume that the contribution of that part of the relaxation is very small and as a result we do not consider this in the DR dynamics. That means dipole density fluctuation is everything to describe the DR. We have reported our calculated relaxation time scales for the ILs in Table 2. Experimentally measured slowest time constants ($\tau_D^{expt.}$) are also given in the same table in order to compare with our theoretical values. Interestingly the theoretically calculated numbers, τ_D are seen to deviate a lot from $\tau_D^{expt.}$. This huge difference is very much surprising and may be interesting to explain several unique microscopic properties of ILs. We have also studied the same theoretical DR behaviour of five common dipolar liquids in room temperature in order to see whether the timescales matches with experimental data. The dipolar liquids, we have studied, are water (H_2O), methanol (CH_3OH), acetonitrile (CH_3CN), ethanol (CH_3CH_2OH), and 1-propanol ($CH_3CH_2CH_2OH$. The theoretical DR time constants (τ_D) along with the experimentally measured data are provided in Table 2. τ_D for these dipolar liquids show overwhelming agreement with experimentally measured slowest time constant[5], $\tau_D^{expt.}$ .For the five dipolar liquids, $\tau_D^{expt.}$ have been taken from different sources.[76,77] This supports our theory as well as establishes a unique difference between ILs and dipolar liquids. The difference between

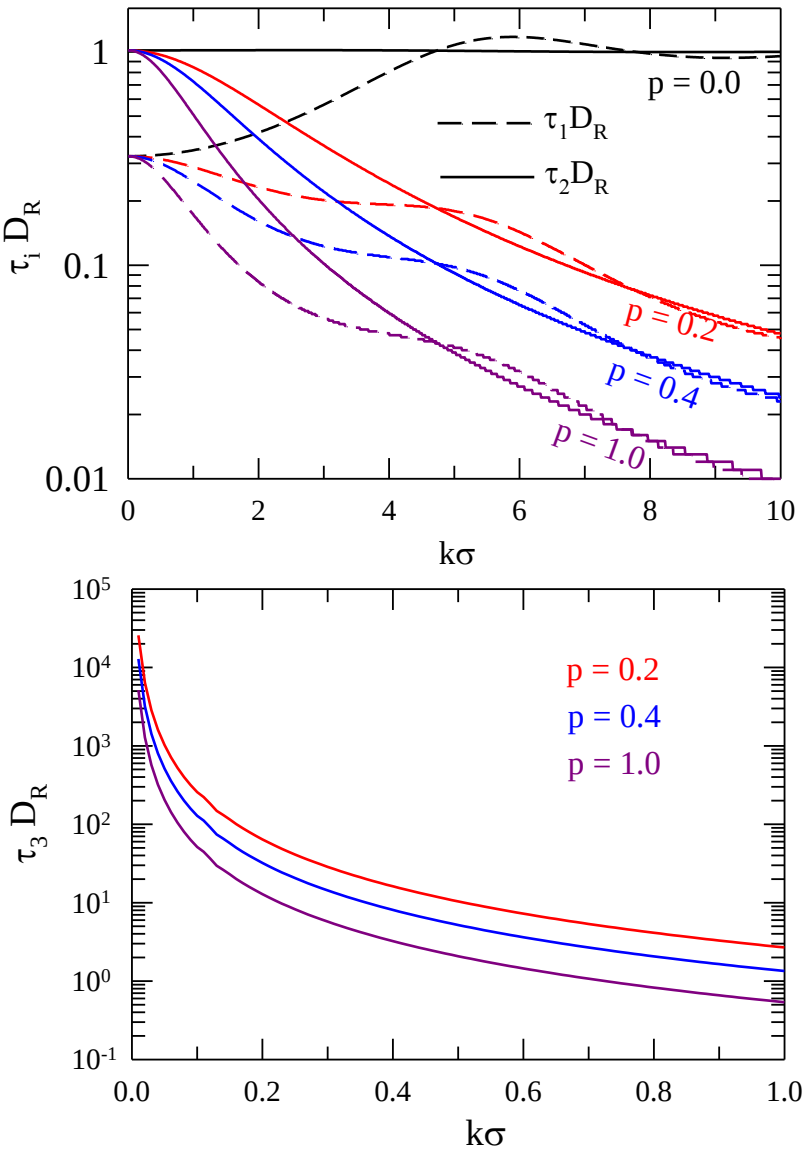

Fig. 8.2: Wavenumber dependence of three relaxation time constants of generalized orientation correlation. The effect of translational contribution ($p = D_T / 2D_R$) has also been shown here.

Table 8.1: Collective orientation correlation time constants and their respective coefficients

IL	X	τ_{M_1} (ps)	Y	τ_{M_2} (ns)	Z	τ_{M_3} (μs)
[Bmim][BF_4]	0.05	4528	0.48	15.47	0.47	21
[Bmim][PF_6]	0.02	7043	0.49	40.55	0.49	29
[Emim][DCA]	0.07	908	0.47	27.35	0.46	4.6
[Hmim][NTf_2]	0.02	2632	0.49	155.6	0.49	19
[Emim][BF_4]	0.03	994	0.49	4.224	0.48	5.1
[Na][TOTO]	0.04	1.4×10^7	0.48	5.6×10^4	0.48	1050

Table 8.2: Comparison between the experimental and theoretical DR time for common dipolar liquids and ILs

Dipolar Liquids				
System	T (K)	τ_D (ps)	$\tau_D^{expt.}$ (ps)	ξ
H_2O	298	8	8	1
CH_3OH	298	50	60	0.8
CH_3CN	298	10	11	0.9
CH_3CH_2OH	298	60	90	0.7
$CH_3CH_2CH_2OH$	298	84	134	0.6
ILs				
$[Bmim][BF_4]$	298	15463	284	54
$[Bmim][PF_6]$	298	40547	1178	34
[Emim][DCA]	298	2734	31	88
$[Hmim][NTf_2]$	298	15567	233	67
$[Emim][BF_4]$	298	4223	46.6	90
[Na][TOTO]	294	5.6×10^7	1.1×10^7	5

predicted and experimental time scales may be due to various reasons. One reason may be the presence of heterogeneity in IL system which is well studied and established by many researchers.[31-40] Recent theoretical study has shown that density inhomogeneity or heterogeneity in IL can guide the mode of dynamics extensively.[78] It should be noted here that our theory is completely devoid of heterogeneity aspect of liquid system and hence the theoretical predicted data does not carry any heterogeneity information of the liquid. Now let us define a new parameter, ξ, which is defined by the ratio of theoretical and experimentally measured DR time, meaning $\xi = \tau_D / \tau_D^{expt.}$. ξ is the degree of deviation of theoretically predicted time scale with experimental one. As we see in Table 2, ξ is close to unity in case of dipolar liquid, and simple dipolar liquids are generally devoid of microscopic heterogeneity in large extent, we can map ξ as a heterogeneity parameter. This is the central focus of this article and one of the significant results pointed here. In the present ILs, ξ ranges between ~30 – 90 except in the case of [Na][TOTO], where ξ is only ~5.

Next, temperature dependence has been investigated to explore the effects of temperature on τ_D and ξ and get a signature of temperature-induced homogenization, a well known phenomenon for most liquids.[79,80,81] Recently, simulation studies have shown that cations and anions of ILs diffuse at a different rate and this difference decreases with increasing temperature. This is a clear signature for increased homogenization at higher temperature. We have compared our predicted DR times with the experimental data in Table 3 for four representative ILs at a wide range of temperature. ξ has also been calculated for these cases and given in the same table. It is evident from Table 3 that with increase of temperature the agreement between τ_D and $\tau_D^{expt.}$ becomes closer; in other words, ξ decreases with increasing temperature. This suggests high temperature homogenization of ILs. A closer inspection of Table 3 further reveals that for imidazolium ILs, 60 K rise in temperature, decreases τ_D and $\tau_D^{expt.}$ by a factor of ~10 – 20 and ~3 – 13 respectively, and that effects the decrease of ξ by a factor of ~1.5 – 2. This suggests a small reduction of microscopic heterogeneity upon temperature rise. This observation is supported by the recent simulation of imidazolium IL, which suggests that at sufficiently high temperature microscopic heterogeneity still exists. This observation is important because the present semimolecular theory can predict the extent of heterogeneity of IL qualitatively. For $[\mathrm{Na}][\mathrm{TOTO}]$, the picture is slightly different from imidazolium ILs. Here in Table 3 we can see that upon 90 K rise in temperature $\tau_D^{theo.}$ and $\tau_D^{expt.}$ decrease by a factor of ~3×10^8 and ~3×10^4 respectively, resulting ~3×10^4 times decrease of ξ value. The most interesting point is that above 324 K the value of ξ almost goes to unity meaning the microscopic heterogeneity of this IL almost vanishes at sufficiently high temperature. Simulation study of this particular IL may be interesting for exploring the temperature effects. The experimental DR study of this IL shows that at the highest temperature condition the DR is almost Debye type as the relaxation time distribution parameters (α and β) of Habriliak-Negami (HN) equation becomes almost unity.[5] The Debye type of relaxation is generally found for microscopically homogeneous systems and thus this type of relaxation indirectly acts as an evidence of microscopic homogeneity of the system.

.Next we have investigated the disagreement of τ_D from $\tau_D^{expt.}$ more precisely and examined the quantities involved in Eq. 8.5, 8.30, 8.31, and 8.34. We have identified the quantity V_{eff}

which is very different from its expected value. Experimental DR study shows that V_{eff} is only ~0.5 - 3.3% of cationic volume, V_{cat}.[5] Experimentally obtained V_{eff} and the volumes of the constituent ions are provided in Table 4. Ratio of V_{eff} and V_{cat} has been defined by χ

Table 8.3: Temperature dependence of τ_D

	$T\ (K)$	$\rho\left(g/cm^3\right)$	$\eta\ (P)$	$\tau_D(ps)$	$\tau_D^{expt.}(ps)$	$\chi\left(=\tau_D/\tau_D^{expt.}\right)$
$[Bmim][BF_4]$	278.15	1.217	3.192	52411	670	78
	288.15	1.209	1.947	31072	351	89
	298.15	1.202	0.996	15463	284	54
	308.15	1.195	0.582	8799	140	63
	318.15	1.189	0.378	5570	93.7	59
	328.15	1.183	0.290	4168	59.4	71
	338.15	1.177	0.208	2919	52.5	56
$[Emim][DCA]$	278.15	1.098	0.403	5554	46.4	120
	288.15	1.082	0.288	3856	34.5	112
	298.15	1.066	0.210	2734	30.7	89
	308.15	1.050	0.156	1977	25.2	78
	318.15	1.034	0.119	1470	18.9	77
	328.15	1.018	0.091	1096	16.7	64
	338.15	1.002	0.072	846	16.1	53
$[Emim][BF_4]$	278.15	1.295	0.761	9164	99.3	92
	288.15	1.288	0.532	6216	60.7	102
	298.15	1.279	0.372	4223	46.6	91
	308.15	1.272	0.256	2826	36.6	77
	318.15	1.265	0.188	2020	21.9	92
	328.15	1.258	0.127	1330	18.4	72
	338.15	1.250	0.089	909	15.5	59
$[Na][TOTO]$	254	1.268	2855724768	5.8×10^{13}	2.2×10^{9}	26364
	264	1.263	12245323	2.4×10^{11}	2.4×10^{9}	100
	274	1.259	31374	6.0×10^{9}	2.4×10^{8}	25
	284	1.254	22563	4.2×10^{8}	4.6×10^{7}	9
	294	1.249	3108	5.6×10^{7}	1.1×10^{7}	5
	304	1.245	662	1.2×10^{7}	3.3×10^{6}	4
	314	1.240	191	3.2×10^{6}	1.1×10^{6}	3
	324	1.235	69	1.1×10^{6}	4.0×10^{5}	3
	334	1.230	30	1.4×10^{5}	1.6×10^{5}	1
	344	1.226	14	2.2×10^{5}	7.0×10^{4}	3

which has also been given in the same table. This is surprising to note that V_{eff} is so much low compared to V_{cat}, which essentially suggests that an extremely low volume of the entire cation is rotating instead of the whole. Low value of V_{eff} has also been obtained by recent simulation work of IL, where the authors have mainly focussed on the validity of hydrodynamic relations.[82] They have suggested that the relations are not valid for IL system and the reason of this is stated as heterogeneity of the medium. They have obtained the effective volume of $[\text{Emim}][\text{NTf}_2]$ is as low as ~ 5 Å^3, which is ~3% of the cationic volume (149 Å^3) of this IL. All these observations indicate that in IL the rotation of the dipolar constituent is rarely Brownian. The rotation is mainly large angle jump[83] which does not feel the medium viscosity. This may be one of the main reasons of rotational diffusion viscosity decoupling commonly found in ILs. When we use the experimentally observed effective volume of the dipolar constituent, we get a very good agreement of the predicted DR time scales with experimental ones. This again supports the validity of our theory in IL system if the heterogeneity is somehow included.

Table 8.4: Comparison between the effective volume and actual cationic volume

ILs	$V_{eff}\left(10^{-30}\,\text{m}^3\right)$	$V_{cat}\left(10^{-30}\,\text{m}^3\right)$	χ
[Emim][DCA]	0.73	149	0.005
[Bmim][BF_4]	1.4	163	0.009
[Bmim][PF_6]	5.3	163	0.033
[Hmim][NTf_2]	2.2	191	0.012
[Emim][BF_4]	0.81	149	0.005

8.4 Conclusion

The theory developed here is a generalized semi-molecular theory for studying the DR dynamics in ILs. This theory is also applicable in dipolar liquid and supercooled molten mixture where both dipolar and ionic components are present in the system. The present theory predicts triphasic relaxation of generalized orientation correlation. The DR obtained

from this theory has two different channels originated from two different interactions in the medium e.g. dipole-dipole and ion-dipole interactions, although the ion-dipole interaction results too large DR time scale. The ion-ion interaction is seen to be non-contributing in DR process. The relation among single particle rotational time, collective rotational time, and DR time has been constructed here. This theory thus establishes the micro-macro relation in IL for the first time. The theory has also been applied in dipolar liquid to benchmark our result. We have seen the predicted DR time to be extremely large compared to the experimental values in ILs, although the predictions for dipolar liquids show a very good agreement with the experiments. This difference has been understood in terms of microscopic heterogeneity in ILs. We have defined a new parameter, ξ, which represents the ratio of theoretical and experimental time scales and is correlated to the spatial heterogeneity of the medium. Temperature dependence study has been done in ILs in order to investigate the effects of temperature on the relaxation time constants and ξ. It is shown that this theory can produce high temperature homogenization for Ils as ξ decreases with increase in temperature. Our analyses suggest that the difference between the predicted and experimental DR times arises from the coupling of the rotating volume with the spatial heterogeneity of ILs, not from ion-ion interactions.

References

1. Stoppa, A.; Hunger, J.; Buchner, R.; Hefter, G.; Thoman, A.; Helm, H. *J. Phys. Chem. B* **2008**, *112*, 4854.
2. Sangoro, J.; Iacob, C.; Serghei, A.; Naumov, S.; Galvosas, P.; Kärger, J.; Wespe, C.; Bordusa, F.; Stoppa, A.; Hunger, J.; Buchner, R.; Kremer, F. *J. Chem. Phys.* **2008**, *128*, 214509.
3. Hunger, J.; Stoppa, A.; Buchner, R.; Hefter, G. J. Phys. Chem. **112**, 12913 (2008).
4. Schröder, C.; Hunger, J.; Stoppa, A.; Buchner, R.; Steinhauser, O. *J. Chem. Phys.* **2008**, *129*, 184501.
5. Hunger, J.; Stoppa, A.; Schrödle, S.; Hefter, G.; Buchner, R. *Chem. Phys. Chem.* **2009**, *10*, 723.
6. Turton, D. A.; Hunger, J.; Stoppa, A.; Hefter, G.; Thoman, A.; Walther, M.; Buchner, R.; Wynne, K. *J. Am. Chem. Soc.* **2009**, *131*, 11140.
7. Hunger, J.; Stoppa, A.; Buchner, R.; Hefter, G. *J. Phys. Chem. B* **2009**, *113*, 9527.
8. Zech, O.; Hunger, J.; Sangoro, J. R.; Iacob, C.; Kremer, F.; Kunz, W.; Buchner, R. *Phys. Chem. Chem. Phys.* **2010**, *12*, 14341.
9. Bešter-Roga, M.; Stoppa, A.; Hunger, J.; Hefter, G.; Buchner, R. *Phys. Chem. Chem. Phys.* **2011**, *13*, 17588.
10. Lohse, P. W.; Bartels, N.; Stoppa, A.; Buchner, R.; Lenzer, T.; Oum, K. *Phys. Chem. Chem. Phys.* **2012**, *114*, 3596.
11. Huang, M.-M.; Bulut, S.; Krossing, I.; Weingärtner, H. *J. Chem. Phys.* **2010**, *133*, 101101.
12. Daguenet, C.; Dyson, P.; Krossing, I.; Oleinikova, A.; Slattery, J.; Wakai, C.; Weingärtner, H. *J. Phys. Chem. B* **2006**, *110*, 12682.
13. Bottcher, C. G. E.; Bordewijk, P. *Theory of Electric Polarization*, Elsevier: London, 1986.
14. Bagchi, B.; Chandra, A. *Adv. Chem. Phys.* **1991**, *80*, 1.
15. Glarum, S. H. *J. Chern. Phys.* **1960**, *33*, 1371.
16. Powles, J. G.; *J. Chem. Phys.* **1953**, *21*, 633.
17. Deutch, J.; Faraday, J. *Sym. Chem. Soc.* **1977**, *11*, 26.
18. Kirkwood, J. G. *J. Chem. Phys.* **1939**, *7*, 911.
19. Kivelson, D.; Madden, P. *Mol. Phys.* **1975**, *30*, 1749.

20. Madden, P.; Kivelson, D. *Adv. Chem. Phys.* **1984**, *56*, 467.
21. Chandra, A.; Bagchi, B. *J. Chem. Phys*. **1989**, *91*, 1829.
22. Chandra, A.; Bagchi, B. *J. Chem. Phys*. **1989**, *91*, 3056.
23. Chandra, A.; Bagchi, B. *Chem. Phys. Lett.* **1989**, *161*, 413.
24. Chandra, A.; Bagchi, B. *J. Chem. Phys.* **1990**, *90*, 1832.
25. Chandra, A.; Bagchi, B. *J. Chem. Phys*. **1990**, *94*, 3152.
26. Bagchi, B.; Chandra, A. *Phys. Rev. Lett.* **1990**, *64*, 455.
27. Bagchi, B.; Chandra, A. *J. Chem. Phys.* **1990**, *93*, 1955.
28. Chandra, A.; Bagchi, B. *J. Phys. Chem.* **1991**, *95*, 2529.
29. Hunger, J.; Niedermayer, S.; Buchner, R.; Hefter, G. *J. Phys. Chem. B* **2010**, *114*, 13617.
30. Schröder, C.; Wakai, C.; Weingärtner, H.; Steinhauser, O. *J. Chem. Phys.* **2007**, *126*, 084511.
31. Sarangi, S. S.; Zhao, W.; Müller-Plathe, F.; Balasubramanian, S. *Chem. Phys. Chem.* **2010**, *11*, 2001.
32. Hebasaki, J.; Ngai, K. L. *J. Chem. Phys.* **2008**, *129*, 194501.
33. Hu, Z.; Margulis, C. J. *Acc. Chem. Res.* **2007**, *40*, 1097.
34. Hu, Z.; Margulis, C. J. *Proc. Natl. Acad. Sci. U.S.A.* **2006**, *103*, 831.
35. Jin, H.; Li, X.; Maroncelli, M. *J. Phys. Chem. B Lett.* **2007**, *111*, 13473.
36. Adhikari, A.; Sahu, K.; Dey, S.; Ghosh, S.; Mandal, U.; Bhattacharyya, K. *J. Phys. Chem. B* **2007**, *111*, 12809.
37. Mandal, P. K.; Sarkar, M.; Samanta, A. *J. Phys. Chem. A* **2004**, *108*, 9048.
38. Triolo, A.; Russina, O.; Bleif, H.; Cola, E. D. *J. Phys. Chem. B* **2007**, *111*, 4641.
39. Wang, Y.; Voth, G. A. *J. Am. Chem. Soc.* **2005**, *127*, 12192.
40. Saha, S.; Mandal, P. K.; Samanta, A. *Phys. Chem. Chem. Phys.* **2004**, *6*, 3106.
41. Hunger, J.; Niedermayer, S.; Buchner, R.; Hefter, G. *J. Phys. Chem. B* **2010**, *114*, 13617.
42. Lakowicz, J. R. *Principles of fluorescence spectroscopy*, Plenum: New York, 1983.
43. Dote, J. L.; Kivelson, D.; Schwartz, R. N. *J. Phys. Chem.* **1981**, *85*, 2169.
44. Horng, M. L.; Gardecki, J. A.; Maroncelli, M. *J. Phys. Chem. A* **1997**, *101*, 1030.
45. Das, A.; Biswas, R.; Chakrabarti, J. *J. Chem. Phys.* **2012**, *136*, 014505.
46. Daschakraborty, S.; Biswas, R. *J. Chem. Sci.* **2012**, *124*, 763.
47. Pal, T.; Biswas, R. *Chem. Phys. Lett.* **2011**, *517*, 180.
48. Mazza, M. G.; Giovambattista, N.; Stanley, H. E.; Starr, F. W. *Phys. Rev. E* **2007**, *76*,

031203.
49. Köddermann, T.; Ludwig, R.; Paschek, D. *Chem. Phys. Chem.* **2008**, *9*, 1851.
50. Jin, H.; Baker, G. A.; Arzhantsev, S.; Dong, J.; Maroncelli, M. *J. Phys. Chem. B* **2007**, *111*, 7291.
51. Arzhantsev, S.; Ito, N.; Heitz, M.; Maroncelli, M. *Chem. Phys. Lett.* **2003**, *381*, 278.
52. Ito, N.; Arzhantsev, S.; Maroncelli, M. *Chem. Phys. Lett.* **2004**, *396*, 83.
53. Ito, N.; Arzhantsev, S.; Heitz, M.; Maroncelli, M. *J. Phys. Chem. B* **2004**, *108*, 5771.
54. Bulut, S.; Klose, P.; Huang, M-M.; Weingärtner, H.; Dyson, P. J.; Laurenczy, G.; Friedrich, C.; Menz, J.; Kümmerar, K.; Krossing, I. *Chem. Eur. J.* **2010**, *16*, 13139.
55. Daschakraborty, S.; Biswas, R. *Chem. Phys. Lett.* **2011**, *510*, 202.
56. Roy, D.; Patel, N.; Conte, S.; Maroncelli, M. *J. Phys. Chem. B* **2010**, *114*, 8410.
57. Calef, D. F.; Wolynes, P. G. *J. Chem. Phys.* **1983**, *78*, 4145.
58. Pedlosky, J. *Geophysical fluid dynamics*, Springer, 1987.
59. Lebowitz, J.; Percus, J. K. *J. Math. Phys.* **1963**, *4*, 116.
60. Kashyap, H. K.; Biswas, R. *J. Phys. Chem. B* **2010**, *114*, 254.
61. Daschakraborty, S.; Biswas, R. *J. Phys. Chem. B* **2011**, *115*, 4011.
62. Bagchi, B.; Biswas, R. *Adv. Chem. Phys.* **1999**, *109*, 207.
63. Bagchi, B. *Phys. Letters A* **1987**, *121*, 29.
64. Bagchi, B. *Physica A* **1987**, *145*, 273.
65. Bagchi, B. *Current Sci.* **1986**, *55*, 691.
66. Gray, C. G.; Gubbins, K. E. *Theory of Molecular Fluids*, Clarendon: Oxford, UK, 1984, Vol. I.
67. Hansen, J. P.; McDonald, I. R. *Theory of Simple Liquids*, 3rd ed. Academic: San Diego, 2006.
68. See Appendix A for various tables.
69. De Gennes, P.G. *Physica* **1959**, *25*,825.
70. Chandra, A.; Wei, D.; Patey, G. N. *J. Chem. Phys.* **1993**, *98*, 4959.
71. Chandra, A.; Patey, G. N. *J. Chem. Phys.* **1994**, *100*, 8385.
72. Chandra, A.; Jana, D.; Bhattacharjee, S. *J. Chem. Phys.* **1996**, *104*, 8662.
73. Mahajan, K.; Chandra, A. *J. Chem. Phys.* **1997**, *106*, 2360.
74. Gazi, H. A. R.; Guchhait, B.; Daschakraborty, S.; Biswas, R. *Chem. Phys. Lett.* **2011**, *501*, 358.
75. Guchhait, B.; Daschakraborty, S.; Biswas, R. *J. Chem. Phys.* **2011**, *136*, 174503.

76. Kindt, J. T.; Schmuttenmayer, C. A. *J. Chem. Phys.* **1996**, *100*, 10373.
77. Asaki, M. L. T.; Redondo, A.; Zawodzinski, T. A.; Taylor, A. J. *J. Chem. Phys.* **2002**, *116*, 10377.
78. Daschakraborty, S.; Biswas, R. *J. Chem. Phys.* **2012**, *137*, 114501.
79. Karimi-Varzaneh, H. A.; Müller-Plathe, F.; Balasubramanian, S.; Carbone, P. *Phys. Chem. Chem. Phys.* **2010**, *12*, 4714.
80. Cadena, C.; Zhao, Q.; Snurr, R. Q.; Maginn, E. J. *J. Phys. Chem. B* **2006**, *110*, 2821.
81. Pal, T.; Biswas, R. *Theo. Chem. Acc.* **2013**, *132*, 1348.
82. Ködermann, T.; Ludwig, R.; Pashchek, D. *Chem. Phys. Chem.* **2008**, *9*, 1851.
83. Anderson, J. E. *Faraday Symp. Chem. Soc.* **1972**, *6*, 82.

Chapter 9

Influence of Polar Interaction on Medium Viscosity: A Computer Simulation Investigation Using Model Liquids

9.1 Introduction

Viscosity coefficient (η, hereafter simply viscosity) is one of the most important dynamical properties of a fluid as it can be experimentally accessed. In conjunction with diffusion coefficients, translational (D_T) and rotational (D_R), η provides crucial information about solute-solvent coupling.[1,2] Moreover, a molecular level understanding can be achieved via using the macro-micro relationships, for example, that between the experimentally measurable viscosity and the corresponding computationally accessible stress tensor autocorrelation function.[1] This provides a description in which one can modify various molecular properties such as molecular diameter and dipole moment and investigate the subsequent effects on individual transport properties (η and D_x, x being T or R) and also on coupling between them. Thermodynamic parameters like solvent density and temperature can affect at the molecular level the coupling between D_x and η. Traditionally, the coupling is expressed via the hydrodynamic relations, Stokes-Einstein (SE)[1] for the centre-of-mass (translational) motion and Stokes-Einstein-Debye (SED)[2] for the rotational motion. Deviations from SE and SED relations often attract special attention because of the possibility of accessing rich, often new, information regarding dynamical pathways to the environmental coupling.[3-9]

Since the viscosity being discussed here is the shear viscosity and related to the rate of momentum transfer from one fluid layer to the adjacent one while moving,[1] it is expected that the interactions with nearest neighbors would dominate the process. At typical liquid densities, the short range repulsive interactions mainly dictate the spatial distribution of nearest neighbors. Consequently, it has been argued that consideration of only the region around the peak of the static structure factor in calculations would suffice to predict the liquid viscosity.[10-11] One would then be naturally interested to ask the following questions: at typical

liquid densities what would be the effects of the longer-ranged dipole-dipole interaction on η and how temperature would modulate such effects? The main focus of this chapter is to investigate the above two questions via simulation studies of model liquids. In addition, solute-solvent coupling as a function of the strength of the dipolar interaction (through the variation of molecular dipole moment, μ) and temperature have been systematically explored.

We would like to mention here that simulation studies have already explored dependences of viscosity on thermodynamic parameters (temperature, density and pressure) in various model liquids, ranging from L-J neat fluids[12] and binary mixtures [13] to explosive materials.[14] In addition, attempts to correlate viscosity with various physical parameters of a substance have shown viscosity to be proportional to the square root of molar mass, cube root of refractive index and linear to the dipole-moment.[15] These correlations, however, lack microscopic explanations and thus warrant molecular level investigation. Here we have carried out such a study with two different model liquids, namely, Lennard-Jones[1] and Stockmayer (SM) fluids.[16,17] The advantage of choosing such a pair is that SM potential, being a sum-total of L-J and dipole-dipole interactions, facilitates an easy exploration of the effects of dipolar interaction on liquid transport properties by simply changing the magnitude of the molecular dipole moment. Note that applicability of integral equations method has already been tested[18] for predicting the pressure and viscosity of SM fluids. In addition, simulation studies have investigated static dielectric properties,[19-21] dynamic solvation response,[22-25] structural aspects,[26] freezing transition[27] for the neat SM fluids, and interfacial properties of electrolyte solutions[28] and binary mixtures of these model fluids.[29] Therefore, SM fluids are one of the most studied model fluid systems and further studies on the transport properties will help better characterizing these systems.

The rest of the chapter is arranged as following. Necessary theoretical discussions and simulation details are presented in the next section. Simulated results and their implications are illustrated in Sec. III. Concluding remarks are provided in Sec. IV.

9.2 Simulation Details and Necessary Statistical Mechanical Relations

Molecular dynamics simulations were performed for one Lennard-Jones system and four Stockmayer (SM) systems covering the dipole-moment range from 0.6 Debye to 3.0 Debye in NVT ensembles with a total number of 216 particles in each of the cases at 300 K, 350 K and 400 K (using argon parameters). The non-dipolar system is characterized by the L-J pair potential,

$$V_{LJ}(r_{ij}) = 4\varepsilon\left[\left(\frac{\sigma}{r_{ij}}\right)^{12} - \left(\frac{\sigma}{r_{ij}}\right)^{6}\right], \tag{9.1}$$

where, σ corresponds to the diameter of an L-J particle, r_{ij} the distance between the ith and jth L-J particles, and ε the energy parameter connected to the well-depth. Here we considered all the systems having particles of same σ and ε which are those of argon, i.e. σ = 3.41 Å and ε/k_B = 119.8 K, k_B being the Boltzmann constant. The Stockmayer fluids are characterized by the following pair interaction

$$V_{SM}(r_{ij}) = 4\varepsilon\left[\left(\frac{\sigma}{r_{ij}}\right)^{12} - \left(\frac{\sigma}{r_{ij}}\right)^{6}\right] + \left[\frac{\vec{\mu}_i.\vec{\mu}_j}{r_{ij}^3} - \frac{3}{r_{ij}^5}(\vec{\mu}_i.\vec{r}_{ij})(\vec{\mu}_j.\vec{r}_{ij})\right], \tag{9.2}$$

where the second term in Eq. 9.2 represents the dipole-dipole interaction ($V_{DD}(r_{ij})$) between ith and jth dipolar particles whose dipole moments are denoted as μ_i and μ_j. Neat systems were only considered and thus $\mu_i = \mu_j$.

The initial configuration was started from a simple cubic lattice in a cubic box with periodic boundary condition and minimum image convention. The scaled density of the system, $\rho^* = \rho\sigma^3$ = 0.7. The volume of the simple cubic box was determined from the density considered. The longer-ranged dipolar interaction was dealt with the Ewald summation technique.[30] The cut-off radius for the L-J and dipolar interaction potentials was taken as half of the box length. Nose-Hoover thermostat[31-33] was employed to maintain constancy of a fixed temperature. Equations of motions were integrated by using the Verlet leapfrog integration scheme[30] with a time-step of 2 fs. First 300 ps of each of the simulation runs were treated as equilibration period and the later 700 ps as production run. Translational self-diffusion coefficients (D_T) for the L-J and SM systems were calculated from both the

mean squared displacements ($\left\langle \left|\Delta\vec{r}(t)\right|^2 \right\rangle$) and velocity autocorrelation functions (VACF). The MSDs were calculated from the simulated centre-of-mass positional vectors ($\vec{r}_i^{\,c}(t)$)[34,35]

$$\left\langle \left|\Delta\vec{r}(t)\right|^2 \right\rangle = \frac{1}{N}\left\langle \sum_{i=1}^{N} \left|\vec{r}_i^{\,c}(t) - \vec{r}_i^{\,c}(0)\right|^2 \right\rangle, \tag{9.3}$$

which produced D_T via the connection

$$D_T = \left[\frac{1}{6t}\left(\left\langle \left|\Delta\vec{r}(t)\right|^2 \right\rangle\right)\right]_{t\to\infty}. \tag{9.4}$$

D_T from the VACF were obtained by the following manner[34]

$$D_T = \frac{1}{3}\int_0^\infty dt\left\langle \vec{v}_i(t).\vec{v}_i(0)\right\rangle, \tag{9.5}$$

where, $\vec{v}_i$ is the centre-of-mass velocity vector associated with the ith particle and averaging was done over both time and number of particles.

Rotational diffusion coefficient (D_R) was obtained from the angular velocity autocorrelation function ($C_\omega(t)$) as follows[1,36]

$$D_R \equiv D_R(t\to\infty) = \frac{k_B T}{I}\int_0^t ds\left(1-\frac{s}{t}\right)C_\omega(s), \tag{9.6}$$

where I denote the moment of inertia and $C_\omega(t) = \left\langle \vec{\omega}(0).\vec{\omega}(t)\right\rangle$.

Shear viscosity coefficient (η) was calculated using the Green-Kubo relation,[1]

$$\eta = \frac{V}{k_B T}\int_0^\infty \left\langle P_{\alpha\beta}(t)\,P_{\alpha\beta}(0)\right\rangle dt, \tag{9.7}$$

where, $\alpha,\beta = x,y,z$ and $P_{\alpha\beta}$ denotes the off-diagonal term of the pressure tensor

$$P_{\alpha\beta} = \frac{1}{V}\left(\sum_i \frac{p_{i\alpha}\,p_{i\beta}}{m_i} + \sum_i\sum_{j>i} r_{ij\alpha}\,f_{ij\beta}\right). \tag{9.8}$$

As before, the above correlation functions were also averaged over paricles and time.

The pressure can then be readily obtained from the simulated force, $f_{ij\alpha}$, data by employing the following expression

$$P = \frac{1}{3V}\sum_{\alpha}\left[\sum_{i} p_{i\alpha}\, p_{i\alpha}/m_i + \sum_{\mathrm{i}}\sum_{\mathrm{j>i}} r_{ij\alpha}\, f_{ij\alpha}\right]$$

$$= \frac{1}{3V}\sum_{\alpha}\left[k_B T + \left\{\sum_{i}\sum_{j>i} - r_{ij\alpha}\,\frac{\partial}{\partial r_{ij\alpha}}\left\{4\varepsilon\left[\left(\frac{\sigma}{r_{ij\alpha}}\right)^{12} - \left(\frac{\sigma}{r_{ij\alpha}}\right)^{6}\right] + \left[\frac{\vec{\mu}_{\mathrm{i}}\cdot\vec{\mu}_{\mathrm{j}}}{r_{ij\alpha}^{\ 3}} - \frac{3}{r_{ij\alpha}^{\ 5}}\left(\vec{\mu}_{\mathrm{i}}\cdot\vec{\mathrm{r}}_{\mathrm{ij}}\right)\left(\vec{\mu}_{\mathrm{j}}\cdot\vec{\mathrm{r}}_{\mathrm{ij}}\right)\right]\right\}\right\}\right],$$

(9.9)

9.3 Results and Discussions

Effects of longer-ranged dipolar interaction and temperature on spatial distribution of particles are depicted in Fig. 9.1 where the radial distribution functions (RDFs), $g(r)$, calculated after varying the dipole moment (μ) values at two different temperatures, are shown as a function of the scaled distance ($r^* = r/\sigma$). Note that eventhough the first peak of the RDF increases both with the increase in dipole moment and lowering of temperature, the enhancement factor always remains very small. This indicates that η will increase with decrease in temperature (at a fixed μ) and increase in μ (at a constant temperature) because η is largely determined by the value of the RDF at contact, $g(\sigma)$.[36,37] The small increase of RDF peak value, however, suggests that enhancement of liquid structure upon switching on of the solvent-solvent dipolar interaction. Diffusion coefficient is then expected to reflect this enhanced solvent structure of SM fluids. The similarity in the RDFs obtained earlier by using the hard sphere and L-J potentials have already indicated the dominance of liquid structure by the repulsive part of the potential.[38] In addition, the well-depth of the L-J potential have secondary effects on the height of the first peak of the calculated $g(r)$.[39] A small increase in the simulated $g(r)$ with μ in the present study is therefore in accordance with earlier results obtained for model fluids.

Average mean square displacements (MSDs) obtained for L-J and two SM fluids at two different temperatures are presented in Fig. 9.2 where the simulated $\left\langle\left|\Delta\vec{r}(t)\right|^2\right\rangle$ are shown as a function of the scaled time, $t^* = t/\sqrt{m\sigma^2/\varepsilon}$. Clearly, the slope of the $\left\langle\left|\Delta\vec{r}(t)\right|^2\right\rangle$ versus t^*

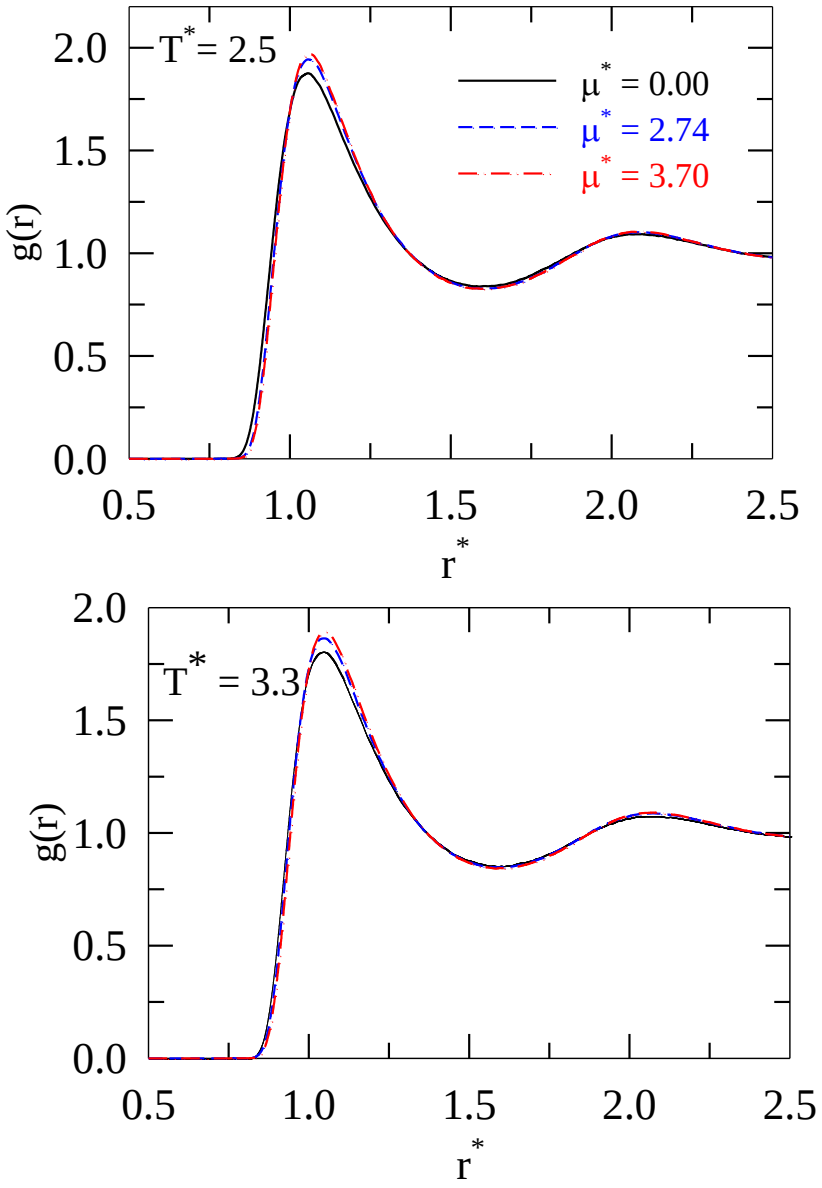

Fig. 9.1: Plots of simulated radial distribution function for systems with different dipole moments. Two panels are for two different temperatures. Different curves are color-coded and explained in the respective panels.

decreases with increase in μ, indicating decrease in translational diffusion coefficient (D_T) as the L-J fluid is replaced by the SM ones. However, the plots in the lower panel suggest that effects of dipole moment become weaker as increase in temperature induces loosening of the liquid structure. The enhancement of decay rates of the normalized velocity autocorrelation

function with μ, shown in Fig. 9.3, further reflects the effects of solution structure and 'loosening' of it upon temperature-rise on particle diffusion. Physically this can be

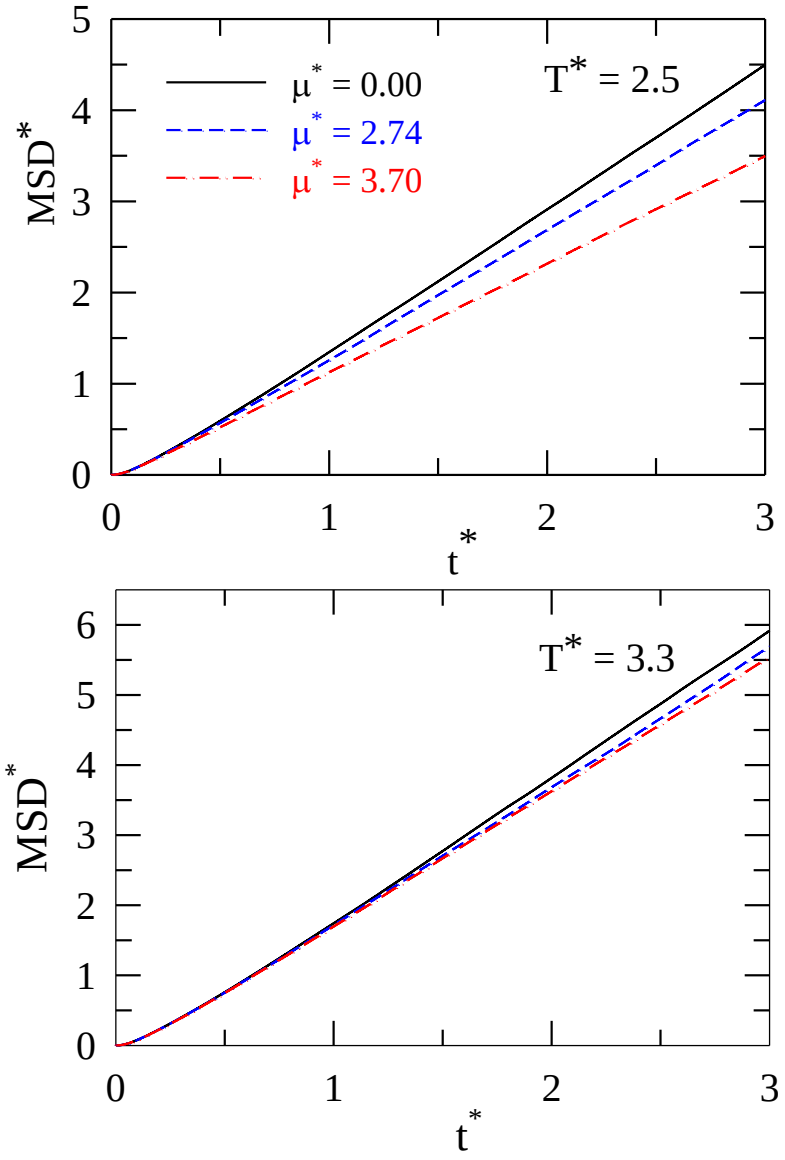

Fig. 9.2: Simulated mean square displacements (MSDs) as a function of time at two different temperatures. Note the dipole moment dependence, particularly at the lower temperature.

understood by realizing that the enhanced solvent structure upon switching on of the dipolar interaction decorrelates the velocity vector at any given time from that at the beginning rather quickly through increased collision against the environment. Eventhough no analytical theory or simulations exist for neat dipolar systems that have investigated the dependence of collision frequency with μ, theoretical studies with (ion + dipole) binary mixtures have

predicted linear dependence of collision frequency with the dipole moment of the polar species at a fixed temperature.[40,41]

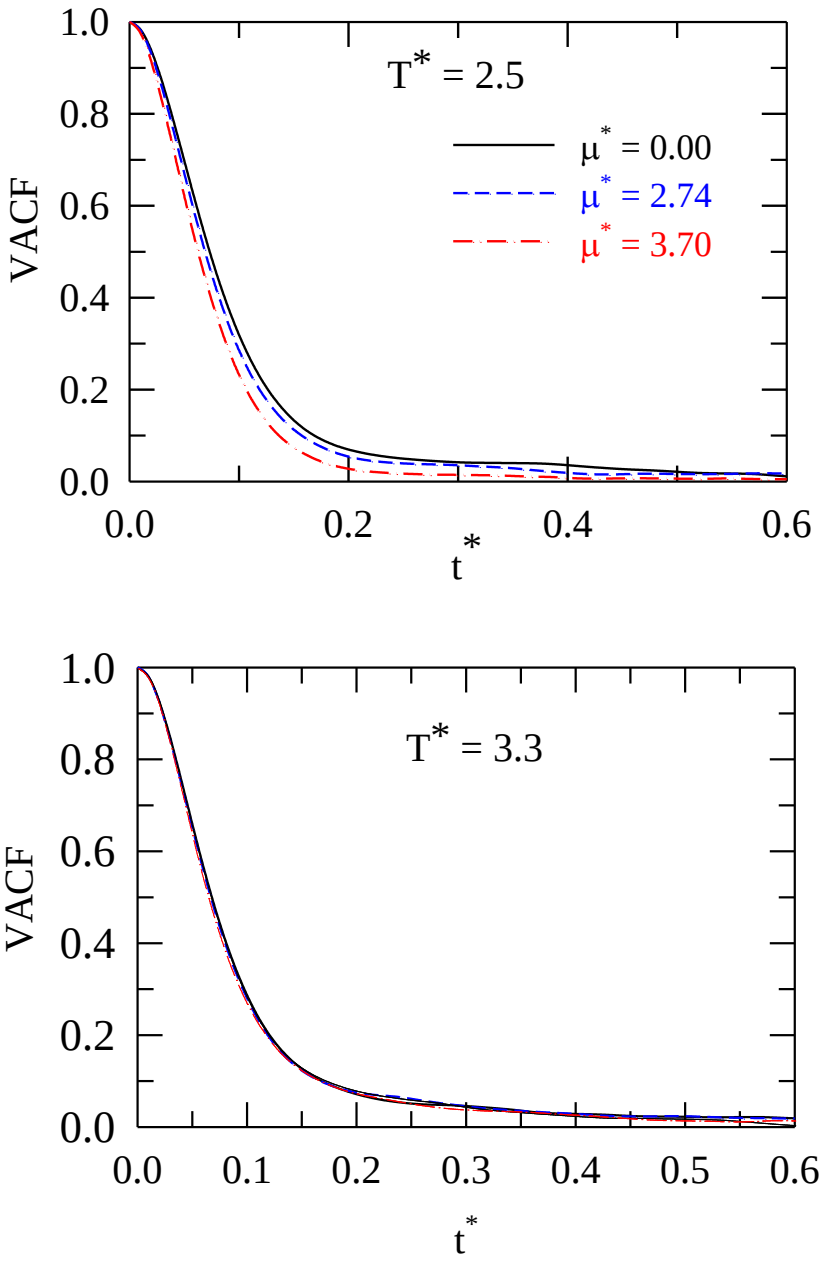

Fig. 9.3: Simulated velocity autocorrelation functions (VACFs) as a function of time for systems with different dipole moments at two different temperatures.

Fig. 9.4 presents the simulated translational diffusion coefficient of a tagged solvent particle ($D_T^* = D_T\sqrt{m/\sigma^2\varepsilon}$) as a function of dipole moment ($\mu^* = \sqrt{\mu^2/\sigma^3\varepsilon}$) for three different temperatures ($T^* = k_BT/\varepsilon$). D_T^* shown here are the arithmetic means of the values obtained

via the MSD and VACF routes. As expected, particle diffusion is larger at higher temperature when all other thermodynamic parameters kept fixed. Note, however, that the dependence on

dipole moment of D_T^* becomes weaker at higher temperature. This can be understood from the temperature dependencies of the simulated MSD and VACF already shown in Figs. 9.2 and 9.3, and originates from the less rigid solvent structure at higher temperature. If parameters for argon is used to calculate diffusion coefficient from the simulated data for L-J systems (that is at $\mu^* = 0$) at $T^* = 2.5$, we find $D_T \approx 1.4\ x\ 10^{-4}$ cm^2s^{-1} , a value in semi-quantitative agreement to earlier simulation results obtained by using 108 L-J particles at comparable density and temperature.[42] The insensitivity to dipole moment of D_T^* in the $0 \le \mu^* \le 1.5$ range at these temperatures, however, indicates that the liquid structure is indeed governed by the shorter-ranged interactions where the longer-ranged dipolar interactions have minimal effects on the liquid structure that dictates diffusion.

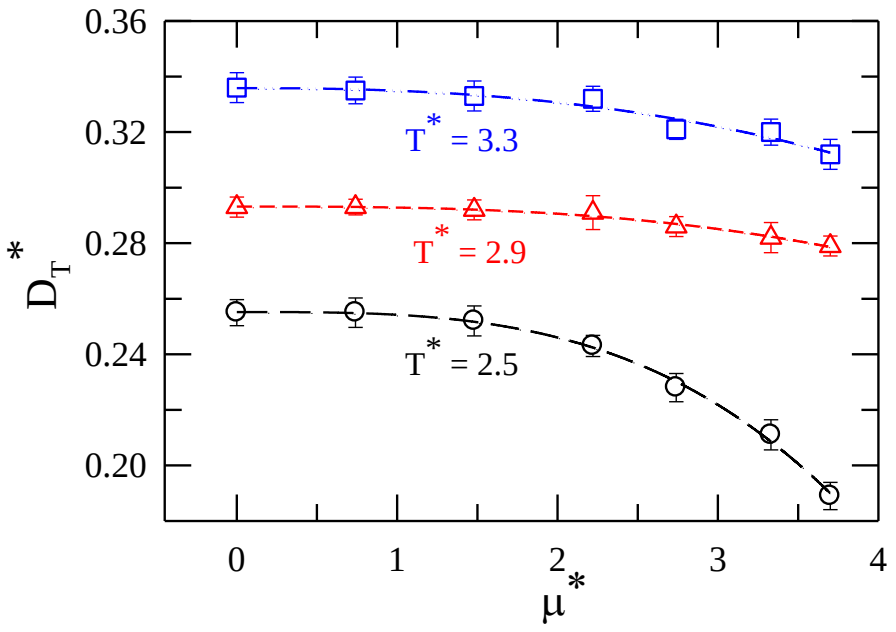

Fig. 9.4: Dipole moment dependence of simulated translational diffusion coefficient at three different temperatures. Error bars have been computed via block average. Lines going through the data are for visual guide.

Fig. 9.5 shows the effects of dipole moment on rotational diffusion at three different temperatures. The interesting aspect to note here is that D_R^* $(= D_R\sqrt{m\sigma^2/\varepsilon})$ is much more

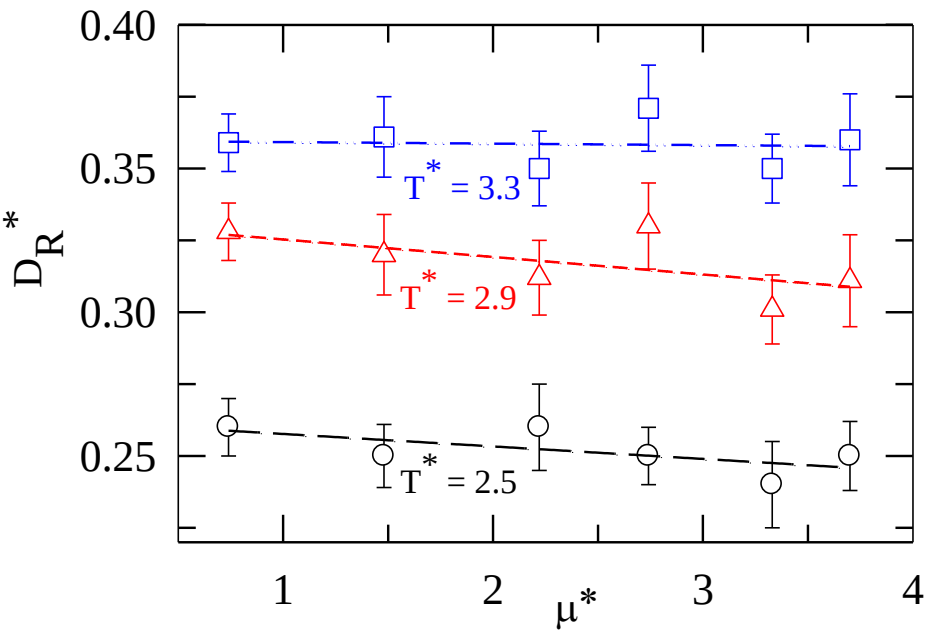

Fig. 9.5: Dipole moment dependence of rotational diffusion coefficient at three different temperatures. As in the previous figure, error bars have been determined via block averaging.

insensitive to μ^* than what has been observed for D_T^* in Fig. 9.4. The microscopic reason for such a behavior arises from the dipole moment insensitivity of the decay of angular velocity autocorrelation function (AVCF), shown in Fig. 9.6. The AVCF decays presented in two panels of Fig. 9.6 for two different temperatures demonstrate insignificant effects of dipole moment. In contrast, VACF decays and MSDs, particularly those at lower temperatures, exhibit much stronger μ^* dependence. The difference lies in the fact that while breaking of solvent structure is necessary for translational diffusion, rotational diffusion does not require centre-of-mass motion and thus can remain largely immune to whatever effects that the longer-ranged dipolar interactions might have on solvent structure.

Next we present in the upper panel of Fig. 9.7 the simulated viscosity as a function of dipole moment at $T^* = 2.5$. It is clear from this figure that η^* rises rather rapidly with μ^* particularly at the high end and the increase could be as large as ~60% over the value of the corresponding L-J fluid. This suggests that the longer-ranged dipole-dipole interaction does affect the medium viscosity, and the effects become stronger for systems with higher dipole

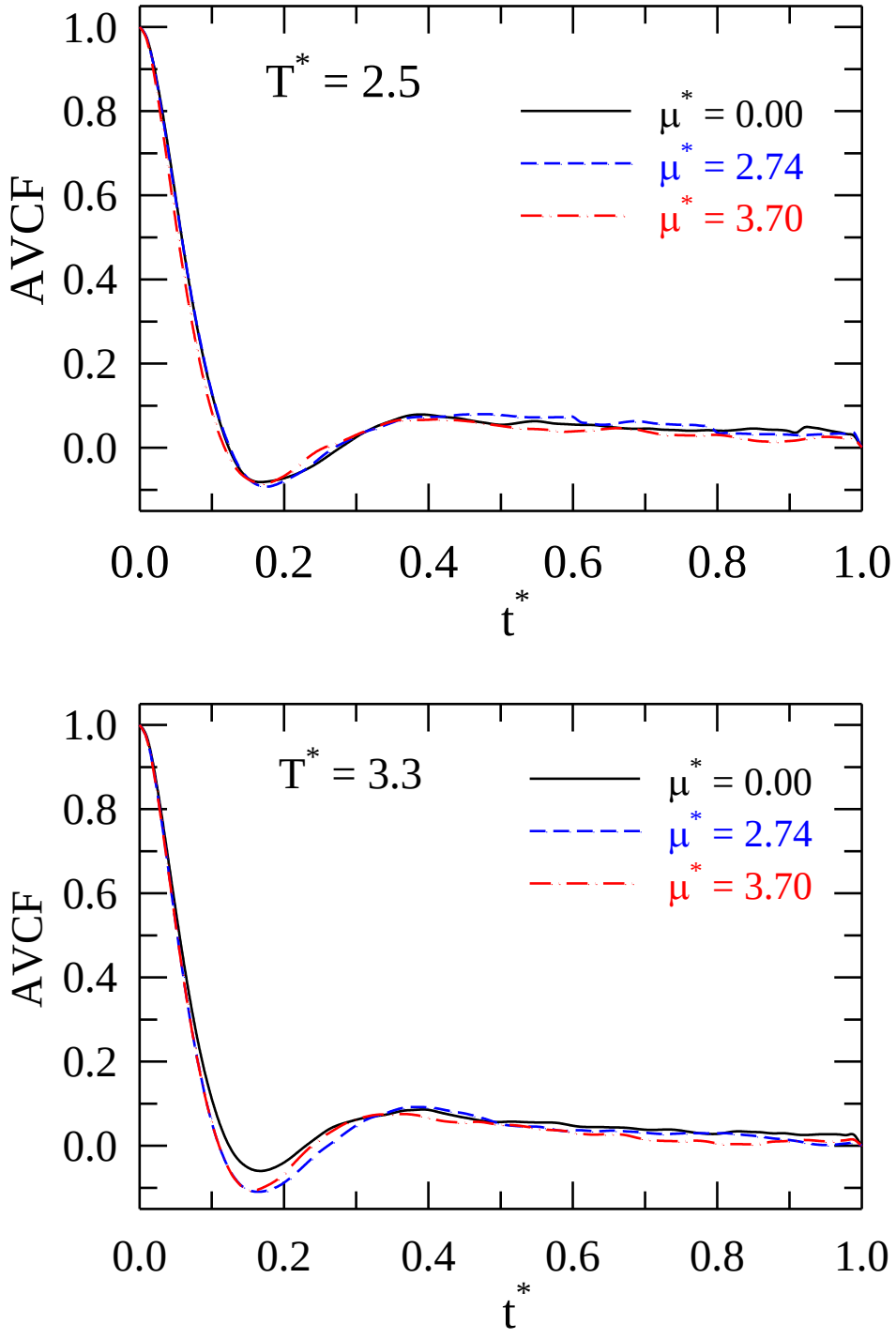

Fig. 9.6: Plots of angular velocity correlation functions (AVCFs) as a function of time at two different temperatures. For further details, see text.

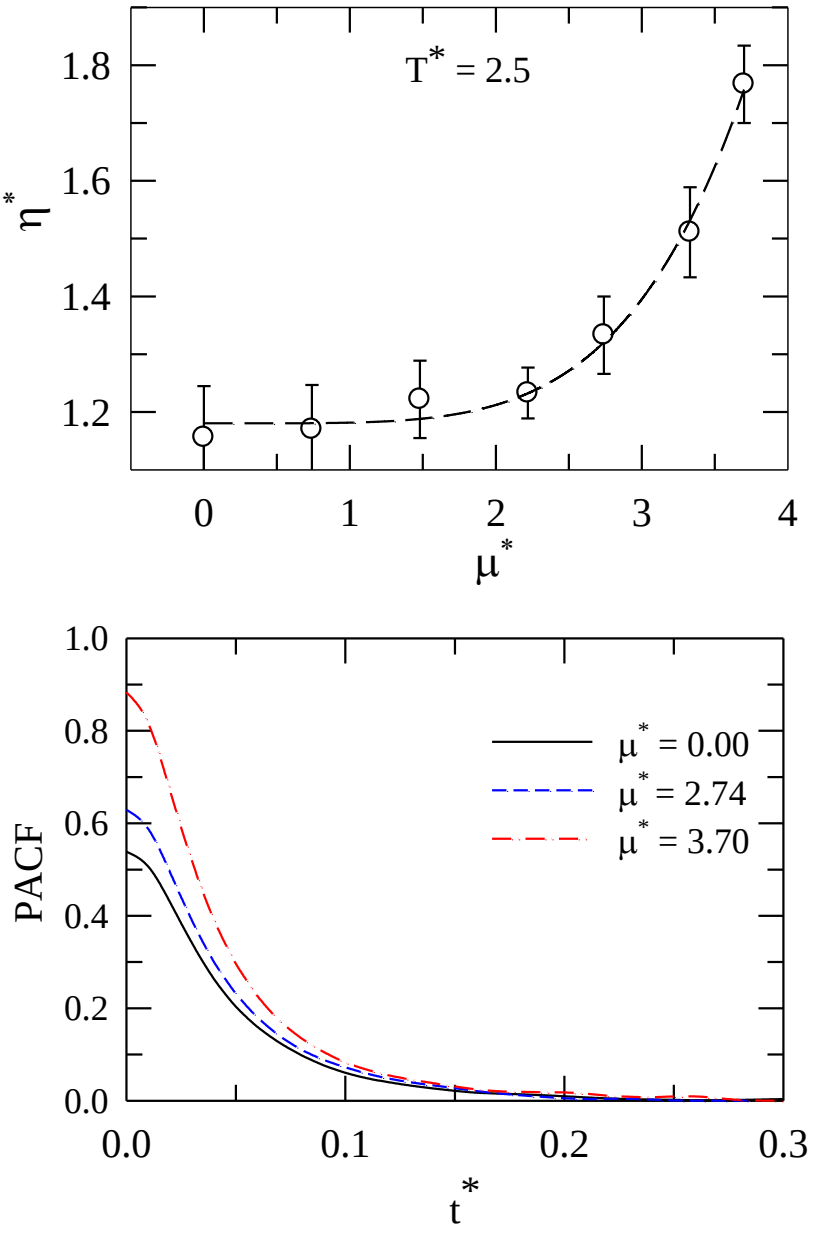

Fig. 9.7: Effects of dipole moment on simulated viscosity (upper panel) and on pressure autocorrelation function, PACF (lower panel). Time integration of this correlation function (multiplied by a prefactor) provides the numerical values for the shear viscosity coefficient.

moments. As the lower panel of this figure suggests, the increase of η^* with μ^* at a fixed temperature and density emerges from the steady increase of the value at $t^* = 0$ of the pressure autocorrelation function (PACF) with dipole moment. We would like to mention

here that, η^* being more collective in nature than diffusion coefficient (D_x^*), simulations of the former is trickier than the latter and the simulated η^* values are often associated with larger error bars, particularly those covering the temperature range considered here.[42] As a result, the present simulations have not been able to capture quite cleanly the temperature dependence of viscosity coefficient as observed for real liquids. However, the dependence of the simulated η^* on μ^* at the other two higher temperatures ($T^* = 2.9$ and 3.3) remained qualitatively the same as that observed at $T^* = 2.5$. When compared for L-J argon (that is, at μ^*=0) at 300 K, the present simulations predict $\eta \approx 1.1\times10^{-3} P$ which is in satisfactory agreement with earlier simulation results.[42] This and the agreement found for translational diffusion coefficient earlier provides us with the necessary confidence that the present simulations have been carried out properly.

Fig. 9.8 shows the simulated mean pressure ($P^* = P\sigma^3/\varepsilon$) as a function of μ^* for the three temperatures considered. The dependence of P^* on μ^* can be understood from Eq. 9.9 which predicts, in the limit of low μ^*, a linear dependence on T^*. At higher μ^*, however, quadratic dependence on dipole moment supersedes the linear temperature dependence and P^* changes approximately as μ^{*2}. This is also the reason for η^* showing nearly a μ^{*2} dependence at large dipole moments (upper panel, Fig. 9.7) at a given temperature.

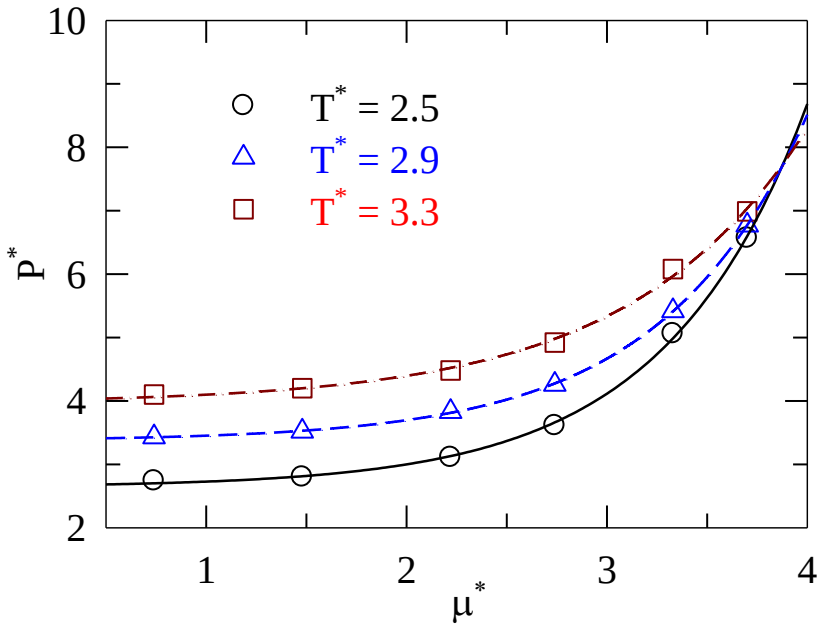

Fig. 9.8: Dipole moment dependence of simulated mean pressure for SM fluids at three different temperatures. While the symbols represent simulated values, lines going through them act as visual guides. Circles, triangles and squares represent data respectively at T^*=2.5, 2.9 and 3.3.

Next we investigate in Fig. 9.9 the applicability of the SE and the SED relations where we show the simulated dipole moment dependence of the diffusion coefficient multiplied by the temperature-scaled viscosity coefficient ($D_x^* \times \eta^* / T^*$). This scaled quantity, $D_x^* \times \eta^* / T^*$, is expected to be constant with μ^* for a given particle if the above hydrodynamic relations (SE and SED) remain valid.

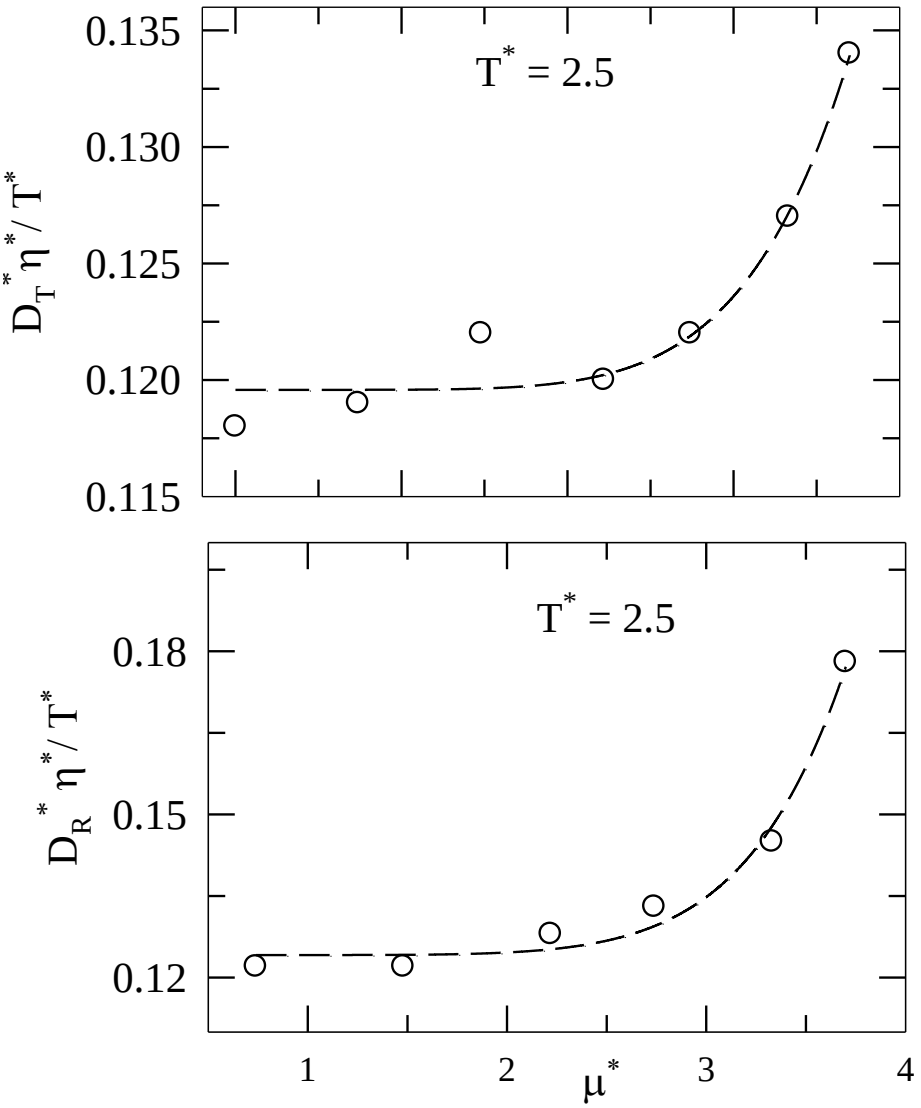

Fig. 9.9: Deviation from the Stokes-Einstein and Stokes-Einstein-Debye relations for the simulated translational (upper panel) and rotational diffusion coefficients (lower panel) as a function of dipole moment.

Earlier simulations have already suggested that such hydrodynamic relations hold in a broad range of density and temperature for pure simple fluids where solute-to-solvent size and interaction ratios are unity.[43] The nature of the curves in the panels of Fig. 9.8 (shown without error bars for the sake of clarity) strongly suggest break-down of SE and SED relations for Stockmayer fluids. The rise of $D_x^* \times \eta^* / T^*$ with μ^* arises because the increase in η^* is not equally reciprocated by the decrease in D_x^*, signaling a partially decoupling between these two transport coefficients. Several works in the last few years have shown that

breaking down of the hydrodynamic relations may occur for diverse systems ranging from as simple as hard sphere or L-J fluids[44-48] to as complex as sucrose benzoate,[49] supercritical fluids[50] and ionic liquids.[51-53] The deviations from the SE and SED relations therefore suggest that diffusion-viscosity decoupling is not an exclusive aspect of deeply supercooled systems where dynamic heterogeneity is traditionally attributed to the observed decoupling [54-55], different rate of particle motions may play an important role as well in deciding environmental coupling in these model systems at temperatures much away from supercooling.

The presence of dynamic heterogeneity is next investigated for these model systems by following the deviation of the self-part of the van Hove correlation function, $G_s(\vec{r},t)$, at intermediate times (times between inertial and diffusive regimes) from the Gaussian distribution with respect to particle displacement, and a non-Gaussian parameter, $\alpha(t)$.[56-58] The time-dependent self-part of the van Hove correlation function is give as[1,9]

$$G_s(\vec{r},t) = \frac{1}{N}\left\langle \sum_{i=1}^{N} \delta\left(\vec{r}_i^{\,c}(t) - \vec{r}_i^{\,c}(0) - \vec{r}\right)\right\rangle, \tag{9.10}$$

where r^c denotes the centre-of-mass of a particle. The Maxwell-Boltzmann velocity distribution at extermely short time (that is, $t \to 0$) and hydrodynamic behavior at $t \to \infty$, forces $G_s(\vec{r},t)$ to be Gaussian with particle displacement, $\Delta\vec{r}(t)$. The non-Gaussian parameter is defined as follows[58]

$$\alpha(t) = \frac{3}{5}\frac{\left\langle \left|\Delta\vec{r}(t)\right|^4 \right\rangle}{\left\langle \left|\Delta\vec{r}(t)\right|^2 \right\rangle^2} - 1, \tag{9.11}$$

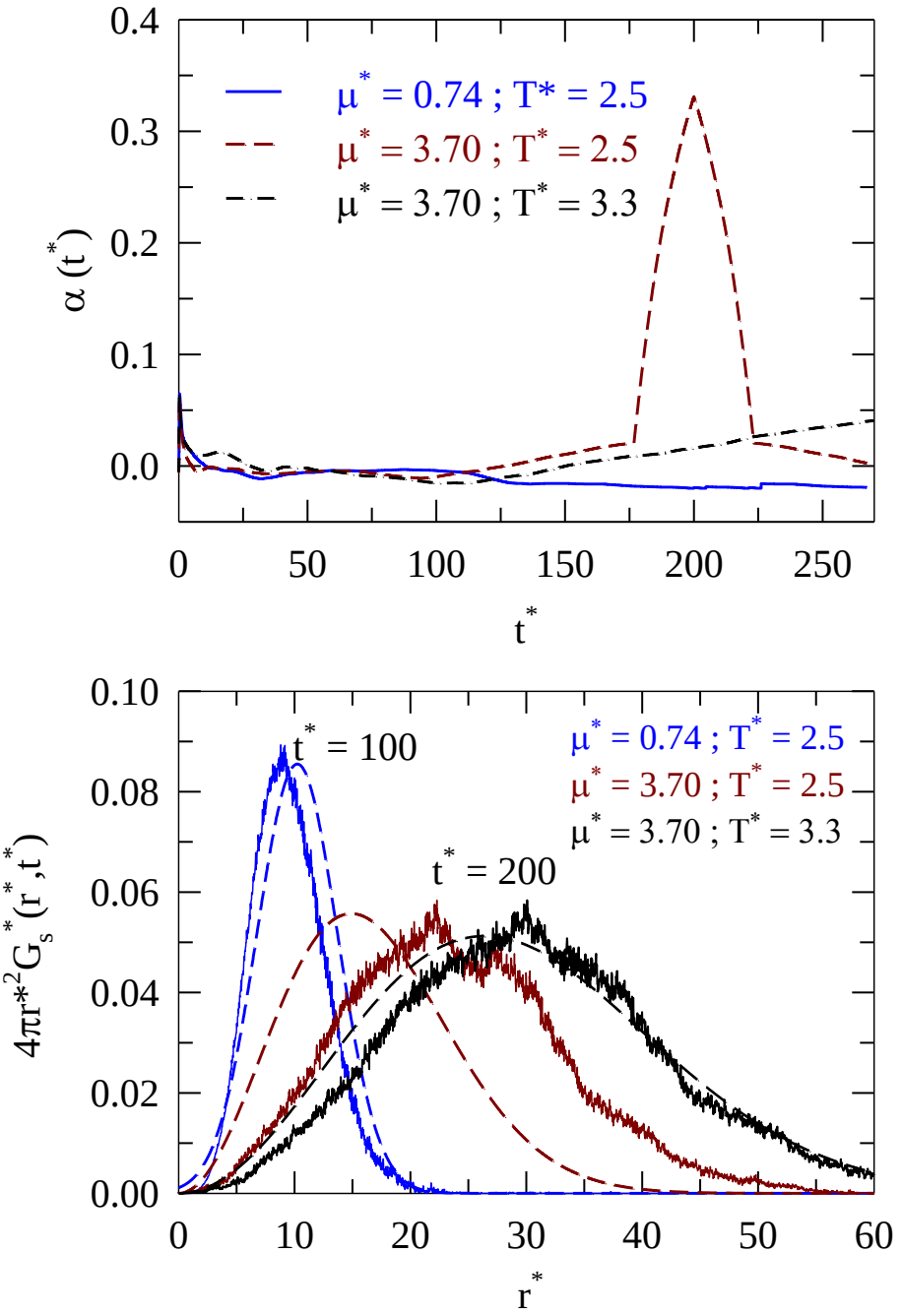

Fig. 9.10: Signatures of dynamic heterogeneity in SM fluids and its temperature and dipole moment dependences. Upper panel shows plots of the simulated non-Gaussian parameter, $\alpha(t)$, associated with centre-of-mass motion of particles for three different values of dipole moment. The curves are color-coded. Lower panel depicts the deviation from Gaussian statistics for particle displacements for SM fluids with different dipole moments and temperatures. As before, the curves are color coded. While the simulated curves are shown by solid lines, dashed lines denote calculations using the following Gaussian approximation[9,35]: $G_s^0(r,t) = \left[3/2\pi\left\langle|\Delta\vec{r}(t)|^2\right\rangle\right]^{3/2} \exp\left(-3r^2/(2\left\langle|\Delta\vec{r}(t)|^2\right\rangle)\right)$.

with $\left\langle \left|\Delta\vec{r}(t)\right|^2 \right\rangle = \frac{1}{N}\left\langle \sum_{i=1}^{N} \left|\vec{r}_i^{\,c}(t) - \vec{r}_i^{\,c}(0)\right|^2 \right\rangle$. For homogeneous harmonic vibrations and in the cases of random walk, $G_s(\vec{r},t)$ is Gaussian and $\alpha(t) = 0$.[9] For hot liquids, $\alpha(t) = 0$ for both at $t = 0$ and $t = \infty$ but $\alpha(t) = 0.2$ (a maximum) at intemediate times.[9]

The simulated $\alpha(t)$ and $G_s(\vec{r},t)$ are presented in Fig. 9.10 for SM fluids with μ^*=0.74 and 3.70. At $T^* = 2.5$ for SM fluid with μ^*=3.7, simulated $\alpha(t)$ curve shows a rather sharp peak at $t^* \approx 200$ which indicates presence of a substantial degree of dynamic heterogeneity in this fluid. Interestingly, the peak vanishes at $T^* = 3.3$, indicating 'homogenization' of particle motions upon raising the solution temperature. In addition, for SM fluids with μ^*=0.74 at $T^* = 2.5$, $\alpha(t)$ remains structureless for the entire simulation period. The displacement statistics shown in the lower panel clearly reveals a significant deviation for the simulated $G_s(\vec{r},t)$ at $t^* \approx 200$ from the predicted Gaussian behaviour for SM fluid at $T^* = 2.5$ with μ^*=3.7 but becomes closer to the Gaussian approximation (dashed lines) either upon decreasing the dipole moment or increasing the solution temperature. The variation of dynamic heterogeneity with dipole moment and temperature for SM fluids therefore explains in microscopic terms (i) the weakening of dipole moment effects on translational diffusion coefficient upon temperature-rise (shown in Fig. 9.4) and (ii) deviation from the SE behaviour for SM fluids with larger dipole moment at relativley lower temperature.

9.4 Conclusion

In this chapter the dipole-moment dependence of transport properties have been studied by molecular dynamics simulations. Medium viscosity has been found to increase as large as by ~60% with dipole moment over the value for the corresponding L-J system at a fixed density and temperature. While the translational diffusion coefficients show a moderate dipole moment dependence which softens up upon raising the solution temperature, rotational diffusion coefficients appear to be insensitive to the magnitude of dipole moment. The

different dependence of the translational and rotational diffusion coefficients has been found to originate from the different sensitivity of the mean square displacements and angular velocity autocorrelation functions to the dipolar interactions. Simulated diffusion coefficients have been found not to follow the conventional hydrodynamic relations with the simulated viscosity coefficients, supporting the notion that break-down of these relations is more widespread than expected. Simulated particle motions at intermediate time have been found to show a substantial deviation from the Gaussian distribution (with respect to particle displacements) for SM fluids with larger dipole moment which reverts back to approximately Gaussian behavior upon either raising the temperature or lowering the dipole moment.

Since the present work has explored the relationship between transport coefficients which are collective properties, a discussion on system size dependence is very much relevant and important. There exist several in-depth studies[12,46,60-61] exploring system size dependences of diffusion coefficients and viscosity and subsequent determination of the stick-slip boundary conditions.[61] All these studies have found, depending upon density and interaction potentials, moderate to small system size dependences. At higher densities like the one considered here, effects of number of particles have been found generally small. Therefore, the numerical values for the transport coefficients reported in the present work may slightly vary if compared with simulations using larger number of particles. However, those variations will not affect the qualitative features reflected by the present simulation study.

References

1. Hansen, J. P.; McDonald, I. R. *Theory of Simple Liquids*, Academic Press: London, 1986.
2. Lakowicz, J. R. *Principles of Fluorescence Spectroscopy*, Kluwar Academic /Plenum: New York, 1999
3. Ediger, M. D. *Annu. Rev. Phys. Chem.* **2000**, *51*, 99.
4. Chakrabarti, D.; Bagchi, B. *Phys. Rev. Lett.* **2006**, *96*, 187801.
5. Abraham, S. E.; Bhattacharyya, S. M.; Bagchi, B. *Phys. Rev. Lett.* **2008**, *100*, 167801.
6. Guchhait, B.; Gazi, H. A. R.; Kashyap, H. K.; Biswas, R. *J. Phys. Chem. B* **2010**, *114*, 5066.
7. Gazi, H. A. R.; Guchhait, B.; Daschakraborty, S.; Biswas, R. *Chem. Phys. Lett.* **2011**, *501*, 358.
8. Guchhait, B; Daschakraborty, S; Biswas, R. *J. Chem. Phys.* **2012**, *136*, 174503.
9. Pal, T; Biswas, R. *Chem. Phys. Lett.* **2011**, *517*, 180.
10. Kirkpatrick, T. R. *Phys. Rev. Lett.* **1984**, *53*, 1735.
11. Kirkpatrick, T. R. *J. Non-Cryst. Solids* **1985**, *75*, 437.
12. Meier, K.; Laesecke, A.; Kabelac, S. *J. Chem. Phys.* **2005**, *122*, 014513.
13. Mukherjee, A.; Bhattacharyya, S.; Bagchi, B. *J. Chem. Phys.* **2002**, *116*, 4577.
14. Bendrov, D.; Smith, G. D.; Sewell, T. D. *J. Chem. Phys.* **2000**, *112*, 7203.
15. Biswanath, D. S. *Viscosity of liquids: Theory, estimation, experiment and data*, Springer, 2007.
16. Stockmayer, W. H. *J. Chem. Phys.* **1941**, *9*, 398.
17. Vesely, F. J. *J. Comput. Phys.* **1977**, *24*, 361.
18. Khordad R, Hosseini F and Papari M M 2009 *Chem. Phys.* **360** 123.
19. Pollock, E. L.; Alder, B. J. *Physica* **1980**, *102A*, 1.
20. Pollock, E. L.; Alder, B. J.; Patey, G. N. *Physica* **1981**, *108A*, 14.
21. Gray, C. G.; Sainger, Y. S.; Joslin, C. G.; Cummings, P. T.; Goldman, S. *J. Chem. Phys.* **1986**, *85*, 1502.
22. Neria, E.; Nitzan, A. *J. Chem. Phys.* **1992**, *96*, 5433.
23. Perera, L.; Berkowitz, M. L. *J. Chem. Phys.* **1992**, *97*, 5253.
24. Roy, S.; Bagchi, B. *J. Chem. Phys.* **1993**, *99*, 1310.
25. Chandra, A. *Chem. Phys. Lett.* **1995**, *235*, 133.
26. Stevens, M. J.; Grest, G. S. *Phys. Rev. E* **1995**, *51*, 5962.
27. Gao, G. T.; Zeng, X. C. *Phys. Rev. E* **2000**, *61*, R2188.

28. Paul, S.; Chandra, A. *J. Phys. Chem. B* **2003**, *107*, 12705.
29. Paul, S.; Chandra, A. *J. Phys. Chem. B* **2007**, *111*, 12500.
30. Allen, M. P.; Tildesley, D. J. *Computer Simulations of Liquids*, Oxford University Press: New York, 1987.
31. Nosé, S. *J. Chem. Phys.* **1984**, *81*, 511.
32. Evans, D. J.; Holian, B. L. *J. Chem. Phys.* **1985**, *83*, 4069.
33. Frenkel, D.; Smit, B. *Understanding Molecular Simulation: From Algorithm to Applications*, Academic Press: London, UK, 1996.
34. McQuarrie, D. A. *Statistical Mechanics*, Viva Books: New Delhi, 2003.
35. Del Popolo, M. G.; Voth, G. A. *J. Phys. Chem. B* **2004**, *108*, 1744.
36. Boon, J. P.; Yip, S. *Molecular Hydrodynamics*, McGraw-Hill: New York, 1980.
37. Biswas, R.; Bagchi, B. *J. Chem. Phys.* **1996**, *105*, 7543.
38. Goharshadi, E. K.; Mansoori, G. A. *Chem. Phys.* **2007**, *331*, 332.
39. Matteoli, E.; Mansoori, G. A. *J. Chem. Phys.* **1995**, *103*, 11.
40. Turulski, J.; Forys, M. *J. Phys. Chem.* **1979**, *83*, 22.
41. Ridge, D. P.; Beauchamp, J. L. *Chem. Phys. Lett.* **1976**, *41*, 2.
42. Borgelt, P.; Hoheisel, C.; Stell, G. *Phys. Rev. A* **1990**, *42*, 789.
43. Cappelezzo, M.; Capellari, C. A.; Pezzin, S. H.; Coelho, L. A. F. *J. Chem. Phys.* **2007**, *126*, 224516.
44. Harris, K. R. *J. Chem. Phys.* **2009**, *131*, 054503.
45. Meier, K.; Laesecke, A.; Kabelac, S. *J. Chem. Phys.* **2004**, *121*, 3671.
46. Meier, K.; Laesecke, A.; Kabelac, S. *J. Chem. Phys.* **2004**, *121*, 9526.
47. Sharma, M.; Yashonath, S. *J. Phys. Chem. B* **2006**, *110*, 17207.
48. Kumar, S. K.; Szamel, G.; Douglas, J. F. *J. Chem. Phys.* **2006**, *124*, 214501.
49. Rajian, J. R.; Huang, W.; Richert, R.; Quitevis, E. L. *J. Chem. Phys.* **2006**, *124*, 014510.
50. Funazukuri, T.; Kong, C. Y.; Kagei, S. *J. Supercrit. Fluids* **2008**, *46*, 280.
51. Kanakubo, M.; Harris, K. R.; Tsuchihashi, N.; Ibuki, K.; Ueno, M. *J. Phys. Chem. B* **2007**, *111*, 2062.
52. Kanakubo, M.; Harris, K. R.; Tsuchihashi, N.; Ibuki, K.; Ueno, M. *J. Phys. Chem. B* **2007**, *111*, 13867.
53. Harris, K. R.; Kanakubo, M.; Tsuchihashi, N.; Ibuki, K.; Ueno, M. *J. Phys. Chem. B* **2008**, *112*, 9830.
54. Sillescu, H. *J. Non-Cryst. Solids* **1999**, *243*, 81.

55. Kumar, P.; Buldyrev, S. V.; Becker, S. R.; Poole, P. H.; Starr, F. W.; Stanley, H. E. *Proc. Natl. Acad. Sci. USA* **2007**, *104*, 9575.
56. Wang, Y.; Voth, G. A. *J. Am. Chem. Soc.* **2005**, *127*, 12192.
57. Roy, D.; Patel, N.; Conte, S.; Maroncelli, M. *J. Phys. Chem. B* **2010**, *114*, 12629.
58. Rahman, A. *Phys. Rev.* **1964**, *136*, 405.
59. Sigurgeirsson, H.; Heyes, D. M. *Mol. Phys.* **2003**, *101*, 469.
60. Yeh, I-C.; Hummer, G. *J. Phys. Chem. B* **2004**, *108*, 15873.
61. Heyes, D. M. *J. Phys.: Condens. Matter* **2007**, *19*, 376106.

Chapter 10

Transport Properties of Binary Mixtures of Asymmetric Particles: A Simulation Study

10.1 Introduction

Study of transport properties of asymmetric particles is of fundamental importance because real molecules more often than not are asymmetric in nature.[1-8] The structural aspects and transport properties of fluids and fluid mixtures containing asymmetric particles are significantly different from those made of spherical entity. Asymmetry in particle shape and interaction can lead to microscopic heterogeneity in solution structure even in model systems at normal condition. Hard rod and disk model is the simplest example of this type of systems which have been used by many authors to study the different structural and dynamical behaviours.[1-7] These model systems are governed by hard repulsive interactions only and therefore attractive interaction among particles find no role in determining various properties of either neat or mixed systems. Gay-Berne (GB) potential, on the other hand, includes both the repulsive and attractive interactions and thus somewhat more realistic for studying properties of liquids made of asymmetric particles. At a very simplistic level, GB interaction has some similarities with that between Lennard – Jones particles.[8,9] Several simulations using GB potential have already explored structural and dynamical aspects of several asymmetric systems.[10-12] The phase behavior of GB fluids is also very interesting because the modified form of GB potential[13] can give rise to liquid crystal. This is an important observation as opto-electronic industries require materials which could be used intelligently for designing and fabricating liquid crystal display devices.

The phase behavior has been extensively studied for GB fluid and three distinctly different phases have been identified namely isotropic, nematic and smectic phase.[14-16] Among these three phases while the smectic phase is the most orientationally ordered, isotropic phase has no orientational ordering, and nematic one lies in between these two. The dynamics of pure GB fluid has been seen to be different for different phases. Interestingly, the diffusion coefficient parallel to the molecular axis shows an anomalous increase with density as the

system enters from the isotropic to nematic region. The Debye diffusion model appears to explain the reorientational mechanism for nematic phase although fails to explain in the isotropic region.[11,12] Both bulk and shear viscosities have been simulated by several researchers and a good agreement between simulations and experiments observed.[17] Molecular dynamics simulations for molecules represented by GB ellipsoid particles and transverse point dipoles have also been reported.[18] Results for polar GB fluid has been compared with the nonpolar GB fluid and it has been seen that for polar one, smectic phase is formed at lower density compared to the nonpolar variety.

Several simulation studies have already been carried out on the translational and rotational dynamics of GB fluid near the isotropic-nematic phase transition (I-N) point as well as in the isotropic phase region.[11,12] These works are more focused towards the verification of hydrodynamic relationships in these regions. Simulations of single particle and collective reorientation correlation functions reveal some interesting results. For example, the decay of the second rank $(l = 2)$ collective orientational relaxation slows down as the I–N transition point is approached. Moreover, the rank dependence predicted by the Debye law also breaks down in this region. The translational diffusion coefficient (D_T) and reorientational correlation time (τ_l) have also been simulated where the product, $D_T \times \tau_l$, remains independent only at higher density and lies in between the slip and stick limits of the Stokes-Einstein-Debye relation only for the GB particles having lower aspect ratio $(\kappa \leq 1.5)$. For higher aspect ratio $(\kappa \sim 3.0)$, however, it rarely shows the above behavior.

Detailed molecular dynamics simulations have been carried out also for GB particles in the sea of spheres. These studies have indicated anisotropic diffusion for the ellipsoids at higher density. In addition, the ratio between parallel and perpendicular diffusion coefficients rises from unity to the value of aspect ratio as density of the system increases.[19-21] The product of the translational diffusion coefficient and reorientational correlation time behaves in a manner similar to that found for pure GB fluid.

The above survey suggests that the binary mixture of GB fluid has not been studied so far by simulation or numerical methods although, as already mentioned, this is important because real systems are more likely to possess either size, shape or interaction asymmetry, or, any

combination of them. The verification of hydrodynamic relations is important for uncovering the nature of solute-solvent interactions in these more complex but model systems. This will certainly help understand the composition dependence of the binary mixture of GB fluids. One expects in these studies a high degree of non-linearity in composition dependence because asymmetric interaction induced non-ideal solution behavior has been observed for LJ mixtures of size-symmetric particles.[22,23]

In this chapter, we have carried out equilibrium molecular dynamics simulations for binary mixtures of GB fluid containing two components of varying aspect ratios near I-N transition in order to study the transport properties of the binary mixture and investigate the non-ideality in this system. Our objective is to investigate the composition dependence of radial distribution function (*g(r)*), pressure (*P*), shear viscosity coefficient (η), translational diffusion coefficients (D_T) (overall, self, and mutual), and rotational correlation time constants (τ_l) of rank, l=1 and 2. We report the product, $D_T \times \tau_l$, which has been found to be nearly independent of mixture composition. The rotational dynamics has been studied where the Debye diffusion model fails to explain the reorientational mechanism. Non ideality has been observed for pressure, self and over-all diffusion coefficients eventhough the extent of non-ideality is always less than 10%. Interestingly, non-ideality is absent for viscosity and mutual diffusion coefficients. The mutual diffusion coefficient remains nearly independent throughout the mole fraction range which qualitatively suggests the mixture is probably homogeneous at all compositions although further analyses are required for a definitive answer.[24]

10.2 Model and Simulation Details

In this section we will discuss about the model we have used and the details of the simulation method.

Molecular dynamics simulations were carried out for binary mixtures using 500 ellipsoids interacting via the following Gay-Berne interaction potential.[9,13]

$$U_{GB}\left(\hat{u}_i,\hat{u}_j,\hat{r}_{ij}\right)=4\varepsilon\left(\hat{u}_i,\hat{u}_j,\hat{r}_{ij}\right)\times \left[\left(\frac{d_w\sigma_0}{r_{ij}-\sigma\left(u_i,u_j,r_{ij}\right)+d_w\sigma_0}\right)^{12}-\left(\frac{d_w\sigma_0}{r_{ij}-\sigma\left(u_i,u_j,r_{ij}\right)+d_w\sigma_0}\right)^{6}\right] \quad (235)$$

, (10.1)

σ_0 is the diameter of the major axis of the ellipsoid, and $\sigma(\hat{r}_{ij}, \hat{u}_i, \hat{u}_j)$ is given by,

$$\sigma(\hat{u}_i, \hat{u}_j, \hat{r}_{ij}) = \sigma_0\left[1-\left\{\frac{\chi\alpha^2(\hat{u}_i\cdot\hat{r}_{ij})+\chi\alpha^{-2}(\hat{u}_j\cdot\hat{r}_{ij})-2\chi^2(\hat{u}_i\cdot\hat{r}_{ij})(\hat{u}_j\cdot\hat{r}_{ij})(\hat{u}_i\cdot\hat{u}_j)}{1-\chi^2(\hat{u}_i\cdot\hat{u}_j)}\right\}\right], \quad (10.2)$$

and

$$\chi = \left[\frac{(l_i^2-d_i^2)(l_j^2-d_j^2)}{(l_j^2-d_i^2)(l_i^2+d_j^2)}\right]^{1/2}, \quad (10.3)$$

$$\alpha^2 = \left[\frac{(l_i^2-d_i^2)(l_j^2+d_i^2)}{(l_j^2-d_j^2)(l_i^2+d_j^2)}\right]^{1/2}, \quad (10.4)$$

where *l* and *d* denote the length and breadth of each particle.

The total well depth parameter can be computed as follows

$$\varepsilon(\hat{u}_i, \hat{u}_j, \hat{r}_{ij}) = \varepsilon_0\,\varepsilon_1^{\nu}(\hat{u}_i, \hat{u}_j)\,\varepsilon_2^{\mu}(\hat{u}_i, \hat{u}_j, \hat{r}_{ij}), \quad (10.5)$$

The orientation-dependent strength terms are calculated in the following manner:

$$\varepsilon_1(\hat{u}_i, \hat{u}_j) = \left[1-\chi^2(\hat{u}_i\cdot\hat{u}_j)\right]^{-1/2}, \quad (10.6)$$

$$\varepsilon_2(\hat{u}_i, \hat{u}_j, \hat{r}_{ij}) = 1-\left\{\frac{\chi'\alpha'^2(\hat{u}_i\cdot\hat{r}_{ij})+\chi'\alpha'^{-2}(\hat{u}_j\cdot\hat{r}_{ij})-2\chi'^2(\hat{u}_i\cdot\hat{r}_{ij})(\hat{u}_j\cdot\hat{r}_{ij})(\hat{u}_i\cdot\hat{u}_j)}{1-\chi'^2(\hat{u}_i.\hat{u}_j)}\right\}, \quad (10.7)$$

where

$$\alpha'^2 = \left[1+\left(\varepsilon_E/\varepsilon_S\right)^{1/\mu}\right]^{-1/2}, \text{ and } \quad \chi' = \frac{1-\left(\varepsilon_E/\varepsilon_S\right)^{1/\mu}}{1+\left(\varepsilon_E/\varepsilon_S\right)^{1/\mu}} \tag{10.8}$$

The total number of particles were kept constant (N=500) across the composition and NVT ensembles were considered for simulations. A cubic box with the conventional periodic boundary conditions was employed for binary mixtures of 500 Gay-Berne prolate ellipsoids with components having different aspect ratios. The first component (C1) was of aspect ratio, κ_1=2.0, and the second component (C2) of κ_2 =1.5. The mole-fraction of C1 was then varied to have binary mixtures at different compositions. All the quantities in the simulation were scaled to appropriate units and the scaled quantities of density, temperature and time denoted by ρ^*, T^*, t^*, respectively. Present simulations were carried out at ρ^*=0.4 and T^* =1.0. The time step Δt^* used was 0.001. The system was equilibrated for 2 × 10^5 time steps and the production involved 1.3 × 10^6 steps for all the mixtures. The d_w in the potential form was set to 1 and the parameters μ and v were set to their canonical values of 2.0 and 1.0, respectively. The asymmetry in energy, $\kappa' = \frac{\varepsilon_s}{\varepsilon_E}$ was set to 5.0 for all the mixtures with ε_s and ε_E denoting the energy parameters for the ellipsoids having end – end and end – side configurations, respectively.

Translational self-diffusion coefficients (D_T) were calculated from both the mean squared displacements ($\left\langle\left|\Delta\vec{r}(t)\right|^2\right\rangle$) and velocity autocorrelation functions (VACF). The mean squared displacements (MSDs) were calculated from the simulated centre-of-mass positional vectors ($\vec{r}_i^{\,c}(t)$)[25,26] using Eq. 9.3 of Chapter 9, which produced D_T via Eq. 9.4. D_T from the VACF were obtained by the Eq. 9.5 of Chapter 9,[25,26] where, $\vec{v}_i$ is the centre-of-mass velocity vector associated with the i^{th} particle and averaging was done over both time and number of particles.

In binary mixtures, mutual diffusion describes the ability of one species diffusing into another. The mutual diffusion coefficient $D_{12}(=D_{21})$ in a binary mixture of species 1 and 2 is defined by Green-Kubo relation as[27-29]

$$D_{12} = \frac{Q}{3Nx_1x_2}\int_0^\infty \left\langle \vec{J}_{12}(t)\cdot \vec{J}_{12}(0)\right\rangle dt\,, \tag{10.9}$$

where relative velocity $\vec{J}_{12}$ is defined as

$$\vec{J}_{12}(t) = x_2\sum_{k=1}^{N_1}\vec{v}_k(t) - x_1\sum_{l=1}^{N_2}v_l(t). \tag{10.10}$$

N denote the total number of particles, x_1 and x_2 mole fractions of species 1 and 2, respectively. $\vec{v}_k(t)$ is the velocity of k^{th} particle of species 1 at time t and $\vec{v}_l(t)$ the velocity of l^{th} particle of species 2 at time t. The thermodynamic factor Q can be expressed as

$$Q = \left[1 + x_1x_2\rho\left(G_{11} + G_{22} - 2G_{12}\right)\right]^{-1} \tag{10.11}$$

with

$$G_{ij} = 4\pi\int_0^\infty r^2\left[g_{ij}(r) - 1\right]dr \tag{10.12}$$

where ρ is the number density and $g_{ij}(r)$ the radial distribution function for pair of species ij.

To study the reorientational motion associated with l = 1 and 2, we calculated the single-particle reorientational correlation functions defined by[25]

$$C_l^{(s)}(t) = \frac{\left\langle P_l\left(\hat{e}_i(0)\cdot\hat{e}_i(t)\right)\right\rangle}{\left\langle P_l\left(\hat{e}_i(0)\cdot\hat{e}_i(0)\right)\right\rangle}\,, \tag{10.13}$$

where $\hat{e}_i(t)$ is the unit vector along the symmetry axis of molecule i and P_l is the l-th order Legendre polynomial. In the above equations, the angular bracket implies an average over the particles as well as over the time origins.

Shear viscosity coefficient (η) was calculated using the Green-Kubo relation,[30,31] given in Eq. 9.7 of Chapter 9, where, $\alpha, \beta = x, y, z$ and $P_{\alpha\beta}$ denotes the off-diagonal term of the pressure tensor (Eq. 9.8 of Chapter 9).

As before, the above correlation functions were also averaged over particles and time.

The pressure was then obtained from the simulated diagonal terms of the pressure tensor by employing the following expression

$$P = \frac{1}{3} Tr[P] = \frac{1}{3} \sum_{\alpha} P_{\alpha\alpha} \qquad (10.14)$$

10.3 Results and Discussion

Effects of C1 (component with higher aspect ratio) on the *average* radial distribution function ($g(r)$) has been depicted in Fig. 10.1 for four representative compositions. It is evident from this figure that the simulated $g(r)$ undergoes several modifications as mixture composition is altered by changing mole-fraction (x_1) of C1. The peak position of $g(r)$ shifts towards longer distance along with decrease in peak height as x_1 in the mixture is increased. Interestingly, a hump at r ~ 0.75 may be noticed which becomes more prominent upon increasing x_1. These two regions have been shown separately in the insets for better visualization. This indicates the gradual rise of the probability of cross configuration over end – end and side - side configurations as the binary mixture becomes enriched with particles of higher aspect ratio. This is supported by the potential energy diagram for the Gay-Berne interaction where it has been found that the depth of the potential energy well for cross configuration is higher than that for end – end and side – side configurations both for ellipsoids and disks.[32] It should be noted that the formation of hump at r ~ 0.75 has been found previously by other researchers as well for isotropic and discotic-nematic phase.[33]

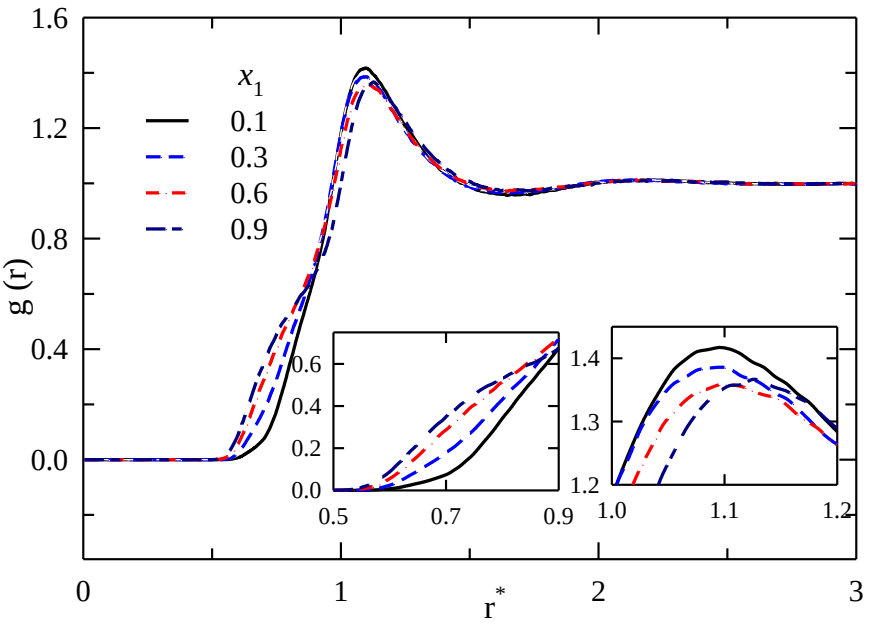

Fig. 10.1: Plots of simulated over-all radial distribution function ($g(r)$) for systems with different compositions. Two insets represent $g(r)$ for r ~0.75 and 1 for better visualization. Different curves are color-coded and explained in the plot. x_1 represents the mole-fraction of the first component ($\kappa = 2$) in the binary mixture.

Fig. 10.2 represents the mean square displacement (MSD), normalized velocity autocorrelation function (VACF) as a function of time in the upper and middle panel respectively, and translational diffusion coefficient ($D^*_{overall}$) as a function of x_1 in lower panel.

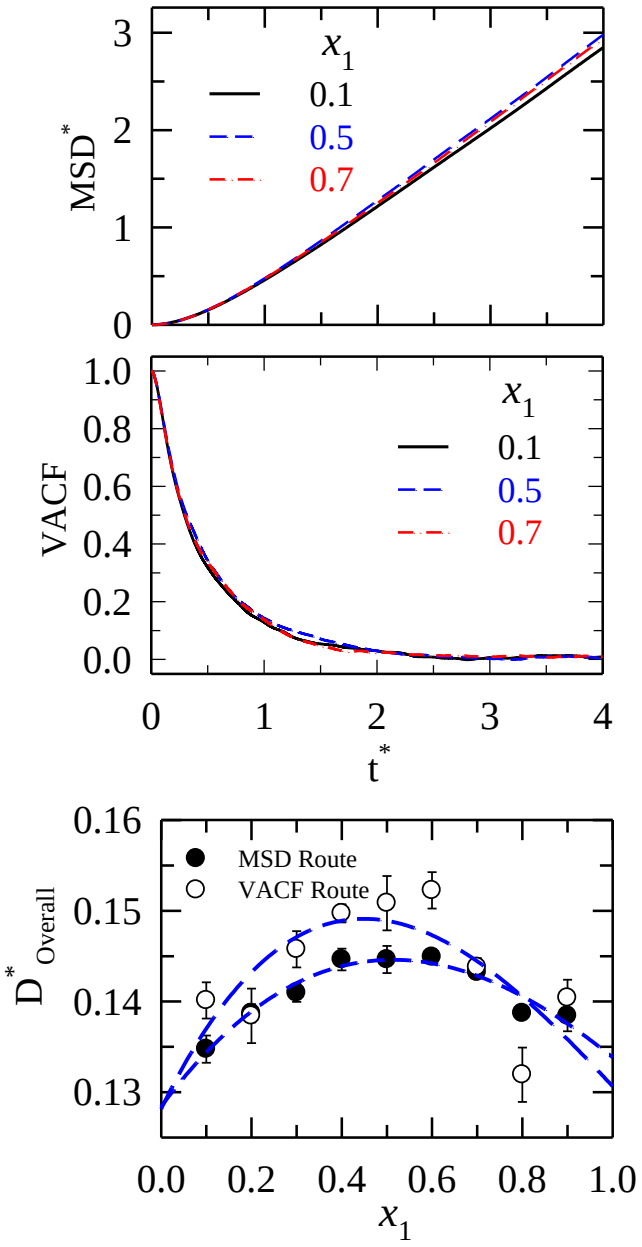

Fig. 10.2: Upper Panel: Simulated mean square displacements (MSDs) for the overall systems as a function of time at four representative compositions. Middle Panel: Simulated normalized velocity auto-correlation function (VACF) as a function of time at the same four representative compositions. Lower Panel: Overall Translational diffusion coefficient, $D^*_{Overall}$ (calculated from VACF and MSD plot) as a function of mole fraction of 1st species. Error bars have been computed via block average. Lines going through the data are for visual guide.

Both the MSD and VACF plots suggest weak composition dependence. This is reflected in the lower panel where $D^*_{overall}$ (calculated from both Eqs. 9.4, and 9.5) has been plotted as a function of x_1. $D^*_{overall}$ increases to a maximum value at x_1~0.5 and then decreases upon

further increase of x_1 . Although the magnitude of variation is small (~13%), the systematic decrease probably suggests a kind of structural transition of the binary mixture. As the system passes through the 0.5 mole fraction, the system makes a transition from C2 dominated to C1 enriched regime. The higher diffusion coefficient at x_1 ~ 0.5 mole fraction may arise due to the least effective packing of the ellipsoids in the system. A previous theoretical investigation involving binary mixtures of hard spheres and ellipsoids predicted relatively less compact packing nearly at 50:50 composition.[34] The extrapolated value of diffusion coefficient ($D^*_{overall}$) for pure C1 is ~ 0.13 which is in close agreement to earlier simulated value obtained by using pure Gay-Berne particles having aspect ratio $\kappa = 2$ at comparable density and temperature.[12]

Self diffusion coefficients for the two components have been calculated separately by using Eqs. 9.4 (MSD route) and 9.5 (VACF route) and finally the mean values have been plotted in Fig. 10.3. The upper and middle panels of the Fig. 10.3 are the plots for self diffusion coefficients of C1 (D_1^*) and C2 (D_2^*) respectively as a function of x_1. D_1^* decreases almost steadily with x_1, although the extent of decrease is somewhat small (~12 %). D_1^* is nearly equal to $D^*_{overall}$ at x_1=0.9 which is expected because the self diffusion of any species in a binary mixture dominated by that species should be nearly equal to the overall diffusion of the system. Unlike D_1^*, D_2^* exhibits a non-monotonic composition dependence with a peak at $x_1 \approx 0.6$, although the overall change is only ~11% of the initial value of D_2^*. As expected, D_2^* is also nearly equal to $D^*_{overall}$ at x_1=0.1. A closer inspection of these two plots in Fig. 10.3 reveals that the self diffusion coefficients of two species are nearly the same at x_1=0.5. This probably signals a structural transition occurring at this composition. This structural transition has not been seen earlier for asymmetric binary fluid mixtures. The lower panel of Fig. 10.3 represents the mutual diffusion coefficient of the species as a function of x_1. In binary liquid mixtures, mutual diffusion is related to the ability of one species diffusing into the other. This is different from self-diffusion which is a measure of mobility of each component in the absence of any external force that means the diffusion of a given species in an environment created only by that species. Therefore, mutual diffusion involves collective motion of many particles of different species together in the mixture and arises due to the gradient of the composition (or chemical potential). Mutual diffusion can be expressed in

terms of velocity correlation functions of the collective motion of the system or in terms of mean square displacement of the centre of mass of the particles of either of the two components. The mutual diffusion coefficient, $D_{12}\ (=D_{21})$ in a binary mixture of species 1 and 2 has been obtained by using the Green – Kubo relation[27-29] expressed in Eq. 10.12. The lower panel of the Fig. 10.3 shows the mutual diffusion coefficient is nearly constant to the variation in composition within the uncertainty limits. The statistical error in mutual diffusivity is of great concern and could be reduced up to some extent by averaging over more simulation runs. This insensitivity of mutual diffusion

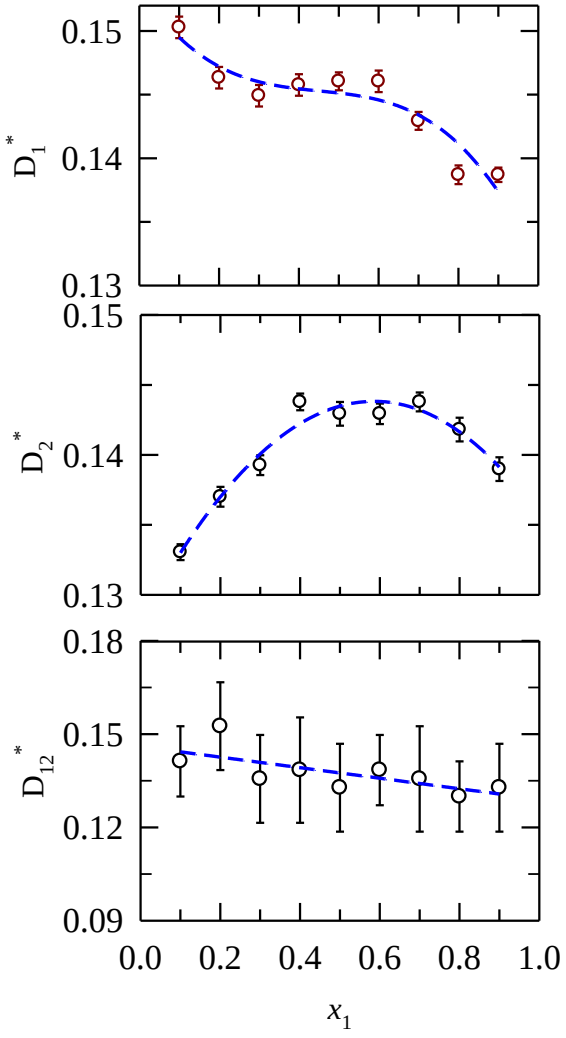

Fig. 10.3: Composition dependence of simulated self diffusion coefficient of 1st component having aspect ratio, $\kappa = 2.0$ (Upper Panel), 2nd component having $\kappa = 1.5$ (Middle panel), and the mutual diffusion coefficient (Lower panel). Error bars have been computed via block average. Lines going through the data are for visual guide.

coefficient to mixture composition may arise from the strong miscibility of components in the binary mixture, but a more precise study warrants simulations using thermodynamic integration method[24].

Fig. 10.4 represents the plot for viscosity coefficient (η^*) as a function of x_1. η^* has been calculated from the integration of stress auto-correlation function,[30,31] by using Eq. 10.17.

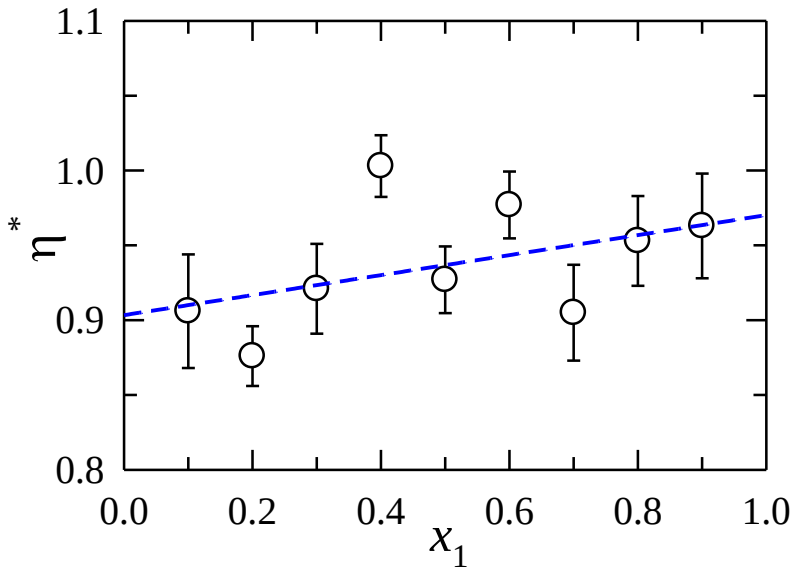

Fig. 10.4: Plot for shear viscosity coefficient as a function of mole fraction of 1st species. computed via block average. Lines going through the data are for visual guide.

The figure shows that η^* remains almost constant in the entire mole fraction range and, more interestingly, does not show any type of non-ideal behavior which is not expected from diffusion behaviour (Fig. 10.3). The absence of non-ideality of η^* may be due to the large estimation error which is very much clear from the plot. We would like to mention here that, η^* being more collective in nature than diffusion coefficient, simulations of the former is less trivial than the latter. Thus the collectiveness and large error of estimation of viscosity coefficient have made the simulated viscosities more imprecise than the diffusion

coefficients. Molecular dynamics simulations have been done previously for the GB model of liquid crystals in the nematic and isotropic phases.[17] The temperature dependence of shear viscosities is in good agreement with experimental data.[35,36] The viscosity obtained in that calculation is two to three times higher than our result for nearly pure GB fluid of higher aspect ratio. This may arise due to lower aspect ratio of the ellipsoid used in this calculation compared to previous study.

Pressure has been computed by using Eq. 10.19 from the simulated pressure tensor and plotted in Fig. 10.5 as a function of x_1.

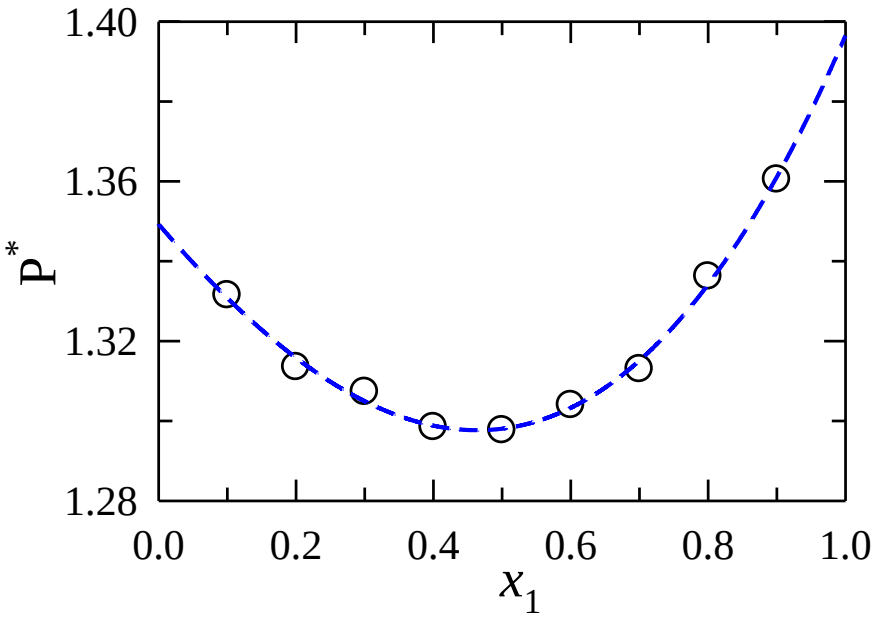

Fig. 10.5: Composition dependence of simulated pressure. Lines going through the data are for visual guide.

The simulated pressure shows a non-ideal composition dependence which can be explained in terms of packing. Pressure derives contributions from thermal energy, and virial term which is the product of inter-particle distance (r_{ij}) and force (F_{ij}) (Eq. 9.9 (Chapter 9)).

Being thermal energy constant throughout the composition range, the virial term is only responsible for variation. That means at the equal proportion of the two species in the

mixture, the total interaction is the least and that may arise due to loose packing. As aspect ratios are different, the packing will not be as tight as in same aspect ratios case, and consequently, the presence of void space produces lower pressure. Note this aspect has not been clearly reflected in the viscosity coefficient (Fig. 10.4) because of inaccuracy involved with the simulated values. Fig. 10.5 also suggests that eventhough the simulated pressure at x_1 = 0.9 is somewhat smaller (~ 1.36) than that (~ 2.0) for pure GB fluid (x_1 = 1.0) at comparable conditions,[12] the slope of the present data indicates very similar value for pressure at x_1 = 1.0.

Fig. 10.6 depicts reorientational time correlation function (RTCF) of ranks, l = 1 and 2 for a representative composition, x_1=0.1 (upper panel) and the product of translational diffusion coefficient and rotational correlation time ($D_T \times \tau_L$) as a function of x_1 (lower panel). RTCF has been calculated by Eq. 10.13. The upper panel shows that RTCF of first rank (l = 1) decays at a rate slower than that of second rank (l = 2). This is expected. For other compositions, this trend remains the same. Rotational correlation time constant has been obtained via time-integration of RTCF as follows

$$\tau_L = \int_0^\infty dt\, C_l^{(S)}(t) \qquad (10.21)$$

In the Table 10.1, we have shown x_1 dependence of τ_1 and τ_2, where it is observed that both the time constants are almost invariant with composition of the mixture. In the same table the ratio, τ_1/τ_2, has also been shown. Interestingly, the ratio is ~1.5, which is half of the predicted value by Debye's law for the rank dependence of reorientational motion in normal liquids. This deviation is also seen previously for pure GB fluid near the I-N transition .[11] In the lower panel of the Fig. 10.6, we have plotted $D_T \times \tau_L$ as a function of x_1. Interestingly, this remains constant throughout the mole fraction range. The hydrodynamic values (combined SE and SED relation) predicted for this case are also plotted in the same figure. Tangs and Evans[37] have reported the Stokes-Einstein products $\mu = D_T \eta$, for neat hard

ellipsoids of aspect ratio ranging from 1 to 10 and both for slip and stick boundary conditions. The rotational diffusion coefficient $D_R = k_B T/\xi_R$ can be computed from rotational friction ξ_R given by[12]

$$\xi_R = \pi\eta a^3 \xi_z, \tag{10.22}$$

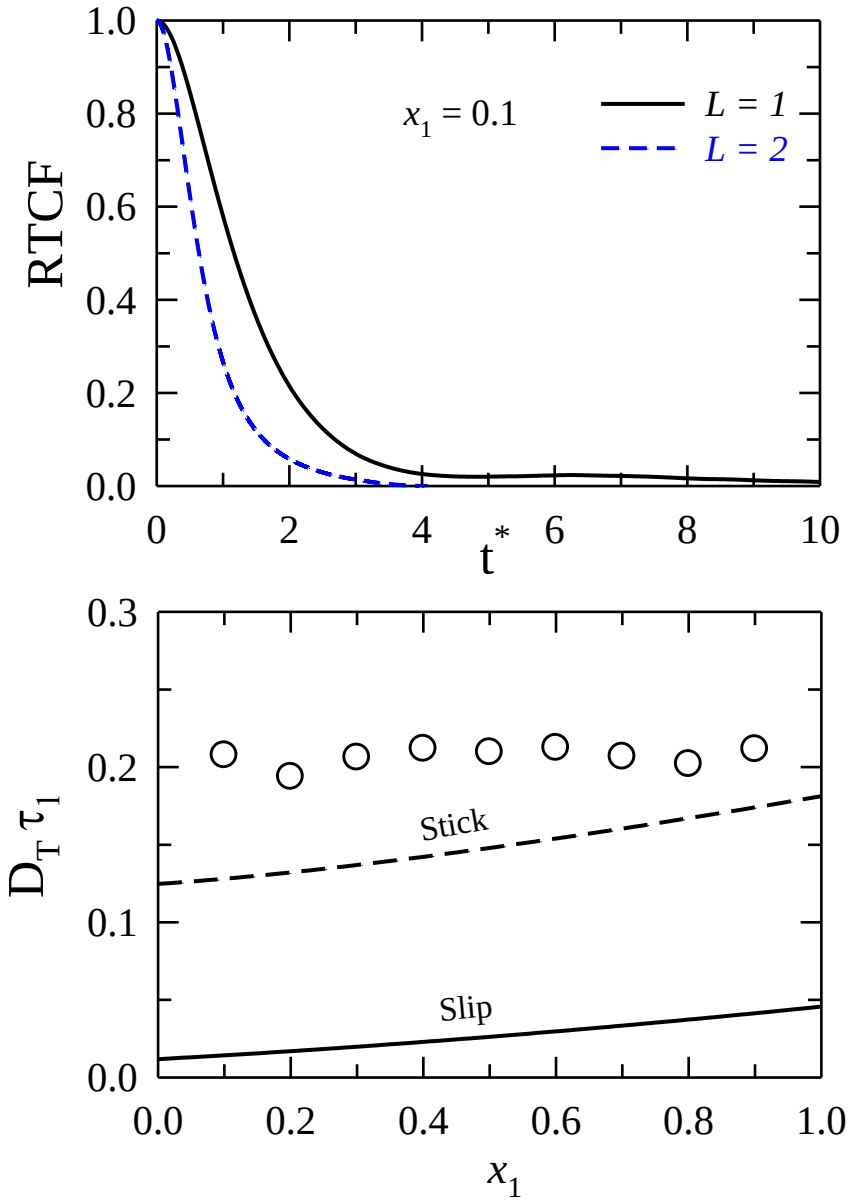

Fig. 10.6: Upper Panel: Plot for the reorientational correlation function against time for a representative composition ($x_1 = 0.1$). Lower Panel: The product of the translational diffusion coefficient, D_T and the average orientational correlation time, τ_1 of the first-rank correlation function, as a function of composition. Note that the solid line and dashed line indicate the hydrodynamic predictions with the stick and slip boundary conditions, respectively.

Table 10.1: Composition dependence of orientational correlation time of rank = 1 and 2, and the ratio between the two. x_1 denote the mole-fraction of the first component ($\kappa = 2$) in the binary mixture.

x_1	τ_1^*	τ_2^*	τ_1/τ_2
0.1	1.51	0.99	1.53
0.2	1.40	0.96	1.46
0.3	1.45	0.96	1.51
0.4	1.44	0.94	1.53
0.5	1.46	0.94	1.55
0.6	1.44	0.93	1.55
0.7	1.48	0.96	1.50
0.8	1.44	0.96	1.54
0.9	1.44	0.94	1.53

where ξ_z may be computed by using the formalism proposed in Ref. 37. Such a calculation has been done for the neat GB fluid as a function of density.[12] Using the relation, $\tau_L^{(S)} = \left[L(L+1)D_R\right]^{-1}$ we can now express the product, $D_T \times \tau_L$ in terms of μ and ξ_z as follows:

$$D_T \tau_L = (\mu \xi_z) \frac{\pi}{16} \frac{\kappa^{8/3}}{L(L+1)} \sigma_0^2 \qquad (10.23)$$

This expression holds for pure GB fluid for stick and slip conditions with the corresponding values for μ and ξ_z. We have modified this expression for our systems containing GB particles having different aspect ratios. We have plotted the ξ_z values as function of effective aspect ratio, $\kappa = x_1\kappa_1 + x_2\kappa_2$, from Ref. 38 and fitted with a cubic equation to get the following equation,

$$\begin{aligned} \xi_z^{Stick} &= 0.5132 + 4.0441\left(\kappa^{-1}\right) - 9.874\left(\kappa^{-1}\right)^2 + 5.3315\left(\kappa^{-1}\right)^3, \\ \xi_z^{Slip} &= \left[0.9336 - 1.4186\left(\kappa^{-1}\right) - 0.2804\left(\kappa^{-1}\right)^2 + 0.7814\left(\kappa^{-1}\right)^3\right] \times \left[\xi_z^{Stick}\right], \end{aligned} \qquad (10.24)$$

Unlike ξ_z, when we plotted the parameter μ as a function of κ from Ref. 36, we found linear dependence and to obey the following relations,

$$\mu^{Stick} = 0.1083 - 0.042(\kappa)$$
$$\mu^{Slip} = 0.1427 + 0.0128(\kappa) \qquad (10.25)$$

calculated products obeying stick and slip limits are denoted by the lines in the lower panel of Fig. 10.6. More interestingly, the simulated product, $D_T \times \tau_1$, is nearly constant and lies above the calculated product obeying stick hydrodynamic condition.

10.4 Conclusion

In this chapter the binary mixture of GB particles of different aspect ratios have been studied by Molecular Dynamics simulation. The composition dependence of different static and dynamic properties has been studied. The radial distribution function has been found to show some interesting features. Simulated pressure and over-all diffusion coefficient exhibit non-ideal composition dependence. However, simulated viscosity does not show any clear non-ideality. The mole fraction dependence of self diffusion coefficients qualitatively signal some kind of structural transition in the 50:50 mixture. The rotational correlation study shows non-Debye behavior in its rank dependence. The product of translational diffusion coefficient and rotational correlation time (first rank) has been found to remain constant across the mixture composition and lie above the stick prediction.

References

1. Rebertus, D. W.; Sando, K. M. *J. Chem. Phys.* **1977**, *67*, 2585.
2. Allen, M. P.; Frenkel, D. *Phys. Rev. Lett.* **1987**, *58*, 1748.
3. Talbot, J.; Allen, M. P.; Evans, G. T.; Frenkel, D.; Kivelson, D. *Phys. Rev. A* **1988**, *39*, 4330.
4. Frenkel, D.; Maguirre, J. F. *Mol. Phys.* **1983**, *49*, 503.
5. Kushik, J.; Berne, J. *J. Chem. Phys.* **1976**, *64*, 1362.
6. Frenkel, D.; Mulder, B. M.; McTague, J. P. *Phys. Rev. Lett.* **1984**, *52*, 287.
7. Allen, M. P. *Phys. Rev. Lett.* **1990**, *65*, 2881.
8. Magda, J. J.; Davis, H. T.; Tirrell, M. *J. Chem. Phys.* **1986**, *85*, 6674.
9. Berne, B. J.; Pechukas, P. *J. Chem. Phys.* **1972**, *56*, 4213.
10. Miguel, E. D.; Rull, L. F.; Gubbins, K. E. *Phys. Rev. A* **1992**, *45*, 3813.
11. Perera, A.; Ravichandran, S.; Morean, M.; Bagchi, B. *J. Chem. Phys.* **1997**, *106*, 1280.
12. Ravichandran, S.; Perera, A.; Morean, M.; Bagchi, B. *J. Chem. Phys.* **1997**, *107*, 8469.
13. Berne, B. J.; Pechukas, P. *J. Chem. Phys.* **1981**, *74*, 3316.
14. Miguel, E. D.; Rull, L. F.; Chalam, M. K.; Gubbins, K. E. *Mol. Phys.* **1991**, *74*, 405.
15. Luckhurst, G. R.; Stephens, R. A.; Phippen, R. W. *Liq. Cryst.* **1990**, *8*, 451.
16. Luckhurst, G. R.; Simmonds, P. S. J. *Mol. Phys.* **1993**, *80*, 233.
17. Smondyrev, A. M.; Loriot, G. B.; Pelcovits, R. A. *Phys. Rev. Lett.* **1995**, *75*, 2340.
18. Gwóźdź, E.; Bródka, A.; Pasterny, K. *Chem. Phys. Lett.* **1997**, *267*, 557.
19. Ravichandran, S.; Bagchi, B. *J. Chem. Phys.* **1999**, *111*, 7505.
20. Vasanthi, R.; Ravichandran, S.; Bagchi, B. *J. Chem. Phys.* **2001**, *114*, 7989.
21. Vasanthi, R.; Ravichandran, S.; Bagchi, B. *J. Chem. Phys.* **2001**, *115*, 10022.
22. Mukherjee, A.; Bagchi, B. *J. Phys. Chem. B* **2001**, *105*, 9581.
23. Srinivas, G.; Mukherjee, A.; Bagchi, B. *J. Chem. Phys.* **2001**, *114*, 6220.

24. Jedlovszky, P.; Idrissi, A.; Jancsó, G. *J. Chem. Phys.* **2009**, *130*, 124516.

25. McQuarrie, D. A. *Statistical Mechanics* **2003** (Viva Books, New Delhi).

26. Del Pópolo, M. G.; Voth, G. A. *J. Phys. Chem. B* **2004**, *108*, 1744.

27. Kamala, C. R.; Ayappa, K. G.; Yashonath, S. *Phys. Rev. E* **2002**, *65*, 061202.

28. Zhou, Z.; Todd, B. D.; Travis, K. P.; Sadus, R. J. *J. Chem. Phys.* **2005**, *123*, 054505.

29. Zhang, L.; Liu, Y.; Wang, Q. *J. Chem. Phys.* **2005**, *123*, 144701.

30. Hansen, J. P.; McDonald, I. R. *Theory of Simple Liquids*, Academic Press: London, 1986.

31. Allen, M. P.; Tildesley, D. J. *Computer Simulations of Liquids*, Oxford University Press: New York, 1987

32. Luckhurst, G. R.; Simmonds, P. S. J. *Mol. Phys.* **1993**, *80*, 233.

33. Chakraborty, D.; Wales, D. J. *Phys. Rev. E* **2008**, *77*, 051709.

34. Perera, A.; Cassou, K.; Ple, F.; Dubois, S. *Mol. Phys.* **2002**, *100*, 3409.

35. Miesowicz, M. *Nature (London)* **1946**, *158*, 27.

36. Chmielewski, A. G. *Mol. Cryst. Liq. Cryst.* **1986**, *132*, 339.

37. Tang, S.; Evans, T. *Mol. Phys.* **1993**, *80*. 1443.

38. Hu, C-M,; Zwanzig, R. *J. Chem. Phys.* **1974**, *60*, 4354.

Chapter 11

Heterogeneity in Structure and Dynamics of Binary Mixture of Asymmetric Particles inside a Cylindrical Nanopore: Investigation Using Molecular Dynamics Simulation

11.1 Introduction

Study of various liquids under confinement is extremely interesting not only from basic scientific view but also for their possible applications in nano-fluidics and drug delivery.[1-16] Both experimental and simulation studies have shown that the macroscopic behaviour of a liquid can change considerably when it is encapsulated.[17,18] For example, it is seen that the static dielectric constant of pure water in confinement remarkably decreases from high value (~80) to such a low value that it behaves almost like a low-polar liquid.[1,3] Water in carbon-nanotube has been extensively studied using computer simulations in order to understand the effect of confinement on various structural and dynamical characteristics.[11-19] Recently, a combined dynamic fluorescence and all-atom molecular dynamics simulation study on solute and solvent dynamics in neutral and reverse micelles have been carried out to investigate the confinement effects on solute-centred relaxation processes.[8] Dimensional crossover in model fluids under nano confinement and the influence of the nature of the boundary wall (attractive or repulsive) have also been studied recently using computer simulation technique.[20]

Studies of transport properties of asymmetric particles is of fundamental importance because the structural aspects and transport properties of fluids and fluid mixtures are expected to be different from those made of spherical entity.[21-24] Gay-Berne[25,26], being the simplest form of potential to mimic the real liquid crystal phase, is extremely interesting and has attracted many researchers to investigate the various properties of this model liquid both in bulk phase[21-30] and in confined environment[31,32]. We have also seen in the previous chapter (Chapter 10) that molecular dynamics simulations of binary mixture of Gay-Berne particles

(interacting via Gay-Berne potential) of different aspect ratios in liquid phase can provide clear understanding on the composition dependence of structural and dynamical properties of these mixtures.[21]

These binary mixtures show non-ideal composition dependence for static (e.g. pressure) and dynamical quantities (e.g. diffusion).[21] Whereas the structural property, such as, radial distribution function ($g(r)$) has been seen to be little influenced by the composition of the binary mixture, the transport properties (diffusion coefficient, viscosity etc.) exhibit more sensitivity.[21]

The confinement on the binary mixture of Gay-Berne liquids can lead to a dramatic change of structure and dynamics from the bulk behavior. This system is interesting due to the applications in the field of nanotechnology and optoelectronic research. Recently the confinement effect on the structure and dynamics of Gay-Berne fluid has been studied using molecular dynamics simulation, where pronounced confinement effects on density distribution, translational and rotation diffusion has been found.[31,32]

The effects of confinement on the microscopic properties of binary mixture of Gay-Berne fluids having two different aspect ratios of the particles are worth studying. In this chapter, we present the molecular dynamics (MD) simulation studies of structural and dynamical characteristics of binary mixture of Gay-Berne fluids of different shapes, confined in a cylindrical nano-channel of diameter ~1 nm. The wall of the channel, being made of Lennard-Jones (LJ) particles having attractive and repulsive parts, can mimic a realistic wall. Previous studies have shown that the aspect ratio of Gay-Berne particles play a major role in determining the microscopic structure and dynamics of this liquid.[23] Transition among different phases (isotropic, nematic and smectic) can be attained simply by changing the aspect ratio of the Gay-Berne particles. In this work we have varied the aspect ratio of one component in order to see the effects on various structural and transport properties of the binary mixture. Density profile along the radius of the channel has been simulated to check whether there is any density inhomogeneity in the system. In addition, dynamical

heterogeneity can be visualized by calculating the translational diffusion coefficient of the particles depending upon the distance from the wall.

11.2 Model and Simulation Details

In this section we will discuss about the model used, and the details of the simulation method. Molecular dynamics simulations were carried out for binary mixtures using 500 ellipsoids interacting via the Gay-Berne interaction potential.[25,26] The Gay-Berne potential form has been discussed in details in the previous Chapter 10 (Eq. 10.1 – Eq. 10.8). We have made the cylindrical channel of diameter 10σ and length 20σ by placing 1176 LJ particles in such a way that there is no gap in the wall having larger size than a Gay-Berne particle and thus the movement of the liquid particles through the wall can be restricted. The interaction between the wall particles (LJ-LJ) has not been taken into account because the channel has been assumed to be rigid. The interaction potential, acting between Gay-Berne ellipsoid and LJ particle, is written as following,

$$U_{GB}\left(\hat{u}_j,\hat{r}_{ij}\right)=4\varepsilon\left(\hat{u}_j,\hat{r}_{ij}\right)\times\left[\left(\frac{d_w\sigma_0}{r_{ij}-\sigma\left(u_j,r_{ij}\right)+d_w\sigma_0}\right)^{12}-\left(\frac{d_w\sigma_0}{r_{ij}-\sigma\left(u_j,r_{ij}\right)+d_w\sigma_0}\right)^{6}\right], \qquad (11.1)$$

$$\text{where } \sigma\left(u_j,r_{ij}\right)=\sigma_0\left[1-\left\{\chi\alpha^{-2}\left(\hat{u}_j\cdot\hat{r}_{ij}\right)\right\}\right];\ \ \chi\alpha^{-2}=\left[\frac{\left(l_j^{\,2}-d_j^{\,2}\right)}{\left(l_j^{\,2}-d_i^{\,2}\right)\left(l_j^{2}+d_i^{\,2}\right)}\right], \qquad (11.2)$$

$$\text{and } \varepsilon\left(\hat{u}_j,\hat{r}_{ij}\right)=\varepsilon_0\left[1-\chi'\alpha'^{2}\left(\hat{u}_i\cdot\hat{r}_{ij}\right)\right];\ \alpha'^{2}=\left[1+\left(\varepsilon_E/\varepsilon_S\right)^{1/\mu}\right]^{-1/2} \text{ and } \chi'=\frac{1-\left(\varepsilon_E/\varepsilon_S\right)^{1/\mu}}{1+\left(\varepsilon_E/\varepsilon_S\right)^{1/\mu}} \quad (11.3)$$

Here *l* and *d* denote the length and breadth of each particle. Note that d_i is the diameter of the LJ particle.

A total of 500 Gay-Berne particles of two different aspect ratios were placed inside a cylindrical channel in cuboid lattice as an initial configuration, and periodic boundary condition along z-axis has been employed. The initialized system has been shown in Scheme 1. Four different mixtures of fixed compositions were considered varying the aspect ratio (κ_1) of first component (C1) keeping the aspect ratio (κ_2) of second constituent (C2) fixed. Thus, the four binary mixtures differ by the value of $R(\kappa_I/\kappa_{II})$. Table 11.1 shows the detailed information about the systems. All the quantities in the present simulations were scaled to appropriate units and the scaled quantities of density, temperature and time denoted by ρ^*, T^*, t^*, respectively. This simulations were carried out at ρ^*=0.32 and T^*=1.0.

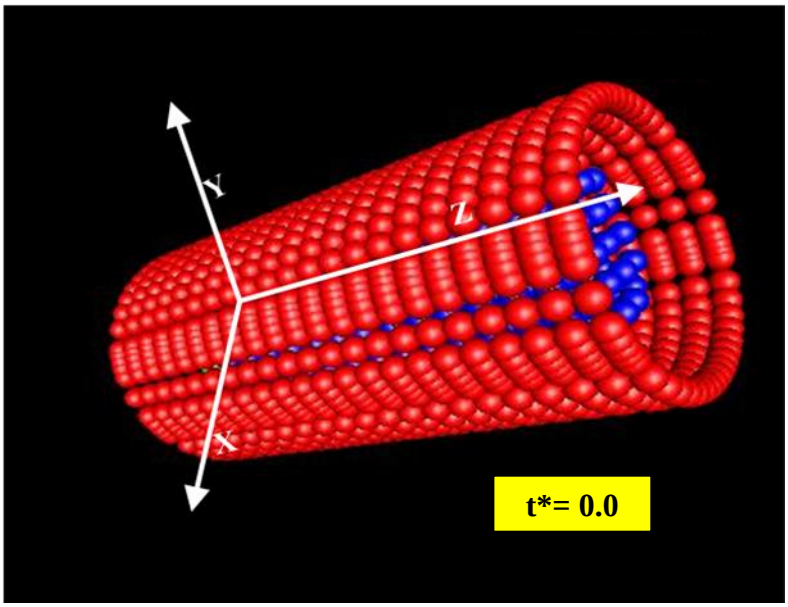

Scheme 11.1: Snapshot of the simulated system at initial configuration (t* = 0.0)

Velocity Verlet algorithm has used for the integration where the time step Δt^* is 0.001. The system was equilibrated for 2×10^5 time steps and the production involved 1.3×10^6 steps for all the mixtures. The d_w in the potential form was set to 1 and the parameters μ and ν were set to their canonical values of 2.0 and 1.0, respectively. The asymmetry in energy,

$\kappa' = \varepsilon_s / \varepsilon_E$ was set to 5.0 for all the mixtures with ε_s and ε_E denoting the energy parameters for the ellipsoids having end – end and end – side configurations, respectively.

Table 11.1: Table for defining the binary mixtures

System	κ_1	κ_2	$R = \kappa_I / \kappa_{II}$	x_1	ρ^*	T^*
Mixture-1	1.2	1.2	1.00	0.5	0.32	1.0
Mixture-2	1.8	1.2	1.50	0.5	0.32	1.0
Mixture-3	2.4	1.2	2.00	0.5	0.32	1.0
Mixture-4	2.7	1.2	2.25	0.5	0.32	1.0

11.3 Results and Discussion

11.3.1 Radial Density Profile

Radial Density profile for these systems has been shown in Fig. 11.1, where the upper and lower panels represent the radial profile for density of C1 and C2 respectively. Here densities (ρ_1^* and ρ_2^*) of the two components, depending upon the distance from the wall, has been simulated in order to

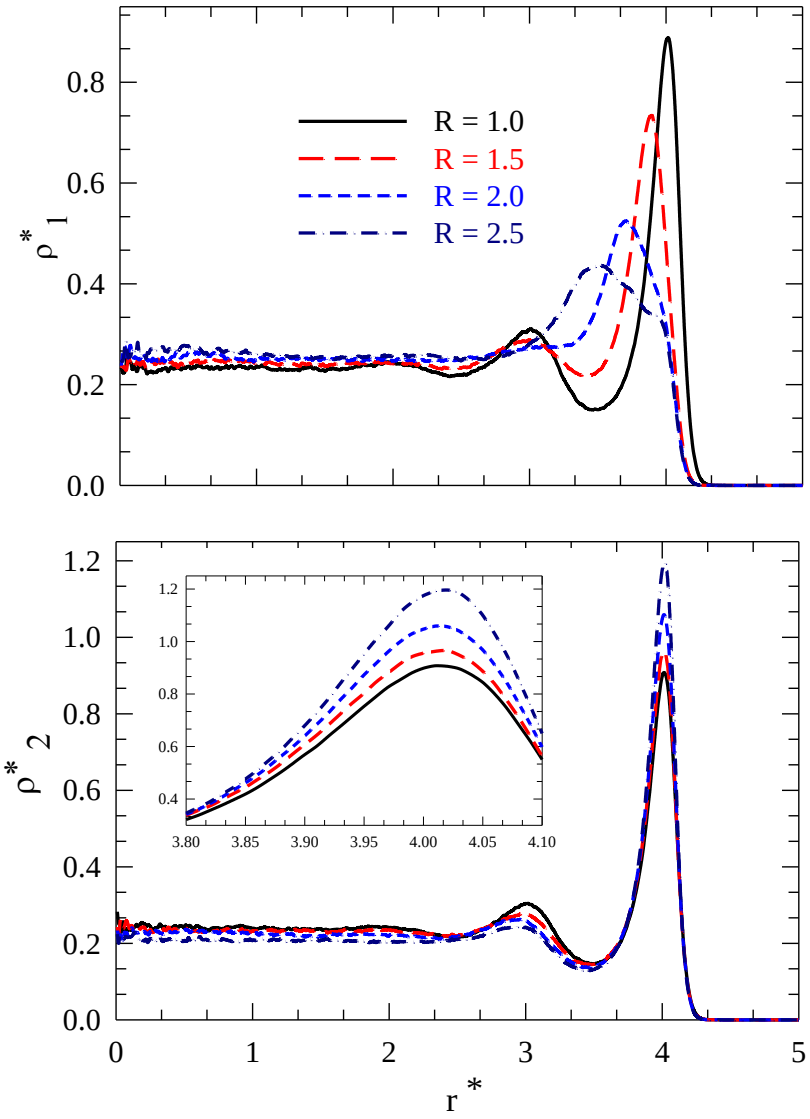

Fig. 11.1: The plot for radial density profile of the two different constituents in the confinement. Whereas the upper panel represents for C1, the radial density profile for C2 has been shown in lower panel.

understand the density distribution of the ellipsoidal particles as a function of distance from the centre of the channel. Fig. 11.1 clearly indicates strong density inhomogeneity in the system and ordering of several liquid layers around the wall of the channel. The typical distance between two maxima is about σ, which is the side-by-side contact distance of the

ellipsoids. This pseudoperiodic modulation of the local density has been seen to propagate into the pore volume but is damped and progressively disappears and thus the liquid near the centre behaves almost like bulk liquid. The similar profile for density has also been obtained in simulation studies in pure Gay-Berne liquid confined in cylindrical nanopore.[31,32] Interestingly, the density profile in real liquid like water has also been seen to behave similarly when confined in a real environment like carbon nanotube.[12-14]

When the aspect ratios of the two constituents are same ($R = \kappa_1/\kappa_2 = 1.0$), the binary mixture is essentially transformed into a neat liquid and thus the density profiles for both the constituents are identical. But as we increase the value of R by 2.5 times of its initial value (by 2.5 times increment of κ_1) the density of C1 near the wall significantly reduces, and this reduction is almost twice of its initial value. In addition, the peak position also shifts towards the centre of the channel as κ_1 is increased. This essentially tells that as the ellipsoids become more asymmetric in shape the particles prefer to relocate towards the centre of the channel. This can be explained in terms of curvature induced jamming, which has been recently observed in reverse micelles.[8] As an ellipsoid becomes more needle shaped (larger κ_1) the particle feel more repulsion with the wall due to larger curvature of the channel, which effectively leads into jamming and as a result its location is shifted towards the centre to get stabilisation. Now the removal of C1 (the needle shaped ellipsoids) facilitates C2 (smaller κ_2) to unite more near the wall. This is clearly reflected in the radial density profile of C2 (lower panel) as the peak height increases with increase in κ_1 without shifting towards the centre of the channel. This behaviour qualitatively indicates the effect of confinement on microscopic order of phase separation between two components of largely different shapes.

11.3.2 Radial profile of the average speed

Once the density inhomogeneity, as a structural information, is observed, one can look into the similar inhomogeneity in dynamics in the present system due to the imposed confinement. The simplest way to understand that is to simulate the radial distribution of average speed

(along Z-direction), <Speed>$_Z$, of the ellipsoidal particles. In Fig. 11.2, we have plotted <Speed>$_Z$

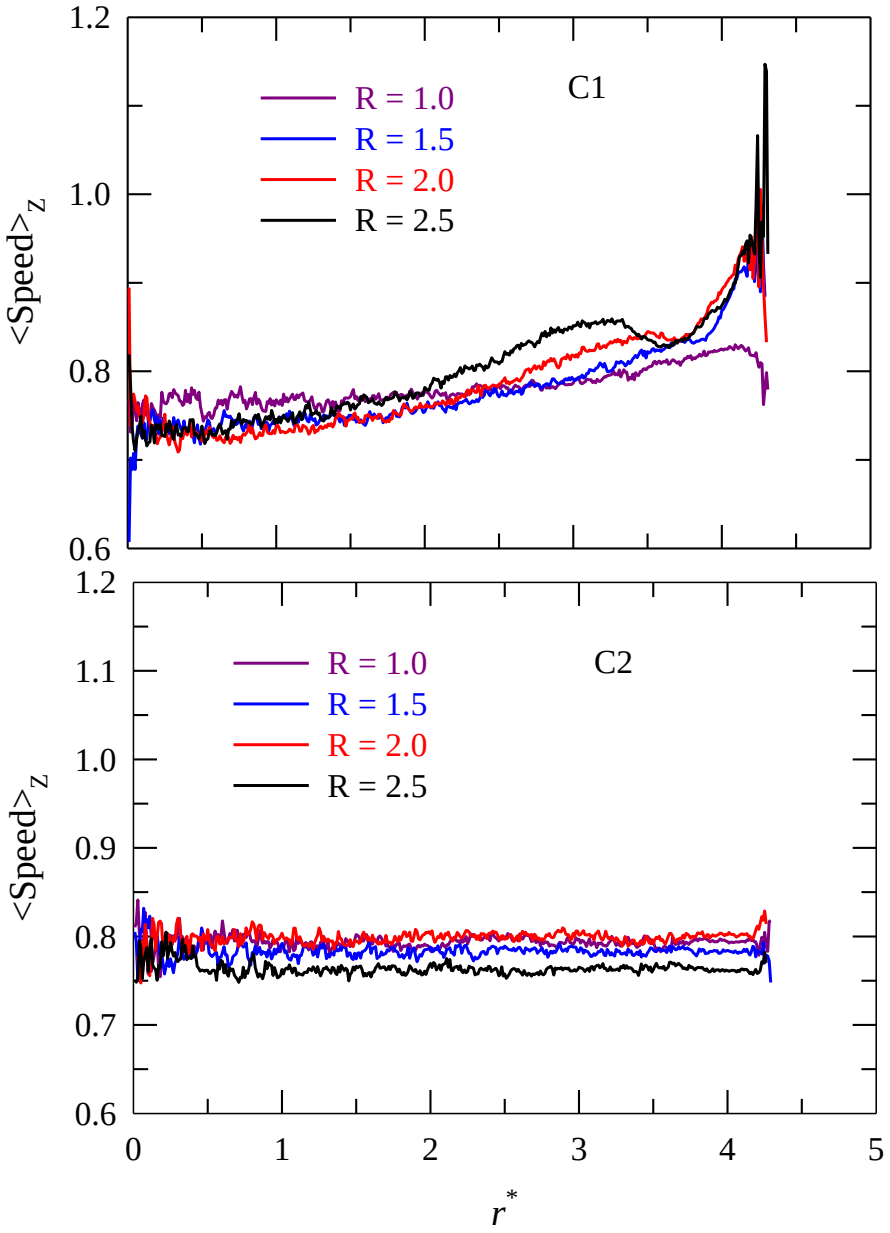

Fig. 11.2: Radial profile of average speed of ellipsoidal particles along Z direction

as a function of distance from the centre of the channel, r^*, for the components, C1 and C2 in the upper and lower panel respectively and the effect of R (κ_1/κ_2) on these distribution. The figure shows that when $\kappa_1 = \kappa_2$ (neat liquid) <Speed>$_Z$ remains almost insensitive towards r^*, meaning uniform speed in this confined environment. But when κ_1 is gradually increased the speed of C1 particles starts fluctuating along the radius and this fluctuation is seen to be maximum near the wall of the channel. In contrast, the fluctuation of speed of C2 particles along the radius is very less. This clearly indicates that the asymmetry in shape can lead into the dynamical inhomogeneity in liquid.

11.3.2 Overall Translational Diffusion

Translational diffusion coefficient of the confined particles has been calculated from two conventional routes: mean square displacement (MSD)[33,34] and velocity auto-correlation function (VACF)[33]. Note that both the MSD and VACF have been calculated only along the Z-direction due to the presence of confinement along X and Y direction. Eq. 9.3 of Chapter 9 has been used here to calculate the mean square displacement in the present system. The upper panel of Fig. 11.3 represents the plot of MSD as a function of time and the influence of R (κ_1/κ_2) on it. The conventional ballistic regime has been seen at small time of MSD plots followed by the linear part, where the later is the reflection of diffusive dynamics. A closer inspection further reveals that as R is increased from R = 1 ($\kappa_1 = \kappa_2$) to R = 1.5 the MSD immediately increases and then remains almost constant on further enhancement of the value of R. This essentially tells that as the shape of two different constituent particles in a binary liquid mixture becomes different, the time dependence of centre of mass position shows its effects. VACF for four different binary mixtures have been plotted against time in the middle panel of the same figure (Fig. 11.3), where it has been seen that the correlation becomes slower immediately after increasing the value of R from R = 1.0 to R = 1.5 and then remains almost insensitive. We have calculated the translation diffusion coefficient (D_T^*) from MSD using Eq. 9.4 (Chapter 9) by measuring the slope of the MSD line at large time window and from VACF using Eq. 9.5 (Chapter 9) by measuring the area under the plot and then plotted D_T^* against R in the lowest panel of Fig. 11.3. The plot shows a nonlinear variation of

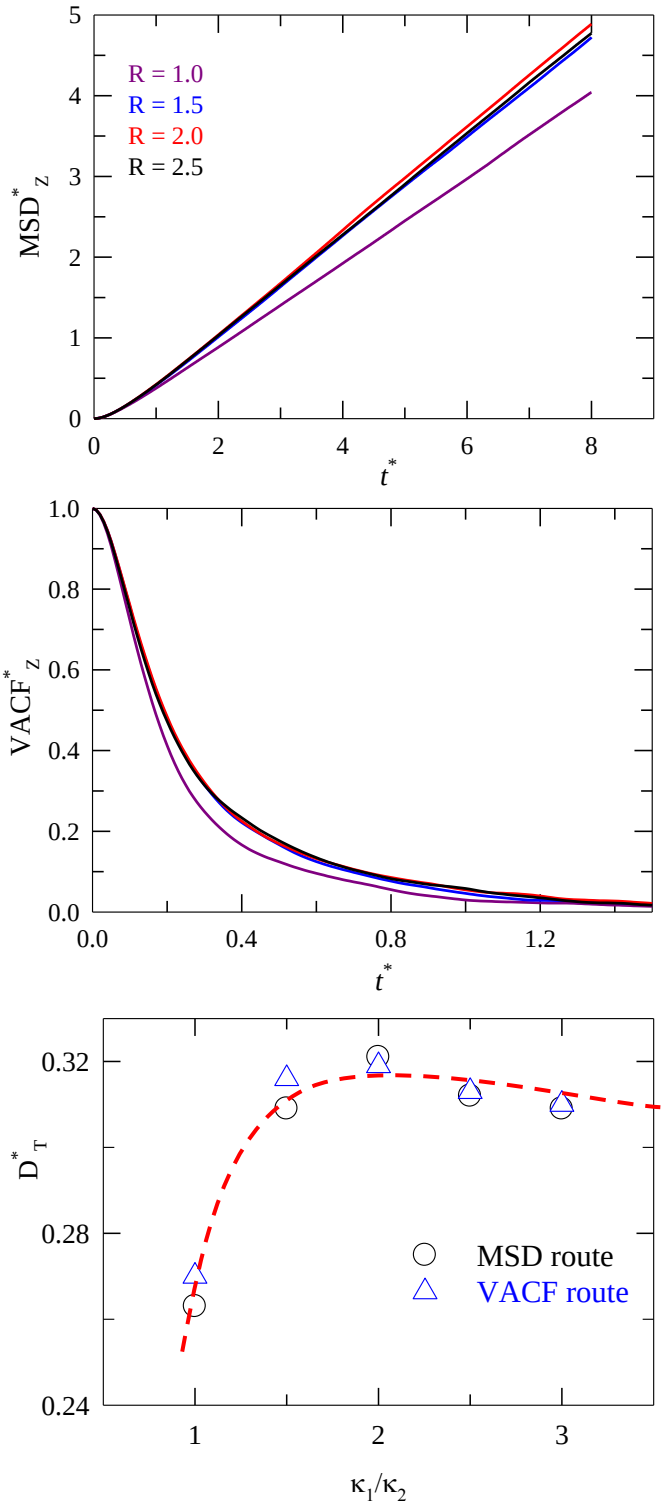

Fig. 11.3: R (κ_1/κ_2) dependence of means square displacement (upper panel), velocity auto correlation function and translation diffusion coefficient along Z-axis. The dotted line in lowest panel is drawn for visual guide.

translation diffusion coefficient on changing R. The plot further tells that as we increase the value of R from R = 1.0 to R = 1.5, D_T^* increases almost 25% of the initial value and then remains almost constant. It should be noted that earlier experiments and simulations have shown that the liquid binary mixtures of n-alkanes, which can be successfully modelled as Gay-Berne particles, the diffusion coefficient gradually decreases as the chain length of one component increases.[35,36] This qualitative picture can be compared with our simulated diffusion behaviour as a function of one component's elongation. Surprisingly, our simulated diffusion does not follow the above behaviour. This can be understood in light of confinement effects on dynamics of the liquids.

11.3.3 Translational Self Diffusion

Translation self diffusion coefficients ($D_{T(Self)}^*$) for the two different components (C1 and C2) have been calculated using the same method, discussed in Chapter 10. In Fig. 11.4, we have plotted $D_{T(Self)}^*$ against R (κ_1/κ_2) for C1 and C2, where we see a distinct difference between C1 and C2 at R > 1, and this difference gradually increases with R. As the value of R is increased to 2.5, $D_{T(Self)}^*$ for C1 increases ~40% of its initial value, whereas C2 shows a slight increase followed by a slight decrease of the value of $D_{T(Self)}^*$. This observation is obvious, because in this case the value of R is changed by changing the aspect ratio (κ_1) of C1 keeping κ_2 constant and thus the impact on the diffusion of C1 will be more than C2. The different behaviours of C1 and C2 are effectively playing the role to get the overall diffusion which has been seen in the lower panel of Fig. 11.3 as a function of R.

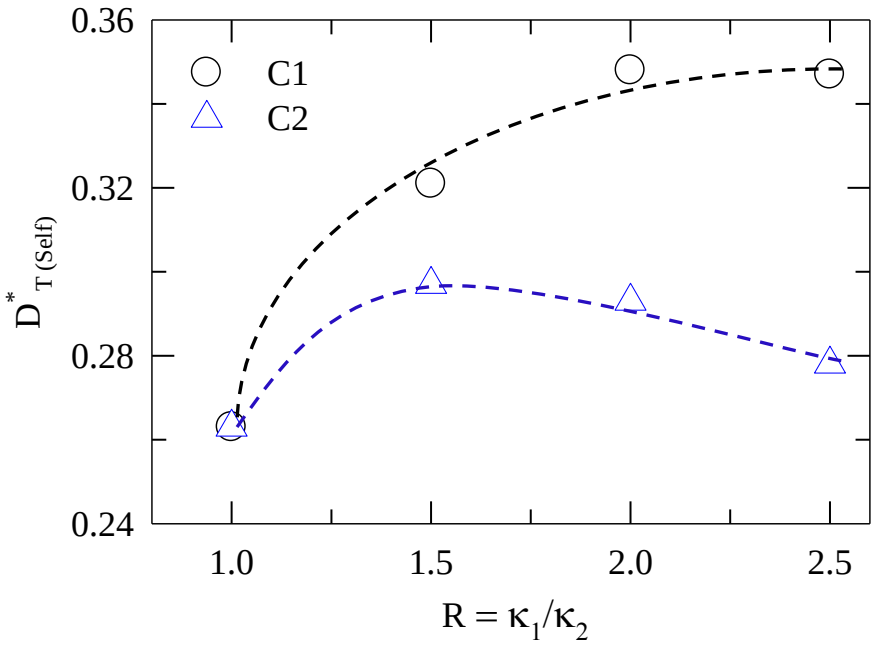

Fig. 11.4: R (κ_1/κ_2) dependence of self-diffusion coefficients of two components along Z-axis. The dotted line is drawn for visual guide.

11.3.4 Radial profile of Translational Diffusion

The radial profile of translation diffusion (along Z-axis) of liquid molecules inside a cylindrical pore is extremely important and interesting to understand the dynamical inhomogeneity in the system as a direct consequence of confinement. Fig. 11.5 represents the radial profile of diffusion of the binary mixture of C1 and C2, where the effect of R has also been shown in order to see the influence of aspect ratio of one component particle on this profile. From the figure it is seen that translation diffusion coefficient at the centre of the channel is maximum and rapidly falls towards the wall of the channel. It is noted that for pure liquid (R = 1), the diffusion coefficient at the centre is ~75% higher than that near the wall. This is understood in terms of friction of the liquid molecules with the wall of the channel. Near the wall of the channel this friction is the maximum and decreases the Z-directional diffusion to its minimum value. At the centre, the liquid shows more *bulk* behaviour and thus feel minimum confinement effect and therefore the friction is minimum. As we increase the

value of R, the radial profile remains qualitatively similar but the diffusion coefficient first increases and then remains constant, as we see in Fig. 11.3 (lower panel).

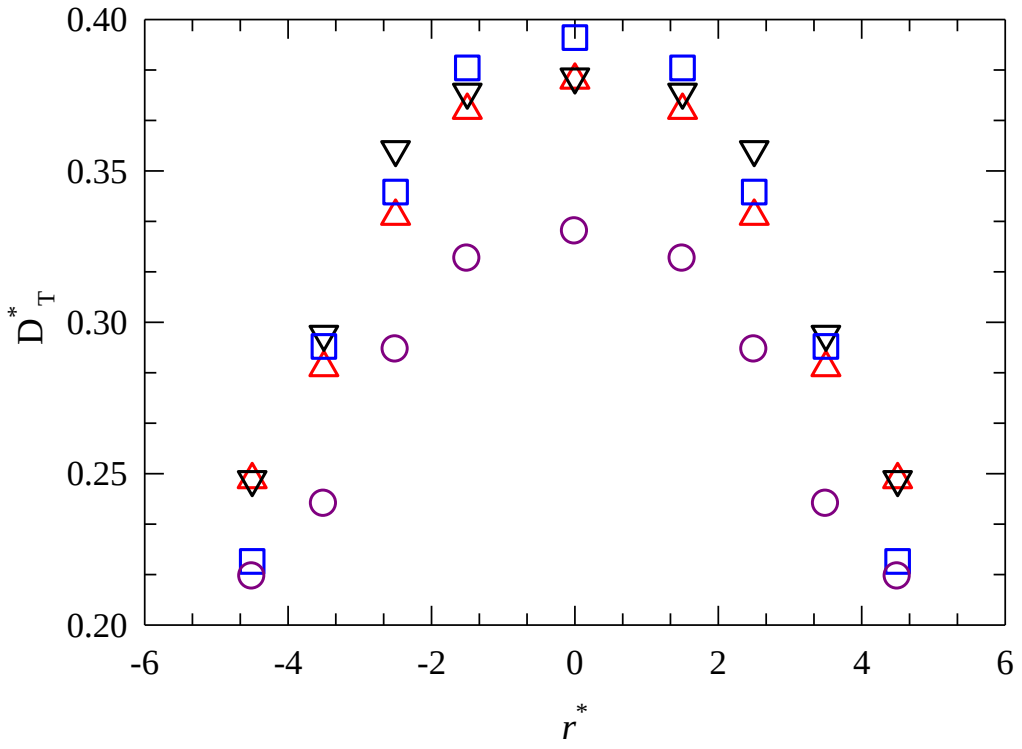

Fig. 11.5: Radial profile of translation diffusion coefficient and the influence of R (R (κ_1/κ_2)) for the binary mixture

11.4 Conclusion

In this chapter we have presented the simulation results regarding the effects of confinement on structure and dynamics of binary mixture of liquids containing asymmetric particles. The large density oscillation near the wall of the nanopore has been seen for all the binary mixtures. As particle becomes more asymmetric in shape (large aspect ratio), its population

near the wall decreases and the distance of the first peak of radial density profile from the wall gradually increases. This is quite interesting because this confinement can play an indirect role to separate the two types of particles in a mixture where one particle has large asymmetry than the other one. The density inhomogeneity of the liquid inside the channel is also an important finding. The radial profile of the speed of the particles also show strong inhomogeneous environment, which can modify the dynamics of a liquid extensively. The diffusion coefficient has been seen to increase when one component in the mixture becomes differently asymmetric in shape. We have also seen that particles with larger aspect ratio diffuse faster in the cylindrical confinement. The radial profile of diffusion coefficient has show a dramatically slow dynamics near the wall compared to the centre of the channel. This is explained in terms of increased interaction of liquid particles with the wall.

References

1. Biswas R.; Rohman, N.; Pradhan, T.; Buchner, R. *J. Phys. Chem. B* **2008**, *112*, 9379.

2. Stanely, H. E.; Buldyrev, S. V.; Franzese, G.; Kumar, P.; Mallamace, M.; Mazza, M. G.; Stokely, K.; Xu, L. *Journal Phys.: Condens. Matter* **2010**, *22*, 2842101.

3. Senapati, S.; Chandra, A. *J. Phys. Chem. B* **2001**, *105*, 5106.

4. Senapati, S.; Chandra, A. *Chem. Phys.* **2001**, *105*, 5106.

5. Bankura, A.; Chandra, A. *J. Phys. Chem. B* **2012**, *116*, 9744.

6. Pal, S. K.; Peon, J.; Zewail, A. H. *Proc. Natl. Acad. Sci. USA* **2002**, *99*, 1763.

7. Thompson, W. H. *Annu. Rev. Phys. Chem.* **2011**, *62*, 599.

8. Guchhait, B.; Biswas, R.; Ghorai, P. K. *J. Phys. Chem. B* **2013**, *117*, 3345.

9. Pradhan, T.; Gazi, H. A. R.; Guchhait, B.; Biswas, R. *J. Chem. Sci.* **2012**, *124*, 355.

10. Biswas, R.; Pal, S. K. *Chem. Phys. Lett.* **2004**, *387*, 221.

11. Mann, D. J.; Halls, M. D. *Phys. Rev. Lett.* **2003**, *90*, 195503.

12. Hummer, G.; Rasaiah, J. C.; Noworyta, J. P. *Nature* **2001**, *414*, 188.

13. Alexiadis, A.; Kassinos, S. *Chem. Rev.* **2008**, *108*, 5014.

14. Cicero, G.; Grossman, J. C.; Schwegler, E.; Gygi, F.; Galli, G. *J. Am. Chem. Soc.* **2008**, *130*, 1871.

15. Rivera, J. L.; McCabe, C.; Cumming, P. T. *Nano Lett.* **2002**, *2*, 1427.

16. Majumder, M.; Chopra, N.; Andrews, R.; Hinds, B. J. *Nature* **2005**, *438*, 44.

17. Alba-Simionesco, C.; Coasne, B.; Dosseh, G.; Dudziak, G.; Gubbins, K. E.; Radhakrishnan, R.; Sliwinska-Bartkowiak, M. *J. Phys.: Condens. Matter* **2006**, *18*, R15.

18. Jahnert, S.; Chavez, F. V.; Schaumann, G. E.; Schreiber, A. ; Schonhoffb, M.; Findenegg, G. H. *Phys. Chem. Chem. Phys.* **2008**, *10*, 6039.

19. Martí, J.; Nagy, G.; Guàrdia, E.; Gordillo, M. C. *J. Phys. Chem. B* **2006**, *110*, 23987.

20. Das, A.; Chakrabarti, J. *Phys. Rev. E* **2012**, *85*, 050601.

21. Daschakraborty, S.; Biswas, R. Transport Properties of Binary Mixtures of Asymmetric Particles: A Simulation Study. In *Concepts and Methods in Modern Theoretical Chemistry (Vol-2)*; Ghosh, S. K., Chattaraj, P. K. Eds.; CRC Press; Taylor & Francis Group: London, UK, 2013; pp 21-35.

22. Perera, A.; Ravichandran, S.; Moreau, M.; Bagchi, B. *J. Chem. Phys.* **1997**, *106*, 1280.

23. Ravichandran, S.; Perera, A. ; Bagchi, B. *J. Chem. Phys.* **1997**, *107*, 8469.

24. Ravichandran, S.; Bagchi, B. *J. Chem. Phys.* **1999**, *111*, 7505.

25. Berne, B. J.; Pechukas, P. *J. Chem. Phys.* **1972**, *56*, 4213.

26. Berne, B. J.; Pechukas, P. *J. Chem. Phys.* **1981**, *74*, 3316.

27. Miguel, E. D.; Rull, L. F.; Gubbins, K. E. *Phys. Rev. A* **1992**, *45*, 3813.

28. Miguel, E. D.; Rull, L. F.; Chalam, M. K.; Gubbins, K. E. *Mol. Phys.* **1991**, *74*, 405.

29. Luckhurst, G. R.; Stephens, R. A.; Phippen, R. W. *Liq. Cryst.* **1990**, *8*, 451.

30. Luckhurst, G. R.; Simmonds, P. S. J. *Mol. Phys.* **1993**, *80*, 233.

31. Ji, Q.; Lefort, R.; Busselez, R.; Morineau, D. *J. Chem. Phys.* **2009**, *130*, 234501.

32. Karjalainen, J.; Lintuvuori, J.; Telkki, V.-V.; Lantto, P.; Vaara, J. *Phys. Chem. Phys. Chem.* **2013**, DOI: 10.1039/C3CP51241J

33. McQuarrie, D. A. *Statistical Mechanics*, Viva Books: New Delhi, 2003.

34. Del Popolo, M. G.; Voth, G. A. *J. Phys. Chem. B* **2004**, *108*, 1744.

35. Leroy, F.; Rousseau, B.; Fuchs, A. H. *Phys. Chem. Chem. Phys.* **2004**, *6*, 775.

36. Srinivasan, S.; Alonso de Mezquia, D.; Bou-Ali, M. M.; Saghir, M. Z. *Philosophical Magazine* **2011**, *91*, 4332.

Chapter 12

Concluding Remarks and Future Problems

In this thesis various interrelated problems have been studied in detail and results discussed. The theory for Stokes shift dynamics and dielectric relaxation in ionic liquids (ILs) have been either discussed or developed and numerical results presented in Chapters 2 – 8 of the present thesis. Chapter 9, 10 and 11 describe various structural and dynamical features of simple model liquids (Stockmayer and Gay-Berne) in bulk and confined environments, which have been studied using molecular dynamics simulation technique. Therefore, this thesis broadly includes both the theoretical and simulation investigation of structural and dynamical aspects of liquids possessing different kinds of interactions. Concluding remarks have been given at the end of every chapter and, therefore, a separate chapter on conclusion is not necessary. However, we take this opportunity to briefly outline the main results presented in this thesis, and mention some related interesting problems that can be studied in future.

In Chapter 1, a general introduction has been presented where the motivational part for studying the dynamics in liquid state has been discussed in great detail in reference to various literature survey related to the studies.

In Chapter 2 and 3, we have described the theoretical Stokes shift dynamics study of a fluorescent probe (C153) in two different ILs,[1-6] having lower and higher viscosity compared to conventional imidazolium ILs[7]. A number of new results have been predicted for these fascinating ILs.[1,2] In case of low viscous IL (Chapter 2), the solvation energy for C153 has been seen to be dominated by the solute-IL dipolar interaction rather than the anticipated solute-IL dipole-ion interaction and the ultrafast response has been found to originate from the collective orientational response of the ILs.[1] In case of high viscous IL (Chapter 3) it is seen that although the magnitude of the calculated total dynamic Stokes shift is somewhat less and the temperature dependence is weaker than those in imidazolium ILs, the relative

contributions of dipole-dipole and ion-dipole interactions are comparable.[2] The dynamics of this IL is extremely slow and it appears that phosphorescence spectroscopy might be a better choice for experimental study of solvation dynamics in these ILs.

Chapter 4 describes probe dependence, effects of IL libration, self-motion and frequency window employed in a given DR measurements on solvation energy relaxation in several ILs. No significant probe dependence has been predicted but libration has been found to affect the rate of solvation considerably. Frequency window has effects on the relaxation dynamics but does not affect too much the average rate of solvation. The effects of experimental technique on measured solvation response is clarified in the next chapter (Chapter 5), where it has been shown that two different experimental techniques may probe different aspects of solute-IL interaction,[8] revealing different relaxation profiles.

In Chapter 6 and 7, we have described the theoretical scheme for understanding the Stokes shift dynamics of a fluorescent probe in the binary mixture of (IL + dipolar solvent).[9,10] The interesting features of solvation in these binary mixtures, observed in experiment, in terms of dynamic Stokes shift and solvation energy relaxation have been quantitatively explained.

Chapter 8 describes molecular level theory for dielectric relaxation (DR) in IL, which has been developed in order to understand the basic dielectric behaviour seen in experimental DR spectroscopy. The DR obtained from this theory has two different channels originated from two solute-IL interactions in the medium (dipole-dipole and ion-dipole), where it has been shown that the ion-dipole interaction results too large DR time scale to contribute to measured DR data. Hence it is concluded that the translation of ions has negligible contribution towards the DR of ILs.

In Chapter 9, 10, and 11, we have presented molecular dynamics simulation studies of model fluids having simple interaction potential between two molecules.[11,12] We have studied the

structural and dynamical features of these systems and checked the effect of single molecular information on the macroscopic properties.

12.1 Future Problems

12.1.1 Stokes Shift Dynamics in Binary mixture of (IL + non dipolar solvent)

The good quantitative agreement of our theoretical studies of Stokes shift dynamics in binary mixture of (IL + dipolar solvent)[9,10] (Chapter 6 and 7) with experiment motivates us to investigate on the Stokes shift dynamics in binary mixture of (IL + non dipolar solvent). The experimental study[13] on the effect of nonpolar solvents on solute rotation and solvation dynamics in imidazolium IL adds further interest for theoretical investigation. Although the steady-state absorption or fluorescence spectra show no effect of the co-solvent on the steady-state absorption or fluorescence spectra of the probe, time-resolved fluorescence anisotropy measurements show a decrease of the probe rotational time with gradual addition of the cosolvent.[13] Solvation dynamics in this mixture is seen to be biphasic, and a decrease of the average solvation time is observed with increasing amount of the co-solvent in solution. Interestingly, dynamic Stokes shift in binary mixture increases with the concentration of non-polar co-solvent in the system. These interesting features can be investigated using molecular level theory as well as computer simulations.

12.1.2 Computer Simulation Investigation of Stokes Shift Dynamics in Binary Mixtures of (IL + dipolar solvent)

Recently, computer simulations has become extremely useful in the study of Stokes shift dynamics in neat IL[14-24] because of its excellent ability to capture the molecular level explanation of experimental Stokes shift dynamics. In comparison to neat systems, binary mixtures of (IL + dipolar solvent) have not been extensively explored via computer simulations. As we have discussed earlier, the experimental time resolved fluorescence spectroscopic technique has shown some interesting results for binary mixtures.[25,26] The increase of dielectric constant with increasing dipolar solvent (e.g. water, acetonitrile etc.), as seen in dielectric relaxation spectroscopy[27], has fuelled further interest. This surprising

behaviour demands further investigation using computer simulation method. The microscopic origin of various solvation timescales observed in experiments should be investigated via realistic simulations.

12.1.3 Theory of Dielectric Relaxation of Binary Mixture of (IL + dipolar solvent)

The successful execution of the dielectric relaxation theory of IL (Chapter 8) further motivates to construct the similar theory for binary mixture of (IL + dipolar solvent). We have seen that in neat IL the dielectric relaxation is primarily governed by the dipole-dipole interaction. The ion-dipole interaction originates a very high relaxation time constant and thus the relaxation process chooses faster channel (dipole-dipole interaction). Now in binary mixture of (IL + dipolar solvent), dipole-dipole interactions are of 3 types, where two of them are self part (IL dipole – IL dipole and dipolar solvent dipole – dipolar solvent dipole) and the third one is the cross (IL dipole – dipolar solvent dipole) interactions. Therefore, these three different interactions can contribute to the total dielectric relaxation in different proportions. The theoretical dielectric relaxation study for this mixture thus can explore different roles played by these interactions in a quantitative manner. Recent experimental dielectric relaxation studies[26,27] in these binary mixtures also raise some important points. These aspects need further investigation via simulations and analytical works.

12.1.4 Solvation and Rotational Dynamics in (Amide + Salt) Deep Eutectic Mixtures

It has been known that acetamide, when mixed with some salts, becomes liquid even at room temperature and these mixtures supercool until the glass transition temperature, T_g is reached. These supercooled molten mixtures possess some similarity to ILs in terms of interaction and various physic-chemical properties. The dynamical study for these mixtures show extremely interesting features. In particular, dielectric spectroscopy[28,29], NMR studies[30], florescence spectroscopy[31-33] indicate that these mixtures possess pronounced spatial and temporal microscopic heterogeneities. These interesting observations have hardly been reexamined by using computer simulations except one model simulation study[34].

References

1. Daschakraborty, S.; Biswas, R. *Chem. Phys. Lett.* **2011**, 510, 202.
2. Daschakraborty, S.; Biswas, R. *Chem. Phys. Lett.* **2012**, *545*, 54.
3. Zech, O.; Kellermeir, M.; Thomaier, S.; Maurer, E.; Klein, R.; Schreiner, C.; Kunz, W. *Chem. Eur. J.* **2009**, *15*, 1341.
4. Zech, O.; Hunger, J.; Sangoro, J. R.; Iacob, C.; Kremer, F.; Kunz, W.; Buchner, R. *Phys. Chem. Chem. Phys.* **2010**, *12*, 14341.
5. Bulut, S.; Klose, P.; Huang, M.-M.; Weingartner, H.; Dyson, P. J.; Laurenczy, G.; Friedrich, C.; Menz, J.; Kummerer, K.; Crossing, I. *Chem. Eur. J.* **2010**, *16*, 13139.
6. Huang, M.-M.; Bulut, S.; Crossing, I.; Weingartner, H. *J. Chem. Phys.* **2010**, *133*, 101101.
7. Jin, H.; O'Hare, B.; Dong, J.; Arzhantsev, S.; Baker, G. A.; Wishart, J. F.; Benesi, A.; Maroncelli, M. *J. Phys. Chem. B* **2008**, *112*, 81.
8. Daschakraborty, S.; Biswas, R. *J. Chem Phys.* **2012**, *137*, 114501.
9. Daschakraborty, S.; Biswas, R. *J. Phys. Chem. B* **2011**, *115*, 4011.
10. Daschakraborty, S.; Biswas, R. *J. Phys. Chem. B* **2013** (Submitted).
11. Daschakraborty, S.; Biswas, R. *J. Chem. Sci.* **2012**, *124*, 763.
12. Daschakraborty, S.; Biswas, R. Transport Properties of Binary Mixtures of Asymmetric Particles: A Simulation Study. In *Concepts and Methods in Modern Theoretical Chemistry (Vol-2)*; Ghosh, S. K., Chattaraj, P. K. Eds.; CRC Press; Taylor & Francis Group: London, UK, 2013; pp 21-35.
13. Paul, A.; Samanta, A. *J. Phys. Chem. B* **2008**, *112*, 947.
14. Roy, D.; Maroncelli, M. *J. Phys. Chem. B* **2012**, *116*, 5951.
15. Jeong, D.; Shim, Y.; Choi, M. Y.; Kim, H. J. *J. Phys. Chem. B* **2007**, *111*, 4920.
16. Shim, Y.; Kim, H. J. *J. Phys. Chem. B* **2008**, *112*, 11028.
17. Shim, Y.; Kim, H. J. *J. Phys. Chem. B* **2009**, *113*, 12964.
18. Shim, Y.; Kim, H. J.; *J. Phys. Chem. B* **2007**, *111*, 4510.
19. Streeter, I.; Lynden-Bell, R. M.; Compton, R. G. *J. Phys. Chem. C* **2008**, *112*, 14538.
20. Bhargava, B. L.; Balasubramanian, S. *J. Chem. Phys.* **2005**, *123*, 144505.
21. Kobrak, M. N.; Znamenskiy, V. *Chem. Phys. Lett.* **2004**, *395*, 127.
22. Kobrak, M. N. *J. Chem. Phys.* **2006**, *125*, 064502.
23. Kobrak, M. N. *J. Chem. Phys.* **2007**, *127*, 184507.

24. Kobrak, M. N. *J. Chem. Phys.* **2007**, *127*, 099903.
25. Liang, M. Solvation and Electron transfer in Ionic Liquids. Ph.D. Thesis, The Pennsylvania State University, August 2012.
26. Zhang, X. –X.; Liang, M.; Hunger, J.; Buchner, R.; Maroncelli, M. *J. Phys. Chem. B*, 2013, DOI: 10.1021/jp4043528
27. Stoppa, A.; Hunger, J.; Hefter, G.; Buchner, R. *J. Phys. Chem. B* **2012,** *116*, 7509–7521.
28. Amico, A.; Berchiesi, G.; Cametti, C.; Biasio, A. D. *J. Chem. Soc. Faraday Trans. 2* **1987**, *83*, 619.
29. Berchiesi, G.; Angelis, M. D.; Rafaiani, G.; Vitali, G. *J. Mol. Liq.* **1992**, *51*, 11.
30. Berchiesi, G.; Rafaiani, G.; Vitali, G.; Farhat, F. *J. Therm. Anal.* **1995**, *44*, 1313.
31. Guchhait, B.; Gazi, H. A. R.; Kashyap, H. K.; Biswas. R. *J. Phys. Chem. B* **2010**, *114*, 5066.
32. Gazi, H. A. R.; Guchhait, B.; Daschakraborty, S.; Biswas. R. *Chem. Phys. Lett.* **2011**, *501*, 358.
33. Guchhait, B.; Daschakraborty, S.; Biswas. R. *J. Phys. Chem. B* **2012**, *136*, 174503.
34. T. Pal and R. Biswas, *Chem. Phys. Lett.*, **2011**, *517*, 180.

Appendix A

Table A1: Experimentally measured frequency dependent dielectric relaxation data for the aluminate ionic liquids at ~343 K as reported in Ref. 3 of Chapter 2.

Ionic Liquid	S	α	τ (ps)	ε_0
$[allyl\text{-}mim]^+$ $[Al(hfip)_4]^-$	12.0	0.30	805	17.0
$[C4\text{-}mim]^+$ $[Al(hfip)_4]^-$	9.4	0.19	280	14.4
$[C2\text{-}mim]^+$ $[Al(hfip)_4]^-$	8.1	0.29	161	12.6
$[C6\text{-}mim]^+$ $[Al(hfip)_4]^-$	11.6	0.13	840	17.5
$[C2\text{-}mmim]^+$ $[Al(hfip)_4]^-$	14.1	0.29	178	17.7
$[C4\text{-}mmim]^+$ $[Al(hfip)_4]^-$	14.9	0.20	440	18.4

Table A2: Parameters required for calculations; T = 343 K

Ionic Liquid	T (K)	ρ (g/cm^3)	η (cp)	σ_+ (Å)	σ_- (Å)
$[allyl\text{-}mim]^+$ $[Al(hfip)_4]^-$	343	1.55	9.5	6.84	12.5
$[C4\text{-}mim]^+$ $[Al(hfip)_4]^-$	343	1.51	9.0	7.21	12.5
$[C2\text{-}mim]^+$ $[Al(hfip)_4]^-$	343	1.55	10.3	6.58	12.5
$[C6\text{-}mim]^+$ $[Al(hfip)_4]^-$	343	1.47	10.1	7.76	12.5
$[C2\text{-}mmim]^+$ $[Al(hfip)_4]^-$	343	1.52	11.9	6.92	12.5
$[C4\text{-}mmim]^+$ $[Al(hfip)_4]^-$	343	1.47	9.6	7.46	12.5

Table A3: Comparison between effective dipole moments calculated from MSA and Cavell's equation for various ionic liquids

Ionic Liquid	μ_{eff}^{MSA} (Debye)	$\mu_{eff}^{Cavell's}$ (Debye)
[C4-mim][BF_4]	4.0	4.6
[C4-mim][PF_6]	4.4	5.3
[C4-mim][DCA]	3.8	3.8
[C6-mim][BF_4]	4.1	4.4
[C2-mim][BF_4]	3.7	3.9
[C2-mim][DCA]	3.4	3.1
[C6-mim][NTf_2]	5.1	5.9
[allyl-mim] [Al(hfiP)$_4$]	7.7	9.0
[C4-mim] [Al(hfiP)$_4$]	7.4	8.2
[C2-mim] [Al(hfiP)$_4$]	6.9	7.4
[C6-mim] [Al(hfiP)$_4$]	8.2	9.4
[C2-mmim] [Al(hfiP)$_4$]	7.9	9.9
[C4-mmim] [Al(hfiP)$_4$]	8.3	10.5

Table A4: Measured and Calculated shift data for various ILs

Cation	Anion	Cation radius (Å)	Anion radius (Å)	Cation/Anion radius ratio (R)	Estimated Stokes shift (cm^{-1})	Average Solvation time (ns)	T (K)
[Bmim]	[PF_6]	3.39[4]	2.72[8]	1.25	2000[1]	1.0[1]	298
[Bmim]	[BF_4]	3.39	2.29[8]	1.48	1900[2]	0.41	298
[Bmim]	[Tf_2N]	3.39	3.39[8]	1.00	1800[3]	0.21	298
[Dmpim]	[Tf_2N]	3.33[3]	3.39	0.98	1700[3]		298
[Bmim]	[Cl]	3.39	2.02[8]	1.68	2200[4]		333
[Bmim]	[Tf_3C]	3.39	3.81[8]	0.89	2000[4]	1.22	298
[Hmim]	[Cl]	3.57[4]	2.02	1.77	2160[4]		298
[Pr_{31}]	[Tf_2N]	3.41[8]	3.39	1.01	2130[4]	0.28[4]	298
[Pr_{41}]	[Tf_2N]	3.47[8]	3.39	1.02	1810[4]	0.38[4]	298
[Pr_{61}]	[Tf_2N]	3.71[8]	3.39	1.09	1840[4]	0.59[4]	298
[$Pr_{10,1}$]	[Tf_2N]	4.10[8]	3.39	1.21	1870[4]	1.3[4]	298
[N_{ip311}]	[Tf_2N]	3.41[8]	3.39	1.01	2100[4]	0.51[4]	298
[N_{ip411}]	[Tf_2N]	3.58[8]	3.39	1.06	2080[4]	0.64[4]	298
[N_{ip611}]	[Tf_2N]	3.76[8]	3.39	1.11	2030[4]	0.97[4]	298
[$N_{ip10,11}$]	[Tf_2N]	4.16[8]	3.39	1.23	1980[4]	2.0[4]	298
[N_{4441}]	[Tf_2N]	4.00[3]	3.39	1.18	1600[3]		298
[N_{3111}]	[Tf_2N]		3.39		1665[5]		298
[N,N-Dmea]	[HCOO]				1670		
[$P_{14,\ 666}$]	[Cl]	5.34[4]	2.02[4]	2.64	1610[6]	4.5[4]	343

$[P_{14,\ 666}]$	[Br]	5.34	2.26[4]	2.36	1610[6]	5.1[4]	343
$[P_{14,\ 666}]$	$[BF_4]$	5.34	2.29[4]	2.33	1440[6]	1.98[4]	343
$[P_{14,\ 666}]$	[DCA]	5.34	2.51[4]	2.13	1520[6]	0.78[4]	343
$[P_{14,\ 666}]$	$[Tf_2N]$	5.34	3.39[4]	1.58	1470[6]	0.99[4]	343
[Bmim]	$[PF_6]$	3.39	2.72	1.25	1748[7]	1.20[7]	298
[Bmim]	$[BF_4]$	3.39	2.29	1.48	1879[7]	0.44[7]	298
[Bmim]	[DCA]	3.39	2.51	1.35	2169[7]	0.12[7]	298
[Hmim]	$[BF_4]$	3.57	2.29	1.56	1966[7]	1.01[7]	298
[Emim]	$[BF_4]$	3.03[9]	2.29	1.32	2062[7]	0.12[7]	298
[Emim]	[DCA]	3.03	2.51	1.21	2331[7]	0.05[7]	298
[Hmim]	$[Tf_2N]$	3.57	3.39	1.05	1655[7]	0.36[7]	298
[Allyl-mim]	$[Al(hfip)_4]$	3.42[10]	6.25[11]	0.55	3389	0.095	343
[Bmim]	$[Al(hfip)_4]$	3.39[10]	6.25	0.54	2691	0.121	343
[Emim]	$[Al(hfip)_4]$	3.03[10]	6.25	0.48	2837	0.108	343
[Hmim]	$[Al(hfip)_4]$	3.57[10]	6.25	0.57	2312	0.181	343
[Emmim]	$[Al(hfip)_4]$	3.46[10]	6.25	0.55	3700	0.089	343
[Bmmim]	$[Al(hfip)_4]$	3.73[10]	6.25	0.60	3237	0.096	343
$[P_{14,\ 666}]$	[Br]	5.34	2.26[4]	2.36	1590[12]	4.65[12]	343
$[P_{14,\ 666}]$	[Cl]	5.34	2.02[4]	2.64	1500[12]	5.13[12]	343
$[P_{14,\ 666}]$	$[BF_4]$	5.34	2.29[4]	2.33	1370[12]	3.22[12]	343

* Blacks are experimental and Blues are theoretical shift values

Table A5: Dynamic Stokes shift measured using a polar probe, C153, in polar solvents and ionic liquids.

Serial #	Solvent[a]	T(K)	μ (D)	ε_0	$\Delta\nu^t$ (10^3 cm^{-1})
1.	Ethyl Acetate	295	1.8	6.02	1.41
2.	Methyl Acetate	295	1.7	6.68	1.49
3.	1-Decanol	295	1.7	7.2	1.77
4.	1-Chlorobutane	295	1.9	7.39	0.81
5.	Tetrahydrofuran	295	1.8	7.58	1.19
6.	Dichloromethane	295	1.1	8.93	0.98
7.	Benzyl alcohol	295	1.7	11.92	1.65
8.	1-Pentanol	295	1.7	13.9	1.83
9.	Cyclohexanone	295	3.1	16.1	1.48
10.	1-Butanol	295	1.8	17.51	1.96
11.	Propionaldehyde	295	2.5	18.5	2.00
12.	Acetone	295	2.7	20.56	1.72
13.	[Bmim][PF_6]	298	~4.0[b]	~12[c]	2.00[d]
14.	[$P_{14,666}$][Br]	343	-	-	1.59[e]
15.	[$P_{14,666}$][Cl]	343	-	-	1.50
16.	[$P_{14,666}$][BF_4]	343	-	-	1.37

(a) $\Delta\nu^t$ for polar solvents (#1-12) are from M. Maroncelli & coworkers, J. Phys. Chem. B 99 (1995**)** 17311; (b) R. Biswas and coworker, Indian. J. Chem. 49A (2010) 685; (c) R. Buchner and coworkers, J. Phys. Chem. B 112 (2008) 4854; (d) $\Delta\nu^t$ for imidazolium ionic liquid (#13) from M. Maroncelli and coworkers, Chem. Phys. Lett. 396 (2004) 83; for C153 in other imidazolium ILs, experimental estimate for $\Delta\nu^t$ is also ~2000 cm^{-1}; see, for example, A. Samanta, J. Phys. Chem. B 110 (2006) 13704; (e) $\Delta\nu^t$ for phosphonium ionic liquids (#14-16) from M. Maroncelli and coworkers, J. Phys. Chem. B 108 (2004) 5771.

Table A6: Experimental dielectric relaxation data for [Na][TOTO] at the temperatures ranging from 254 K to 344 K, as reported in Ref. 2 of Chapter 3.

T (K)	ε_0	τ (sec)	α'	β'	ε_∞
254	19.89	2.2×10^{-2}	0.00	0.20	6.53
264	21.59	2.4×10^{-3}	0.21	0.31	6.84
274	22.03	2.4×10^{-4}	0.27	0.40	7.17
284	22.03	4.6×10^{-5}	0.23	0.40	7.11
294	22.06	1.1×10^{-5}	0.21	0.42	7.01
304	21.93	3.3×10^{-6}	0.18	0.41	6.78
314	21.92	1.1×10^{-6}	0.17	0.45	7.00
324	22.03	4.0×10^{-7}	0.18	0.49	7.00
334	22.17	1.6×10^{-7}	0.21	0.56	7.00
344	22.03	7.0×10^{-8}	0.20	0.62	7.00

Table A7: Table for necessary input parameters for the calculation. Data has been taken from Ref. 1 of Chapter 3.

T (K)	ρ_{IL} (g/cm^3)	η (Poise)	μ_{MSA}^{eff}(Debye)
254	1.268	2855724768	4.23
264	1.263	12245323	4.44
274	1.259	313714	4.56
284	1.254	22563	4.66
294	1.249	3108	4.75
304	1.245	662	4.83
314	1.240	191	4.91
324	1.235	69	5.01
334	1.230	30	5.11
344	1.226	14	5.18

Table A8: Table summarizing fit parameters for the dipole-dipole and ion-dipole interaction contributions to the total solvation response function at different temperatures.

$\langle \tau_{sx} \rangle = \int_0^\infty dt\, S_{sx}$ with $x = d$ or i

T (K)	$S(t)$	a_1	τ_1 (ps)	a_2	τ_2 (ps)	α	$\langle \tau_{sx} \rangle$ (sec)
254	$S_{sd}(t)$			1.00	1.0×10^{9}	0.26	5.4×10^{-3}
		0.35	6.1×10^{9}	0.65	1.2×10^{8}	0.35	5.5×10^{-3}
	$S_{si}(t)$	0.44	5.6×10^{12}	0.56	8.1×10^{11}	1	2.9
264	$S_{sd}(t)$			1.00	1.6×10^{8}	0.30	1.2×10^{-3}
		0.22	9.8×10^{8}	0.78	8.3×10^{7}	0.26	1.3×10^{-3}
	$S_{si}(t)$	0.30	3.6×10^{10}	0.70	4.8×10^{9}	1	1.4×10^{-2}
274	$S_{sd}(t)$			1.00	2.9×10^{7}	0.32	1.0×10^{-4}
		0.19	1.0×10^{8}	0.81	1.7×10^{7}	0.32	1.1×10^{-4}
	$S_{si}(t)$	0.43	6.8×10^{8}	0.57	7.3×10^{7}	1	3.3×10^{-4}
284	$S_{sd}(t)$			1.00	4.9×10^{6}	0.34	1.3×10^{-6}
		0.23	1.1×10^{7}	0.77	2.8×10^{6}	0.34	1.3×10^{-6}
	$S_{si}(t)$	0.57	3.6×10^{7}	0.43	4.3×10^{6}	1	2.2×10^{-5}
294	$S_{sd}(t)$			1.00	9.4×10^{5}	0.44	2.5×10^{-6}
		0.21	2.3×10^{6}	0.79	6.7×10^{5}	0.38	2.4×10^{-6}
	$S_{si}(t)$	0.46	5.4×10^{6}	0.54	8.1×10^{5}	1	2.9×10^{-6}
304	$S_{sd}(t)$			1.00	2.3×10^{5}	0.47	4.6×10^{-7}
		0.21	6.8×10^{5}	0.79	1.6×10^{5}	0.41	4.7×10^{-7}
	$S_{si}(t)$	0.34	1.6×10^{6}	0.66	2.0×10^{5}	1	6.8×10^{-7}
314	$S_{sd}(t)$			1.00	9.2×10^{4}	0.51	1.8×10^{-7}
		0.23	1.9×10^{5}	0.77	6.9×10^{4}	0.45	1.6×10^{-7}
	$S_{si}(t)$	0.41	3.9×10^{5}	0.59	4.4×10^{4}	1	1.8×10^{-7}
324	$S_{sd}(t)$			1.00	3.7×10^{4}	0.55	6.3×10^{-8}
		0.14	7.2×10^{4}	0.86	3.2×10^{4}	0.50	6.3×10^{-8}
	$S_{si}(t)$	0.36	1.5×10^{5}	0.64	1.9×10^{4}	1	6.6×10^{-8}
334	$S_{sd}(t)$			1.00	1.8×10^{4}	0.57	2.9×10^{-8}
		0.11	2.5×10^{4}	0.89	1.7×10^{4}	0.54	2.6×10^{-8}
	$S_{si}(t)$	0.45	5.0×10^{4}	0.55	7.1×10^{3}	1	2.9×10^{-8}
344	$S_{sd}(t)$			1.00	9.3×10^{3}	0.61	1.4×10^{-8}
		0.08	8.9×10^{3}	0.92	9.2×10^{3}	0.59	1.4×10^{-8}
	$S_{si}(t)$	0.61	3.4×10^{3}	0.39	2.7×10^{3}	1	3.1×10^{-9}

Table A9: Table for fitting parameters of $S_{sd}(t)$, $S_{si}(t)$, and $S_{ss}(t)$, obtained after including the model faster time scale.

T (K)	$S(t)$	a_1	τ_1 (ns)	a_2	τ_2 (ns)	α	$\langle\tau_{ss}\rangle$ (sec)
304	$S_{sd}(t)$	0.37	1.75	0.63	150	0.42	2.7×10^{-7}
	$S_{si}(t)$	0.66	200	0.34	1600	1	6.8×10^{-7}
	$S_{ss}(t)$	0.35	1.71	0.65	199	0.45	3.2×10^{-7}

Table A10: Dielectric relaxation parameters of ionic liquids measured in different frequency windows

ILs	ε_0	S_1	τ_1 (ps)	α	β	S_2	τ_2 (ps)	S_3	τ_3	ε_∞ [a]	Ref. in Chapter 4	Frequency range
$[Im_{21}][DCA]$	11.0	4.97	30.7	0.16	1	1.90	1.84			4.13	30	200 MHz - 89 GHz
$[Im_{21}][BF_4]$	14.5	8.70	46.6	0.36	1	2.05	1.22			3.75	30	200 MHz -89 GHz
	13.6	9.70	21.0	0.00	1	0.90	160			3	31	10 MHz - 20 GHz
$[Im_{21}][TF_2N]$	12.3	7.59	261	0.00	0.34	1.43	24.2			3.28	32	200 MHz -20 GHz
	12.3	4.00	145	0.00	1	3.60	23.0			4.7	31	10 MHz - 20 GHz
$[Im_{41}][DCA]$	11.3	6.42	63.0	0.33	1	0.75	2.09			4.13	30	200 MHz -89 GHz
$[Im_{41}][BF_4]$	14.6	10.0	284	0.52	1	2.04	0.62			2.56	30	200 MHz -89 GHz
	12.2	8.94	1140	0	0.21	0.37	73.1	1.15	0.39	1.74	33	100MHz-300 GHz
$[Im_{41}][PF_6]$	16.1	12.0	1178	0.57	1	1.86	0.47			2.24	30	200 MHz -89 GHz
$[Im_{41}][TF_2N]$	13.7	2.70	21.0	0.00	1	3.20	140	3.5	1.0	4.3	31	10 MHz - 20 GHz
	12.6	7.80	57.0	0.00	1	2.20	6.3			2.6	35	40 MHz - 40 GHz
$[Im_{61}][TF_2N]$	12.7	9.40	233	0.47	1	0.68	0.80			2.62	30	200 MHz -89 GHz
$[Im_{81}][TF_2N]$	16.8	8.30	4100	0.00	0.92	3.10	200	1.8	20.0	3.6	31	10 MHz - 20 GHz
$[Pr_{41}][TF_2N]$	11.7	8.48	454	0.00	0.33	0.77	15.3			2.45	34	200 MHz -20 GHz
$[S_{222}][TF_2N]$	13.2	10.2	235	0.00	0.34	0.95	17.2			2.05	34	200 MHz -20 GHz

Table A11: Various physical properties on the ILs

ILs	M_w	ρ (g/cm^3)	η (P)	σ_+ (Å)	σ_- (Å)	μ (Debye)
$[Im_{21}][DCA]$	179.2	1.07[a]	0.210[a]	6.06[a]	5.00[a]	3.40
$[Im_{21}][BF_4]$	200.0	1.28[a]	0.370[a]	6.06	4.58[a]	3.70
$[Im_{21}][TF_2N]$	393.3	1.52[b]	0.340[b]	6.06	6.78[a]	4.64
$[Im_{41}][DCA]$	205.2	1.057[a]	0.293[a]	6.78[a]	5.00	3.80
$[Im_{41}][BF_4]$	226.0	1.202[a]	0.996[a]	6.78	4.58	3.70
$[Im_{41}][PF_6]$	284.2	1.368[a]	2.496[a]	6.78	5.44[a]	4.40
$[Im_{41}][TF_2N]$	419.3	1.440[b]	0.510[b]	6.78	6.78	4.93
$[Im_{61}][TF_2N]$	447.4	1.366[a]	0.678[a]	7.14[a]	6.78	5.00
$[Im_{81}][TF_2N]$	475.2	1.320[b]	0.950[b]	8.80[d]	6.78	5.89
$[Pr_{41}][TF_2N]$	422.1	1.387[c]	0.870[c]	7.50[c]	6.78	4.74
$[S_{222}][TF_2N]$	399.1	1.465[c]	0.400[c]	6.96[c]	6.78	4.71

a) From Ref. 9 of Chapter 4; b) From Ref. 31 of Chapter 4; c) From Ref. 34 of Chapter 4; d) diameter of $[Im_{81}]^+$ has been aproximated by comparing the diameters of $[Im_{21}]^+$, $[Im_{41}]^+$, and $[Im_{61}]^+$ cations.

Table A12: Fitting parameters of the solvation response functions of C153 probe in the remaining ILs.

ILs	$S(t)$	a_1	τ_1 (ps)	a_2	τ_2 (ps)	β	$\langle\tau_{solv}\rangle$ (ns)	$\langle\tau_{solv}\rangle^{theo.}$ / $\langle\tau_{solv}\rangle^{expt.}$
$[Im_{21}]$ $[BF_4]$	$S_{sd}(t)$	0.23	1.05	0.77	30.3	0.47	0.049	1.58
	$S_{si}(t)$	0.38	133	0.62	1378	1	0.814	
	$S_{ss}(t)$	0.21	1.11	0.79	35.2	0.40	0.098	
	$S_{expt.}(t)$	0.45	0.21	0.55	50.0	0.40	0.062	
$[Im_{21}]$ $[TF_2N]$	$S_{sd}(t)$			1.00	41.0	0.46	0.081	1.28
	$S_{si}(t)$	0.34	152	0.66	1552	1	1.029	
	$S_{ss}(t)$			1.00	57.3	0.45	0.118	
	$S_{expt.}(t)$	0.25	0.23	0.75	60.0	0.44	0.092	
$[Im_{41}]$ $[TF_2N]$	$S_{sd}(t)$	0.33	0.78	0.67	51.6	0.65	0.042	1.18
	$S_{si}(t)$	0.19	132	0.81	1781	1	1.414	
	$S_{ss}(t)$	0.20	0.76	0.80	65.1	0.46	0.179	
	$S_{expt.}(t)$	0.39	0.34	0.61	190	0.60	0.151	

Table A13: Table for fitting parameters of the solvation response of C153 after adding the libration part in DR data in remaining ILs

ILs	$S(t)$	a_1	τ_1 (ps)	a_2	τ_2 (ps)	β	$\langle\tau_{solv}\rangle$ (ns)	$\langle\tau_{solv}\rangle^{theo.}$ / $\langle\tau_{solv}\rangle^{expt.}$
$[Im_{21}]$ $[BF_4]$	$S_{sd}(t)$	0.26	0.08	0.74	6.31	0.33	0.024	1.26
	$S_{si}(t)$	0.38	133	0.62	1378	1	0.814	
	$S_{ss}(t)$	0.24	0.08	0.76	13.4	0.29	0.078	
	$S_{expt.}(t)$	0.45	0.21	0.55	50.0	0.40	0.062	
$[Im_{21}]$ $[TF_2N]$	$S_{sd}(t)$	0.25	0.05	0.75	27.2	0.42	0.032	1.05
	$S_{si}(t)$	0.34	152	0.66	1552	1	1.029	
	$S_{ss}(t)$	0.19	0.04	0.81	38.4	0.41	0.097	
	$S_{expt.}(t)$	0.25	0.23	0.75	60.0	0.44	0.092	
$[Im_{41}]$ $[TF_2N]$	$S_{sd}(t)$	0.35	0.08	0.65	10.0	0.34	0.039	0.93
	$S_{si}(t)$	0.19	132	0.81	1781	1	1.414	
	$S_{ss}(t)$	0.31	0.08	0.69	12	0.33	0.141	
	$S_{expt.}(t)$	0.39	0.34	0.61	190	0.60	0.151	

Table A14: Size ratios of solute (C153) to cations, anions and the ionic liquids as a whole.

Ionic Liquids	$\sigma_{C153}/\sigma_{Cation}$	$\sigma_{C153}/\sigma_{Anion}$	$\sigma_{C153}/\sigma_{IL}$
[Bmim][Cl]	1.15	1.87	1.07
[Bmim][BF_4]	1.15	1.70	1.05
[Bmim][PF_6]	1.15	1.43	1.0
[Bmim][TFSI]	1.15	1.02	0.86
[Emim][TFSI]	1.19	1.02	0.87
[Hmim][TFSI]	1.01	1.02	0.80
[Phos][Cl]	0.73	1.87	0.72

Table A15: Input parameters necessary for numerical calculations

Ionic Liquid	Experimental	Reduced	Diameter of	Diameter of
[Bmim][Cl]	1.080	1.35	6.78	4.18
[Bmim][BF_4]	1.202	1.23	6.78	4.58
[Bmim][PF_6]	1.368	1.28	6.78	5.40
[Bmim][TFSI]	1.430	1.41	6.78	7.62
[Emim][TFSI]	1.519	1.45	6.58	7.62
[Hmim][TFSI]	1.366	1.40	7.20	7.62
[Phos][Cl]	0.891	1.24	10.68	4.18

Table A16: Composition dependence of viscosity coefficient for binary mixtures of ionic liquids and polar solvents[13].

[BMIM][PF_6] + H_2O	
x_w	Viscosity (cp)
0.00	261
0.03	228
0.10	150
0.18	108
0.22	89.0
[BMIM][BF_4] + H_2O	
x_w	Viscosity (cp)
0.0	116
0.1	80.9
0.2	59.5
0.3	42.1
0.4	28.1
0.5	20.8
0.6	14.6
0.7	9.53
0.8	5.92
0.9	3.20
1.0	0.89
[BMIM][BF_4] + CH_3CN	
x_{an}	Viscosity (cp)
0.0	116
0.1	76.0
0.2	50.0
0.3	32.6
0.4	21.1
0.5	13.9
0.6	9.02
0.7	5.80
0.8	3.76
0.9	2.50
1.0	1.60

Table A17: Solvation response function for C153 in the binary mixture of [Bmim][PF_6] and water at 0.03 mole fraction of water.

S(t)	*f*	a_1	τ_1 (ps)	α	a_2	τ_2 (ps)	β	$< \tau >$ (ps)
$S_{si}(t)$		0.08	132	1	0.92	3333	1	3080
$S_{sd}(t)$		0.28	0.33	1	0.72	384	0.33	840
$S_{sp}(t)$		0.59	0.005	1	0.41	0.52	1	0.22
$S_{ss}(t) = 0.90\,[f\,S_{sd}+(1-f)S_{sp}] + 0.10S_{si}$	0.0	0.90	0.15	1	0.10	2406	1	232
	0.1	0.85	0.09	0.40	0.15	2110	0.66	345
	0.2	0.79	0.10	0.41	0.21	1520	0.51	423
	0.3	0.73	0.11	0.43	0.27	1133	0.45	482
	0.4	0.66	0.13	0.45	0.34	895	0.42	549
	0.5	0.60	0.14	0.48	0.40	746	0.40	599
	0.6	0.48	0.19	1	0.52	497	0.32	743
	0.7	0.43	0.21	1	0.57	496	0.34	772
	0.8	0.37	0.24	1	0.63	490	0.35	825
	0.9	0.32	0.27	1	0.68	482	0.36	859
	1.0	0.26	0.32	1	0.74	473	0.37	899
Experiment[14]		0.81	807	1	0.19	11870	1	2910

Table A18: Solvation response function for C153 in the binary mixture of [Bmim][PF_6] and water at 0.18 mole fraction of water.

S(t)	*f*	a_1	τ_1 (ps)	α	a_2	τ_2 (ps)	β	$< \tau >$ (ps)
$S_{si}(t)$		0.13	118	1	0.87	2000	1	1760
$S_{sd}(t)$		0.31	0.31	1	0.69	221	0.41	420
$S_{sp}(t)$		0.56	0.005	1	0.44	0.54	1	0.24
$S_{ss}(t) = 0.90\,[f\,S_{sd}+(1-f)S_{sp}] + 0.10S_{si}$	0.0	0.90	0.17	1	0.10	1742	1	173
	0.1	0.85	0.11	0.41	0.15	1428	0.66	259
	0.2	0.79	0.12	0.42	0.21	1001	0.54	309
	0.3	0.73	0.13	0.44	0.27	755	0.48	353
	0.4	0.66	0.14	0.46	0.34	611	0.46	396
	0.5	0.60	0.16	0.49	0.40	520	0.44	433
	0.6	0.49	0.21	1	0.51	373	0.37	533
	0.7	0.44	0.23	1	0.56	369	0.39	544
	0.8	0.38	0.25	1	0.62	363	0.40	577
	0.9	0.33	0.28	1	0.67	357	0.41	596
	1.0	0.27	0.31	1	0.73	352	0.41	643
Experiment[14]		0.86	570	1	0.14	9460	1	1810

Table A19: Solvation response function for C153 in the binary mixture of [Bmim][PF_6] and water at 0.22 mole fraction of water.

S(t)	*f*	a_1	τ_1 (ps)	α	a_2	τ_2 (ps)	β	$< \tau >$ (ps)
$S_{si}(t)$		0.15	115	1	0.85	1667	1	1430
$S_{sd}(t)$		0.31	0.31	1	0.69	217	0.43	380
$S_{sp}(t)$		0.56	0.005	1	0.44	0.55	1	0.24
$S_{ss}(t) = 0.90\,[f\,S_{sd}+(1-f)S_{sp}] + 0.10S_{si}$	0.0	0.90	0.18	1	0.10	1591	1	158
	0.1	0.85	0.12	0.42	0.15	1281	0.66	237
	0.2	0.79	0.13	0.43	0.21	892	0.54	283
	0.3	0.73	0.14	0.45	0.27	674	0.49	319
	0.4	0.66	0.15	0.57	0.34	546	0.47	355
	0.5	0.60	0.16	0.49	0.40	469	0.45	390
	0.6	0.49	0.21	1	0.51	340	0.38	484
	0.7	0.44	0.23	1	0.56	336	0.40	492
	0.8	0.39	0.25	1	0.61	331	0.41	513
	0.9	0.33	0.28	1	0.67	326	0.42	538
	1.0	0.27	0.31	1	0.73	320	0.42	578
Experiment[14]		0.90	540	1	0.10	6760	1	1160

Table A20: Composition dependence of the solvation response function for C153 in the binary mixture of [Bmim][BF_4] and water with $f = 0.9$ at $x_w \neq 0$.

x_w	S(t)	a_1	τ_1 (ps)	α	a_2	τ_2 (ps)	β	$<\tau>$ (ns)
0.0	$S_{si}(t)$	0.11	115	1	0.89	2500	1	2240
	$S_{sd}(t)$	0.10	0.22	1	0.90	61	0.30	380
	$S_{ss}(t)$	0.09	0.25	1	0.91	108	0.29	616
0.1	$S_{si}(t)$	0.14	110	1	0.86	2000	1	1740
	$S_{sd}(t)$	0.09	0.24	1	0.91	38	0.29	290
	$S_{sp}(t)$	0.55	0.0051	1	0.45	0.54	1	0.25
	$S_{ss}(t)$	0.12	0.27	1	0.88	60	0.26	532
0.2	$S_{si}(t)$	0.18	105	1	0.82	1428	1	1190
	$S_{sd}(t)$	0.17	0.19	1	0.89	40	0.31	250
	$S_{sp}(t)$	0.57	0.005	1	0.43	0.54	1	0.24
	$S_{ss}(t)$	0.13	0.21	1	0.87	50	0.26	454
0.3	$S_{si}(t)$	0.22	98	1	0.78	1250	1	1000
	$S_{sd}(t)$	0.12	0.17	1	0.88	41	0.32	230
	$S_{sp}(t)$	0.56	0.005	1	0.44	0.55	1	0.24
	$S_{ss}(t)$	0.16	0.17	1	0.84	66	0.30	396
0.4	$S_{si}(t)$	0.26	85	1	0.74	909	1	700
	$S_{sd}(t)$	0.14	0.15	1	0.86	39	0.34	180
	$S_{sp}(t)$	0.54	0.005	1	0.46	0.56	1	0.26
	$S_{ss}(t)$	0.17	0.16	1	0.83	60	0.32	294
0.5	$S_{si}(t)$	0.27	71	1	0.73	769	1	580
	$S_{sd}(t)$	0.14	0.14	1	0.86	35	0.35	150
	$S_{sp}(t)$	0.53	0.005	1	0.47	0.57	1	270
	$S_{ss}(t)$	0.17	0.15	1	0.83	53	0.33	244
0.6	$S_{si}(t)$	0.14	25	1	0.86	476	1	410
	$S_{sd}(t)$	0.14	0.12	1	0.86	29	0.36	110
	$S_{sp}(t)$	0.52	0.006	1	0.48	0.58	1	0.28
	$S_{ss}(t)$	0.17	0.15	1	0.83	43	0.33	204
0.7	$S_{si}(t)$	0.16	19	1	0.84	323	1	220
	$S_{sd}(t)$	0.14	0.11	1	0.86	22	0.36	90
	$S_{sp}(t)$	0.50	0.006	1	0.50	0.59	1	0.30
	$S_{ss}(t)$	0.25	0.14	0.45	0.75	42	0.38	120
0.8	$S_{si}(t)$	0.19	16	1	0.81	213	1	180
	$S_{sd}(t)$	0.14	0.10	1	0.86	15	0.36	60
	$S_{sp}(t)$	0.49	0.006	1	0.51	0.59	1	0.30
	$S_{ss}(t)$	0.28	0.14	0.44	0.72	32	0.39	82

Table A21: Composition dependence of the solvation response function for C153 in the binary mixture of [Bmim][BF_4] and acetonitrile with $f = 0.9$ at $x_{AN} \neq 0$.

x_{AN}	S(t)	a_1	τ_1 (ps)	α	a_2	τ_2 (ps)	B	$<\tau>$ (ns)
0.0	$S_{si}(t)$	0.11	115	1	0.89	2500	1	2240
	$S_{sd}(t)$	0.10	0.22	1	0.90	61	0.30	380
	$S_{ss}(t)$	0.09	0.25	1	0.91	108	0.29	616
0.1	$S_{si}(t)$	0.13	100	1	0.13	2000	1	1750
	$S_{sd}(t)$	0.12	0.19	1	0.88	66	0.33	310
	$S_{sp}(t)$	0.78	0.06	1	0.22	0.44	1	0.14
	$S_{ss}(t)$	0.18	0.14	1	0.82	113	0.31	503
0.2	$S_{si}(t)$	0.15	85	1	0.85	1667	1	1430
	$S_{sd}(t)$	0.13	0.18	1	0.87	53	0.33	260
	$S_{sp}(t)$	0.77	0.06	1	0.23	0.45	1	0.15
	$S_{ss}(t)$	0.18	0.14	1	0.82	89	0.32	396
0.3	$S_{si}(t)$	0.17	69	1	0.83	1429	1	1200
	$S_{sd}(t)$	0.14	0.16	1	0.86	49	0.35	200
	$S_{sp}(t)$	0.75	0.07	1	0.25	0.46	1	0.17
	$S_{ss}(t)$	0.20	0.14	1	0.80	80	0.34	308
0.4	$S_{si}(t)$	0.15	44	1	0.85	1000	1	860
	$S_{sd}(t)$	0.14	0.14	1	0.86	41	0.37	140
	$S_{sp}(t)$	0.72	0.07	1	0.28	0.47	1	0.18
	$S_{ss}(t)$	0.20	0.14	1	0.80	65	0.35	240
0.5	$S_{si}(t)$	0.11	18	1	0.89	714	1	640
	$S_{sd}(t)$	0.15	0.12	1	0.85	33	0.38	110
	$S_{sp}(t)$	0.69	0.08	1	0.31	0.49	1	0.21
	$S_{ss}(t)$	0.26	0.14	1	0.80	51	0.36	179
0.6	$S_{si}(t)$	0.13	15	1	0.87	526	1	460
	$S_{sd}(t)$	0.15	0.11	1	0.85	25	0.39	180
	$S_{sp}(t)$	0.63	0.08	1	0.37	0.53	1	0.25
	$S_{ss}(t)$	0.19	0.14	1	0.81	38	0.37	127
0.7	$S_{si}(t)$	0.15	12	1	0.85	370	1	320
	$S_{sd}(t)$	0.15	0.09	1	0.85	19	0.39	60
	$S_{sp}(t)$	0.57	0.09	1	0.43	0.62	1	0.32
	$S_{ss}(t)$	0.18	0.15	1	0.82	27	0.37	92
0.8	$S_{si}(t)$	0.18	10	1	0.82	244	1	200
	$S_{sd}(t)$	0.15	0.08	1	0.85	14	0.39	50
	$S_{sp}(t)$	0.51	0.10	1	0.49	0.78	1	0.43
	$S_{ss}(t)$	0.16	0.16	1	0.84	18	0.36	60

Table A22: Table for the necessary input parameters like mass density (ρ), number density of dipole (ρ_N^d), number density of ion (ρ_N^i), viscosity (η), and effective dipole moment (from MSA) (μ_{eff}) for the binary mixture of ($[\text{Bmim}][\text{BF}_4] + \text{CH}_3\text{CN}$).

x_{IL}	ρ (g.cm^{-3})	ρ_N^d (cm^{-3}) × 10^{-21}	ρ_N^i (cm^{-3}) × 10^{-21}	η (cP)	μ_{eff} (D)
0.0	0.777	11.4	0.00	0.341	3.7
0.1	0.912	9.18	0.32	0.887	3.7
0.2	0.995	7.69	0.65	1.792	3.7
0.3	1.052	6.60	0.97	3.344	3.8
0.4	1.090	5.77	1.29	6.069	3.8
0.5	1.119	5.12	1.61	10.22	3.9
0.6	1.145	4.59	1.94	17.59	3.9
0.7	1.164	4.15	2.26	27.71	3.9
0.8	1.179	3.79	2.58	40.27	4.0
0.9	1.198	3.48	2.90	70.91	4.0
1.0	1.211	3.21	3.23	110.3	4.1

Table A23: Table for the necessary input parameters like mass density (ρ), number density of dipole (ρ_N^d), number density of ion (ρ_N^i), viscosity (η), and effective dipole moment (from MSA) (μ_{eff}) for the binary mixture of ($[\text{Bmim}][\text{BF}_4] + \text{H}_2\text{O}$).

x_{IL}	ρ (g.cm^{-3})	ρ_N^d (cm^{-3}) × 10^{-21}	ρ_N^i (cm^{-3}) × 10^{-21}	η (cP)	μ_{eff} (D)
0.0	0.983	32.7	0.00	1.00	2.85
0.1	1.076	12.8	0.32	2.90	2.90
0.3	1.131	6.49	0.97	7.40	3.00
0.5	1.153	4.71	1.61	15.5	3.20
0.7	1.165	3.87	2.26	32.6	3.35
0.9	1.173	3.39	2.90	72.8	3.50
1.0	1.176	3.21	3.23	110	3.70

Table A24: Fitting parameters of solvation responses of C153 probe in the binary mixture of ($[\mathrm{Bmim}][\mathrm{BF_4}] + \mathrm{CH_3CN}$) from experiment and theory, using effective medium calculation approach

x_{IL}	Tool	f_1	τ_1	f_2	τ_2	f_3	τ_3	f_4	τ_4	β	$\langle\tau_f\rangle$	$\langle\tau_s\rangle$	$\langle\tau_{solv}\rangle$
0.2	Theo.			0.26	1.68	0.23	6.20	0.51	21.5	1	1.68	16.7	12.8
	Expt.	0.54	0.26	0.32	1.40	0.07	14.0	0.07	118	1	0.23	22.0	10.0
0.3	Theo.			0.26	2.86	0.36	11.3	0.38	38.8	1	2.86	18.8	14.7
	Expt.	0.42	0.20	0.32	0.76	0.16	9.00	0.10	90.0	1	0.18	19.0	11.0
0.4	Theo.			0.15	1.87	0.48	9.68	0.37	38.0	1	1.87	22.0	19.0
	Expt.	0.60	0.26	0.17	2.00	0.16	37.0	0.07	237	1	0.23	56.0	23.0
0.5	Theo.												
	Expt.	0.19	0.15	0.45	0.41	0.19	16.0	0.16	161	1	0.13	37.0	30.0
0.6	Theo.			0.23	1.38	0.64	21.5	0.13	350	1	1.38	77.0	59.6
	Expt.	0.42	0.17	0.22	0.55	0.17	71.0	0.18	287	1	0.15	112	65.0
0.8	Theo.			0.23	0.93	0.68	37.5	0.09	794	1	0.93	126	97.2
	Expt.	0.34	0.17	0.23	0.65	0.29	86.0	0.14	779	1	0.15	198	131
0.9	Theo.			0.26	0.65	0.64	41.5	0.10	1505	1	0.65	239	177
	Expt.	0.08	0.12	0.45	0.26	0.21	39.0	0.26	648	1	0.11	193	243

Table A25: Fitting parameters of solvation responses of C153 probe in the binary mixture of ($[\mathrm{Bmim}][\mathrm{BF_4}] + \mathrm{H_2O}$) from experiment and theory (using both *new* and *old* DR data)

x_{IL}	Mode	a_1	τ_1 (ps)	a_2	τ_2 (ps)	β	$\langle\tau_f\rangle$ (ps)	$\langle\tau_s\rangle$ (ps)	$\langle\tau_{solv}\rangle$ (ps)
0.1	Theory (*new* DR)	0.86	0.45	0.14	6.2	0.31	0.45	49.8	7.40
	Theory (*old* DR)	0.87	0.44	0.13	4.8	0.28	0.44	61.7	8.40
	Expt.	0.19	0.27	0.81	10.0	0.37	0.27	44.0	36.0
0.3	Theory (*new* DR)	0.71	0.46	0.29	31.0	0.40	0.46	103	30.2
	Theory (*old* DR)	0.73	0.42	0.27	33.9	0.36	0.42	155	42.1
	Expt.	0.09	0.15	0.91	12.0	0.31	0.15	89.0	81.0
0.5	Theory (*new* DR)	0.55	0.47	0.45	60.2	0.43	0.47	166	74.9
	Theory (*old* DR)	0.60	0.40	0.40	73.0	0.39	0.40	261	104
	Expt.	0.25	0.13	0.75	30.0	0.36	0.13	141	106
0.7	Theory (*new* DR)	0.40	0.51	0.60	69.4	0.43	0.51	191	115
	Theory (*old* DR)	0.46	0.38	0.54	114	0.38	0.38	439	237
	Expt.	0.35	0.08	0.65	76	0.41	0.08	231	151
0.9	Theory (*new* DR)	0.27	0.72	0.73	115	0.43	0.72	317	232
	Theory (*old* DR)	0.32	0.38	0.68	152	0.35	0.38	764	520
	Expt.	0.33	0.14	0.67	170	0.48	0.14	362	243

Table A26: Fitting parameters of solvation responses of C153 probe in the binary mixture of ($[\mathrm{Bmim}][\mathrm{BF_4}] + \mathrm{H_2O}$) from experiment and theory, using effective medium calculation approach.

x_{IL}	Mode	a_1	τ_1 (ps)	a_2	τ_2 (ps)	β	$\langle\tau_f\rangle$ (ps)	$\langle\tau_s\rangle$ (ps)	$\langle\tau_{solv}\rangle$ (ps)
0.1	Theory	0.05	4.10	0.95	25.0	0.63	4.10	35.4	33.8
	Expt.	0.19	0.27	0.81	10.0	0.37	0.27	44.0	36.0
0.3	Theory	0.08	3.38	0.92	34.7	0.59	3.38	53.4	49.4
	Expt.	0.09	0.15	0.91	12.0	0.31	0.15	89.0	81.0
0.5	Theory	0.11	1.27	0.89	36.4	0.50	1.27	72.8	64.9
	Expt.	0.25	0.13	0.75	30.0	0.36	0.13	141	106
0.7	Theory	0.17	1.16	0.83	49.3	0.46	1.16	116	96.8
	Expt.	0.35	0.08	0.65	76.0	0.41	0.08	231	151
0.9	Theory	0.20	1.06	0.80	80.0	0.42	1.06	234	187
	Expt.	0.33	0.14	0.67	170	0.48	0.14	362	243

Table A27: Input parameters for ILs necessary for numerical calculations

$T\ (K)$	$\rho\left(g/cm^3\right)$	$\eta\ (P)$	σ_+ (Å)	σ_- (Å)	M_w	μ (D)
$[Bmim][BF_4]$						
278.15	1.217	3.192	6.78	4.58	226.0	3.7
288.15	1.209	1.947				
298.15	1.202	0.996				
308.15	1.195	0.582				
318.15	1.189	0.378				
328.15	1.183	0.290				
338.15	1.177	0.208				
$[Bmim][PF_6]$						
288.15	1.377	5.737	6.78	5.44	284.2	4.4
298.15	1.368	2.496				
308.15	1.360	1.401				
318.15	1.349	0.811				
328.15	1.339	0.531				
338.15	1.329	0.358				
$[Emim][DCA]$						
278.15	1.098	0.403	6.06	5.00	179.2	3.4
288.15	1.082	0.288				
298.15	1.066	0.210				
308.15	1.050	0.156				
318.15	1.034	0.119				
328.15	1.018	0.091				
338.15	1.002	0.072				
$[Hmim][NTf_2]$						
278.15	1.386	2.141	7.14	6.78	447.4	5.0
288.15	1.376	1.146				
298.15	1.366	0.678				
308.15	1.356	0.433				
318.15	1.345	0.294				
328.15	1.335	0.210				
338.15	1.325	0.157				
$[Emim][BF_4]$						
278.15	1.295	0.761	6.06	4.58	200.0	3.7
288.15	1.288	0.532				
298.15	1.279	0.372				
308.15	1.272	0.256				
318.15	1.265	0.188				
328.15	1.258	0.127				
338.15	1.250	0.089				

[Na][TOTO]						
$T\ (K)$	$\rho\left(g/cm^3\right)$	$\eta\ (P)$	σ_+	σ_-	M_w	μ (D)
254	1.268	2855724768	2.30	8.30	244.2	4.56
264	1.263	12245323				
274	1.259	31374				
284	1.254	22563				
294	1.249	3108				
304	1.245	662				
314	1.240	191				
324	1.235	69				
334	1.230	30				
344	1.226	14				

Table A28: Dielectric relaxation parameters of the ILs

T (K)	ε_0	S_1	τ_1 (ps)	α_1	β_1	S_2	τ_2	ε_∞
[Bmim][BF_4]								
278.15	14.4	10.1	670	0.59	1	3.24	0.26	1.10
288.15	14.1	9.64	351	0.54	1	2.78	0.40	1.72
298.15	14.6	10.0	284	0.52	1	2.04	0.62	2.57
308.15	13.8	9.09	140	0.49	1	1.68	0.80	2.98
318.15	13.3	8.43	93.7	0.45	1	1.71	0.94	3.11
328.15	12.5	7.56	59.4	0.40	1	1.76	0.97	3.17
338.15	12.5	7.34	52.5	0.39	1	1.58	1.42	3.56
[Bmim][PF_6]								
288.15	16.7	12.8	2625	0.61	1	1.32	0.50	2.55
298.15	16.1	12.0	1178	0.57	1	1.86	0.47	2.24
308.15	17.2	13.2	905	0.58	1	1.61	0.48	2.30
318.15	16.8	12.9	535	0.56	1	1.39	0.64	2.56
328.15	13.9	9.8	166	0.50	1	1.71	0.61	2.39
338.15	13.0	8.5	106	0.43	1	1.23	1.39	3.27
[Emim]DCA								
278.15	11.7	5.95	46.4	0.23	1	1.49	1.88	4.30
288.15	11.3	5.28	34.5	0.18	1	1.69	2.14	4.37
298.15	11.0	4.97	30.7	0.16	1	1.90	1.84	4.18
308.15	10.5	4.25	25.2	0.13	1	1.95	2.08	4.33
318.15	10.0	3.55	18.9	0.08	1	2.11	2.11	4.31
328.15	10.1	3.74	16.7	0.10	1	2.06	2.11	4.32
338.15	10.0	3.17	16.1	0.03	1	2.38	2.49	4.42
[Hmim][NTf_2]								
278.15	13.8	10.60	925	0.55	1	0.43	0.80	2.77
288.15	12.1	8.72	299	0.47	1	0.65	0.80	2.71
298.15	12.7	9.40	233	0.47	1	0.68	0.80	2.58
308.15	11.6	8.11	128	0.40	1	1.09	0.69	2.40
318.15	11.9	8.40	107	0.39	1	0.97	0.80	2.52
328.15	11.3	7.68	73.1	0.34	1	1.19	0.80	2.38
338.15	11.2	7.56	64.0	0.33	1	1.03	1.2	2.66
[Emim][BF_4]								
278.15	16.3	11.0	99.3	0.46	1	0.85	1.00	3.41
288.15	15.6	10.2	60.7	0.44	1	1.65	1.26	3.69
298.15	14.5	8.70	46.6	0.36	1	2.05	1.22	3.75
308.15	13.6	7.42	36.6	0.31	1	2.13	1.60	4.07
318.15	13.0	7.31	21.9	0.34	1	1.91	1.30	3.75
328.15	12.6	6.51	18.4	0.26	1	2.41	1.24	3.64
338.15	12.1	5.84	15.5	0.20	1	2.48	1.29	3.79

T (K)	ε_0	S	τ (sec)	α_1	β_1	ε_∞
[Na][TOTO]						
254	19.89	13.36	2.2×10^{-2}	0.00	0.20	6.53
264	21.59	14.75	2.4×10^{-3}	0.21	0.31	6.84
274	22.03	14.86	2.4×10^{-4}	0.27	0.40	7.17
284	22.03	14.92	4.6×10^{-5}	0.23	0.40	7.11
294	22.06	15.05	1.1×10^{-5}	0.21	0.42	7.01
304	21.93	15.15	3.3×10^{-6}	0.18	0.41	6.78
314	21.92	14.92	1.1×10^{-6}	0.17	0.45	7.00
324	22.03	15.03	4.0×10^{-7}	0.18	0.49	7.00
334	22.17	15.17	1.6×10^{-7}	0.21	0.56	7.00
344	22.03	15.03	7.0×10^{-8}	0.20	0.62	7.00

References

1. Ito, N.; Arzhantsev, S.; Maroncelli**,** M. *Chem. Phys. Lett.* **2004** *396*, 83.
2. Karmakar, R.; Samanta, A. *J. Phys. Chem. A* **2002**, *106*, 4447.
3. Arzhantsev, S.; Ito, N.; Heitz, M.; Maroncelli**,** M. *Chem. Phys. Lett.* **2003** *381*, 278.
4. Jin, H.; Baker, G. A.; Arzhantsev, S.; Dong, J.; Maroncelli**,** M. *J. Phys. Chem. B* **2007**, *111*, 7291.
5. Pramanik, R.; Rao, V. G.; Sarkar, S.; Ghatak, C.; Setua, P.; Sarkar, N. *J. Phys. Chem. B* **2009**, *113*, 8626.
6. Ito, N.; Arzhantsev, S.; Heitz, M.; Maroncelli, M. *J. Phys. Chem. B* **2004**, *108*, 5771.
7. Kashyap, H. K.; Biswas, R. *J. Phys. Chem. B* **2010**, *114*, 16811.
8. Jin, H.; O'Hare, B.; Dong, J.; Arzhantsev, S.; Baker, G. A.; Wishart, J. F.; Benesei, A. J.; Maroncelli, M. *J. Phys. Chem. B* **2008**, *112*, 81.
9. Tokuda, H.; Hayamizu, K.; Ishii, K.; Susan, Md. A. B. H.; Watanabe, M. *J. Phys. Chem. B* **2005**, *109*, 6103.
10. Huang, M. M.; Bulut, S.; Krossing, I.; Weingärtner, H. *J. Chem. Phys*. **2010**, *133*, 101101.
11. Krossing, I.; Raabe, I. *Angew. Chem. Int. Ed.* **2004**, *43*, 2066
12. Kashyap, H. K.; Biswas, R. *J. Phys. Chem. B* **2010**, *114*, 254.
13. Li, W.; Zhang, Z.; Han, B.; Hu, S.; Xie, Y.; Yang, G. *J. Phys. Chem. B* **2007**, *111*, 6452.
14. Chakrabarty, D.; Chakraborty, A.; Seth, D.; Hazra, P.; Sarkar, N. *Chem. Phys. Lett.* **2004**, *397*, 469.

Appendix B

Calculation of the wave-number dependent orientational dipolar dynamic structure factor, $S^{lm}_{solvent}(k,t)$

The calculation of $S^{lm}_{solvent}(k,t)$ requires, as inputs, (i) orientational static structure factor, (ii) experimental dielectric relaxation data of these ionic liquids and (iii) isotropic liquid dynamic structure factor[7,8,20]. These are necessary to calculate the wavevector and frequency (z) dependent rotational and translational memory kernels - $\Gamma_R(k,z)$ and $\Gamma_T(k,z)$ - which constitute $S^{lm}_{solvent}(k,t)$. The full expression for $S^{lm}_{solvent}(k,t)$ with explicit connection to $\Gamma_R(k,z)$ and $\Gamma_T(k,z)$ is available in Ref. 7. The orientational static structure factor for these ionic liquids, $S^{lm}_{solvent}(k)$, has been obtained from the mean spherical approximation (MSA) model[9] with proper corrections at both $k \to 0$ and $k \to \infty$ limits, using the experimental static dielectric constant after approximating the dipolar species as dipolar hard-spheres. The dipole moment of these ionic liquids has been estimated using the Cavell's equation[10]. The wave-number and frequency dependent rotational frictional kernel, $\Gamma_R(k,z)$, is connected to the experimentally measured frequency dependent dielectric function, $\varepsilon(z)$, as follows[7,8,20]:

$$\frac{2k_BT}{I[z+\Gamma_R(k,z)]} = \frac{z\varepsilon_0[\varepsilon(z)-\varepsilon_\infty]}{f(110;k=0)\varepsilon_\infty[\varepsilon_0-\varepsilon(z)]}, \qquad \text{(B.1)}$$

where ε_∞ is the infinite frequency dielectric constant and *I* the moment of inertia. $f(110,k)$ is connected to the orientational direct correlation function, $c(110,k)$, via the relation[20,21] $f(110,k) = 1-(\rho_d^0/4\pi)c(110,k)$.

Ref. 3 reports that the experimentally measured frequency dependent dielectric function, $\varepsilon(z)$, for these aluminate ionic liquids at ~343 K follows the Cole-Cole distribution

$$\varepsilon(z) = \varepsilon_\infty + \frac{S}{[1+(z\tau)^{\alpha_1}]}, \qquad \text{(B.2)}$$

where τ denotes the relaxation time associated with the S dispersion. Note these experiments have only the coverage up to 20 GHz. The parameter α determines the width of the distribution. The relevant experimental dielectric relaxation data are provided in Table S1.

The isotropic liquid dynamic structure factor is related to the translational frictional kernel ($\Gamma_t(k,z)$) as follows[32]

$$\frac{k_B T}{M\sigma^2[z+\Gamma_T(k,z)]} = \frac{S(k)[S(k)-zS(k,z)]}{k^2 S(k,z)}, \qquad \text{(B.3)}$$

with $S(k,z) = \dfrac{S(k)}{z + D_T k^2 / S(k)}$, where the translational diffusion coefficient of (D_T) is obtained from the experimental viscosity and stick boundary condition using the effective volume of an ionic liquid molecule. The static isotropic structure factor is approximated by that for the Percus-Yevick hard spheres[9]. Subsequently, Laplace inversion (L^{-1}) transforms the frequency dependent quantity into a time dependent one: $S^{lm}_{solvent}(k,t) = L^{-1}\left[S^{lm}_{solvent}(k,z)\right]$.

B. Calculation of the wave-number and time dependent solute dynamic structure factor, $S^{lm}_{solute}(k,t)$

The solute dynamic structure factor, $S^{lm}_{solute}(k,t)$ has been assumed to be given by[7,8]

$$S^{lm}_{solute}(k,t) = \frac{1}{4\pi}\exp\left[-\left(l(l+1)D^s_R + k^2 D^s_T\right)t\right]. \qquad \text{(B.4)}$$

In the above equation D^s_R and D^s_T represent respectively the rotational and translation diffusion coefficients of the solute and have been obtained from experimental viscosity using the *stick* boundary condition.

C. Calculation of the isotropic ion dynamic structure factor, $S^{ion}_{\alpha\beta}(k,t)$

The isotropic static ion structure factor, $S^{ion}_{\alpha\beta}(k)$, is calculated by using the following relation [22,23],

$$S_{\alpha\beta}^{ion}(k) = \delta_{\alpha\beta} - \frac{4\pi\sqrt{n_\alpha^0 n_\beta^0}\, q_\alpha q_\beta}{k_B T \varepsilon_0 (1+k\sigma)} \frac{\kappa^2}{\kappa_D^2} \frac{\cos(k\sigma) + \frac{\kappa}{k}\sin(k\sigma)}{(k^2+\kappa^2)}, \tag{B.5}$$

where q_α is the charge of α^{th} type ion and κ the renormalized screening constant. κ is related to the Debye screening constant, κ_D, as follows

$$\kappa = \frac{\kappa_D}{\sqrt{1-(\kappa_D\sigma)^2/2 + (\kappa_D\sigma)^3/6}}, \tag{B.6}$$

with $\kappa_D = \sqrt{\frac{4\pi}{k_B T \varepsilon_0} \sum_\alpha n_\alpha^0 q_\alpha^2}$. $\delta_{\alpha\beta}$ denotes the Kronecker's delta representation and σ the average ion diameter.

Note the references cited to in the above write-up are those corresponding to the references given in the Chapter 2.

Appendix C

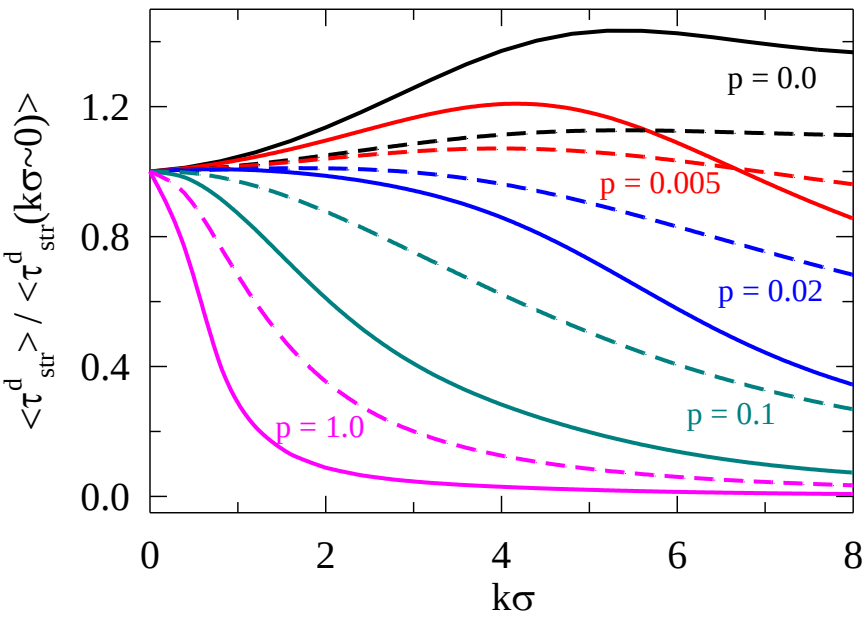

Fig. C1: Pronounced wavevector dependence for inhomogeneous case than in homogeneous one. Calculations are for $[C4\text{-}mim]^+[Al(hfip)_4]^-$ at 343 K. $< \tau^d_{str} >$, average relaxation time for dynamic dipolar structure factor, has been calculated by using the corresponding dielectric relaxation data. Solid lines and broken lines represent for $\alpha = 0.19$ and $\alpha = 0.19$.

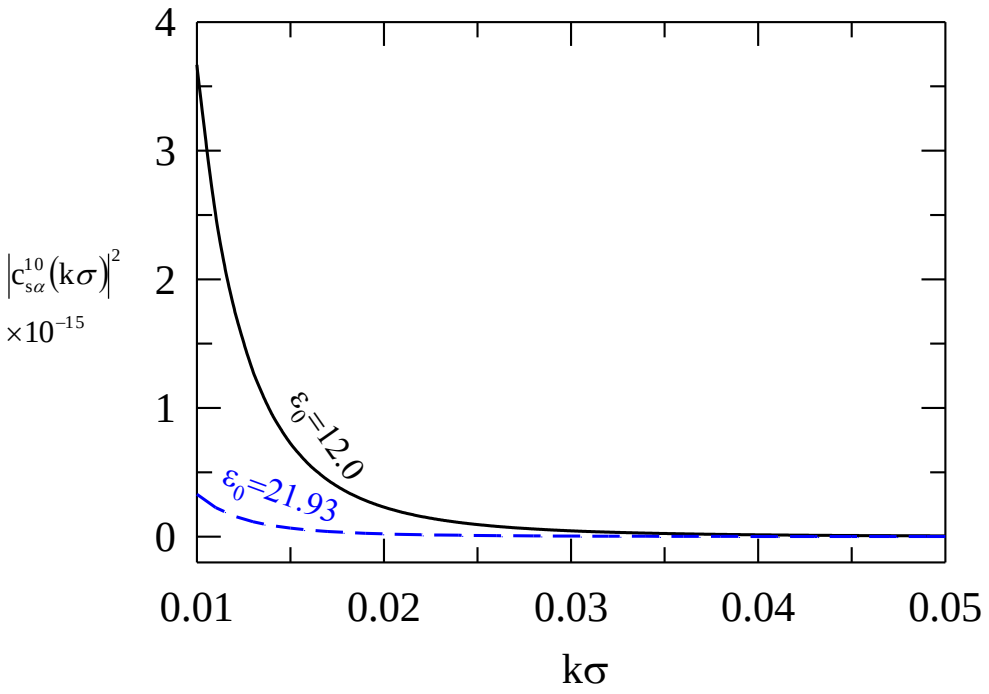

Fig. C2: Static direct correlation functions for Solute dipole – IL ion (dipole-ion) interaction for liquids having different static dielectric constant values but with same size and dipole moment parameters.

.

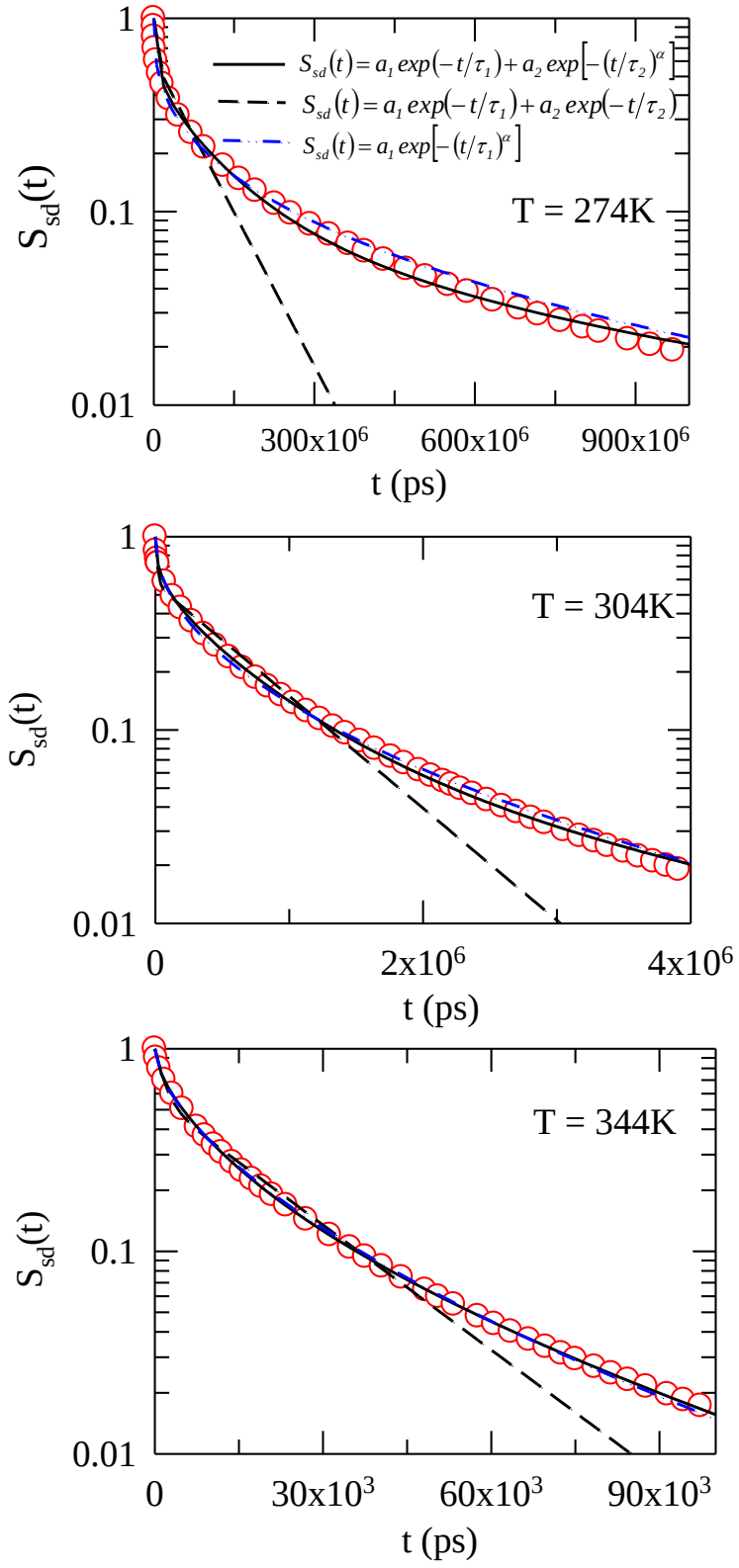

Fig. C3: Fitting of $S_{sd}(t)$ by stretched exponential, bi-exponential and (exponential +stretched exponential) functions at three representative temperatures.

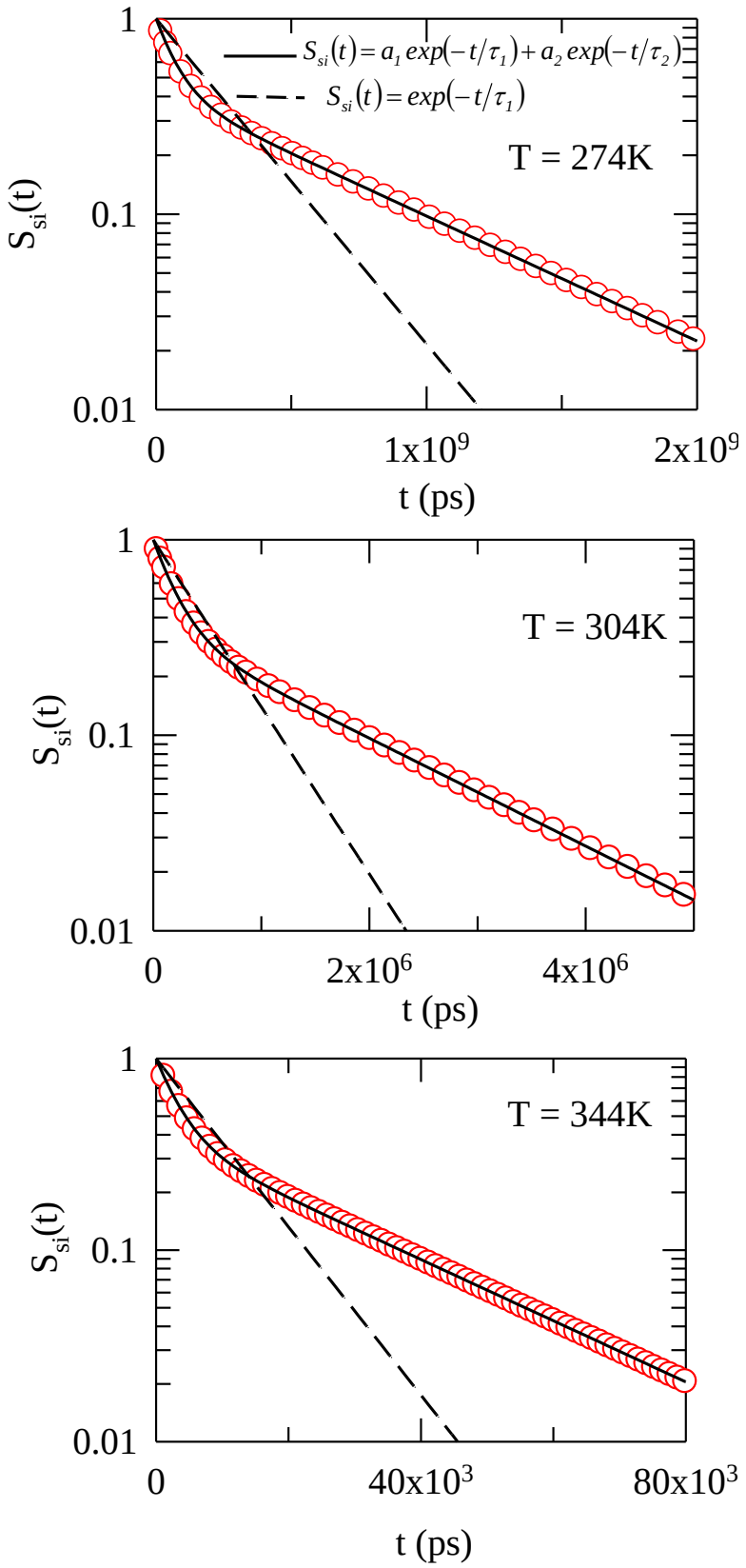

Fig. C4: Fitting of $S_{si}(t)$ using exponential and bi-exponential functions at three representative temperatures.

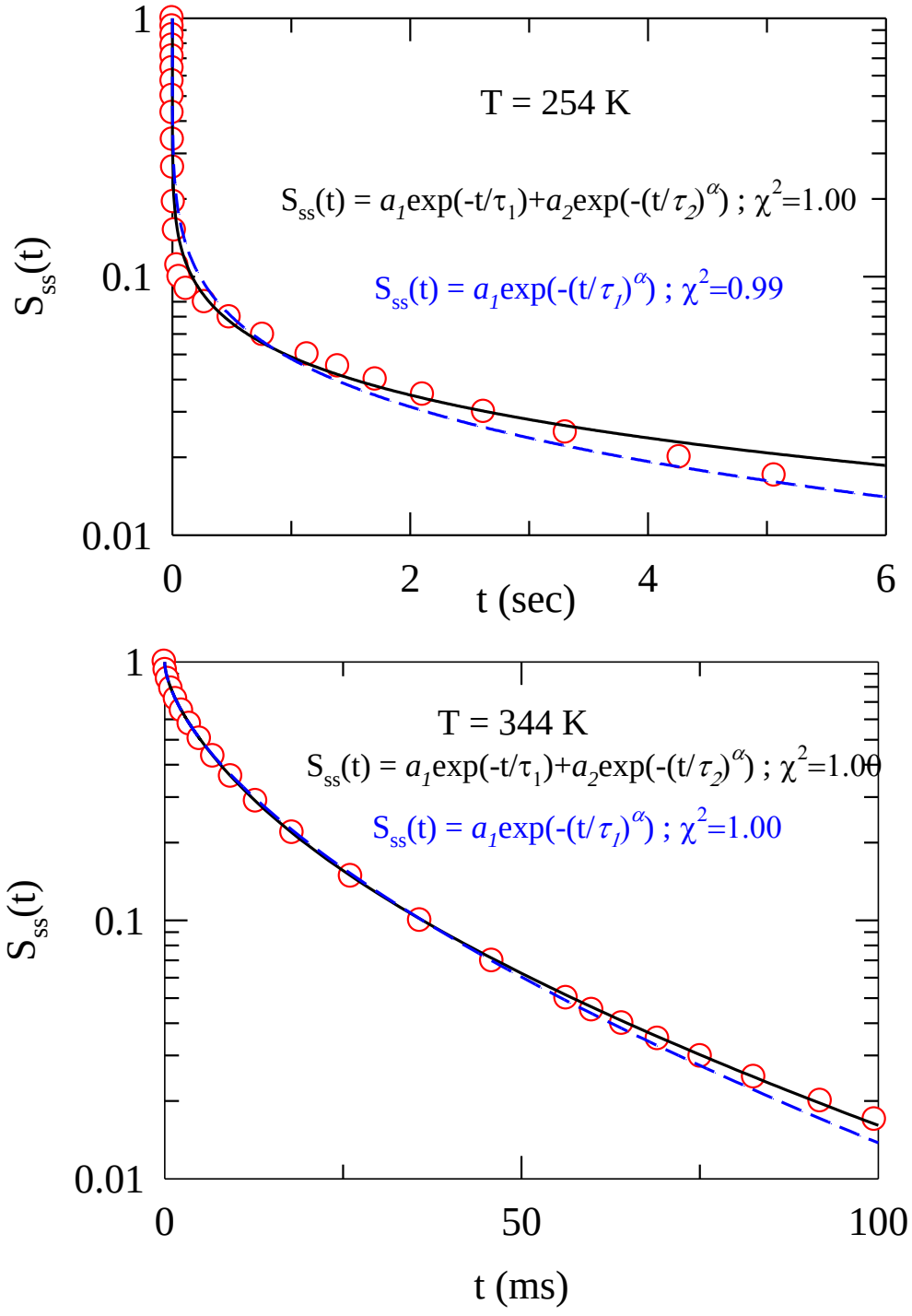

Fig. C5: Fitting of $S_{ss}(t)$ for [Na][TOTO] by stretched exponential and (exponential +stretched exponential) functions at two representative temperatures.

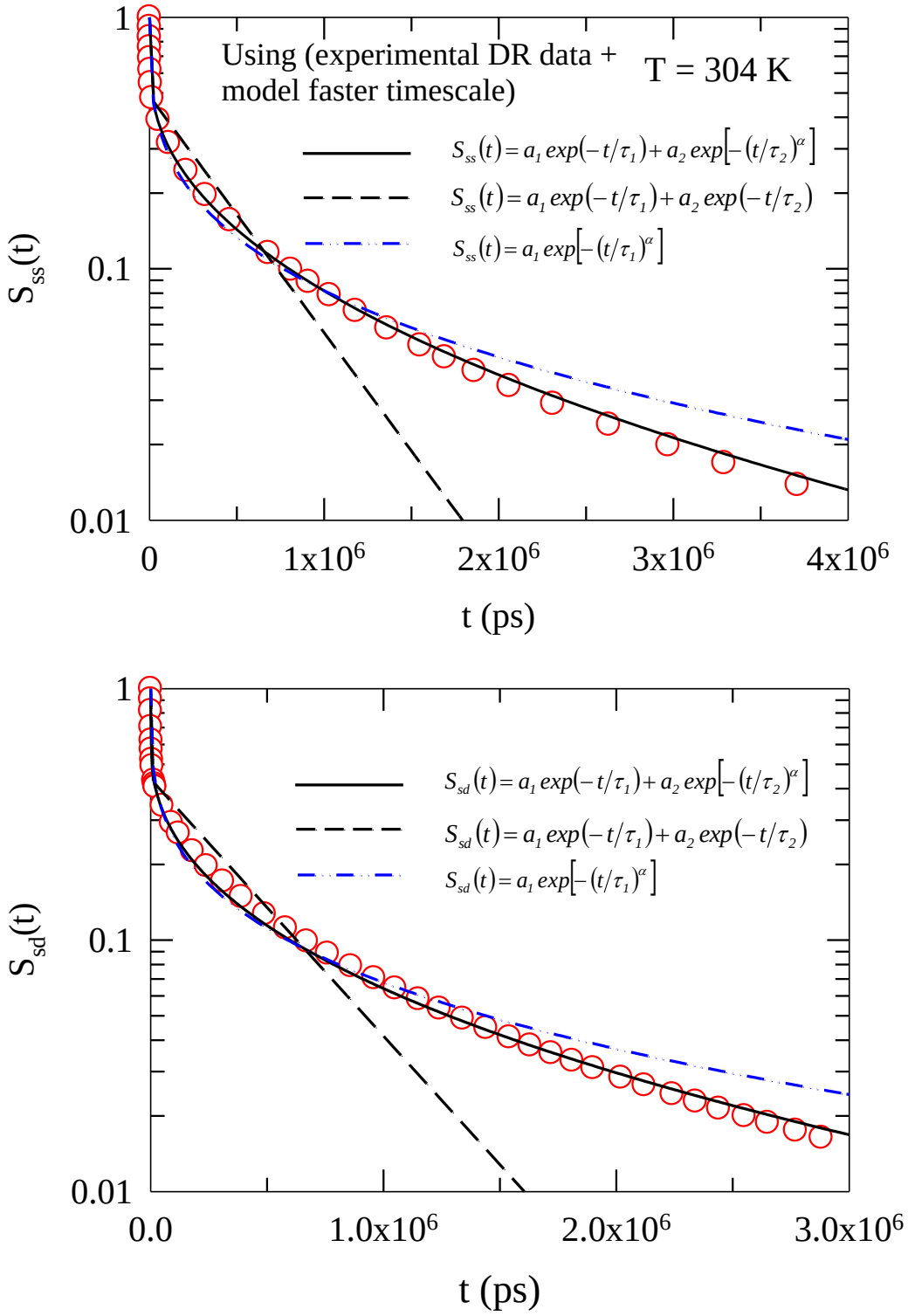

Fig. C6: Fitting of $S_{ss}(t)$ and $S_{sd}(t)$ by stretched exponential, bi-exponential and (exponential +stretched exponential) functions at T = 304 K.

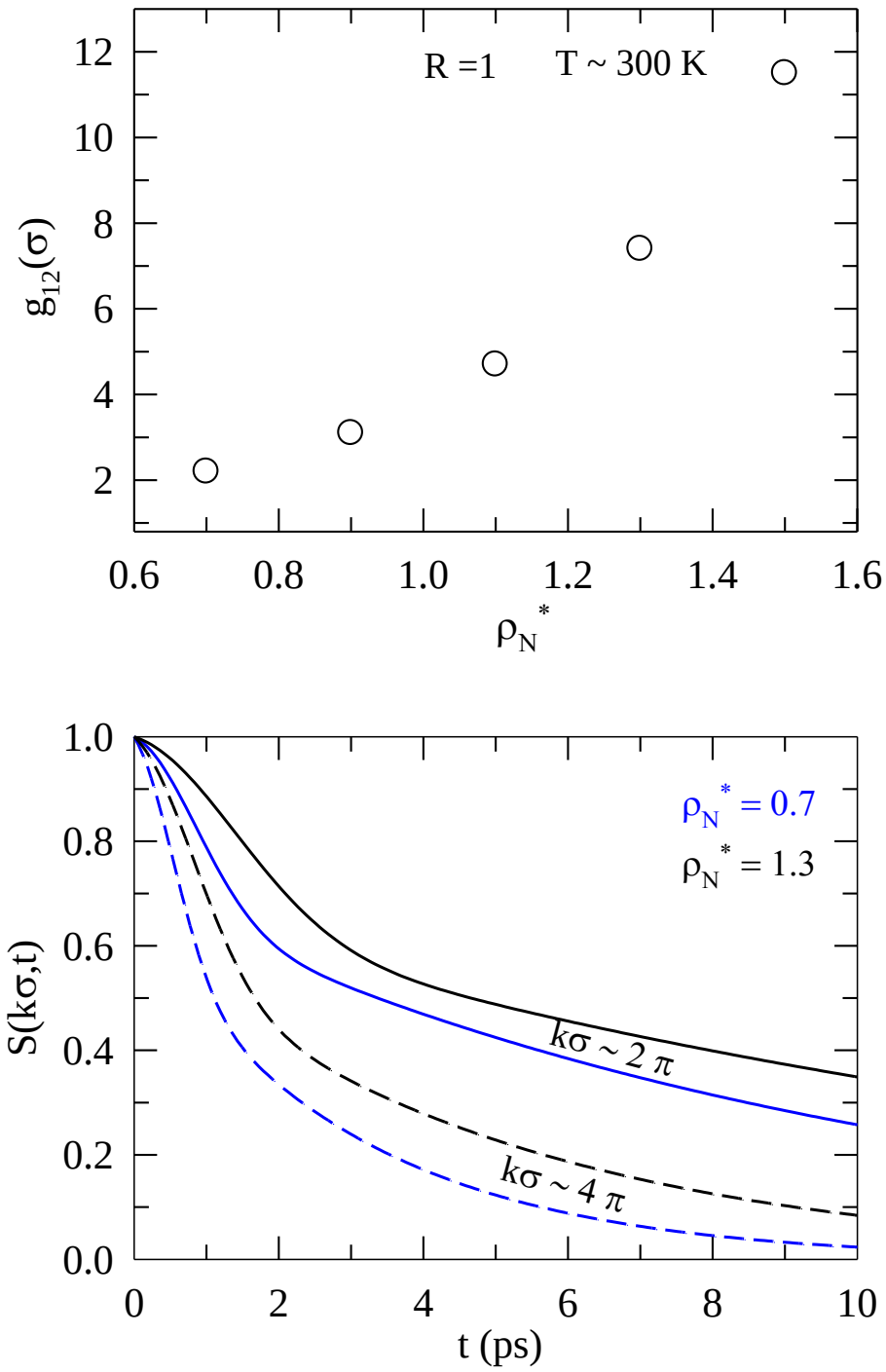

Fig. C7: Upper panel: Density dependence of the value of solute –solvent radial distribution function at contact for a fixed solute-solvent size ratio, R = 1; Lower panel: Relaxation of the isotropic solvent dynamic structure factor at two wavenumbers, $k\sigma \sim 2\pi$ (solid line) and $k\sigma \sim 4\pi$ (broken line) and for two densities (colour coded) specified in the figure.

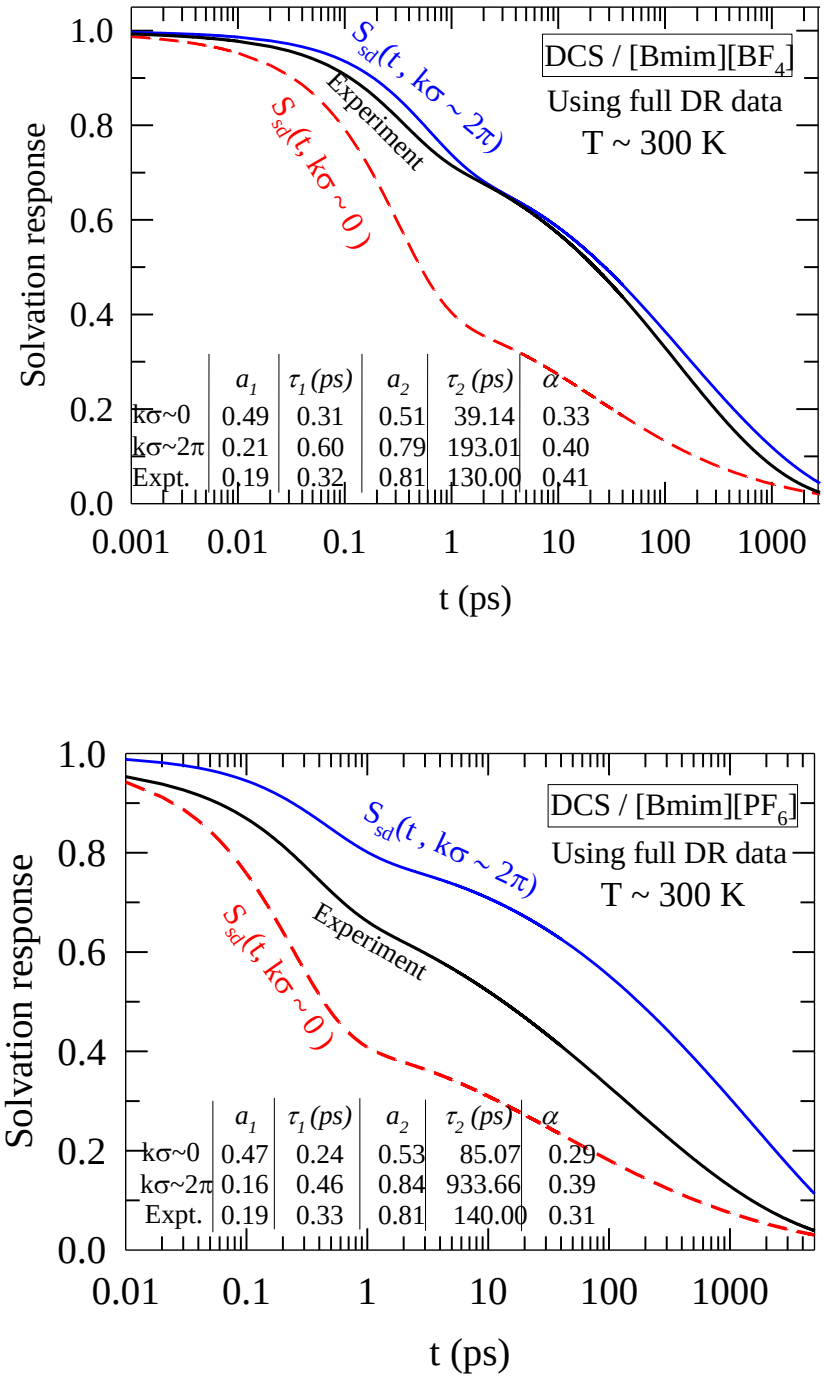

Fig. C8: Comparison between the calculated polar solvation response using the full dielectric relaxation data and the experiments for DCS in [Bmim][BF_4]. Calculations at two wavenumber modes are shown using colour code. Fit parameters are also summarized in each panel for better comparison.

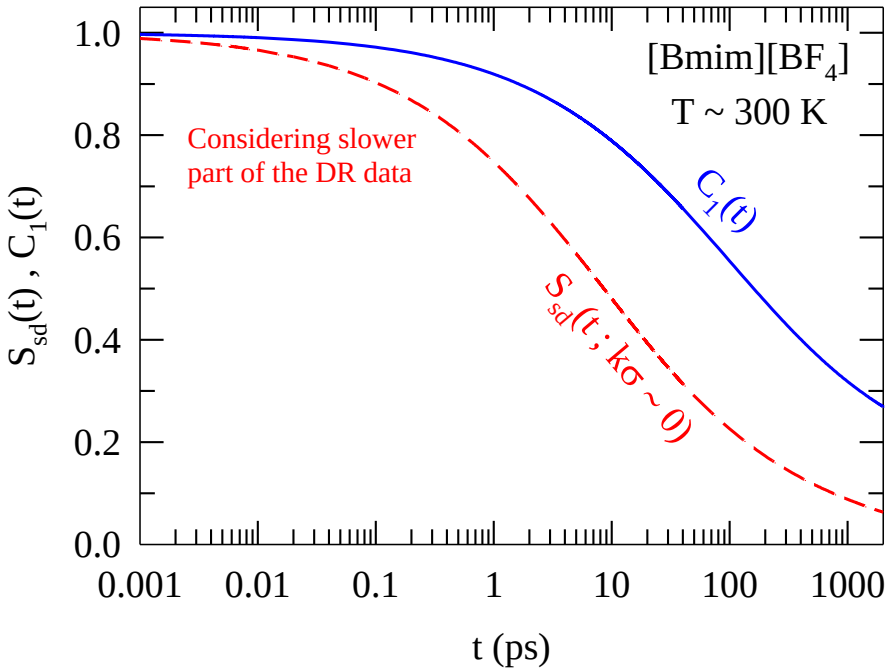

Fig. C9: Comparison between the collective polar solvation energy relaxation due to dipole-dipole solute-IL interaction and the collective single particle reorientation correlation function in [Bmim][BF_4]. The calculated solvation response is for DCS.

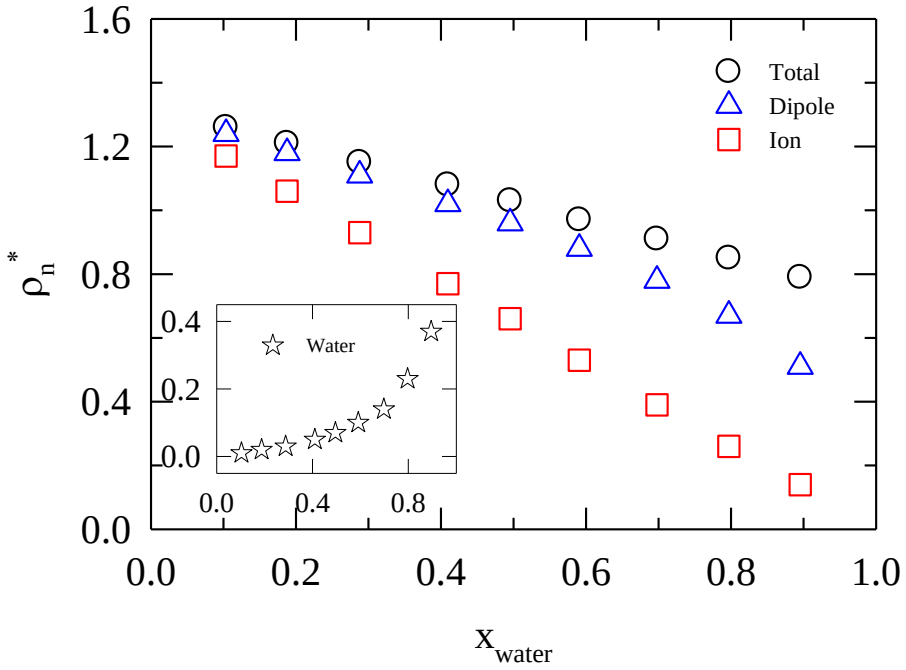

Fig. C10: Composition dependence of the reduced total number density, ion and dipole densities for the binary mixture of ([Bmim][BF_4] + water). The reduced number density of water in this mixture is shown in the inset as a function water mole fraction.

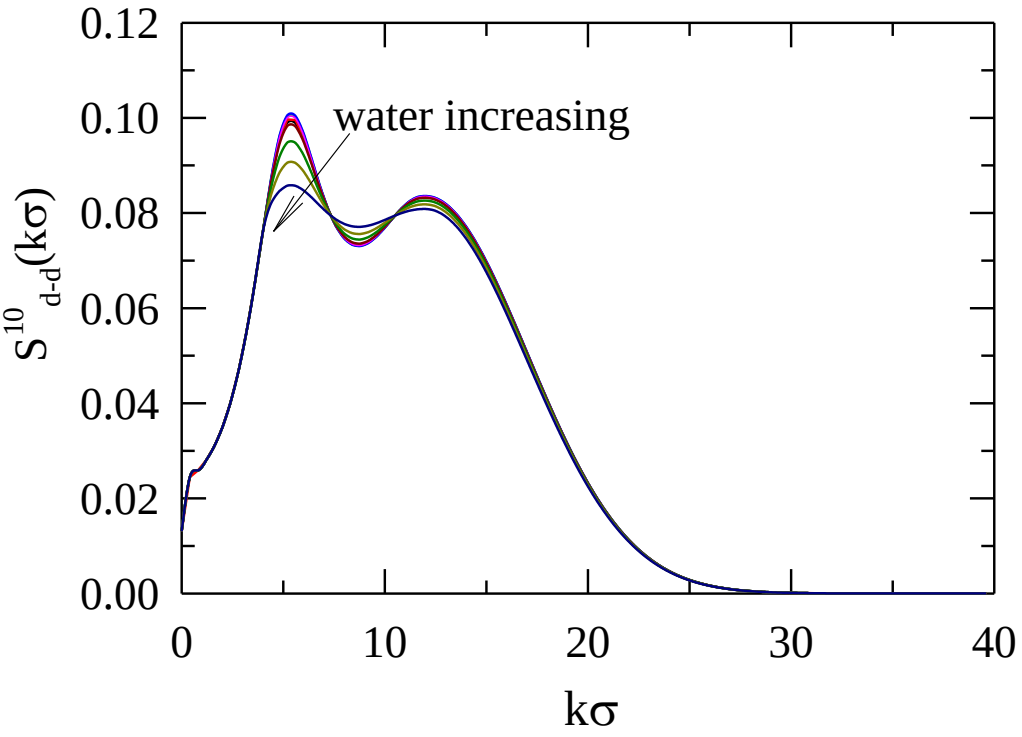

Fig. C11: Composition dependence of the cation – cation dipolar orientational static structural correlation function for aqueous mixtures of [Bmim][BF_4] at water mole fractions 0, 0.1, 0.2, 0.3, 0.4, 0.5, 0.6, 0.7, 0.8 and 0.9.

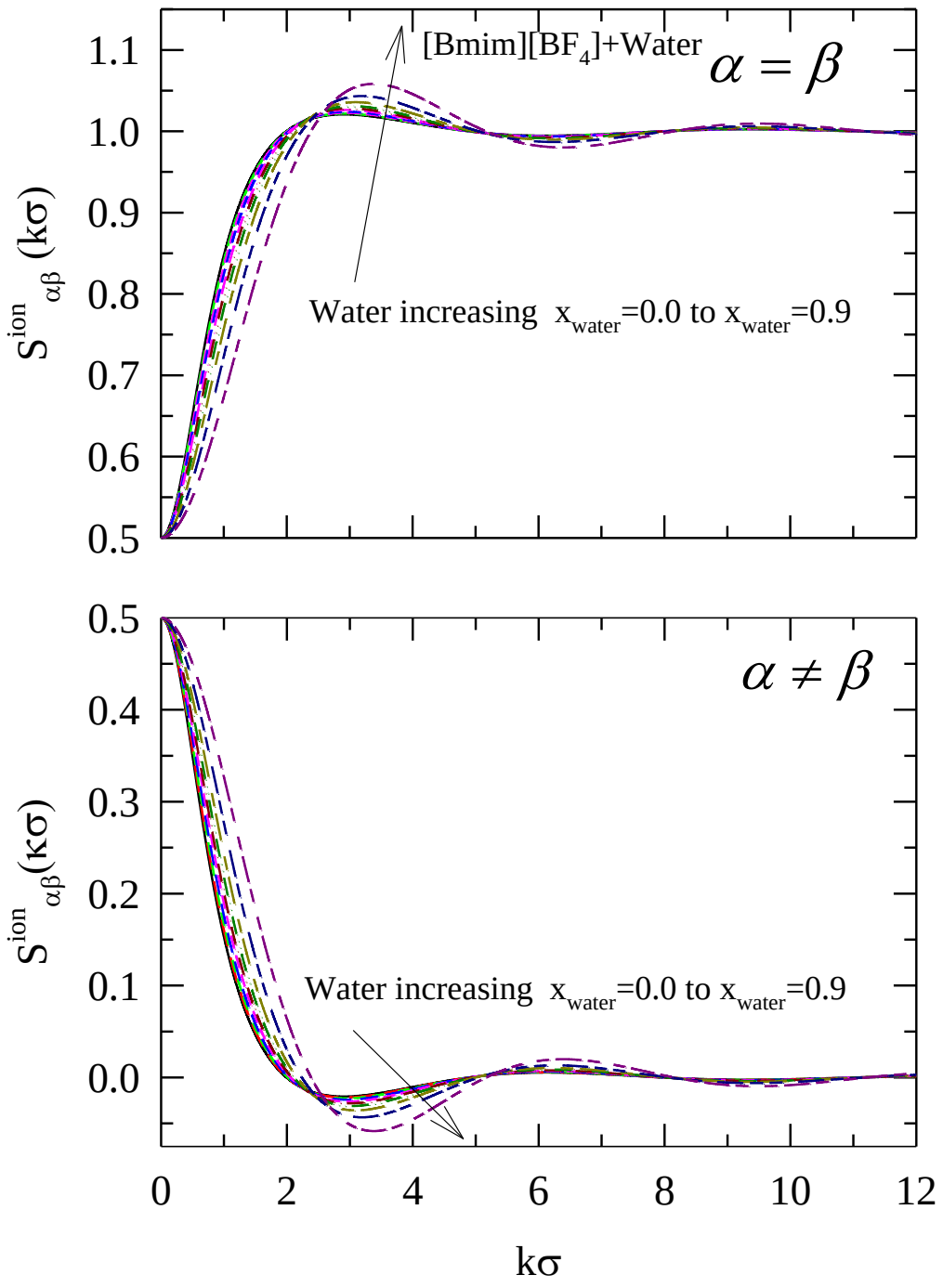

Fig. C12: Static structure factors of ions of same and opposite charges as a function of wavenumber.

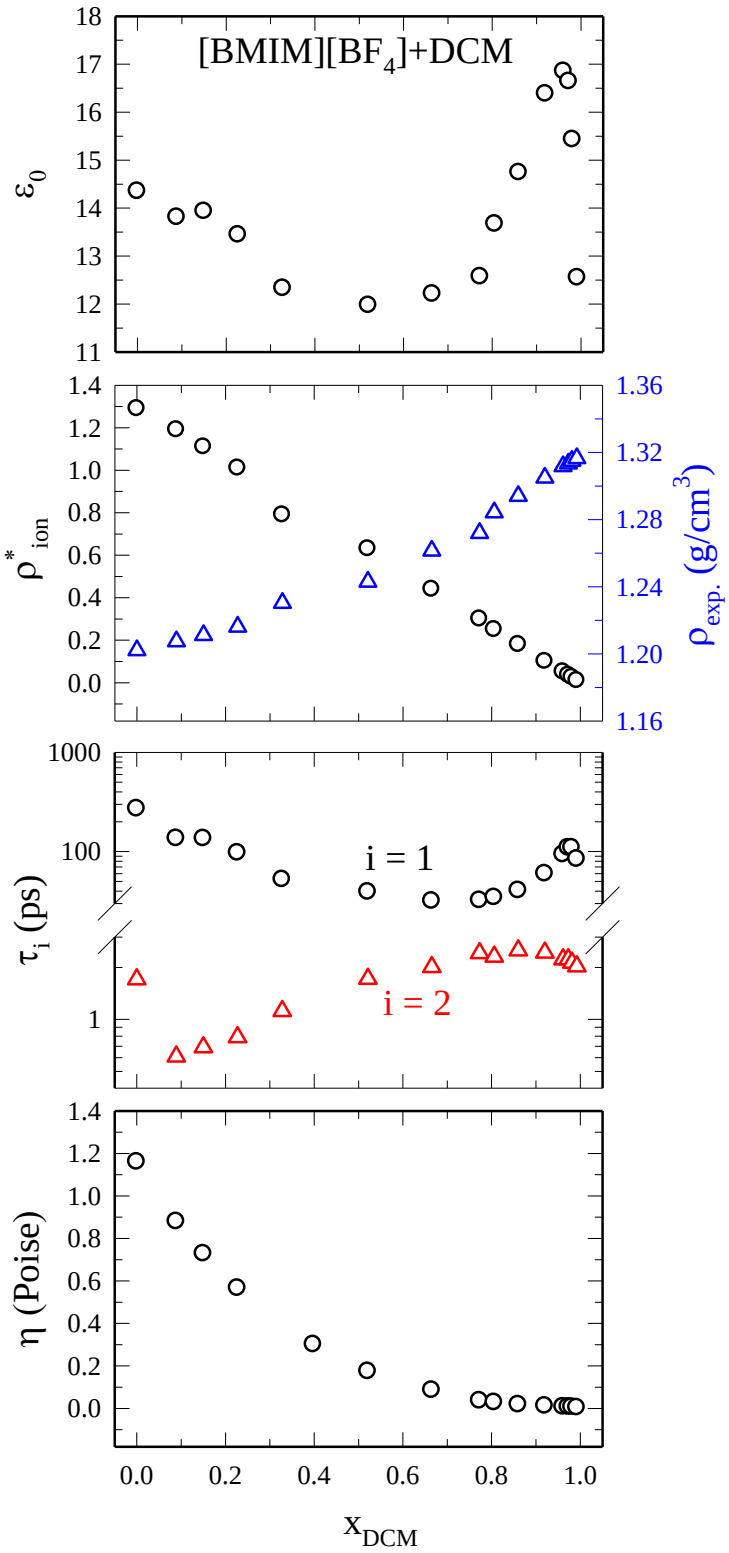

Fig. C13: Composition dependence of experimental static dielectric constant (ε_0, first panel), calculated and experimental densities (second panel), measured dielectric relaxation times (third panel) and experimental viscosities. The references for the experimentally measured quantities are already cited in the main text.

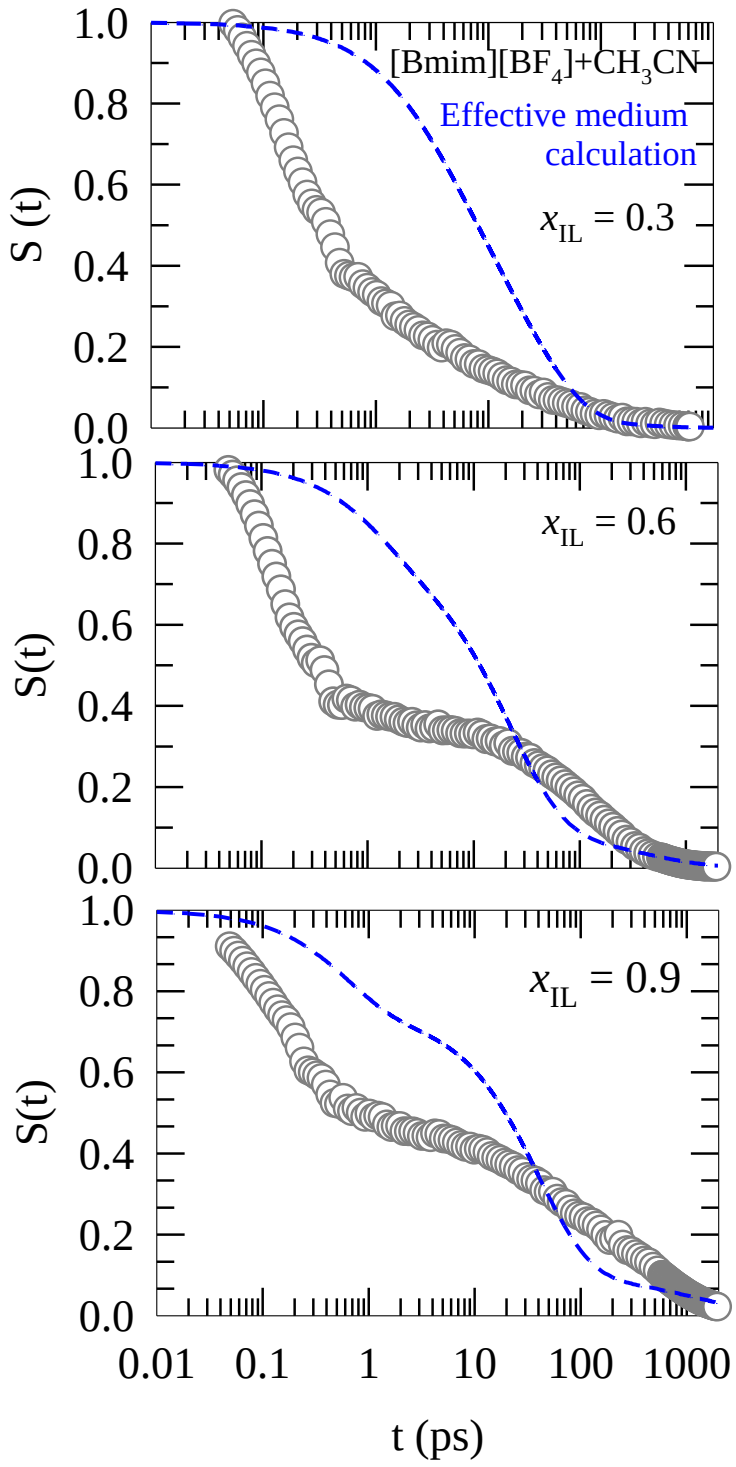

Fig. C14: Decay of the calculated (blue short dashed line) and measured (dark grey open circle) solvation response with time of C153 probe in the binary mixture of $([Bmim][BF_4]+CH_3CN)$ at three representative compositions. The calculated solvation response functions have been obtained from effective medium calculation approach.

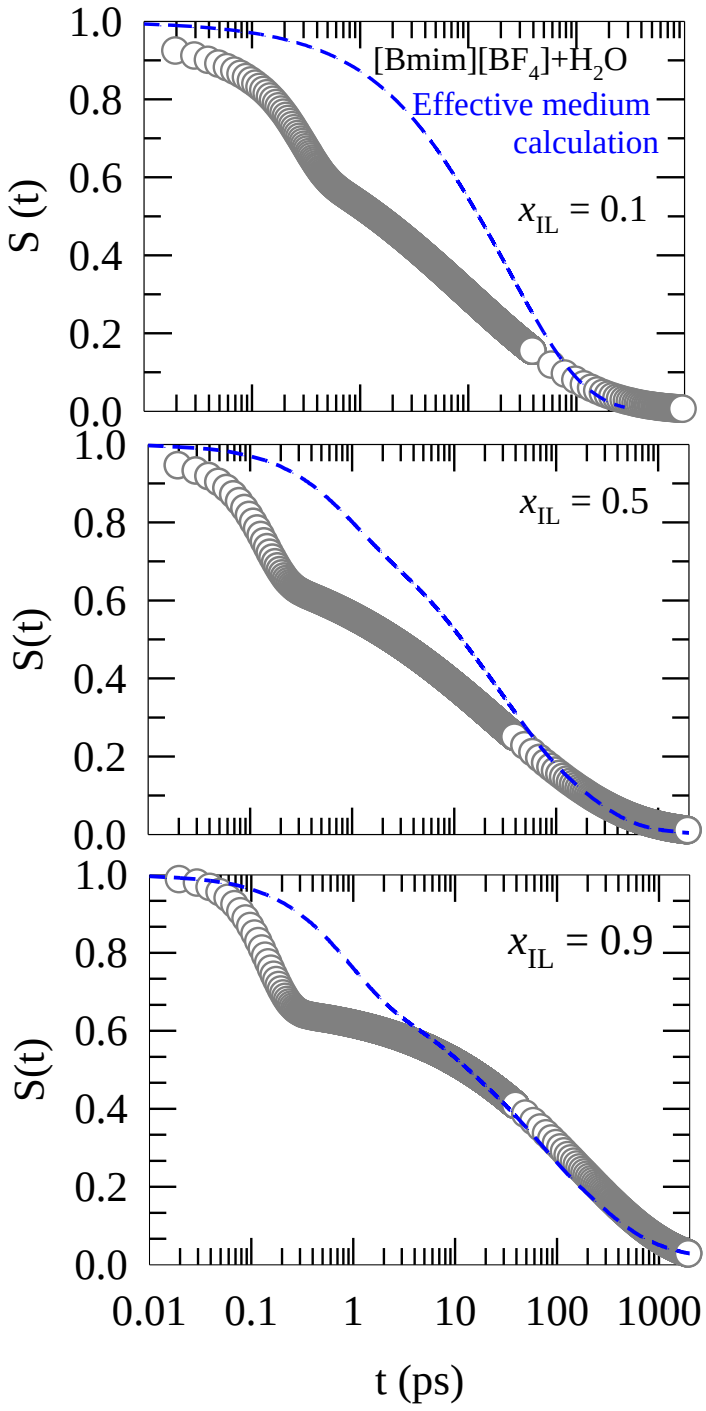

Fig. C15: Decay of the calculated (blue short dashed line) and measured (dark grey open circle) solvation response with time of C153 probe in the binary mixture of $([Bmim][BF_4]+H_2O)$ at three representative compositions. The calculated solvation response functions have been obtained from effective medium calculation approach.

Appendix D

Emergence of bimodal relaxation of $S(t)$ calculated using the Cole-Davidson part of the full experimental dielectric relaxation data

The expression for the generalized rate of orientational polarization density relaxation is given by[10,16-21]

$$\sum_{lm}(k,z) = D_T k^2 f(llm;k) + z\frac{\varepsilon_0[\varepsilon(z)-\varepsilon_\infty]}{\varepsilon_\infty[\varepsilon_0-\varepsilon(z)]}\frac{f(llm;k)}{f(llm;k=0)}\ , \qquad \text{(D.1)}$$

which, in the limit of collective ($k \to 0$) density fluctuation, takes the following form

$$\sum_{lm}(k\to 0,z) = z\frac{\varepsilon_0[\varepsilon(z)-\varepsilon_\infty]}{\varepsilon_\infty[\varepsilon_0-\varepsilon(z)]}. \qquad \text{(D.2)}$$

The experimental $\varepsilon(z)$ for dipolar ILs studied here has been found to fit to either (Cole-Davidson + Debye) or (Cole-Cole + Debye) functions.[23] The Cole-Davidson component is considered here.

$$\varepsilon(z) = \varepsilon_\infty + \frac{S_1}{(1+z\tau_1)^\beta}\ , \qquad \text{(D.3)}$$

with $S_1 = \varepsilon_0 - \varepsilon_\infty$. From Eqs. (2) and (3), one can write

$$\sum_{lm}(k\to 0,z) = z\frac{\varepsilon_0}{\varepsilon_\infty}\left[\frac{1}{(1+z\tau_1)^\beta - 1}\right]\ . \qquad \text{(D.4)}$$

For $k \to 2\pi$ limit, Eq. 4 will be modified by a multiplicative factor, $\frac{f(llm;k\to 2\pi)}{f(llm;k=0)}$, and added to $D_T k^2 f(llm;k)$ evaluated at $k \to 2\pi$.

(**D1**) We first consider $\beta = 0.5$ for analytical tractability

$$\sum_{lm}(k\to 0,z) = z\frac{\varepsilon_0}{\varepsilon_\infty}\left[\frac{1}{\sqrt{(1+z\tau_1)}-1}\right] \qquad \text{(D.5)}$$

Using Taylor series expansion at the $z \to 0$ limit we obtain

$$\sum_{lm}(k\to 0,z)= z\frac{\varepsilon_0}{\varepsilon_\infty}\left[\frac{1}{1+\frac{1}{2}z\tau_1-\frac{1}{8}z^2\tau_1^2-1}\right] = \frac{\varepsilon_0}{\varepsilon_\infty}\left[\frac{1}{\frac{1}{2}\tau_1-\frac{1}{8}z\tau_1^2}\right] \qquad \text{(D.6)}$$

The normalized orientational solvent dynamic structure factor then can be written as

$$S^{lm}_{Solvent}(k\to 0,t)= L^{-1}\left[z+\sum_{lm}(k\to 0,z)\right]^{-1}, \text{where } L^{-1} \text{ represents the Laplace's inverse}$$

$$\begin{aligned} &= L^{-1}\left[z+\frac{\varepsilon_0}{\varepsilon_\infty}\frac{8}{4\tau_1-z\tau_1^2}\right]^{-1} \\ &= L^{-1}\left[\frac{4\varepsilon_\infty\tau_1-\varepsilon_\infty\tau_1^2 z}{4\varepsilon_\infty\tau_1 z-\varepsilon_\infty\tau_1^2 z^2+8\varepsilon_0}\right] \\ &= L^{-1}\left[\frac{A}{z+B}+\frac{C}{z+D}\right] \\ &= L^{-1}\left(\frac{A}{z+B}\right)+L^{-1}\left(\frac{C}{z+D}\right) \\ &= A\exp(-Bt)+C\exp(-Dt) \end{aligned} \qquad \text{(D.7)}$$

where $A=\dfrac{-\frac{2}{\tau_1}\pm\sqrt{\frac{4}{\tau_1^2}+\frac{2\varepsilon_0}{\varepsilon_\infty\tau_1^2}}}{-1-\frac{2}{\tau_1}\pm\sqrt{\frac{4}{\tau_1^2}+\frac{2\varepsilon_0}{\varepsilon_\infty\tau_1^2}}}$, $B=-\frac{2}{\tau_1}\mp\sqrt{\frac{4}{\tau_1^2}+\frac{2\varepsilon_0}{\varepsilon_\infty\tau_1^2}}$

$$C=\frac{-1}{-1-\frac{2}{\tau_1}\pm\sqrt{\frac{4}{\tau_1^2}+\frac{2\varepsilon_0}{\varepsilon_\infty\tau_1^2}}}, \quad D=-\frac{2}{\tau_1}\pm\sqrt{\frac{4}{\tau_1^2}+\frac{2\varepsilon_0}{\varepsilon_\infty\tau_1^2}} \qquad \text{(D.8)}$$

Hence, $S_{sd}(t)$ will be biphasic. Note the above calculations can also be done for any positive fractional value of β but in those cases it has to be solved numerically.

(D2) Consider now for the case with $\boldsymbol{\beta}$ **= 1**

$$\sum_{lm}(k \to 0, z) = \frac{\varepsilon_0}{\varepsilon_\infty \tau_1}, \tag{D.9}$$

$$\begin{aligned} S^{10}_{Solvent}(k \to 0, t) &= L^{-1}\left[z + \sum_{lm}(k \to 0, z) \right]^{-1} \\ &= L^{-1}\left[\frac{1}{z + \frac{\varepsilon_0}{\varepsilon_\infty \tau_1}} \right] \\ &= \exp\left(-\frac{\varepsilon_0}{\varepsilon_\infty \tau_1} t \right) \\ &= \exp\left(-t/\tau_d^{k\to 0} \right) \quad ; \tau_d^{k\to 0} = \frac{\varepsilon_\infty \tau_1}{\varepsilon_0} \end{aligned} \tag{D.10}$$

Hence, $S_{sd}(t)$ will be single exponential if the dielectric response is single Debye type.

Note the references cited to in the above write-up are those corresponding to the references given in the Chapter 5.

Appendix E

Derivation of the expression for the total fluctuating solvation energy of a dipolar solute in a binary mixture of dipolar ionic liquid and a common polar solvent

Following the classical density functional theory, the excess free energy functional for a dipolar probe in a binary mixture of dipolar ionic liquid and a polar solvent may be written as

$$\begin{aligned}
\beta\Delta F\left[\rho_s(\boldsymbol{r},\boldsymbol{\Omega}),\rho_d(\boldsymbol{r},\boldsymbol{\Omega}),\rho_p(\boldsymbol{r},\boldsymbol{\Omega})n_\alpha(\boldsymbol{r})\right] &= \int d\boldsymbol{r}d\boldsymbol{\Omega}\rho_s(\boldsymbol{r},\boldsymbol{\Omega})\left[\ln\frac{\rho_s(r,\Omega)}{\rho_s^0/4\pi}-1\right] \\
&+\int d\boldsymbol{r}d\boldsymbol{\Omega}\rho_d(\boldsymbol{r},\boldsymbol{\Omega})\left[\ln\frac{\rho_d(r,\Omega)}{\rho_d^0/4\pi}-1\right] \\
&+\int d\boldsymbol{r}d\boldsymbol{\Omega}\rho_p(\boldsymbol{r},\boldsymbol{\Omega})\left[\ln\frac{\rho_p(r,\Omega)}{\rho_p^0/4\pi}-1\right] \\
&+\sum_{\alpha=1}^{2}\int d\boldsymbol{r}\,n_\alpha(\boldsymbol{r})\left[\ln\frac{n_\alpha(\boldsymbol{r})}{n_\alpha^0}-1\right] \\
&-\frac{1}{2}\int d\boldsymbol{r}d\boldsymbol{\Omega}d\boldsymbol{r}'d\boldsymbol{\Omega}'\,c_{ss}(\boldsymbol{r},\boldsymbol{\Omega};\boldsymbol{r}',\boldsymbol{\Omega}')\delta\rho_s(\boldsymbol{r},\boldsymbol{\Omega})\delta\rho_s(\boldsymbol{r}',\boldsymbol{\Omega}') \\
&-\frac{1}{2}\int d\boldsymbol{r}d\boldsymbol{\Omega}d\boldsymbol{r}'d\boldsymbol{\Omega}'\,c_{dd}(\boldsymbol{r},\boldsymbol{\Omega};\boldsymbol{r}',\boldsymbol{\Omega}')\delta\rho_d(\boldsymbol{r},\boldsymbol{\Omega})\delta\rho_d(\boldsymbol{r}',\boldsymbol{\Omega}') \\
&-\frac{1}{2}\int d\boldsymbol{r}d\boldsymbol{\Omega}d\boldsymbol{r}'d\boldsymbol{\Omega}'\,c_{\mathrm{pp}}(\boldsymbol{r},\boldsymbol{\Omega};\boldsymbol{r}',\boldsymbol{\Omega}')\delta\rho_p(\boldsymbol{r},\boldsymbol{\Omega})\delta\rho_p(\boldsymbol{r}',\boldsymbol{\Omega}') \\
&-\frac{1}{2}\sum_{\alpha,\beta=1}^{2}\int d\boldsymbol{r}d\boldsymbol{r}'c_{\alpha\beta}(\boldsymbol{r};\boldsymbol{r}')\delta n_\alpha(\boldsymbol{r})\delta n_\beta(\boldsymbol{r}') \\
&-\int d\boldsymbol{r}d\boldsymbol{\Omega}d\boldsymbol{r}'d\boldsymbol{\Omega}'\,c_{\mathrm{sd}}(\boldsymbol{r},\boldsymbol{\Omega};\boldsymbol{r}',\boldsymbol{\Omega}')\delta\rho_s(\boldsymbol{r},\boldsymbol{\Omega})\delta\rho_d(\boldsymbol{r}',\boldsymbol{\Omega}') \\
&-\int d\boldsymbol{r}d\boldsymbol{\Omega}d\boldsymbol{r}'d\boldsymbol{\Omega}'\,c_{\mathrm{sp}}(\boldsymbol{r},\boldsymbol{\Omega};\boldsymbol{r}',\boldsymbol{\Omega}')\delta\rho_s(\boldsymbol{r},\boldsymbol{\Omega})\delta\rho_p(\boldsymbol{r}',\boldsymbol{\Omega}') \\
&-\int d\boldsymbol{r}d\boldsymbol{\Omega}d\boldsymbol{r}'d\boldsymbol{\Omega}'\,c_{\mathrm{dp}}(\boldsymbol{r},\boldsymbol{\Omega};\boldsymbol{r}',\boldsymbol{\Omega}')\delta\rho_d(\boldsymbol{r},\boldsymbol{\Omega})\delta\rho_p(\boldsymbol{r}',\boldsymbol{\Omega}') \\
&-\sum_{\alpha=1}^{2}\int d\boldsymbol{r}d\boldsymbol{\Omega}d\boldsymbol{r}'\,c_{s\alpha}(\boldsymbol{r},\boldsymbol{\Omega};\boldsymbol{r}')\delta\rho_s(\boldsymbol{r},\boldsymbol{\Omega})\delta n_\alpha(\boldsymbol{r}') \\
&-\sum_{\alpha=1}^{2}\int d\boldsymbol{r}d\boldsymbol{\Omega}d\boldsymbol{r}'\,c_{d\alpha}(\boldsymbol{r},\boldsymbol{\Omega};\boldsymbol{r}')\delta\rho_d(\boldsymbol{r},\boldsymbol{\Omega})\delta n_\alpha(\boldsymbol{r}') \\
&-\sum_{\alpha=1}^{2}\int d\boldsymbol{r}d\boldsymbol{\Omega}d\boldsymbol{r}'\,c_{p\alpha}(\boldsymbol{r},\boldsymbol{\Omega};\boldsymbol{r}')\delta\rho_p(\boldsymbol{r},\boldsymbol{\Omega})\delta n_\alpha(\boldsymbol{r}')
\end{aligned} \tag{E.1}$$

where $\delta\rho_s(\boldsymbol{r},\boldsymbol{\Omega}) = \rho_s(\boldsymbol{r},\boldsymbol{\Omega}) - \rho_s^0/4\pi$, $\delta\rho_d(\boldsymbol{r},\boldsymbol{\Omega}) = \rho_d(\boldsymbol{r},\boldsymbol{\Omega}) - \rho_d^0/4\pi$, $\delta\rho_p(\boldsymbol{r},\boldsymbol{\Omega}) = \rho_p(\boldsymbol{r},\boldsymbol{\Omega}) - \rho_p^0/4\pi$, and $\delta n_\alpha(\boldsymbol{r}) = n_\alpha(\boldsymbol{r}) - n_\alpha^0/4\pi$ represent the density fluctuations of solute dipole, dipolar ion , co-solvent dipole and ions over their bulk values. In equilibrium, excess free energy functional is minimum with respect to the bulk density of solute, $\rho_s(\boldsymbol{r},\boldsymbol{\Omega})$. That is,

$$\frac{\delta\beta\Delta F\left[\rho_s(\boldsymbol{r},\boldsymbol{\Omega}),\rho_d(\boldsymbol{r},\boldsymbol{\Omega}),\rho_p(\boldsymbol{r},\boldsymbol{\Omega}),n_\alpha(\boldsymbol{r})\right]}{\delta\rho_s(\boldsymbol{r},\boldsymbol{\Omega})} = 0, \qquad \text{(E.2)}$$

This and the subsequent generalization to time domain allows one to write the time dependent fluctuating effective solvation energy

$$\Delta E_{total}(\boldsymbol{r},\boldsymbol{\Omega};t) = -k_B T\int d\boldsymbol{r}'d\boldsymbol{\Omega}'\, c_{sd}(\boldsymbol{r},\boldsymbol{\Omega};\boldsymbol{r}',\boldsymbol{\Omega}')\delta\rho_d(\boldsymbol{r}',\boldsymbol{\Omega}';\boldsymbol{t}) - k_B T\int d\boldsymbol{r}'d\boldsymbol{\Omega}'\, c_{sp}(\boldsymbol{r},\boldsymbol{\Omega};\boldsymbol{r}',\boldsymbol{\Omega}')\delta\rho_p(\boldsymbol{r}',\boldsymbol{\Omega}';\boldsymbol{t})$$
$$- k_B T\sum_{\alpha=1}^{2}\int d\boldsymbol{r}'c_{s\alpha}(\boldsymbol{r},\boldsymbol{\Omega};\boldsymbol{r}')\delta n_\alpha(\boldsymbol{r}',\boldsymbol{t}),$$

(E.3)

Eq. 3 expresses the fluctuating total solvation energy for an immobile solute. The same for a mobile dipolar solute can be written as follows:

$$\Delta E_{total}(r,\Omega,t) = -k_B T\rho_s(r,\Omega,t)\left[\int d\mathbf{r}'d\boldsymbol{\Omega}'c_{sd}(\mathbf{r},\boldsymbol{\Omega};\mathbf{r}',\boldsymbol{\Omega}')\delta\rho_d(\mathbf{r}',\boldsymbol{\Omega}';t) + \int d\mathbf{r}'d\boldsymbol{\Omega}'c_{sp}(\mathbf{r},\boldsymbol{\Omega};\mathbf{r}',\boldsymbol{\Omega}')\delta\rho_p(\mathbf{r}',\boldsymbol{\Omega}';t) + \sum_{\alpha=1}^{2}\int d\mathbf{r}'c_{s\alpha}(\mathbf{r},\boldsymbol{\Omega};\mathbf{r}')\delta n_\alpha(\mathbf{r}',t)\right]$$

(E.4)

The above expression (Eq. E.4) is the Eq. 6.1 of the Chapter 6.

Appendix F

Calculation detail of the generalized rate, $\Sigma_{lm}(k,z)$

The (l,m)th component of the generalized rate of orientational solvent polarization density relaxation has been shown to be given by,[88,106-109]

$$\Sigma_{lm}(k,z) = \frac{k_B T k^2 f_{llm}(k)}{M\sigma^2\left[z+\Gamma_T(k,z)\right]} + \frac{k_B T l(l+1) f_{llm}(k)}{I\left[z+\Gamma_R(k,z)\right]}, \qquad \text{(F.1)}$$

where σ, M, and I denote respectively the diameter, mass, and average moment of inertia of the solvent molecule. $\Gamma_T(k,z)$ and $\Gamma_R(k,z)$ are respectively the wave number and frequency dependent translational and rotational dissipative kernels.

The translational dissipative kernel, $\Gamma_T(k,z)$, is related to the isotropic liquid dynamic structure factor, *S(k,z)*.[88] If one considers only the diffusive dynamics for the relaxation of the isotropic dynamic structure factor then in time plane one can write $S(k,t) = S(k)\exp[-D_T k^2 t/S(k)]$ which leads to the following relation for

$$\frac{k_B T}{M\sigma^2[z+\Gamma_T(k,z)]} = \frac{D_T}{\sigma^2}. \qquad \text{(F.2)}$$

The translational diffusion coefficient, $D_T\,(=2k_BT/C\eta\sigma)$ can be obtained from hydrodynamics by using effective diameter of a given ionic liquid molecule and experimentally measured medium viscosity (η). The calculation of the rotational kernel ($\Gamma_R(k,z)$), on the other hand, is somewhat involved and has already been discussed in detail in many of our earlier works.[84-88,106-109] In short, $\Gamma_R(k,z)$ was first approximated by its long wavelength limit ($\Gamma_R(k,z) \approx \Gamma_R(k=0,z)$) and then connected to the experimentally measured frequency dependent dielectric function $\varepsilon(z)$ as follows

$$\frac{2k_B T}{I\left[z+\Gamma_R(k,z)\right]} = \frac{z\varepsilon_0\left[\varepsilon(z)-\varepsilon_\infty\right]}{f_{110}(k=0)\varepsilon_\infty\left[\varepsilon_0-\varepsilon(z)\right]}, \qquad \text{(F.3)}$$

where ε_∞ is the optical frequency dielectric constant of the pure medium. Since Eq. 6.2 (Chapter 6) expresses the total solvation energy as a sum-total of contributions from pure components, $\varepsilon(z)$ used in the calculations are those measured for pure systems. Subsequently, we have calculated $\Sigma_{11}(k,z)$ by multiplying Eq. F.3 with $f_{111}(k)$.

Note the references cited to in the above Appendix are those corresponding to the references given in the Chapter 6.